UNIVERSITÉ DU LUXEMBOURG

PhD-FSTC-2019-35
The Faculty of Sciences, Technology and Communication

DISSERTATION

Defence held on 29/05/2019 in Esch-sur-Alzette

to obtain the degree of

DOCTEUR DE L'UNIVERSITÉ DU LUXEMBOURG

EN BIOLOGIE

by

Lisa Maria SMITS

Born on 28th July 1989 in Goch, (Germany)

GENERATION OF MIDBRAIN ORGANOIDS AS A MODEL TO STUDY PARKINSON'S DISEASE

Dissertation defence committee

Dr Jens C. Schwamborn, dissertation supervisor
Professor, Université du Luxembourg

Dr Liliana Bernardino
Associate Professor, University of Beira Interior

Dr Anne Grünewald, Chairman
Associate Professor, Université du Luxembourg

Dr Wim Mandemakers
Erasmus MC, Rotterdam

Dr Alexander Skupin, Vice Chairman
Université du Luxembourg

University of Luxembourg

Doctoral Thesis

Generation of midbrain organoids as a model to study Parkinson's disease

Author:
Lisa M. Smits

Supervisor:
Prof. Dr. Jens C. Schwamborn

A thesis submitted in partial fulfilment of the requirements for the degree of Doctor of Philosophy in Biology

in the

Developmental and Cellular Biology Group
Luxembourg Centre for Systems Biomedicine

2nd September 2019

Declaration of Authorship

I, Lisa M. Smits, declare that this thesis titled, 'Generation of midbrain organoids as a model to study Parkinson's disease' and the work presented in it are my own. I confirm that:

- This work was done wholly while in candidature for a research degree at the University of Luxembourg.
- No part of this thesis has previously been submitted for a degree or any other qualification at the University of Luxembourg, or any other institution.
- Where I have consulted the published work of others, this is always clearly attributed.
- Where I have quoted from the work of others, the source is always given. With the exception of such quotations, this thesis is entirely my own work.
- I have acknowledged all main sources of help.
- Where the thesis is based on work done by myself jointly with others, I have made clear exactly what was done by others and what I have contributed myself.

Signed: _____

Date: _____

" I have no special talent. I am only passionately curious."

Albert Einstein

Abstract

Generation of midbrain organoids as a model to study Parkinson's disease

by Lisa M. Smits

The study of 3D cell culture models not only bridges the gap between traditional 2D *in vitro* experiments and *in vivo* animal models, it also addresses processes that cannot be recapitulated by these traditional models. Therefore, it offers an opportunity to better understand complex biology, for instance brain development, where conventional models have not proven successful. The so–called brain organoid technology provides a physiologically relevant context, which holds great potential for its application in modelling neurological diseases.

To obtain these highly specialised structures, resembling specifically key features of the human midbrain, we derived a human midbrain–specific organoid (hMO) system from regionally patterned neural stem cells (NSCs). The resulting neural tissue exhibited abundant neurons with midbrain dopaminergic neuron (mDAN) identity, as well as astroglia and oligodendrocyte differentiation. Within the hMOs, we could observe neurite myelination and the formation of synaptic connections. Regular fire patterning and neural network synchronicity were determined by multielectrode array (MEA) recordings. In addition to electrophysiologically functional mDANs producing and secreting dopamine (DA), we also detected responsive neuronal subtypes, like GABAergic and glutamatergic neurons.

To investigate Parkinson's disease (PD)–relevant pathomechanisms, we derived hMOs from PD patients carrying the *LRRK2*–G2019S mutation and compared them to healthy control hMOs. In addition to a reduced number and complexity of mDANs, we determined a significant increase of the stem cell marker FOXA2 in the patient–derived hMOs. This suggests a neurodevelopmental defect induced by a PD–specific mutation and emphasises the importance of advanced three–dimensional (3D) stem cell–based *in vitro* models.

The in this thesis described hMOs are suitable to reveal PD–relevant phenotypes, thus constitute as a powerful tool for human–specific *in vitro* disease modelling of neurological disorders with a great potential to be utilised in advanced therapy development.

Dissemination

During the course of this PhD project, the work carried out resulted in six co-authored articles, out of which four have been published and three have been submitted. All articles can be found in the results part or in the respective appendices.

Published

Anna S. Monzel, Lisa M. Smits, Kathrin Hemmer, Siham Hachi, Edinson Lucumi Moreno, Thea van Wuellen, Javier Jarazo, Jonas Walter, Inga Brüggemann, Ibrahim Boussaad, Emanuel Berger, Ronan M.T. T Fleming, Silvia Bolognin and Jens C. Schwamborn (May 2017). 'Derivation of Human Midbrain-Specific Organoids from Neuroepithelial Stem Cells'. In: *Stem Cell Reports* 8.5, pp. 1–11

Athanasios D Spathis, Xenophon Asvos, Despina Ziavra, Theodoros Karampelas, Stavros Topouzis, Zoe Cournia, Xiaobing Qing, Lisa M Smits, Christina Dalla, Hardy J Rideout, Jens C Schwamborn, Constantin Tamvakopoulos, Demosthenes Fokas and Demetrios K Vassilatis (Apr. 2017). 'Nurr1:RXRα heterodimer activation as monotherapy for Parkinson' s disease'. In: *PNAS* 114.15, pp. 3999–4004

Asad Jan, Brandon Jansonius, Alberto Delaidelli, Forum Bhanshali, Yi Andy An, Nelson Ferreira, Lisa M. Smits, Gian Luca Negri, Jens C. Schwamborn, Poul H. Jensen, Ian R. Mackenzie, Stefan Taubert and Poul H. Sorensen (Dec. 2018). 'Activity of translation regulator eukaryotic elongation factor-2 kinase is increased in Parkinson disease brain and its inhibition reduces alpha synuclein toxicity'. In: *Acta Neuropathologica Communications* 6.1

Kathrin Hemmer, Lisa M Smits, Silvia Bolognin and Jens C Schwamborn (May 2018). 'In vivo Phenotyping of Human Parkinson' s Disease-Specific Stem Cells Carrying the LRRK2 -G2019S Mutation Reveals Increased a-Synuclein Levels but Absence of Spreading'. In: *Opera Medica et Physiologica* 4.2

Lisa M. Smits, Lydia Reinhardt, Peter Reinhardt, Michael Glatza, Anna S. Monzel, Nancy Stanslowsky, Marcelo D. Rosato-Siri, Alessandra Zanon, Paul M. Antony, Jessica Bellmann, Sarah M. Nicklas, Kathrin Hemmer, Xiaobing Qing, Emanuel Berger, Norman Kalmbach, Marc Ehrlich, Silvia Bolognin, Andrew A. Hicks, Florian

Wegner, Jared L. Sterneckert and Jens C. Schwamborn (Dec. 2019). 'Modeling Parkinson's disease in midbrain-like organoids'. In: *npj Parkinson's Disease* 5.1, p. 5

Submitted

Lisa M Smits, Stefano Magni, Kamil Grzyb, Paul MA Antony, Rejko Krüger, Alexander Skupin, Silvia Bolognin and Jens C Schwamborn (2019). 'Single-cell transcriptomics reveals multiple neuronal cell types in human midbrain-specific organoids'. In: *bioRxiv*

Contents

Abbreviations

2D	two–dimensional
3D	three–dimensional
6–OHDA	6–hydroxydopamine
AA	ascorbic acid
Aβ	amyloid–β
AADC	aromatic l–amino acid decarboxylase
AD	Alzheimer's disease
AMPA	α–amino–3–hydroxy–5–methyl–4–isoxazolepropionic acid
AQP4	Aquaporin
BDNF	brain–derived neurotrophic factor
BMP	bone morphogenic protein
BSA	bovine serum albumin
CC3	cleaved Caspase–3
CHIR	CHIR–99021
CNPase	2', 3'–cyclic nucleotide 3'–phosphodiesterase
CNS	central nervous system
DA	dopamine
DAN	dopaminergic neuron
DAPT	N-(N-(3, 5–difluorophenacetyl–L–alanyl))–S–phenylglycine t–butyl ester
DAT	dopamine transporter
dbcAMP	dibutyryladenosine cyclic monophosphate
DCX	doublecortin
DDC	DA decarboxylase
DEM	digital expression matrix
DEG	differentially expressed genes
DM	Dorsomorphin
DMEM	modified Dulbecco's Eagle's medium
DMSO	dimethylsulfoxide
DNA	deoxiribonucleic acid

EBF3	early B–cell factor 3
EBs	embryoid bodies
EDTA	ethylenediaminetetraacetic acid
EGF	epidermal growth factor
ELISA	enzyme–linked immunosorbent assay
EN–1	homeobox protein engrailed–1
ENT	engineered nervous tissue
ESC	embryonic stem cell
FACS	fluorescence–activated cell sorting
FGF	fibroblast growth factor
FOXA2	forkhead box protein A2
FOXG1	forkhead box protein G1
FP	floor plate
GABA	γ–aminobutyric acid
GBA	glucocerebrocidase
GBX2	gastrulation brain homeobox 2
GD	GDNF
GDNF	glial cell–derived neurotrophic factor
GFAP	glial fibrillary acidic protein
GIRK2	G–protein–regulated inward–rectifier potassium channel 2
GSK–3β	glycogen synthase kinase 3β
hBDNF	human brain–derived neurotrophic factor
hGDNF	human glial cell–derived neurotrophic factor
hiPSC	human induced pluripotent stem cell
hMO	human midbrain–specific organoid
hNESC	human neuroepithelial stem cell
H_2O_2	hydrogen peroxide
HPLC	high–performance liquid chromatography
HTS	high–throughput screening
ICM	inner cell mass
IRX3	Iroquois–class homeobox protein 3
IsO	isthmic organiser
KLF4	Kruppel–like factor 4
L1CAM	L1 cell adhesion molecule
LBs	Lewy bodies
LDN	LDN–193189
LMX1A	LIM homeobox transcription factor 1α
LNs	Lewy neurites
LRRK2	leucine–rich repeat kinase 2
LSM	laser scanning microscope

MAP2	microtubule–associated protein 2
MEA	multielectrode array
mDAN	midbrain dopaminergic neuron
mfNPC	midbrain floor plate neural precursor cell
MAO–B	monoamine oxidase B
MBP	myelin basic protein
MPP+	1–methyl–4–phenylpyridinium
MPTP	1–methyl–4–phenyl–1,2,3,6–tetrahydropyridine
mRNA	messenger RNA
NEAA	non–essential amino acids
NGN2	neurogenin 2
NFT	neurofibrillary tangle
NM	neuromelanin
NMDA	N–methyl–D–aspartate
NPC	neural precursor cell
NSC	neural stem cell
NT3	neurotrophic factor 3
NURR1	nuclear receptor related 1 protein
OCT–3/4	octamer binding factor 3/4
OTX2	orthodenticle homologue 2
p	passage
PRKN	parkin
PAX3	paired box protein 3
PAX6	paired box protein 6
PBS	phosphate–buffered saline
PCR	polymerase chain reaction
PD	Parkinson's disease
PFA	paraformaldehyde
PINK1	PTEN induced kinase 1
PITX3	paired–like homeodomain 3
PMA	Purmorphamine
PNS	peripheral nervous system
pS129	phosphorylated at serine 129
PSC	pluripotent stem cell
PTEN	phosphatase and tensin homolog
qRT–PCR	quantitative real–time polymerase chain reaction
RA	retinoid acid
RGMB	repulsive guidance molecule B
RNA	ribonucleic acid
R–NSC	rosette neural stem cell

ROS	reactive oxygen species
RT	room temperature
SAG	smoothened agonist
SB	SB–431542
SC	stem cell
scRNA–seq	single–cell RNA sequencing
SD	standard deviation
SEM	standard error of the mean
SFEBq	serum–free floating culture of embryoid body–like aggregates with quick re–aggregation
SHH	sonic hedgehog
smNPC	small molecule neural precursor cell
SN	*substantia nigra*
SNCA	α–synuclein
SNc	*substantia nigra pars compacta*
SOX1	sex determining region Y–box 1
SOX2	sex determining region Y–box 2
SVZ	subventricular zone
TBS	Tris–buffered saline
TEM	transmission electron microscopy
TGF–β	transforming growth factor β
TH	tyrosine hydroxylase
t–SNE	t–distributed stochastic neighbourhood embedding
TTX	tetrodotoxin
TUJ1	βIII Tubulin
UCHL1	ubiquitin C–terminal hydrolase L1
VIM	Vimentin
VMAT2	vesicular monoamine transporter 2
VPS35	vacuolar protein sorting–associated protein 35
VZ	ventricular zone
w/o	without
WHO	World Health Organization
ZIKV	Zika virus

List of Figures

List of Tables

CHAPTER 1

Introduction

1.1 Parkinson's disease

In 1817 James Parkinson published the first clinical description of the Shaking Palsy, a neurological disease today well–known by his own name. In his *Essay on the Shaking Palsy* he composed his observation about six people that he partially encountered on the streets of London (Parkinson 2002). Despite the small number of patients and the fact that he did not perform physical examinations, he was able to perfectly document the clinical symptoms of the disease.
200 years after drawing attention for the first time, Parkinson's disease (PD) is one of the most prevalent neurodegenerative disorders in the world. The recently published Global Burden of Disease Study estimated that there are currently 6.2 million PD patients (Feigin et al. 2017; Dorsey et al. 2018). For the majority of these cases, the aetiological factors causing the disease are unknown.
The loss of neuromelanin (NM)–containing midbrain dopaminergic neurons (mDANs) in the *substantia nigra pars compacta* (SNc) and thereby the disruption of the basal ganglia network of the midbrain, striatum, and cortex, is characterised as a hallmark for the diagnosis of PD (Byers et al. 2012; Recasens et al. 2014; Rodriguez et al. 2014). The progressive neuronal degeneration leads to a reduced thalamus

activity, which in turn fails to adequately control motor cortical functions (Tepper et al. 2007; Blesa, Trigo-Damas et al. 2017). As a consequence, PD–patients show clearly observable movement abnormalities, such as tremor at rest, inability to initiate movement (akinesia), slowness of movement (bradykinesia), muscular rigidity and postural instability (Obeso et al. 2002; Lindvall et al. 2009; Ruitenberg et al. 2015; Kalia et al. 2015). In addition to these cardinal PD clinical features, patients develop an attendant extranigral pathology, which gives rise to non–motor symptoms (Braak, Del Tredici et al. 2003). The loss of mDANs in the olfactory bulb can lead to an impairment of the sense of smell, furthermore patients often suffer from sleeping disorder, depression, and dementia (Braak, Del Tredici et al. 2003; Langston 2006; Nass et al. 2008).

The presence of protein aggregations and the formation of intracellular inclusion bodies, like Lewy bodies (LBs) in the neuronal soma or Lewy neurites (LNs) in neuritic projections, is another neuropathological feature of PD (Forno 1996; Wakabayashi et al. 1997; Engelhardt et al. 2017; Byers et al. 2012; Recasens et al. 2014). Intriguingly, after decades of research on PD, the molecular mechanisms underlying the initiation and progression of the neurodegenerative disease, commonly occurring as sporadic idiopathic form, could not have been entirely disclosed and remain largely elusive (Roybon et al. 2004). Nevertheless, 5–10 % of all PD cases are caused by mutations or deletions in dominantly or recessively inherited genes (Klein et al. 2012; Schwamborn 2018). Among these eleven Mendelian inherited genes, some are involved in mitochondria biogenesis (*DJ–1, LRRK2, PRKN, PINK1, SNCA*), the autophagy–lysosome–pathway (*ATP13A2, LRRK2, SNCA, VPS35*) and the endosome–lysosome–pathway (*DNAJC6, SNCA, VPS35*). They can lead to monogenic forms of PD or increased PD susceptibility, which indicates that these genes are important in the pathogenesis (Dawson and Dawson 2003; Lesage et al. 2009; Nuytemans et al. 2010; Byers et al. 2012; Schwamborn 2018). Furthermore, non–genetic factors, like the exposure to toxins, herbicides, and pesticides, as well as infection and psychological stress might induce changes in the brain connectivity and gene expression that can contribute to the risk to suffer from PD (Kamel et al. 2014; Austin et al. 2016; Jagmag et al. 2016; Schwamborn 2018).

1.1.1 Models of Parkinson's disease

As primary brain cells from PD patients are not accessible, disease modelling tools are required, in order to understand the molecular mechanisms underlying and driving the pathogenesis of PD. In the last years, these tools typically were animal models or two–dimensional (2D) cell cultures (Sterneckert et al. 2014). The advantage of animal models is the possibility of disease examination *in vivo* and it allows to study the disease progression as well as to analyse treatment options (Jagmag et al. 2016). Even though, animal models largely contributed to our actual knowledge of PD, these models cannot entirely phenocopy this human disease. And apart from ethical concerns, the isolation of primary animal cells is not suited for applications like high–throughput screenings (HTSs) (Sterneckert et al. 2014; Jagmag et al. 2016). With the establishment of the human induced pluripotent stem cell (hiPSC) technology and thereby the ability to generate all cell types of the human body that were previously unobtainable in large quantities, the methodology in the field of stem cell research advanced tremendously (Takahashi et al. 2007; Byers et al. 2012). Patient–specific as well as genome edited hiPSCs are able to express disease–causing genes of interest, thus enabled a substantial progress in *in vitro* disease modelling (Sterneckert et al. 2014).
Usually, the experimental models can be categorised as toxin or genetic models. For instance, there are several neurotoxins known, that allow modelling of the nigrostrial mDAN degeneration (Jagmag et al. 2016). One established component of the neurotoxins is 6–hydroxydopamine (6–OHDA), a structural analogue of the catecholamines DA and noradrenaline (Ungerstedt 1968; Sachs et al. 1975; Emborg 2007). 6–OHDA is able to cross the dopamine transporter (DAT), which leads to a toxin accumulation in the cell. This promotes the formation of hydrogen peroxide (H_2O_2) and other reactive oxygen species (ROS) by auto–oxidation and is followed by neuronal damage (Jagmag et al. 2016). The neurotoxin precursor 1–methyl–4–phenyl–1,2,3,6–tetrahydropyridine (MPTP) can be oxidased by glial cells via monoamine oxidase B (MAO–B) to 1–methyl–4–phenylpyridinium (MPP+), which causes damage to the nigrostriatal DA pathway. MPP+ has a high affinity for the DAT and leads to a significant mDAN damage in the striatum and SNc by inhibiting the mitochondrial complex I (Jackson-Lewis et al. 2007; Emborg 2007; Jagmag et al. 2016). Rotenone, known as an insecticide and pesticide, blocks the electron transport chain via the same pathway and additionally inhibits cell proliferation (Jagmag et al. 2016). Even though, the application of rotenone in rats

can reproduce almost all the features of PD, including α–synuclein aggregation and the formation of LBs as well as the slow and specific loss of mDANs, the high mortality rate makes the experimental reproducibility difficult (Fleming et al. 2004; Tanner et al. 2011; Blesa, Trigo-Damas et al. 2016; Jagmag et al. 2016). Paraquat, a broadly used herbicide, was suggested to have parkinsonian toxic effects due to its similar structure to MPP+. And indeed, it has been shown to cause mDAN degeneration and, like rotenone, also induces LB formation in rodent mDANs (McCormack et al. 2002; Berry et al. 2011; Tanner et al. 2011; Blesa, Trigo-Damas et al. 2016). Nevertheless, it is still elusive how the cell damage, caused by the generation of ROS, is linked to paraquat and there are even contradictory findings, stating that paraquat does not cause changes in the nigrostriatal DA system (Miller 2007; Jagmag et al. 2016; Blesa, Trigo-Damas et al. 2016). Another neurotoxic candidate is methamphetamine, which promotes an increased stimulation–independent DA release (Sulzer 2011). While interacting with DAT and vesicular monoamine transporter 2 (VMAT2), it causes changes in the DA distribution from synaptic vesicles to the cytosol (Howard et al. 2011). DA oxidation within the cytosol leads to oxidative stress and ROS generation, which can cause neuronal death (Jagmag et al. 2016). Although methamphetamine abuse and PD have distinct symptomatic profiles, it has been shown that methamphetamine users have an increased risk to develop PD (Sulzer 2011; Granado et al. 2013).

In addition to the toxin models, PD–specific disease modelling is conducted with genetic models that reproduce the most known mutations observed in familial PD. This approach aims to elucidate pathways associated with the investigated gene and to evaluate potential therapeutics (Blesa, Trigo-Damas et al. 2016; Jagmag et al. 2016). As stated above, mutations in α–synuclein (SNCA), like encoding the substitutions A30P, A53T, and E46K, have been identified to predispose to an autosomal–dominant form of PD (Polymeropoulos et al. 1997; Krüger et al. 1998; Zarranz et al. 2004). These missense mutations enhance SNCA aggregation and fibril formation (Schapira and Gegg 2011; Schapira and Jenner 2011; Stefanis 2012; Proukakis et al. 2013; Jagmag et al. 2016). It has been further shown, that also the duplication or triplication of *SNCA* is sufficient to cause PD by a dose–dependent SNCA aggregation (Singleton et al. 2003; Jagmag et al. 2016; Blesa, Trigo-Damas et al. 2016). Despite of the development of numerous animal models exhibiting a mutated form of *SNCA* to replicate SNCA–dependent neurodegeneration and SNCA propagation, no significant mDAN degeneration has been found in most of these genetic models (Blesa, Trigo-Damas et al. 2016). There are suggestions that SNCA

plays a role as a presynaptic regulator of DA release, synthesis or storage, but its exact function is still unknown (Maries et al. 2003; Venda et al. 2010; Dettmer et al. 2016; Jagmag et al. 2016). Also mutations in *leucine–rich repeat kinase 2 (LRRK2)* are known to predispose to an autosomal–dominant type of PD, like the most frequent mutations G2019S and R1441C (Blesa, Trigo-Damas et al. 2016). Genetic models like LRRK2 knockout mice exhibit abnormal SNCA or ubiquitin accumulation, however they do not display a functional disruption of the basal ganglia (Li, Tan et al. 2007; Li, Liu et al. 2009; Tong et al. 2010; Ramonet et al. 2011; Hinkle et al. 2012; Tsika et al. 2014). Also the overexpression of *LRRK2*–G2019S or *LRRK2*–R1441C in both, mice and rats, cannot recapitulate the loss of mDANs in the SNc or alterations in the locomotor activity (Ramonet et al. 2011; Shaikh et al. 2015; Blesa, Trigo-Damas et al. 2016).

Genetic and toxin models are important for the disease modelling of PD, however, these models bear limitations. The pathological and behavioural phenotypes are often quite different from the actual human condition and cannot truly recapitulate hallmarks of the disease, like a significant loss of mDANs (Chesselet et al. 2008; Potashkin et al. 2011; Blesa, Trigo-Damas et al. 2016). This might partly explain why many promising drug candidates, examined via these disease models, are not effective in patients when they are tested in clinical trials (Sterneckert et al. 2014; Abe-Fukasawa et al. 2018). This highlights the need for more advanced models that can recapitulate the human physiology to enable exploring complex biological processes.

1.2 Brain organoids

The development of the organoid methodology counts today as a major technological breakthrough in stem cell research. It allowed an immense advancement in the application of hiPSCs and was even celebrated as the 'Method of the Year' in 2017 ('Method of the Year 2017: Organoids' 2018, see Figure 1.1).

1.2.1 Derivation of neuroepithelial 3D cultures

Initial experiments on self-organisation of PSCs under 3D conditions have been performed already more than ten years ago. Mototsugu Eiraku and co–workers

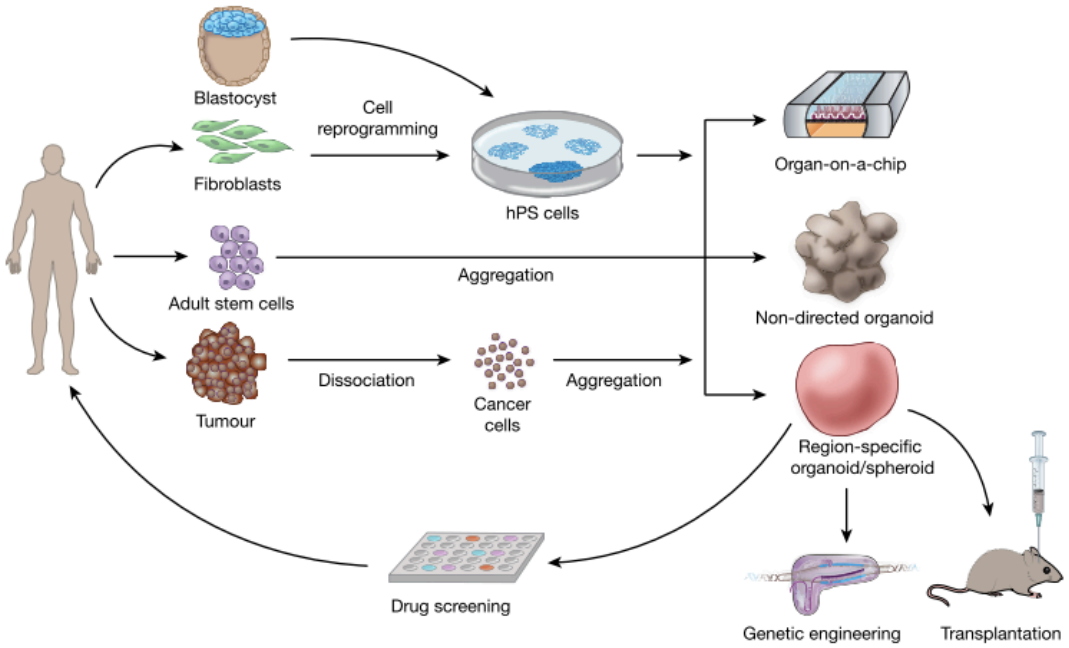

FIGURE 1.1: **Different approaches for deriving human 3D cultures.** Potential cellular sources for organoid derivation are hpluripotent stem cells (PSCs) derived from a blastocyst or by reprogramming of fibroblast, adult stem cells or primary tissue–derived cancer cells. The can be applied for microfluidics–based organ–on–a–chip (top), undirected organoids (middle), and region–specific organoid (bottom) derivation. These 3D cultures can be used for drug screening, manipulated with CRISPR–Cas9 genome–editing technologies or transplanted into animals (from Pasca 2018).

described the generation of a serum–free floating culture of embryoid body–like aggregates with quick re–aggregation (SFEBq) and its utilisation for a reproducible formation of apico–basally polarised cortical neuroepithelia (Eiraku, Watanabe et al. 2008). With this first PSC–based model, early aspects of corticogenesis were recapitulated *in vitro* by manipulating embryologically relevant patterning signals. Five years later, the same group published an optimised SFEBq–based protocol for an up to 13 weeks long–term culture of cortical neuroepithelia (Kadoshima et al. 2013). They were able to recapitulate the continuous self–development of the cortex, including a cortical curvature and a self–forming dorsocaudal–ventrorostral axis. This work highlights the necessity of intrinsic cues for the development of neocortex–specific complexity *in vitro*. Furthermore, SFEBq were also the basis for further advancement in 3D cell culture approaches, leading to the derivation of several other brain regions (e.g. adenohypophysis (Suga et al. 2011), retina (Eiraku,

Takata et al. 2011), cerebellum (Muguruma et al. 2015), hippocampus (Sakaguchi et al. 2015) and forebrain (Mariani et al. 2015)).

1.2.2 Cerebral organoids

Yet, it were the findings of Madeleine Lancaster and co–workers that actually launched a new era in the research on human brain by introducing the 'cerebral organoids', (Latin: *of* or *relating to the brain*) (Lancaster, Renner et al. 2013, Kelava et al. 2016b). Supporting Kadoshima's conclusions, Lancaster et al. took advantage of the PSCs' nature of intrinsic self–organisation and derived neuroepithelium under 3D conditions. To avoid limitations on specific brain region identities, they pass on adding patterning growth factors. Instead, after aggregation, the cells were embedded in Matrigel, a surrogate matrix that has been introduced already before, in the generation of intestinal organoids (Sato et al. 2009). It serves as a structural support, induces the correct polarity signal to promote the complex outgrowth of large, apicobasally polarised neuroepithelial buds (Lancaster and Knoblich 2014b, Lancaster and Knoblich 2014a, Wang, Allen et al. 2018). These buds expand during the course of culture and acquire not only various brain identities but also fluid–filled lumens reminiscent of brain ventricles. To improve nutrient supply and oxygen exchange, the floating cerebral organoids were cultured in spinning bioreactors or on orbital shaker plates, this allowed an organoid to size up to 4 mm in diameter (Lancaster and Knoblich 2014a, Kelava et al. 2016b). These optimised growth conditions and the intrinsic self–organising capacities of PSCs resulted in the formation of a variety of brain regions within a single organoid, including hindbrain, midbrain, forebrain, and even retinal tissue identities (Lancaster, Renner et al. 2013, Lancaster and Knoblich 2014b, Renner et al. 2017, Wang, Allen et al. 2018). Remarkably, a detailed study about the patterning events during the course of cerebral organoid development and differentiation indicates that spatial and temporal patterning events are reminiscent of that determining the human brain development (Renner et al. 2017).

1.2.3 Modification of cerebral organoids

The classic cerebral organoid protocol, describing the generation of rather whole–brain organoids, has been modified by many research groups in the last years

and has resulted in the formation of more regionally restricted 3D cell cultures (Lancaster and Knoblich 2014a, Kelava et al. 2016b). In the study of Anca Paşca and co–workers, both bone morphogenic protein (BMP) and transforming growth factor β (TGF–β) signalling pathways, were inhibited by the small molecules Dorsomorphin (DM) and SB–431542 (SB), to archive an effective neural induction (Paşca et al. 2015). This dual–SMAD inhibition, in combination with fibroblast growth factor (FGF)2, epidermal growth factor (EGF) and the absence of extracellular scaffolding, gave rise to neural progenitors, expressing the dorsal telencephalic markers paired box protein 6 (PAX6) and forkhead box protein G1 (FOXG1). Further neuronal differentiation was promoted by replacing FGF2 and EGF with brain–derived neurotrophic factor (BDNF) and neurotrophic factor 3 (NT3) and led to the generation of various neural and glial identities of the dorsal cortex within each spheroid, including superficial and deep cortical layer neurons (Paşca et al. 2015, Kelava et al. 2016b). With this, Paşca et al. described a method that gave rise to a 3D culture specific of a brain subregion, thereof a culture that exhibited a reduced amount of ectodermal derivatives, compared to the original cerebral organoid protocol.

A similar approach of using a dual–SMAD inhibition was published by Qian et al. in 2016. While maintaining the basis of the Lancaster protocol, like Matrigel embedding and agitation, they have shown that it is possible to culture organoids in 3D–printed miniaturised bioreactors, thus enable more feasible, scaled–up productions of neural 3D cultures (Qian et al. 2016). Another advantage of the self–engineered multi–well spinning device is the possibility of comparing numerous different culture conditions in parallel. Like Paşca and co–workers, they aimed to reduce the tissue heterogeneity of the cerebral organoids and therefore pre–patterned the embryoid bodies (EBs) to obtain specific brain regions. The inhibition of TGF–β signalling by SB and activation of Wnt signalling by glycogen synthase kinase 3β (GSK–3β) inhibitor CHIR–99021 (CHIR) within the first two weeks of culture, resulted in forebrain organoids organised in defined, multi–layered progenitor zones, including homologues to the ventricular zone (VZ), the inner and outer subventricular zone (SVZ). Moreover, neuronal types of all six cortical layers could be detected within these forebrain–specific organoids. With the help of their mini–bioreactors, Qian and co–workers also developed a method to derive hypothalamic–specific organoids. After a dual–SMAD inhibition with SB and LDN–193189 (LDN), they patterned the neuroectodermal cells to a hypothalamic fate, by activating Wnt and sonic hedgehog (SHH) signalling, applying WNT3a, SHH and

Purmorphamine (PMA) to the culture. After 40 days, these organoids contained cell populations expressing markers specific of hypothalamic neuronal lineages (Qian et al. 2016).

1.2.4 Midbrain–specific organoids

Besides developing a modified protocol for forebrain– and hypothalamus–specific organoids, Qian et al. also explored a method to derive organoids with a midbrain identity. Inspired by 2D experiments performed by Kriks et al. and also initial midbrain–like tissue experiments reported by Tieng and co–workers, they induced the floor plate differentiation by activating SMAD inhibition, Wnt and SHH signalling and adding FGF8 to the developing 3D culture (Kriks et al. 2011; Tieng et al. 2014). After 18 days, cells expressed the neural progenitor marker NESTIN and the midbrain floor plate marker forkhead box protein A2 (FOXA2), dopaminergic neuron (DAN) marker tyrosine hydroxylase (TH) however, could only be observed from day 38 on. After keeping the organoids for additional weeks in culture, a sound nuclear receptor related 1 protein (NURR1) and paired–like homeodomain 3 (PITX3)/TH co–expression was observed (Qian et al. 2016).
In the same year, another protocol describing the generation of midbrain–specific organoids was published (Jo et al. 2016). Jo and co–workers based their derivation on the findings of Chambers et al. and used Noggin and SB for a dual–SMAD inhibition (Chambers et al. 2009, see also Table 8.1 on page 87). The originating neural organoids expressed midbrain–specific markers like FOXA2, orthodenticle homologue 2 (OTX2), and LIM homeobox transcription factor 1α (LMX1A) after seven days and a subsequent differentiation of these floor plate precursors into TH+ mDANs was achieved during the development of the hMOs (Jo et al. 2016). Interestingly, after 60 days of culture, TH+ neurons were co–expressing G–protein–regulated inward–rectifier potassium channel 2 (GIRK2), which is enriched in the A9 subtypes of mDANs, forming the SNc in the human brain. This cluster of cells is particularly vulnerable to cell death and progressively degenerates during the course of PD (Xi et al. 2012; Hegarty et al. 2013). Gene expression profiles were generated for the hMOs to further investigate overlapping characteristics with 2D–cultured mDANs and human prenatal midbrain samples. A cluster analysis comparing the differentially expressed genes between the three groups indicated that hMOs share features of gene expression profiles of the prenatal midbrain, which cannot be recapitulated via the conventional 2D derivation method for mDANs

(Jo et al. 2016). Proving that the specific cellular structure and heterogeneity of the midbrain–specific organoid cultures allow us to model biological aspects, which cannot be mimicked with current 2D stem cell cultures. Furthermore, the reproducibility and especially the usability for disease modelling of this organoid protocol has been proven true by another research group, publishing their findings in the beginning of this year (Kim et al. 2019).

1.3 Disease modelling with brain organoids

Similar characteristics on molecular, cellular and also physiological basis between human brain organoids and the actual human brain justify the increasing application of brain organoids in studying brain biology and modelling neurological disorders (Wang, Zhu et al. 2018, see Figure 1.2). Already Lancaster and co–workers dis-

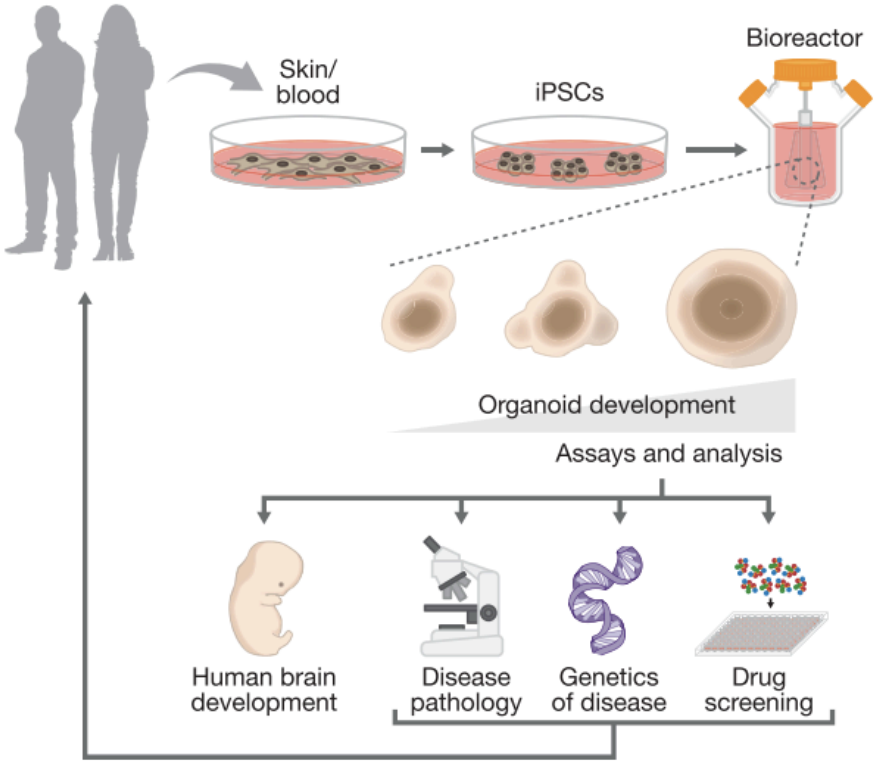

Figure 1.2: **Application for human brain organoids.** Brain organoids derived from human PSCs can be applied for human brain development research. To improve the understanding of human disease and the impact of genetic variation, they can serve as a cellular platform for chemical screens (from Arlotta 2018).

covered the potential of cerebral organoids for being used as a model to detect an

impaired neurodevelopment and they derived organoids carrying a mutation that causes microcephaly (Lancaster, Renner et al. 2013). It was suggested that also a Zika virus (ZIKV) infection was causing microcephaly in neonates. In 2016, the World Health Organization (WHO) declared the ZIKV and its associated complications an emergency of public health (Qian et al. 2016; Dutta et al. 2017). This activation of the global research community led to an accelerated development of vaccines and treatments, with many studies based on cerebral organoids, which were able to recapitulate features of human cortical development *in vitro* (Wells et al. 2016; Garcez et al. 2016; Cugola et al. 2016; Qian et al. 2016; Dang et al. 2016; Nowakowski et al. 2016; Miner et al. 2016; Xu, Yang et al. 2016). The results of these studies indicate that a ZIKV infection affects the neurogenesis, disrupts the cortical layers of the organoids, and like this causing microcephalic–like deficits in the cortical development (Dutta et al. 2017). Due to the specific embryonic formation of human brains, only a human–specific 3D cell culture model exhibiting advanced organisational features could have led to the reported discoveries. Neither murine nor 2D cell culture were able to address the potential link between ZIKV and microcephaly (Qian et al. 2016; Dutta et al. 2017; Setia et al. 2019).

Despite this successful application, brain organoids have not only been proven useful to study neurodevelopmental disorders. Recently, so–called tumouroids have been established from human glioblastoma, the most common and aggressive brain cancer (Dutta et al. 2017). The hypoxic gradients and stem cell heterogeneity found in these tumouroids cannot be resembled via conventional culture methods. Therefore, glioblastoma organoids offer a unique opportunity for their application in brain cancer diagnostics and therapeutics (Hubert et al. 2016; Dutta et al. 2017; Bian et al. 2018).

Furthermore, two different approaches using 3D human neural cell culture system were reported to recapitulate Alzheimer's disease (AD) phenotypes *in vitro* (Choi, Kim, Hebisch et al. 2014; Raja et al. 2016). These 3D cultures provide an environment that promotes the formation of amyloid–β (Aβ) plaques and neurofibrillary tangles (NFTs), pathological events that could not have been serially linked before by using 2D cultured human neurons (Choi, Kim, Hebisch et al. 2014; D'Avanzo et al. 2015; Choi, Kim, Quinti et al. 2016; Raja et al. 2016). This confirms that the evolving brain organoid methodology facilitates the development of more precise human cellular models that can support the research of neurodegenerative disorders.

CHAPTER 2

Aim of the thesis

The technology of more complex 3D cell culture systems not only bridges the gap between traditional 2D *in vitro* experiments and *in vivo* animal models, but also addresses processes that cannot be recapitulated by these traditional models. Therefore, it offers an opportunity to unravel complex biological processes, like the development of the human brain, where conventional models have not proven successful. The establishment of stem cell–derived brain organoids allowed for the resembling of key aspects of the human brain development *in vitro*, by utilising the enormous differentiation potential of PSCs and their ability to self–organise with a specific spatial orientation. With that, this novel technology provides a physiologically relevant context, like interactions between glia cells and neurons in a spatially organised microenvironment, which holds great potential for its application in modelling neurological diseases.

The aim of this thesis was the generation and characterisation of a novel midbrain–specific 3D cell culture system, thereby providing an advanced *in vitro* model to study neurodevelopmental processes and also neurodegenerative diseases of the human midbrain.
In order to achieve the formation of these highly specialised structures, resembling specifically the human midbrain, we derived an organoid system from regionally

patterned neural stem cells. The particular starting population, already committed to the ventral neural tube fate of the mesencephalon, and further application of spatio–temporal specific signalling under 3D culture conditions, led to the establishment of two novel human midbrain–specific organoid (hMO) methods. We aimed to assess the differentiation efficiency into true midbrain dopaminergic neurons and to evaluate their cellular environment within the hMOs. A detailed *in vitro* characterisation of diverse developing cell populations and their functional properties, enabled us to evaluate the identity and potential of hMOs.

As we intended to generate a midbrain-specific model that also holds great potential for its application in modelling neurological diseases, we additionally addressed whether hMOs are suitable to reveal Parkinson's disease (PD)–relevant phenotypes. By deriving hMOs from PD patients carrying the *LRRK2*–G2019S mutation and comparing them to healthy control hMOs, we focused on the investigation of PD–relevant pathomechanisms. With that we aimed to evaluate our newly derived hMO methods that constitute as a powerful tool for human–specific *in vitro* disease modelling of neurological disorders.

CHAPTER 3

Material and Methods

All comprehensive information concerning the material and methods that were used in this thesis can be found in the original articles listed in Chapter 4. In the following section, the experimental procedures which I conducted by myself will be briefly listed and linked to the respective chapter.

Methods

- **hiPSC culture**
  - see Chapter 5 (Monzel et al. 2017)
  - see Chapter 6 (Smits, Magni et al. 2019)
  - see Chapter 7 (Smits, Reinhardt et al. 2019)
- **Derivation of mfNPCs**
  - see Chapter 6 (Smits, Magni et al. 2019)
  - see Chapter 7 (Smits, Reinhardt et al. 2019)
- **Expansion of mfNPCs**
  - see Chapter 6 (Smits, Magni et al. 2019)
  - see Chapter 7 (Smits, Reinhardt et al. 2019)

- **Differentiation of mfNPCs**
  - see Chapter 6 (Smits, Magni et al. 2019)
  - see Chapter 7 (Smits, Reinhardt et al. 2019)
- **Derivation of smNPC**
  - see Chapter 5 (Monzel et al. 2017)
- **Generation of hMOs**
  - see Chapter 7 (Smits, Reinhardt et al. 2019)
- **Immunofluorescence staining**
  - see Chapter 5 (Monzel et al. 2017)
  - see Chapter 6 (Smits, Magni et al. 2019)
  - see Chapter 7 (Smits, Reinhardt et al. 2019)
- **Image analysis**
  - see Chapter 6 (Smits, Magni et al. 2019)
  - see Chapter 7 (Smits, Reinhardt et al. 2019)
- **Quantitative RT–PCR (qRT–PCR)**
  - see Chapter 7 (Smits, Reinhardt et al. 2019)
- **Dopamine ELISA**
  - see Chapter 7 (Smits, Reinhardt et al. 2019)
- **Microelectrode array (MEA)**
  - see Chapter 5 (Monzel et al. 2017)
  - see Chapter 6 (Smits, Magni et al. 2019)

CHAPTER 4

Results

CHAPTER 5

Original article: Derivation of Human Midbrain–Specific Organoids from Neuroepithelial Stem Cells

This article has been published in the *Stem Cell Reports* journal.

5.1 Preface

With the establishment of the hiPSC technology and thereby the ability to generate all cell types of the human body, the methodology in the field of stem cell research advanced tremendously (Takahashi et al. 2007). Patient–specific as well as genome edited hiPSCs enabled a substantial progress in *in vitro* disease modelling over the last decade. However, the traditional, 2D cell culture approaches bear limitations, especially when it comes to recapitulating the complexity of the human brain. These circumstances motivated the establishment of more complex 3D *in vitro* cell culture models. Protocols for the so–called brain–like organoids affirm the enormous differentiation potential of hiPSCs and their ability to self–organise with a specific spatial orientation (Lancaster, Renner et al. 2013; Muguruma et al. 2015; Jo et al. 2016; Qian et al. 2016). To obtain these highly specialised structures, resembling specifically the human midbrain, we derived an hMO system from regionally patterned human neuroepithelial stem cells (hNESCs). The resulting neural tissue exhibited abundant neurons with mDAN identity, as well as astroglia and oligodendrocyte differentiation. Within the hMOs, we could observe neurite myelination with structures as nodes of Ranvier and the formation of synaptic connections. These indications for electrophysiological activity were confirmed by calcium imaging and MEA recordings, determining regular fire patterning and neural network synchronicity. With this advanced 3D *in vitro* cell culture system, we provided a method to model diseases that strongly affect the human midbrain, for instance PD. hMO might be able to reveal disease underlying mechanisms and therefore have great potential to be utilised in advanced disease modelling and therapy development.

In this study, I was taking part in developing the hMO derivation protocol. I supported the other co–authors in designing and compiling experiments for the characterisation of hMOs. I cultured and analysed hNESCs as a starting population for hMOs (Supplementary Figure S1A). To evaluate the electrophysiological activity of hMOs, I elaborated the experimental design for MEA recordings and analysed the collected data. The results are shown in Figure 4C–G and the method is described in Supplemental Experimental Procedures. Lastly, I contributed in writing and editing the manuscript.

Stem Cell Reports
Report
ISSCR
OPEN ACCESS

Derivation of Human Midbrain-Specific Organoids from Neuroepithelial Stem Cells

Anna S. Monzel,[1,4] Lisa M. Smits,[1,4] Kathrin Hemmer,[1,4] Siham Hachi,[2] Edinson Lucumi Moreno,[2] Thea van Wuellen,[1] Javier Jarazo,[1] Jonas Walter,[1] Inga Brüggemann,[1] Ibrahim Boussaad,[3] Emanuel Berger,[1] Ronan M.T. Fleming,[2] Silvia Bolognin,[1] and Jens C. Schwamborn[1,*]

[1]Developmental and Cellular Biology, Luxembourg Centre for Systems Biomedicine (LCSB), University of Luxembourg, 7, avenue des Hauts-Fourneaux, 4362 Esch-sur-Alzette, Luxembourg
[2]Systems Biochemistry
[3]Clinical & Experimental Neuroscience
Luxembourg Centre for Systems Biomedicine (LCSB), University of Luxembourg, 4362 Esch-sur-Alzette, Luxembourg
[4]Co-first author
*Correspondence: jens.schwamborn@uni.lu
http://dx.doi.org/10.1016/j.stemcr.2017.03.010

SUMMARY

Research on human brain development and neurological diseases is limited by the lack of advanced experimental in vitro models that truly recapitulate the complexity of the human brain. Here, we describe a robust human brain organoid system that is highly specific to the midbrain derived from regionally patterned neuroepithelial stem cells. These human midbrain organoids contain spatially organized groups of dopaminergic neurons, which make them an attractive model for the study of Parkinson's disease. Midbrain organoids are characterized in detail for neuronal, astroglial, and oligodendrocyte differentiation. Furthermore, we show the presence of synaptic connections and electrophysiological activity. The complexity of this model is further highlighted by the myelination of neurites. The present midbrain organoid system has the potential to be used for advanced in vitro disease modeling and therapy development.

INTRODUCTION

With the development of methods to generate induced pluripotent stem cells (iPSCs) from somatic cells (Takahashi and Yamanaka, 2006; Yu et al., 2007), human cells with the potential to generate all body cell types in vitro became available. This advance led to tremendous progress in the development of protocols for the differentiation of iPSCs into various human cell types. In addition, disease-specific human iPSCs and their derived cell types are now widely used for in vitro disease modeling. However, particularly with regard to neuronal diseases, it is of importance to consider that the human brain is an extremely complex, three-dimensional (3D) structure. Consequently, the investigation of its development and modeling of disease processes in traditional, two-dimensional cultures has strong limitations. It has been demonstrated that the presence of a 3D matrix promotes many biologically relevant functions, such as differentiation capability (Baharvand et al., 2006; Greiner et al., 2013; Tanaka et al., 2004; Tian et al., 2008), cellular signaling, and lineage specification (Engler et al., 2006; Greiner et al., 2013; McBeath et al., 2004). In addition, 3D culture systems are more physiological concerning cell-cell and cell-matrix interactions (Lee et al., 2007). These observations have, in recent years, prompted the use of human iPSCs for the generation of 3D in vitro models of complete organs, the so-called organoids.

These organoid technologies have been pioneered for the small intestine (Sato et al., 2009) and later extended also to other organs or parts of organs (Nakano et al., 2012). Recently, protocols for the generation of human brain-like organoids have been developed, including protocols for cerebral (Lancaster et al., 2013), cerebellar (Muguruma et al., 2015), midbrain-like (Jo et al., 2016), and forebrain organoids (Qian et al., 2016). These organoids provide a proof of concept that human iPSCs can indeed differentiate into various cell types and even self-organize with a specific spatial orientation, which recapitulates key features of the human brain. These brain organoids have been used successfully to model a genetic form of microcephaly (Lancaster et al., 2013) as well as Zika virus-induced microcephaly (Qian et al., 2016). Importantly, thus far all brain organoids have been generated directly from iPSCs; however, evidence suggesting that these organoids could also be derived from more fate-restricted neural stem cells is lacking. The utilization of neural stem cells as the starting population has the advantage that already patterned cells might differentiate into the desired structures more efficiently (cheaper, faster cell doublings, ease of handling, and so forth). Furthermore, while the generation of certain brain structures, such as the cerebral cortex or cerebellum, is meanwhile well described, a higher degree of prepatterning seems to be required for the generation of other highly specialized structures. This is particularly true for brain regions severely affected by neurodegenerative disorders, such as Alzheimer's disease (hippocampus) or Parkinson's disease (PD; substantia nigra).

To address these challenges, we used our previously described human neuroepithelial stem cell (NESC) culture system (Reinhardt et al., 2013) and differentiated these NESCs under dynamic conditions into human midbrain-specific organoids.

RESULTS

Generation of Human Midbrain-Specific Organoids

Previously described NESCs (Reinhardt et al., 2013) were used as the starting population for the generation of human midbrain organoids (hMOs). Compared with iPSCs as a starting population, NESCs are already patterned toward midbrain/hindbrain identity. Therefore, an efficient differentiation into hMOs was expected.

Typically, NESCs express the neural progenitor markers SOX1, SOX2, PAX6, and Nestin prior to organoid generation (Figure S1A). Cells were seeded on round-bottomed ultra-low-adhesion 96-well plates, enabling the cells to form 3D colonies. They were cultured in the presence of the GSK3b inhibitor CHIR99021 to stimulate the canonical WNT signaling pathway, and the SHH pathway was activated using purmorphamine (PMA). The 3D NESC colonies were embedded into droplets of Matrigel for structural support, and 2 days later differentiation into hMOs was initiated. We kept the organoids on an orbital shaker rotating at 80 rpm (Figure 1A). All experiments were conducted with four different and independent NESC lines, individually derived from four different and independent human iPSC lines (Table S1).

During the first 12 days of culture, the hMOs rapidly increased in size and reached a mean core size of 1.26 mm (±0.06 mm, n = 4) in diameter after 20 days (Figure 1B). Consistent with the finding that organoids increased in size after starting the differentiation, we observed expression of the cell proliferation marker Ki67 at day 27 (referred to as early-stage hMOs), which significantly decreased upon maturation until day 61 (late-stage hMOs) from 2.32% (±0.7%, n = 4) to 0.13% (±0.08%, n = 4) (Figures 1C, 1E, and 1G). Furthermore, young hMOs expressed the neural progenitor marker SOX2, which also significantly decreased during maturation from 35% (±3%, n = 4, day 27) to 18.4% (±1.7%, n = 4, day 61). Interestingly, the localization of SOX2-positive cells became more regionally restricted by day 61, resembling the formation of a stem cell niche (Figures 1D, 1F, and 1G). Although consistent with previous findings (Lancaster and Knoblich, 2014; Lancaster et al., 2013), we found substantial cell death in the core of the hMOs, which resulted from the lack of nutrient support in the center of the organoid. In general we did not observe high levels of apoptotic cell death, revealed by staining of the marker cleaved caspase-3. The basic level of apoptosis that was detectable did not change during the course of differentiation (Figure S1B). Importantly, we were able to reproduce the generation of hMOs from NESCs, which were previously derived from four independent iPSC lines.

Neuronal Differentiation and Self-Organization of NESC-Derived hMOs

After showing a decrease of proliferation and stem cell identity, we assessed neuronal differentiation. Because we are particularly interested in the future utilization of hMOs for in vitro modeling of PD, we also investigated the differentiation of midbrain dopaminergic neurons (mDNs). We were able to see robust differentiation into TUJ1-positive neurons and tyrosine hydroxylase (TH) positive mDNs. These stainings revealed the formation of a complex neuronal network (Figures 2A, 2B, S2A, and S2B).

We further examined whether the organoids undergo differentiation into mDNs with midbrain identity. We observed a large population of TH-, LMX1A-, and FOXA2-positive neurons in late-stage hMOs (Figure 2C). Flow-cytometry analysis of late-stage hMOs revealed that 64% (±2.4%, n = 4) of the cells were triple-positive for TH, LMX1A, and FOXA2 (Figure 2D). To further confirm the regional identity of the hMOs, we stained for the orphan nuclear receptor NURR1, which is widely expressed in mDNs. NURR1 expression was observed in early- and late-stage hMOs. We identified cells that co-expressed NURR1 with the midbrain-specific transcription factor OTX2 (Figure 2E) and the mDN marker TH (Figure S2C). We further found cells that co-expressed NURR1 with the ventral marker NKX6-1 (Figures 2F and S2D). We next examined the expression of PITX3, an important transcription factor for the differentiation and maintenance of mDN during development. We found cells co-expressing PITX3 with TH in the late-stage hMOs (Figure S2E) as well as a small population of cells co-expressing PITX3 with NKX6-1 (Figure S2F). Taken together, these results indicate a differentiation toward ventral midbrain identity in the hMOs described here.

To further address the identity of mDNs in these organoids, we stained for the dopamine transporter (DAT), which is a defining marker for mDNs. In late-stage hMOs we identified cells co-expressing TH and DAT (Figure 1G), as well as cells positive for FOXA2/DAT (Figure S2G) and TH/dopamine decarboxylase (DDC) (Figure S2H). qRT-PCR further confirmed the upregulation of the three mDN differentiation markers *TH*, *DAT*, and *DDC* in late-stage hMOs (Figure 2H). Previously, expression of PAX6 in the midbrain but not in mDNs has been shown (Duan et al., 2013; Schwarz et al., 1999). To further confirm the identity of the mDNs, we stained for PAX6 and TH. We could not identify TH-positive mDNs co-expressing PAX6, further

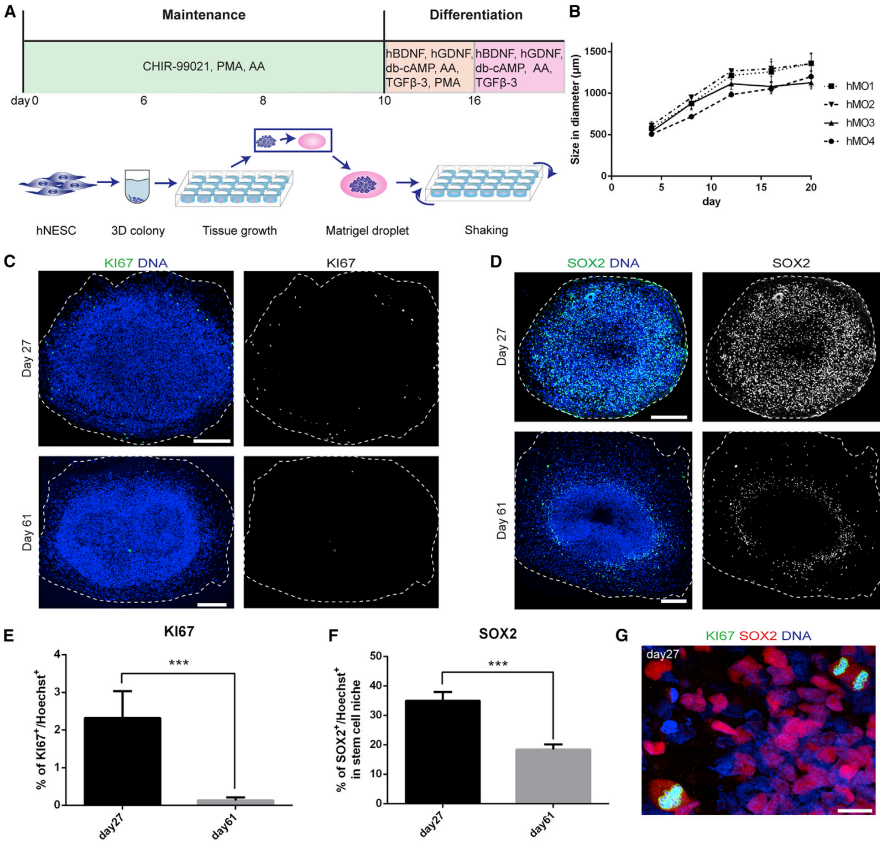

Figure 1. Derivation of hMOs from Human NESCs

(A) Procedure of hMO culture system. Details are described Supplemental Experimental Procedures. hNESC, human neuroepithelial stem cell; AA, ascorbic acid, PMA, purmorphamine.

(B) Growth of hMOs from day 4 to day 20. The diameter size of six organoids (two independent cultures) per organoid line was measured on days 4, 8, 12, 16, and 20 of the organoid culture and the mean was calculated. Error bars represent mean ± SEM.

(C) IF staining of the cell proliferation marker Ki67 at day 27 and day 61 of the organoid culture.

(D) IF staining at day 27 and day 61 of the neural stem cell marker SOX2.

(E) Quantification of the percentage of $Ki67^+$ cells at day 27 and day 61 by cell counting. $Ki67^+$ cells were normalized to $Hoechst^+$ cells. A total of 3,549 $Hoechst^+$ cells (day 27) and 3,309 $Hoechst^+$ cells (day 61) of eight independent organoid cultures derived from four independent lines was counted. Error bars represent mean + SEM (n = 4); ***p < 0.0001.

(F) Quantification of the percentage of $SOX2^+$ cells at day 27 and day 61 by cell counting. $SOX2^+$ cells were normalized to $Hoechst^+$ cells. A total of 3,549 $Hoechst^+$ cells (day 27) and 3,309 $Hoechst^+$ cells (day 61) of eight independent organoid cultures derived from four independent lines was counted. Error bars represent mean + SEM (n = 4); ***p < 0.0001.

(G) Representative image of $Ki67^+/SOX2^+$ proliferative neural progenitor cells at day 27.

Dashed lines indicate the perimeter of the organoid.

Scale bars, 200 µm (C and D) and 20 µm (G).

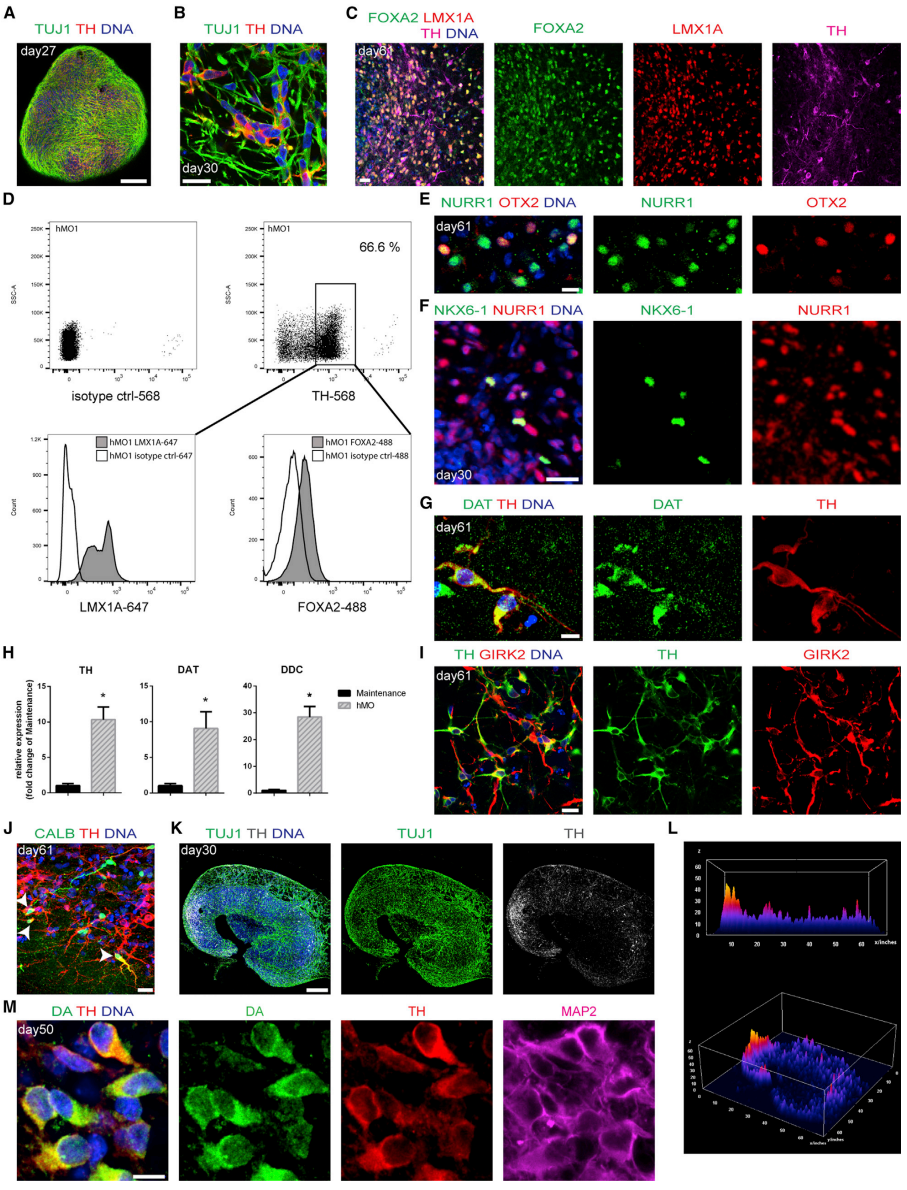

(legend on next page)

supporting that the hMOs contain authentic mDNs (Figure S2I). Intriguingly, we observed robust co-expression of GIRK2 with TH in late-stage hMOs, revealing the presence of the A9 subtype mDNs (Figure 2I), but we also observed cells double-positive for CALBINDIN (CALB) and TH in late-stage hMOs, indicating the presence of A10 subtype mDNs (Figure 2J). These data confirm that our hMOs contain A9 and A10 subtype mDNs.

In previous studies it has been repeatedly shown that stem cells exhibit an enormous potential to self-organize into complex heterogeneous brain organoids (Eiraku and Sasai, 2012; Eiraku et al., 2008; Lancaster et al., 2013; Muguruma et al., 2015). To examine the degree of spatial organization in hMOs, we evaluated the distribution pattern of the mDN markers TUJ1/TH and depicted the results using surface plots. Strikingly, we found that mDNs formed clearly specified clusters within hMOs (Figures 2K and 2L). To further demonstrate the identity of TH-positive neurons as dopaminergic, we analyzed their ability to produce the neurotransmitter dopamine. Immunostaining of mature hMOs demonstrated the presence of dopamine, TH, and MAP2 triple-positive cells (Figure 2M). Intriguingly, we occasionally even observed the formation of Fontana-Masson staining-positive neuromelanin granules in the hMO cultures (Figure S2J).

Altogether these results indicate that mDNs of NESC-derived organoids self-organize into a complex, spatially patterned neuronal tissue.

Glial Differentiation in hMOs

During the development of the fetal human brain, neural tube-derived cells not only differentiate into neurons but also into glia cells, including astrocytes and oligodendrocytes. Therefore, we investigated the presence of these glia cells in the hMOs. In good agreement with brain development, where glia differentiation temporally follows neuronal differentiation, we were unable to detect significant amounts of glia cells in young hMOs (day 27). However, in more mature organoids (day 61), we observed a significant increase of S100B-positive astrocytes (up to 4%) (Figure 3A). We confirmed astrocyte identity by co-staining of S100B with the astrocyte markers Aquaporin (AQP4) and Vimentin (VIM) (Figure 3B). Moreover, we detected a fraction of cells that differentiated into O4-positive oligodendrocytes (Figure S3A). In the CNS, mature oligodendrocytes form myelin sheaths that enwrap axons to accelerate the transmission of action potentials along axons. To analyze whether the oligodendrocytes within the hMOs are able to execute their actual function, i.e., formation of myelin sheets, we performed IF staining against CNPase, a myelin-associated enzyme, together with the neuronal marker TUJ1. A 3D surface reconstruction of these stainings revealed numerous TUJ1-positive neurites that were ensheathed by myelin sheets of CNPase-positive oligodendrocytes (Figures 3C, S3B, and S3C). Interestingly, these neurites often showed gaps of ensheathment, resembling the formation of nodes of Ranvier (Figure 3C) that allow for saltatory fast neuronal transmission. Moreover, CNPase-positive oligodendrocytes that ensheath TUJ1-positive neurites were also positive for the mature oligodendrocyte marker myelin basic protein (MBP) (Figure 3D). Quantification revealed that 29.6% (±2.4%, n = 4) of TUJ1-positive neurites were ensheathed by oligodendrocytes as confirmed by image analysis using MBP and TUJ1 masks.

Functionality of hMOs

One important requirement for neuronal transmission is the development of a mature neuronal network via the formation of synaptic connections. Therefore, synaptic

Figure 2. Neuronal Differentiation and Self-Organization in hMOs

(A) Whole-mount IF staining of an organoid at day 27 for the mDN markers TUJ1 and TH.
(B) IF staining of the mDN markers TUJ1 and TH in a 50-μm section at day 30.
(C) IF staining of the midbrain dopaminergic neuron markers FOXA2, LMX1A, and TH at day 61.
(D) Representative flow-cytometry analysis of cells dissociated from hMO1 at day 61 (six organoids) to quantify TH-, LMX1A-, and FOXA2-positive cells.
(E) IF staining of NURR1 and midbrain marker OTX2 in late-stage hMOs (D61).
(F) IF staining of NKX6-1 and NURR1 in early-stage hMOs (day 30).
(G) IF staining of DAT co-stained with TH in late-stage hMOs (day 61).
(H) qRT-PCR analysis for the mDN markers *TH*, *DAT*, and *DDC*. Data obtained from four independent NESC lines and therefrom derived hMOs. For each hMO culture, five organoids were pooled for RNA isolation. Error bars indicate mean + SEM (n = 4); *p = 0.0286 (TH), *p = 0.0286 (DAT), *p = 0.0571 (DDC).
(I) IF staining of A9 mDN marker GIRK2 co-stained with TH in late-stage hMOs (day 61).
(J) IF staining of A10 mDN marker calbindin and TH in late-stage hMOs (day 61). Arrowheads show cells that are positive for both markers.
(K and L) Asymmetry analysis of mDNs. Immunostaining of mDNs for TUJ1 and TH (K) was analyzed based on fluorescence intensities using a 3D surface plot (L).
(M) IF staining for dopamine (DA), MAP2, and TH at day 50.
Section in (F) is 100 μm and section in (K) is 150 μm. Scale bars, 200 μm (A and K), 20 μm (B, C, F, I, and J), and 10 μm (E, G, and M).

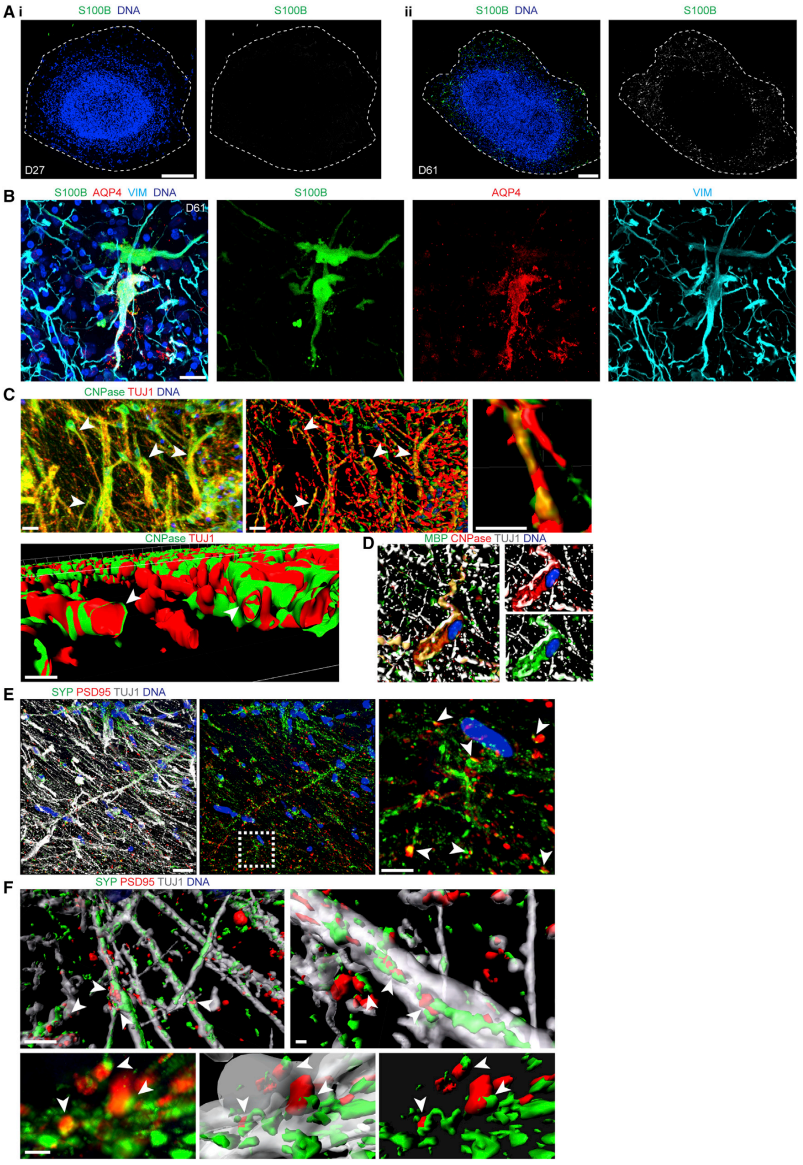

(legend on next page)

connectivity was investigated using IF staining against the presynaptic marker Synaptophysin (SYP) and the postsynaptic marker PSD95 at day 61. To assess the presynaptic and postsynaptic density in hMOs, we quantified the number of presynaptic and postsynaptic counts per μm^2 to an amount of 0.031 (±0.003; n = 4) and 0.016 (±0.004; n = 4), respectively. A subsequent 3D surface reconstruction demonstrated not only the formation of numerous pre- and postsynaptic puncta but also multiple synaptic connections (Figures 3E and S3D). Synaptic connections have been developed between different neurites, indicated by the direct contact of SYP-positive presynapses with PSD95-positive postsynapses (Figure 3F). Accordingly, hMOs fulfill the prerequisite to forward signals via synaptic connections and thus for being electrophysiologically functional.

To further address functionality and neuronal network activity, we performed Fluo-4AM calcium imaging on whole organoids. We measured the spontaneous neuronal activity of six hMOs based on calcium transients evoked by action potentials (Figures 4A, 4B, and S4; Movie S1). Notably, some of the fluorescent traces showed regular firing patterns, which were indicative of tonic electrophysiological activity and resembled the pacemaker activity of mDNs (Hartfield et al., 2014; Moreno et al., 2015). We quantified that 64% (±18%, n = 3) of the cells were actively firing. In addition to calcium imaging, a multielectrode array (MEA) system was used to examine the electrophysiological activity. This methodology allows non-invasive recordings of extracellular field potentials generated by action potentials. At days 82–84, the hMOs were placed on a grid of 16 electrodes in a 48-well tissue culture plate (Figure 4C). Spontaneous activity was detected over several days by individual electrodes in the form of mono- and biphasic spikes (96.13 ± 66.8 spikes/active electrode/measurement [n ≥ 4], Figures 4D and 4E). Furthermore, spikes occurred close in time on multiple electrodes, which represents neuronal network synchronicity (Figure 4F). To further address functionality, we treated the hMOs with the dopamine D_2/D_3 receptor agonist quinpirole (5 μM). Indeed, after this treatment neuronal activity was reduced (Figure 4G), confirming the presence of functional dopamine receptors in the described hMOs. Together, these findings indicate that hMOs develop functional synaptic connections and show spontaneous neuronal activity.

DISCUSSION

One of the main limitations in neuroscience and the modeling of neurological diseases is the lack of advanced experimental in vitro models that truly recapitulate the complexity of the human brain. Here we have presented a human brain organoid system that is highly specific to the midbrain. These hMOs contain spatially patterned groups of dopaminergic neurons, which make them an attractive model for the study of PD. hMOs are characterized in detail with regard to neuronal differentiation and activity as well as for astroglia and oligodendrocyte differentiation.

The presence of astrocytes is crucial for the formation of synapses and regular neuronal activity (Chung et al., 2015). Astrocytes are specified later than neurons during development (Chaboub and Deneen, 2013; Molofsky et al., 2012). Accordingly, hMOs show robust astrocyte immunoreactivity only after 61 days of differentiation. Furthermore, synaptic connections, consisting of a direct contact between pre- and postsynapses, are detectable in the hMOs. These synaptic contacts are the prerequisite for electrophysiological and neuronal network functionality, which we indeed detected in the hMOs by Ca^{2+} imaging and MEA measurements. In addition, fast information transmission between neurons depends on axonal myelination, which is achieved by oligodendrocytes. In most

Figure 3. Differentiation into Glial Cells and Formation of Synaptic Connections

(A) IF staining for the astroglia marker S100B in early-stage (day 27) and late-stage (day 61) hMOs. Dashed lines indicate the perimeter of the organoid.

(B) IF staining for the astrocyte markers S100B, AQP4, and VIM. Dashed lines indicate the perimeter of the organoid.

(C) IF staining of an organoid at day 61 revealing differentiation into CNPase- and MBP-positive oligodendrocytes. 3D surface reconstructions of confocal z stacks visualize the formation of myelin sheaths that enwrap TUJ1-positive neurites (arrowheads) as well as the formation of nodes of Ranvier that are suggested by the presence of gaps of CNPase-positive ensheathment.

(D) 3D surface reconstruction of a confocal z stack of an IF staining of co-stained MBP and CNPase enwrapping a TUJ1-positive neurite.

(E) IF staining of the presynaptic marker SYP and the postsynaptic marker PSD95 at day 61. Arrowheads indicate a direct contact between a pre- and a postsynapse. Dashed box indicates the region of magnification. Images show the 3D view of a confocal z stack.

(F) 3D surface reconstructions of confocal z stacks demonstrate the formation of synaptic connections between different neurites of an organoid as indicated by several direct contacts (arrowheads) between the pre- and postsynaptic markers SYP and PSD95, respectively. Lower panels show high magnifications of a 3D view of a confocal z stack and the corresponding 3D surface reconstruction of several synaptic connections.

Scale bars represent 200 μm (A), 20 μm (B, C upper panel left/middle, E left), 10 μm (C lower panel, D, F upper panel left), 7 μm (E right), 3 μm (F upper panel right), 2 μm (F lower panel), 1 μm C upper panel right.

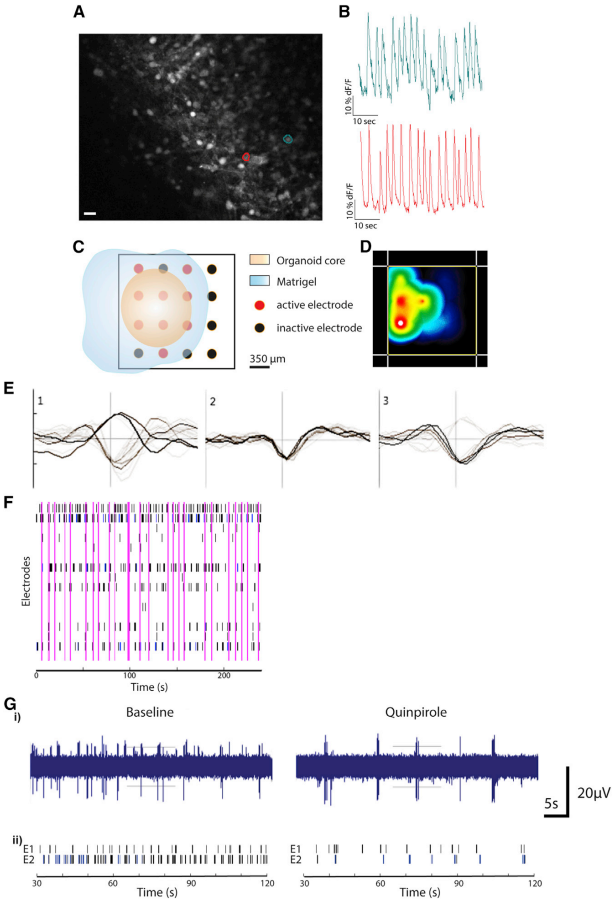

Figure 4. hMOs Reveal Electrophysiological Activity

(A and B) Monitoring of the spontaneous electrophysiological activity in an organoid using Fluo-4AM-based calcium imaging. (A) Mean fluorescence frame of a calcium imaging dataset of a midbrain organoid with two segmented neurons (bordered red and blue) expressing spontaneous activity. Scale bar, 20 µm. (B) Fluorescence traces corresponding to the segmented cell bodies in (A) showing firing patterns with pacemaking-like shape.

(C–F) Evaluation of the spontaneous activity in 16 hMOs of four organoid lines (n = 4) after 82–84 days using an MEA system. (C) Representative scheme of positioned midbrain organoid on a 16-electrode array in a 48-well tissue culture plate. (D) Representative image of the activity map. (E) Examples of mono- and biphasic spikes detected by individual electrodes. (F) Representative image of a spike raster plot showing neuronal network activity in time and space. Spikes occurring on multiple electrodes, closely in time, represent network synchrony, indicated by pink lines. (G) Representative raw data trace (i) and spike raster plots (ii) for single electrodes and the effect of quinpirole on firing frequency of mDNs 30 min after treatment.

stem cell-based differentiation protocols, the differentiation into oligodendrocytes is extremely inefficient (Bunk et al., 2016; Jablonska et al., 2010). However, in the present approach we achieved a robust differentiation into oligodendrocytes and a high degree of neurite myelination. Neurites in these hMOs are ensheathed by oligodendrocytes and even structures such as the nodes of Ranvier, which are of critical importance for saltatory transmission of signals in axons (Faivre-Sarrailh and Devaux, 2013), become apparent.

Compared with other pioneering human brain organoid systems, we are able to generate organoids of a remarkable size (up to 2 mm in diameter) with high reproducibility. Importantly, it was possible to reproducibly generate hMOs based on iPSC lines that come from different origins such as cord blood and fibroblasts. Additionally these fibroblasts have been sampled from individuals at ages from 53 years to 81 years (Table S1). Importantly, in contrast to all other human brain organoid systems, our starting population of cells are not iPSCs but NESCs (Reinhardt et al., 2013), which allows us to achieve an efficient directed differentiation. Our approach is fully focused on the midbrain, as shown by the abundant presence of neurons with mDN identity. These neurons are asymmetrically

distributed in a discrete cluster. This asymmetry mirrors a unique feature of the human brain, where the soma of mDNs reside in the substantia nigra. Furthermore, the presence of neuromelanin, which is a unique feature of the primate brain, is an interesting finding.

The presented hMOs have a great potential to be used for in vitro modeling of diseases that strongly affect the human midbrain, particularly PD (Michel et al., 2016). Patient-specific hMOs might reveal specific phenotypes that are not abundant in 2D cultures and therefore may be used for mechanistic studies and drug testing. Importantly, such a pipeline would be fully suitable for approaches in personalized medicine (Bu et al., 2016; Hillje and Schwamborn, 2016).

Neurodegenerative disorders, such as PD, are typically considered to be age-associated diseases (Sepe et al., 2016; Xu et al., 2016). However, there is accumulating evidence that PD has a strong neurodevelopmental component that probably defines the susceptibility to develop the disease (Garcia-Reitboeck et al., 2013; Le Grand et al., 2014). This finding supports the importance of human brain development models to investigate the disease's underlying mechanisms.

Major limitations of the hMOs presented here, as well as other published brain organoid systems, is the absence of immune cells (microglia) and vasculature. The absence of vasculature might limit the growth of organoids beyond a certain size and the appearance of dead cells in the center of the organoids. While the absence of microglia is a major disadvantage for disease modeling, another option to reduce the problem of the dead cells in the center of organoids might be to produce smaller organoids. However, it seems likely that there is a minimal size of an organoid required to achieve key characteristics such as spatial asymmetry. Despite these limitations, the hMO system presented here along with other models may be a first step toward a more human patient-specific, probably even personalized, era of advanced disease modeling and therapy development.

EXPERIMENTAL PROCEDURES

Authorization from the National Ethics Committee for the work with human iPSCs (CNER No. 201305/04; PDiPS from the Ethic Review Panel of the University of Luxembourg) is in place.

For hMO generation, 9,000 human NESCs were plated in each well of an ultra-low-attachment 96-well round-bottomed plate (Corning) and cultured in N2B27 medium (DMEM-F12 [Invitrogen]/Neurobasal [Invitrogen] 50:50 with 1:200 N2 supplement [Invitrogen], 1:100 B27 supplement lacking vitamin A [Invitrogen], 1% L-glutamine and 1% penicillin-streptomycin [Invitrogen]) containing 3 μM CHIR-99021 (Axon Medchem), 0.75 μM purmorphamine (Enzo Life Science), and 150 μM ascorbic acid (Sigma) (referred to as N2B27 maintenance medium). After 6 days, the colonies were transferred to ultra-low-attachment 24-well plates (Corning) and cultured in N2B27 maintenance medium. On day 8, the 3D colonies were transferred to droplets of hESC-qualified Matrigel (BD Bioscience) as previously described (Lancaster and Knoblich, 2014). Droplets were cultured in N2B27 maintenance medium for 2 more days. On day 10, differentiation was initiated with N2B27 medium supplemented with 10 ng/mL human brain-derived neurotrophic factor, 10 ng/mL human glial-derived neurotrophic factor, 500 μM dibutyryl cyclic AMP (Peprotech), 200 μM ascorbic acid (Sigma), and 1 ng/mL transforming growth factor β3 (Peprotech). In addition, 1 μM purmorphamine (Enzo Life Science) was added to this medium for an additional 6 days. On day 14 of the organoid culture, the plates were placed on an orbital shaker (IKA), rotating at 80 rpm, in an incubator and the organoids were kept in culture with media changes every second or third day. A detailed description is provided in Supplemental Experimental Procedures.

SUPPLEMENTAL INFORMATION

Supplemental Information includes Supplemental Experimental Procedures, four figures, two tables, and one movie and can be found with this article online at http://dx.doi.org/10.1016/j.stemcr.2017.03.010.

AUTHOR CONTRIBUTIONS

A.S.M., L.M.S., K.H., R.M.T.F., S.B., and J.C.S. designed the study; A.S.M., L.M.S., K.H., S.H., E.L.M., T.v.W., J.J., and J.W. conducted the research; A.S.M., L.M.S., K.H., S.H., E.L.M., I. Brüggemann, I. Boussaad, E.B., S.B., and J.C.S. analyzed the data; A.S.M., L.M.S., K.H., S.H., E.L.M., E.B., R.M.T.F., S.B., and J.C.S. wrote the paper.

ACKNOWLEDGMENTS

This project was supported by the LCSB pluripotent stem cell core facility. The J.C.S. laboratory is supported by the Fonds National de la Recherche (FNR) (CORE, C13/BM/5791363) and by a University Luxembourg Internal Research Project grant (MidNSCs). A.S.M., L.M.S., S.H., and E.L.M. are supported by fellowships from the FNR (AFR, Aides à la Formation-Recherche). This is an EU Joint Program - Neurodegenerative Disease Research (JPND) project (INTER/JPND/14/02; INTER/JPND/15/11092422). Further support comes from the SysMedPD project which has received funding from the European Union's Horizon 2020 research and innovation program under grant agreement No. 668738. Finally, we also thank the private donors who support our work at the Luxembourg Center for Systems Biomedicine.

Received: July 1, 2016
Revised: March 10, 2017
Accepted: March 10, 2017
Published: April 13, 2017

REFERENCES

Baharvand, H., Hashemi, S.M., Kazemi Ashtiani, S., and Farrokhi, A. (2006). Differentiation of human embryonic stem cells into

hepatocytes in 2D and 3D culture systems in vitro. Int. J. Dev. Biol. *50*, 645–652.

Bu, L.L., Yang, K., Xiong, W.X., Liu, F.T., Anderson, B., Wang, Y., and Wang, J. (2016). Toward precision medicine in Parkinson's disease. Ann. Transl. Med. *4*, 26.

Bunk, E.C., Ertaylan, G., Ortega, F., Pavlou, M.A., Gonzalez-Cano, L., Stergiopoulos, A., Safaiyan, S., Vols, S., van Cann, M., Politis, P.K., et al. (2016). Prox1 is required for oligodendrocyte cell identity in adult neural stem cells of the subventricular zone. Stem Cells *34*, 2115–2129.

Chaboub, L.S., and Deneen, B. (2013). Astrocyte form and function in the developing central nervous system. Semin. Pediatr. Neurol. *20*, 230–235.

Chung, W.S., Welsh, C.A., Barres, B.A., and Stevens, B. (2015). Do glia drive synaptic and cognitive impairment in disease? Nat. Neurosci. *18*, 1539–1545.

Duan, D., Fu, Y., Paxinos, G., and Watson, C. (2013). Spatiotemporal expression patterns of Pax6 in the brain of embryonic, newborn, and adult mice. Brain Struct. Funct. *218*, 353–372.

Eiraku, M., and Sasai, Y. (2012). Self-formation of layered neural structures in three-dimensional culture of ES cells. Curr. Opin. Neurobiol. *22*, 768–777.

Eiraku, M., Watanabe, K., Matsuo-Takasaki, M., Kawada, M., Yonemura, S., Matsumura, M., Wataya, T., Nishiyama, A., Muguruma, K., and Sasai, Y. (2008). Self-organized formation of polarized cortical tissues from ESCs and its active manipulation by extrinsic signals. Cell Stem Cell *3*, 519–532.

Engler, A.J., Sen, S., Sweeney, H.L., and Discher, D.E. (2006). Matrix elasticity directs stem cell lineage specification. Cell *126*, 677–689.

Faivre-Sarrailh, C., and Devaux, J.J. (2013). Neuro-glial interactions at the nodes of Ranvier: implication in health and diseases. Front. Cell. Neurosci. *7*, 196.

Garcia-Reitboeck, P., Anichtchik, O., Dalley, J.W., Ninkina, N., Tofaris, G.K., Buchman, V.L., and Spillantini, M.G. (2013). Endogenous alpha-synuclein influences the number of dopaminergic neurons in mouse substantia nigra. Exp. Neurol. *248*, 541–545.

Greiner, J., Kaltschmidt, B., Kaltschmidt, C., and Widera, D. (2013). Going 3D—cell culture approaches for stem cell research and therapy. Curr. Tissue Eng. *2*, 8–19.

Hartfield, E.M., Yamasaki-Mann, M., Ribeiro Fernandes, H.J., Vowles, J., James, W.S., Cowley, S.A., and Wade-Martins, R. (2014). Physiological characterisation of human iPS-derived dopaminergic neurons. PLoS One *9*, e87388.

Hillje, A.L., and Schwamborn, J.C. (2016). Utilization of stem cells to model Parkinson's disease—current state and future challenges. Future Neurol. *11*, 171–186.

Jablonska, B., Aguirre, A., Raymond, M., Szabo, G., Kitabatake, Y., Sailor, K.A., Ming, G.L., Song, H., and Gallo, V. (2010). Chordin-induced lineage plasticity of adult SVZ neuroblasts after demyelination. Nat. Neurosci. *13*, 541–550.

Jo, J., Xiao, Y., Sun, A.X., Cukuroglu, E., Tran, H.D., Goke, J., Tan, Z.Y., Saw, T.Y., Tan, C.P., Lokman, H., et al. (2016). Midbrain-like organoids from human pluripotent stem cells contain functional dopaminergic and neuromelanin-producing neurons. Cell Stem Cell *19*, 248–257.

Lancaster, M.A., and Knoblich, J.A. (2014). Generation of cerebral organoids from human pluripotent stem cells. Nat. Protoc. *9*, 2329–2340.

Lancaster, M.A., Renner, M., Martin, C.A., Wenzel, D., Bicknell, L.S., Hurles, M.E., Homfray, T., Penninger, J.M., Jackson, A.P., and Knoblich, J.A. (2013). Cerebral organoids model human brain development and microcephaly. Nature *501*, 373–379.

Le Grand, J.N., Gonzalez-Cano, L., Pavlou, M.A., and Schwamborn, J.C. (2014). Neural stem cells in Parkinson's disease: a role for neurogenesis defects in onset and progression. Cell Mol. Life Sci. *72*, 773–797.

Lee, G.Y., Kenny, P.A., Lee, E.H., and Bissell, M.J. (2007). Three-dimensional culture models of normal and malignant breast epithelial cells. Nat. Methods *4*, 359–365.

McBeath, R., Pirone, D.M., Nelson, C.M., Bhadriraju, K., and Chen, C.S. (2004). Cell shape, cytoskeletal tension, and RhoA regulate stem cell lineage commitment. Dev. Cell *6*, 483–495.

Michel, P.P., Hirsch, E.C., and Hunot, S. (2016). Understanding dopaminergic cell death pathways in Parkinson disease. Neuron *90*, 675–691.

Molofsky, A.V., Krencik, R., Ullian, E.M., Tsai, H.H., Deneen, B., Richardson, W.D., Barres, B.A., and Rowitch, D.H. (2012). Astrocytes and disease: a neurodevelopmental perspective. Genes Dev. *26*, 891–907.

Moreno, E.L., Hachi, S., Hemmer, K., Trietsch, S.J., Baumuratov, A.S., Hankemeier, T., Vulto, P., Schwamborn, J.C., and Fleming, R.M. (2015). Differentiation of neuroepithelial stem cells into functional dopaminergic neurons in 3D microfluidic cell culture. Lab Chip *15*, 2419–2428.

Muguruma, K., Nishiyama, A., Kawakami, H., Hashimoto, K., and Sasai, Y. (2015). Self-organization of polarized cerebellar tissue in 3D culture of human pluripotent stem cells. Cell Rep. *10*, 537–550.

Nakano, T., Ando, S., Takata, N., Kawada, M., Muguruma, K., Sekiguchi, K., Saito, K., Yonemura, S., Eiraku, M., and Sasai, Y. (2012). Self-formation of optic cups and storable stratified neural retina from human ESCs. Cell Stem Cell *10*, 771–785.

Qian, X., Nguyen, H.N., Song, M.M., Hadiono, C., Ogden, S.C., Hammack, C., Yao, B., Hamersky, G.R., Jacob, F., Zhong, C., et al. (2016). Brain-region-specific organoids using mini-bioreactors for modeling ZIKV exposure. Cell *165*, 1238–1254.

Reinhardt, P., Glatza, M., Hemmer, K., Tsytsyura, Y., Thiel, C.S., Hoing, S., Moritz, S., Parga, J.A., Wagner, L., Bruder, J.M., et al. (2013). Derivation and expansion using only small molecules of human neural progenitors for neurodegenerative disease modeling. PLoS One *8*, e59252.

Sato, T., Vries, R.G., Snippert, H.J., van de Wetering, M., Barker, N., Stange, D.E., van Es, J.H., Abo, A., Kujala, P., Peters, P.J., et al. (2009). Single Lgr5 stem cells build crypt-villus structures in vitro without a mesenchymal niche. Nature *459*, 262–265.

Schwarz, M., Alvarez-Bolado, G., Dressler, G., Urbanek, P., Busslinger, M., and Gruss, P. (1999). Pax2/5 and Pax6 subdivide the early neural tube into three domains. Mech. Dev. *82*, 29–39.

Sepe, S., Milanese, C., Gabriels, S., Derks, K.W., Payan-Gomez, C., van, I.W.F., Rijksen, Y.M., Nigg, A.L., Moreno, S., Cerri, S., et al. (2016). Inefficient DNA repair is an aging-related modifier of Parkinson's disease. Cell Rep. *15*, 1866–1875.

Takahashi, K., and Yamanaka, S. (2006). Induction of pluripotent stem cells from mouse embryonic and adult fibroblast cultures by defined factors. Cell *126*, 663–676.

Tanaka, H., Murphy, C.L., Murphy, C., Kimura, M., Kawai, S., and Polak, J.M. (2004). Chondrogenic differentiation of murine embryonic stem cells: effects of culture conditions and dexamethasone. J. Cell Biochem. *93*, 454–462.

Tian, X.F., Heng, B.C., Ge, Z., Lu, K., Rufaihah, A.J., Fan, V.T., Yeo, J.F., and Cao, T. (2008). Comparison of osteogenesis of human embryonic stem cells within 2D and 3D culture systems. Scand. J. Clin. Lab. Invest. *68*, 58–67.

Xu, Y., Yang, J., and Shang, H. (2016). Meta-analysis of risk factors for Parkinson's disease dementia. Transl. Neurodegener. *5*, 11.

Yu, J., Vodyanik, M.A., Smuga-Otto, K., Antosiewicz-Bourget, J., Frane, J.L., Tian, S., Nie, J., Jonsdottir, G.A., Ruotti, V., Stewart, R., et al. (2007). Induced pluripotent stem cell lines derived from human somatic cells. Science *318*, 1917–1920.

Supplemental Information

Derivation of human midbrain-specific organoids from neuroepithelial stem cells

Anna S. Monzel[1#], Lisa M. Smits[1#], Kathrin Hemmer[1#], Siham Hachi[2], Edinson Lucumi Moreno[2], Thea van Wuellen[1], Javier Jarazo[1], Jonas Walter[1], Inga Brüggemann[1], Ibrahim Boussaad[3], Emanuel Berger[1], Ronan M.T. Fleming[2], Silvia Bolognin[1], Jens C. Schwamborn[1]*

[1]Luxembourg Centre for Systems Biomedicine (LCSB), Developmental and Cellular Biology, University of Luxembourg, L-4362 Esch-sur-Alzette Luxembourg
[2]Luxembourg Centre for Systems Biomedicine (LCSB), Systems Biochemistry, University of Luxembourg, L-4362 Esch-sur-Alzette Luxembourg
[3]Luxembourg Centre for Systems Biomedicine (LCSB), Clinical & Experimental Neuroscience, University of Luxembourg, L-4362 Esch-sur-Alzette Luxembourg
*Correspondence: Jens C. Schwamborn, Luxembourg Centre for Systems Biomedicine (LCSB), University of Luxembourg, 7, avenue des Hauts-Fourneaux, L-4362 Esch-sur-Alzette Luxembourg; E-mail: jens.schwamborn@uni.lu
[#]Co-first author

Supplemental Figures and Legends

Figure S1

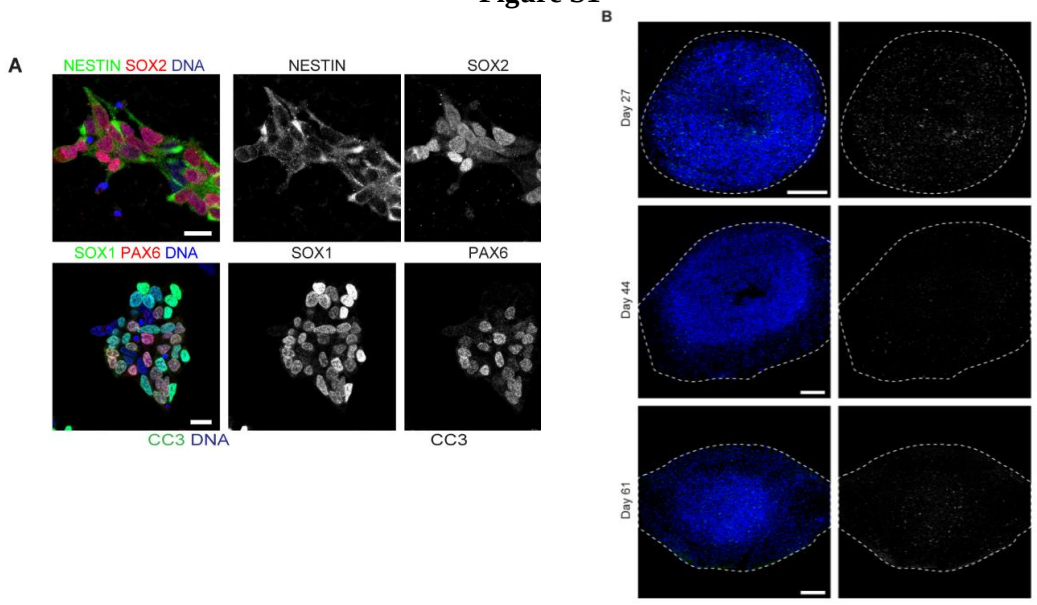

Figure S1: Derivation of hMOs from human NESCs. Related to Figure 1.
(A) Immunocytological staining of human neuroepithelial stem cells for the neural progenitor markers NESTIN and SOX2 (upper panel) and SOX1 and PAX6 (lower panel). (B) Immunohistological staining at days 27, 44, and 61 for the apoptotic marker cleaved caspase-3 (CC3). Scale bars, 20 µm (A), 200 µm (B). Dashed lines indicate the perimeter of the organoid.

Figure S2

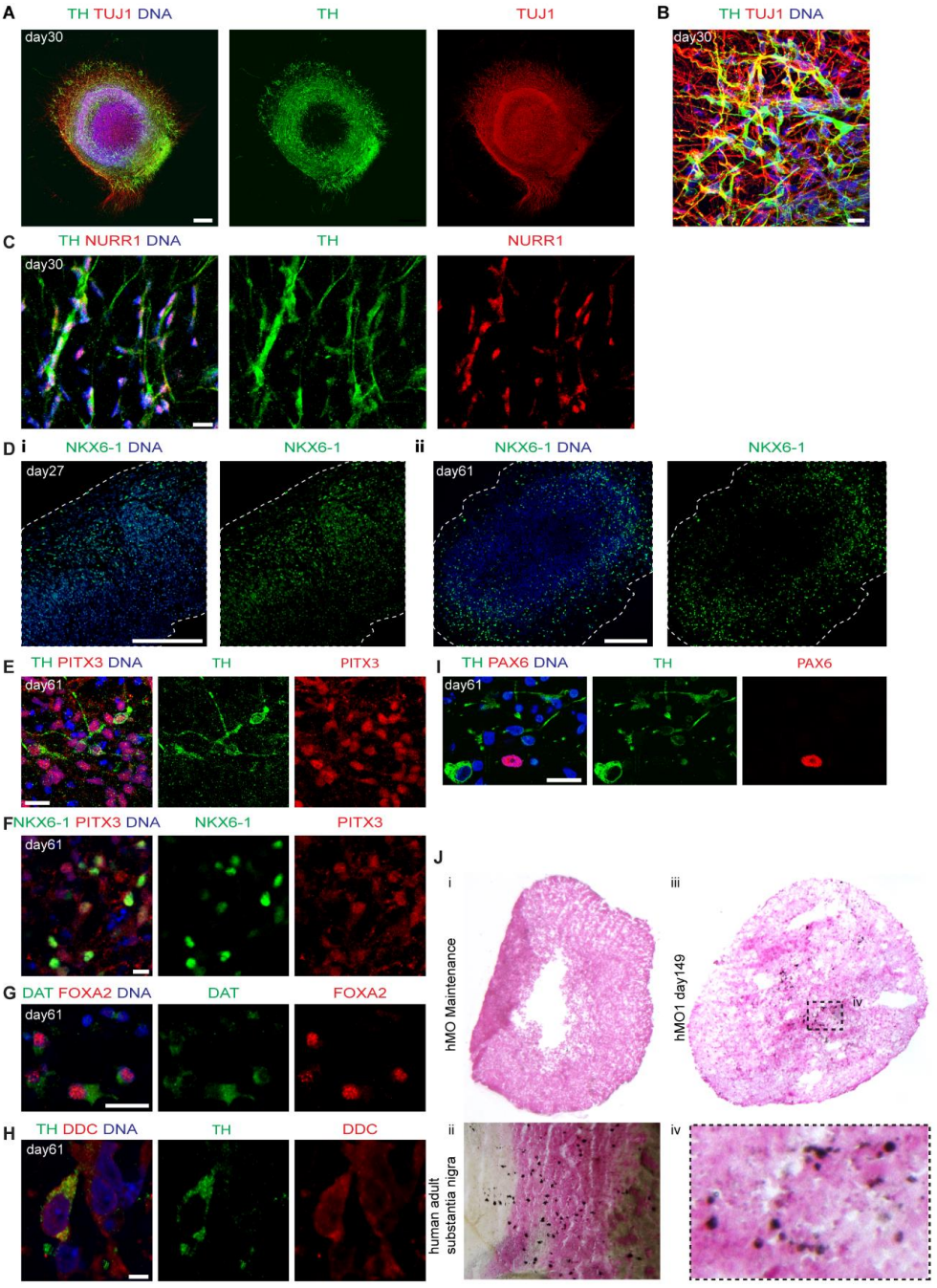

Figure S2: mDN differentiation and specification. Related to Figure 2.
(A) Immunohistological staining of TUJ1 and TH at day 30.(B) Higher magnification of (A) showing an immunohistological staining of TUJ1 and TH at day 30. (C) Immunohistological staining of the mDN markers NURR1 and TH.(D) Immunohistological staining of the ventral marker NKX6-1 in early stage (i) and late stage (ii) organoids. (E) Immunohistological staining of mDN markers PITX3 and TH in late stage organoids. (F) Immunohistological staining of the ventral marker NKX6-1 and PITX3 in late stage organoids.(G) Immunohistological staining of mDN markers DAT and FOXA2 in late stage organoids. (H) Immunohistological staining of DN markers DDC and TH in late stage organoids.

(I) Immunohistological staining of neural progenitor marker PAX6 and DN marker TH in late stage organoids.(F) Fontana Masson staining of (i) an organoid kept under maintenance conditions at d13 (negative control), (ii) human post-mortem substantia nigra tissue as a positive control and (iii) a midbrain organoid at day 149. (iv) Higher magnification of (iii). Scale bars, 200 µm (A, D), 20 µm (B, C, E, G, I) 10 µm (F), 5 µm (H). Dashed lines indicate the perimeter of the organoid.

Figure S3

Figure S3: Robust differentiation into glia cells and formation of synaptic connections. Related to Figure 3.

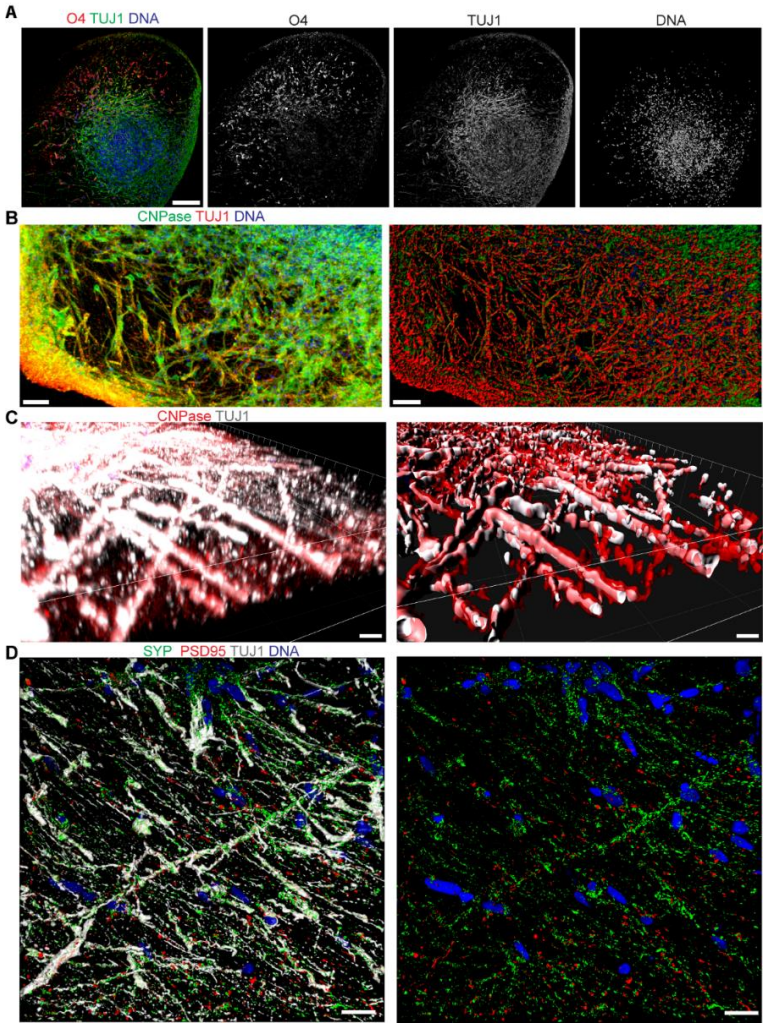

(A) Overview of an organoid at day 44 shows robust differentiation into O4-positive oligodendrocytes and TUJ1-positive neurons. Oligodendrocytes show spatially asymmetric distribution that cluster in the upper left region of the organoid.
(B) Representative 3D view and surface reconstruction at a lower magnification of the confocal z-stack shown in Figure 3C. Cells differentiated into CNPase-positive oligodendrocytes and TUJ1-positive neurons.
(C) Representative 3D view and surface reconstruction at higher magnification of a confocal z-stack illustrate the formation of CNPase-positive myelin sheets that cover TUJ1-positive fibers.
(D) Representative 3D surface reconstructions of the confocal z-stack shown in Figure 3E. Scale bars, 200 µm (A), 50 µm (B), 15 µm (C), 20 µm (D).

Figure S4

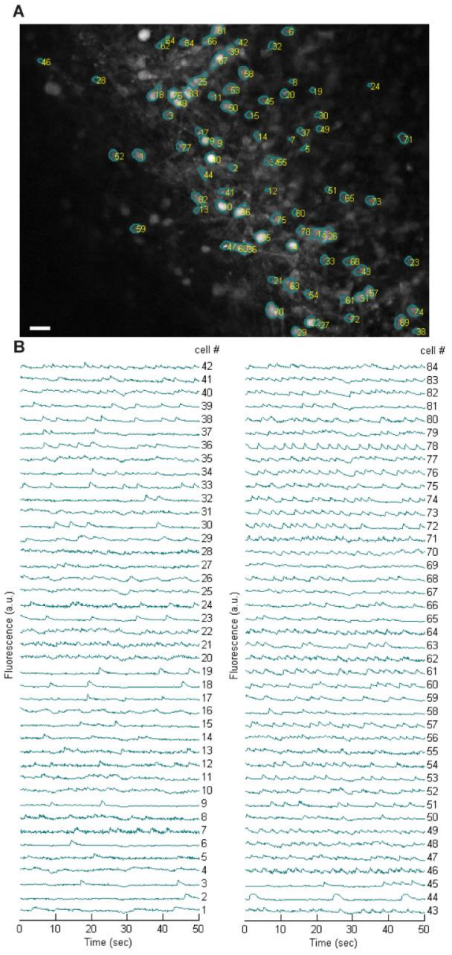

Figure S4: hMOs reveal electrophysiological activity. Related to Figure 4.
(A) Mean fluorescence frame of a Fluo-4AM based calcium imaging dataset of a midbrain organoid with automatically segmented cell bodies. Scale bar, 20 µm.
(B) Fluorescence traces corresponding to the cell bodies segmented in (A)

Table S1

Table S1 Source of hiPSCs	**Age at sampling**	**Gender**	**hNESC ID**	**Corresponding human midbrain organoid culture**
Reinhardt et al. 2013	81	♀	3.0.0.10.0	hMO1
Reinhardt et al. 2013	53	♀	3.0.0.14.0	hMO2
Coriell (ND34769)	68	♀	3.0.0.24.1	hMO3
Gibco (A13777)	Cord Blood	♀	3.0.0.15.0	hMO4

Table S1 related to experimental procedures: Cell lines used in this study to generate hMOs. Human NESCs were derived under 2D conditions from human iPSCs of different origin. Human midbrain-specific organoids were generated with hNESCs as described in the Experimental procedures section.

Table S2

Antibody	Species	Source	Ref.-No.	Dilution
AQP4	rabbit	Santa Cruz	sc-20812	1:100
Calbindin	mouse	swant	300	1:500
CC3	rabbit	Cell Signaling Technology	9661	1:200
CNPase	mouse	Abcam	ab6319	1:200
DAT	rat	Abcam	ab5981	1:500
DDC	rabbit	Thermo Scientific	PA5-25450	1:25
Dopamine	rabbit	ImmuSmol	IS1005	1:500
FOXA2	mouse	Santa Cruz	sc-101060	1:250
GIRK2	goat	Abcam	ab65096	1:200
IgG control	rabbit	Santa Cruz	sc-3888	1:100
IgG2a κ isotype control	mouse	BioLegend	401502	1:300
IgY control	chicken	RnD	AB-101-C	1:50
KI67	mouse	BD Biosciences	550609	1:200
LMX1A	rabbit	Abcam	ab139726	1:200
MAP2	mouse	Millipore	MAB3418	1:200
MBP	rat	Abcam	ab7349	1:200
Nestin	mouse	BD Bioscience	611659	1:200
NKX6-1	mouse	DSHB	F55A10	1:50
NURR1	rabbit	Santa Cruz	sc-991	1:250
O4	mouse	Sigma-Aldrich	O7139	1:400
OTX2	goat	R&D	AF1979	1:200
PAX6	rabbit	Covance	PRB-278P	1:300
PAX6	mouse	DSHB	1-223	1:200
PITX3	rabbit	Millipore	AB5722	1:200
PSD-95	rabbit	Invitrogen	51-6900	1:300
S100B	mouse	Sigma-Aldrich	S2532	1:1000
SOX1	goat	R&D systems	AF3369	1:100
SOX2	goat	R&D systems	AF2018	1:200
SOX2	rabbit	Abcam	ab97959	1:100
SYP	mouse	Abcam	ab8049	1:50
TH	chicken	Abcam	ab76442	1:1000
TH	rabbit	Abcam	ab112	1:1000
TH	rabbit	Santa Cruz	sc-14007	1:1000
TUJ1	mouse	BioLegend	801201	1:600
TUJ1	rabbit	Covance	PRB-435P-0100	1:600
TUJ1	chicken	Millipore	AB9354	1:600
Vimentin	chicken	Abcam	ab24525	1:200

Table S2 related to experimental procedures: Antibodies used in this study.

Supplemental Experimental Procedures

Neuroepithelial stem cell derivation and generation of midbrain organoids

Human NESC lines from four female healthy individuals were generated as described elsewhere (Reinhardt et al., 2013) from human iPSC lines (Table S1). Human NESCs were cultured on Matrigel coated plates in N2B27 media supplemented with 3 µM CHIR-99021 (Axon Medchem), 0.75 µM purmorphamine (Enzo Life Science) and 150 µM ascorbic acid (Sigma) (referred to as N2B27 maintenance media) as previously described (Reinhardt et al., 2013). N2B27 medium consists of DMEM-F12 (Invitrogen)/Neurobasal (Invitrogen) 50:50 with 1:200 N2 supplement (Invitrogen), 1:100 B27 supplement lacking Vitamin A (Invitrogen), 1 % L-glutamine and 1 % penicillin/streptomycin (Invitrogen). On day 0 of the organoid culture, hNESCs at passage <24 were treated with accutase for 5 min at 37 °C, followed by gentle pipetting to generate single cells. A total of 9000 cells were seeded into each well of an ultra-low attachment 96-well round bottom plate (Corning) and cultured in N2B27 maintenance media. The medium was changed every other day for 6 days, and 3D colonies were then transferred to ultra-low attachment 24-well plates (Corning) and cultured in N2B27 maintenance media.

On day 8 of the organoid culture, the 3D colonies were transferred to droplets of hESC-qualified Matrigel (BD Bioscience) as previously described (Lancaster and Knoblich, 2014). Droplets were cultured in N2B27 maintenance media either in 10-cm Petri dishes for short-term cultures or in ultra-low attachment 24-well plates (Corning) with one droplet per well for long-term cultures. On day 10, differentiation was initiated with N2B27 media supplemented with 10 ng/ml hBDNF (Peprotech), 10 ng/ml hGDNF (Peprotech), 500 µM dbcAMP (Peprotech), 200 µM ascorbic acid (Sigma), and 1 ng/ml TGF-β3 (Peprotech). Additionally, 1 µM purmorphamine (Enzo Life Science) was added to this medium for an additional 6 days. On day 14 of the organoid culture, the plates were placed on an orbital shaker (IKA), rotating at 80 rpm, in an incubator (5 % CO_2, 37 °C) and the organoids were kept in culture with media changes every second or third day. In order to measure the size of the organoids, brightfield images were taken of two independently generated organoid cultures of four cell lines (3 organoids per cell line) and the average diameter was measured.

Flow cytometry

For flow cytometry analysis, six organoids for each cell line were dissociated to single cells by incubation in DMEM-F12 (Invitrogen) containing 0.18 % Papain (Sigma), 0.04 % EDTA (Sigma) and 0.04 % L-Cystein (Sigma) at 37 °C under dynamic conditions until the Matrigel disappeared (2-3 h). Organoids were then treated with accutase for further 2-3 h at 37 °C under dynamic conditions. During accutase treatment, organoids were firstly triturated with a 1000 µl pipette and eventually with a 200 µl pipette in order to support the dissociation into single cells. For intracellular staining, transcription factor buffer set (BD Bioscience) was used according to the manufacturer´s instructions. After fixation, cells were filtered through a 5 ml polystyrene round-bottom tube with cell-strainer cap (Corning). 200,000 cells were used per sample and antibodies were used at the following dilutions: chicken anti-TH (1:50, Abcam) mouse anti-FOXA2 (1:300, Santa Cruz Biotechnology) and rabbit anti-LMX1A (1:100, Abcam). Threshold gates were set with the same samples that were stained with the following isotype control antibodies: Normal chicken IgY Control (R&D Systems), normal rabbit IgG control (Santa Cruz Biotechnology), and purified Mouse IgG2a, κ isotype control (BioLegend). Isotype control antibodies were used at the same concentration as the detection antibody. All secondary

antibodies (Invitrogen) were conjugated to Alexa Fluor fluorochromes. Flow cytometry was performed by using BD LSRFortessa Cell Analyzer and data were analyzed and represented by FlowJo software.

Immunohistochemical analysis

Organoids were fixed with 4 % paraformaldehyde overnight at RT and washed 3x with PBS for 1 h. Afterwards, they were embedded in 3 % low-melting point agarose in PBS and incubated for 15 min at 37 °C, followed by 30 min incubation at RT. The solid agarose block was covered with PBS and kept overnight at 4 °C. If not indicated otherwise, 50 µm sections were cut using a vibratome (Leica VT1000s), and sections were permeabilized with 0.5 % Triton X-100 in PBS and blocked for 2 h in 2.5 % normal goat or donkey serum with 2.5 % BSA, 0.1 % Triton X-100, and 0.1 % sodium azide. Permeabilization times varied between 30 min and 2 h depending on the antibody used. Sections were incubated on a shaker for 48-72 h at 4 °C with primary antibodies in the blocking buffer at the following dilutions: rabbit anti-TH (1:1000, Abcam), chicken anti-TH (1:1000, Abcam), rabbit anti-TH (1:1000, Santa Cruz Biotechnology), goat anti-SOX2 (1:200, R&D Systems), rabbit anti-SOX2 (1:100, Abcam), goat anti-SOX1 (1:100, R&D Systems), mouse anti-NESTIN (1:200, BD), mouse anti-KI67 (1:200, BD), rabbit anti-CC3 (1:200, Cell Signalling), mouse anti-FOXA2 (1:250, Santa Cruz Biotechnology), rabbit anti-LMX1A (1:200, Abcam), mouse anti-S100B (1:1000, Abcam), chicken anti-Vimentin (1:200, Abcam), rabbit anti-AQP4 (1:100, Santa Cruz Biotechnology), mouse anti-TUJ1 (1:600, Covance), rabbit anti-TUJ1 (1:600, Covance), chicken anti-TUJ1 (1:600 Millipore), mouse anti-NKX6-1 (1:50, DSHB), rabbit anti-NURR1 (1:250, Santa Cruz Biotechnology), goat anti-OTX2 (1:200, Neuromics), rat anti-DAT (1:500, Abcam), goat anti-GIRK2 (1:200, Abcam), mouse anti-Calbindin (1:500, Swant), rabbit anti-PITX3 (1:200, Millipore), rabbit anti-DDC (1:25, Thermo Scientific), rabbit anti-PAX6 (1:300, Covance), mouse anti-PAX6 (1:200, DSHB), mouse anti-Synaptophysin (1:50 Abcam), rabbit anti PSD-95 (1:300, Invitrogen), mouse anti-MAP2 (1:200, Millipore), mouse anti-CNPase (1:200, Abcam), rat anti-MBP (1:200, Abcam) and mouse anti-O4 (1:400, Sigma). After incubation with the primary antibodies, sections were washed three times in 0.01 % Triton X-100 and blocked for 30 min at RT on a shaker, followed by incubation with the secondary antibodies in 0.01 % Triton X-100 (1:1000). All secondary antibodies (Invitrogen) were conjugated to Alexa Fluor fluorochromes.

For whole mount stainings, whole organoids were blocked and permeabilized with 10% normal goat serum, 0.1% Triton X-100 in PBS at RT overnight. The primary antibodies were diluted in 3% normal goat serum and 0.1% Triton X-100 in PBS at the following dilutions: mouse anti-TUJ1 (1:600, Covance) and rabbit anti-TH (1:1000, Abcam) and incubated on a shaker for 3 days at 4°C. After incubation with the primary antibodies, the whole mounts were washed three times with PBS for 1h and incubated with the secondary antibodies diluted in 3% normal goat serum and 0.1% Triton X-100 in PBS and incubated on a shaker for 2 days at 4°C.

Dopamine was detected using a STAINperfect Immunostaining Kit (ImmuSmol) according to manufacturer's protocol. Prior to fixation, the organoids were treated with DMEM-F12 (Invitrogen) containing 0.18 % Papain (Sigma), 0.04 % EDTA (Sigma) and 0.04 % L-Cystein (Sigma) at 37 °C under dynamic conditions until the Matrigel disappeared (2-3 h). Afterwards, agarose sections were performed as described previously. Sections were co-stained with rabbit anti-Dopamine (ImmuSmol), chicken anti-TH (1:1000, Abcam), mouse anti-MAP2 primary antibody (1:200, Millipore) and

nuclei were counterstained with Hoechst 33342 (Invitrogen). Sections were mounted in Fluoromount-G mounting medium (Southern Biotech) and analyzed with a confocal laser scanning microscope (Zeiss LSM 710). Images were further processed with Zen Software (Zeiss) and ImageJ.
For quantification studies, positive cells of two independently generated organoid cultures of four cell lines were counted and normalized to Hoechst+ cells. For SOX2 and KI67 quantifications, a total of 3549 Hoechst+ cells (day 27) and 3309 Hoechst+ cells (day 61) was counted. For quantification of TUJ1-positive neurites that were ensheathed by oligodendrocytes as well as of pre- and postsynaptic particles, microscopy fields of outer regions of independently generated organoid cultures of four cell lines were chosen and further preprocessed by using ImageJ. After creating masks, image calculator was used to quantify the overlay area of TUJ-1 and MBP positive staining, whereas the tool particle analysis was used to quantify pre- and postsynapses.
Three-dimensional surface reconstructions of confocal z-stacks were created using Imaris software (Bitplane). The asymmetric distribution of mDNs was assessed based on fluorescence intensities with the ImageJ Interactive 3D surface plot plugin.

Quantitative real-time PCR
Total RNA was isolated from 61 days-old organoids. Typically, five organoids were pooled for one isolation. For dissociation, the organoids were snap frozen in liquid nitrogen and afterwards lysed with 1 ml QIAzol lysis reagent (Qiagen), passed through a needle three times and homogenized with QIAshredder columns significance was calculated using the Mann–Whitney test.

Fontana Masson staining
The midbrain organoids were fixed in 4 % PFA overnight at RT, washed 3x in PBS for 1 h, dehydrated in 30 % Sucrose o/n and cryosections were performed using a (Qiagen). For the RNA isolation, 200 µl Chloroform were added to the QIAzol cell lysate. After an incubation of 5 min at 4 °C, the samples were centrifuged at 1500 xg at 4 °C for 5 min. The aqueous phase was collected and mixed with an equal volume of isopropyl alcohol, followed by an incubation o/n at -80 °C. Afterwards the samples were centrifuged at 12.000 xg, 4 °C for 30 min and washed 2x with 70 % Ethanol, centrifuging at 5000 xg, 4 °C for 15 min. The dry pellet was dissolved in H_2O and heated for 10 min at 60 °C. DNA was eliminated using the DNAse I amplification grade endonuclease (Sigma**).** Subsequently, isolated RNA was reverse-transcribed following the protocol of the High Capacity RNA to DNA Kit (Thermo Fisher Scientific). Quantitative real-time polymerase chain reactions (qRT–PCRs) were conducted for four independent maintenance and organoid cultures (20 organoids, n=4) with the Taqman® Gene Expression Master Mix (Applied Biosystems) and the following Taqman® probes: *TH* (Hs00165941_m1), *DAT* (Hs00997374_m1), and *DDC* (Hs01105048_m1). Amplification of 1 µg cDNA was performed in an AriaMx Real-time PCR System (Agilent Technologies) as follows: An initial AmpliTaq Gold activation step, 10 min at 95 °C, 40 cycles of denaturation for 15 s at 95 °C and annealing for 1 min at 60 °C. The expression levels were normalized relative to the expression of the housekeeping gene *GAPDH* using the comparative Ct–method $2^{-\Delta\Delta Ct}$. To evaluate the expression patterns of midbrain organoids, the values were compared to the expression levels of hNESCs, which were set to 1. Statistical

Cryostat (Leica) to a thickness of 10 µm. The sections were stained with a Fontana-Masson staining kit (Abcam). As a negative control, 13 days old organoids kept under maintenance conditions were used. Human post mortem substantia nigra sections served as a positive control.

Evaluation of electrophysiological activity
Calcium imaging and multielectrode array (MEA) recording was used to analyze the spontaneous activity of organoids at day 50-52 (6 Organoids, n=3) and day 82-84 (16 Organoids, n=4), respectively. For calcium imaging, a concentration of 5 µM cell permeant Fluo-4 AM (Life Technologies) in a neurobasal medium was added to the well and incubated for 45 min at 37 °C on an orbital shaker. Fluorescent images were acquired using a live cell spinning disk confocal microscope (Zeiss) equipped with a CMOS camera (Orca Flash 4.0, Hamamatsu). Calcium time-series were acquired at 5 Hz for approximately 2 min and stored as single images. These images were analyzed using the ADINA toolbox (Diego et al., 2013), which is publicly available software that has been developed to automatically segment individual cell bodies and separate the overlapping ones. Fluorescent traces, expressed as relative changes in the fluorescence intensity (ΔF/F), were then measured for segmented cell bodies. In order to quantify the percentage of active neurons, we wrote a custom MATLAB script for automated batch analysis of a set of calcium time-series of organoids.
MEA recording was conducted using the Maestro system from Axion BioSystems. A 48-well MEA plate containing a 16-electrode array per well was precoated with 0.1 mg/ml poly-D-lysine hydrobromide (Sigma-Aldrich) and subsequently coated with 10 µg/ml laminin (Sigma-Aldrich) for 1 h at RT. Midbrain organoids were placed onto the array after day 82-84. A coverslip was placed on top to ensure the contact of the free floating organoid with the electrodes. Spontaneous activity was recorded at a sampling rate of 12.5 kHz for 10 min for up to five days at 37 °C in neuronal maturation media. Using Axion Integrated Studio (AxIS 2.1), a Butterworth band pass filter with 200-3000 Hz cutoff frequency and a threshold of 6 x SD were set to minimize both false-positives and missed detections. The Neural Metric Tool (Axion BioSystems) was used to analyze the spike raster plots. Electrodes with an average of ≥5 spikes/min were defined as active. The spike count files generated from the recordings were used to calculate the number of spikes/active electrode/measurement. Further details regarding the MEA system were previously described (Bardy et al., 2015). Quinpirole (5 µM, Sigma Aldrich) was applied to 16 midbrain organoids (n=4) and spontaneous firing was subsequently recorded every 30 min for 10 min.

Other supplemental data
Movie S1: Calcium time series of an hMO at day 52. Image stacks were acquired at a frequency of 5 Hz for approximately 2 min. The movie is displayed in pseudocolor (lookup table in Image J). 'Cool' colors (blue/green) indicate low fluorescence intensity, 'warm' colors (yellow/red) indicate high fluorescence intensity.

Supplemental References
Bardy, C., van den Hurk, M., Eames, T., Marchand, C., Hernandez, R.V., Kellogg, M., Gorris, M., Galet, B., Palomares, V., Brown, J., *et al.* (2015). Neuronal medium that supports basic synaptic functions and activity of human neurons in vitro. Proceedings of the National Academy of Sciences of the United States of America *112*, E2725-2734.
Diego, F., Reichinnek, S., Both, M., and Hamprecht, F. (2013). Automated identification of neuronal activity from calcium imaging by sparse dictionary learning. Proceedings of the IEEE 10th International Symposium on Biomedical Imaging, pp. 1058–1061, 2013.
Lancaster, M.A., and Knoblich, J.A. (2014). Generation of cerebral organoids from human pluripotent stem cells. Nature protocols *9*, 2329-2340.
Reinhardt, P., Glatza, M., Hemmer, K., Tsytsyura, Y., Thiel, C.S., Hoing, S., Moritz, S., Parga, J.A., Wagner, L., Bruder, J.M., *et al.* (2013). Derivation and expansion using only small molecules of human neural progenitors for neurodegenerative disease modeling. PloS one *8*, e59252.

CHAPTER 6

Original article: Single-cell transcriptomics reveals multiple neuronal cell types in human midbrain organoids

This article is uploaded to *bioRxiv* and submitted to the *Journal of Neuroscience*.

6.1 Preface

Standard *in vitro* models for studying the pathophysiology of human neurons are usually based on pure cultures of neurons, either isolated from neuronal tissue or derived from PSCs, and cultivated under 2D conditions. These monolayers have been proven as useful tools to research disease mechanisms and to identify neuroprotective compounds (Nguyen et al. 2011; Cooper et al. 2012; Sánchez-Danés et al. 2012; Reinhardt, Schmid et al. 2013; Spathis et al. 2017). However, a downside of these cultures is that they cannot recapitulate relevant physiological features of the human brain, like cytoarchitecture and cell–cell interactions. This might cause ineffectiveness in clinical trials of compounds that have been only verified in neuronal monocultures (Abe-Fukasawa et al. 2018). The establishment of stem cell–derived brain organoids enabled to resemble key aspects of the human brain development *in vitro*, and thus provide a platform for advanced drug screening (Kelava et al. 2016a; Di Lullo et al. 2017). To gain more insights about the specific features of hMOs and thereby evaluating their application for potential drug discovery, we investigated the presence of neuronal subtypes and their electrophysiological activity. We demonstrated that hMOs exhibit neuronal functional properties during the course of differentiation and contain dopaminergic, GABAergic, glutamatergic, and serotonergic neurons.
With this detailed characterisation of hMOs, we demonstrated the presence of a progressive maturation of heterogenous, post–mitotic neuronal cell populations, which are functionally interconnected. Thus, this advanced 3D model, recapitulating complex interactions of mDANs with other cells of the central nervous system (CNS), might be able to give novel insights about pathomechanisms of multifactorial diseases, like PD.

This publication is the result of my PhD studies. I derived the midbrain floor plate neural precursor cell (mfNPC) lines and generated all hMOs analysed in this manuscript. S. Bolognin elaborated the MATLAB scripts for the high–content image analysis. The experimental part of the single–cell RNA sequencing (scRNA–seq) was performed by K. Grzyb. S. Magni performed and evaluated the computational analysis of the scRNA–seq data, which can be found in Figure 1C–F and Figure 2C–F. Apart from these mentioned exceptions, I designed and conducted the experiments, prepared the figures and wrote the original manuscript.

Single-cell transcriptomics reveals multiple neuronal cell types in human midbrain-specific organoids

Lisa M. Smits[1], Stefano Magni[1], Kamil Grzyb[1], Paul MA. Antony[1], Rejko Krüger[1], Alexander Skupin[1,2], Silvia Bolognin[1] and Jens C. Schwamborn[1]

[1]Luxembourg Centre for Systems Biomedicine (LCSB), University of Luxembourg, Belvaux Luxembourg

[2]University California San Diego, La Jolla, CA, USA

Corresponding author

Prof. Dr. Jens C. Schwamborn
jens.schwamborn@uni.lu

Keywords: neural stem cells, midbrain organoids, neuronal subtypes, single-cell RNA-sequencing, electrophysiological activity

Abstract

Human stem cell-derived organoids have great potential for modelling physiological and pathological processes. They recapitulate *in vitro* the organisation and function of a respective organ or part of an organ. Human midbrain organoids (hMOs) have been described to contain midbrain-specific dopaminergic neurons that release the neurotransmitter dopamine. However, the human midbrain contains also additional neuronal cell types, which are functionally interacting with each other. Here, we analysed hMOs at high-resolution by means of single-cell RNA-sequencing (scRNA-seq), imaging and electrophysiology to unravel cell heterogeneity. Our findings demonstrate that hMOs show essential neuronal functional properties as spontaneous electrophysiological activity of different neuronal subtypes, including dopaminergic, GABAergic, and glutamatergic neurons. Recapitulating these *in vivo* features makes hMOs an excellent tool for *in vitro* disease phenotyping and drug discovery.

Introduction

Current *in vitro* approaches to model physiology and pathology of human neurons are mainly based on pure cultures of neurons grown under 2D conditions. It has been shown that the differentiation potential of human induced pluripotent stem cells (iPSCs) provides a unique source of different neural cell types (Takahashi and Yamanaka, 2006). Until now, many protocols for generating iPSC-derived neural cultures have been described. The resulting cell culture monolayers have been proven as useful tools to study disease mechanisms and to identify potential neuroprotective compounds (Nguyen et al., 2011; Cooper et al., 2012; Sánchez-Danés et al., 2012; Reinhardt et al., 2013b; Ryan et al., 2013, Spathis et al., 2017). However, these culture conditions do not recapitulate several characteristics, which are relevant to the human brain, like cyto-architecture or complex cell-cell interactions. This may result in inaccurate modelling of the human brain (patho-)physiology with the consequence that candidate compounds might prove efficacy in 2D *in vitro* studies but are ineffective in clinical trials or vice versa (Abe-Fukasawa et al., 2018). The recent establishment of new 3D neuronal cell culture models has contributed to mimic key aspects of human brain development (Lancaster et al., 2013; Tieng et al., 2014; Muguruma et al., 2015; Jo et al., 2016; Qian et al., 2016; Monzel et al., 2017). Studies using human cerebral brain organoids have shown the acquisition of neuronal maturity and network activity (Quadrato et al., 2017; Matsui et al., 2018). Their complex, multicellular architecture enables the study of neuronal diseases and has already led to novel insights on e.g. Zika virus-induced microcephaly (Ming et al., 2016; Qian et al., 2017). Besides this unique *in vitro* disease modelling potential, human brain organoids provide a platform for advanced drug screening (Kelava and Lancaster, 2016; Di Lullo and Kriegstein, 2017). In this study, we focused on a detailed characterisation of the different neuronal subtypes in human midbrain-specific organoids (hMOs). With single-cell transcriptome analysis, we examined the presence of different neuronal subtypes, and subsequently studied the effect of chemical compounds on the electrophysiological activity of the neuronal network. Our findings demonstrate that hMOs contain, beside dopaminergic neurons, other neuronal subtypes including GABAergic, glutamatergic, and serotonergic neurons. hMOs showed essential neuronal functional properties during the course of differentiation, like synapse formation and spontaneous electrophysiological activity. These features indicate that hMOs recapitulate specific characteristics of functional human midbrain tissue, thus making them a valuable resource for *in vitro* disease modelling and drug discovery.

Material and Methods

Ethics Statement

Written informed consent was obtained from all individuals who donated samples to this study and the here conduced work was approved by the responsible ethics commissions. The cell lines used in this study are summarised in Table 1.

Pluripotent Stem Cell culture

hiPSC lines were provided by Bill Skarnes, Wellcome Trust Sanger Institute (iPSC Bill), Alstem (iPS15, derived from human peripheral blood mononuclear cells, episomal reprogrammed) or previously described in Reinhard *et alia* (Reinhardt et al., 2013b). The cells were cultured on Matrigel-coated (Corning, hESC-qualified matrix) plates, maintained in Essential 8 medium (Thermo Fisher Scientific) and cultured with and split 1:6 to 1:8 every four to five days using Accutase (Sigma). 10 µM ROCK inhibitor (Y-27632, Abcam) was added to the media for 24 h following splitting.

Derivation of midbrain floorplate neural progenitor cells

The derivation and maintenance of

midbrain floorplate neural progenitor cells (mfNPCs), has been described previously (Smits et al., 2019).
In brief, embryoid bodies (EBs) were formed with 2,000 iPSCs each, using AggreWell 400 (Stemcell Technologies). The cells were cultured in Knockout DMEM (Invitrogen) with 20 % Knockout Serum Replacement (Invitrogen), 100 µM beta-mercaptoethanol (Gibco), 1 % nonessential amino acids (NEAA, Invitrogen), 1 % penicillin/streptomycin/glutamine (Invitrogen), freshly supplemented with 10 µM SB-431542 (SB, Ascent Scientific), 250 nM LDN-193189 (LDN, Sigma), 3 µM CHIR99021 (CHIR, Axon Medchem), 0.5 µM SAG (Merck), and 5 µM ROCK inhibitor (Sigma). After 24 h, EBs were transferred to a non-treated tissue culture plate (Corning). On day two, medium was replaced with N2B27 medium consists of DMEM-F12 (Invitrogen)/Neurobasal (Invitrogen) 50:50 with 1:200 N2 supplement (Invitrogen), 1:100 B27 supplement lacking vitamin A (Invitrogen) with 1 % penicillin/streptomycin/glutamine, supplemented with 10 µM SB, 250 nM LDN, 3 µM CHIR, 0.5 µM SAG. On day four and six, medium was exchanged with the same but including 200 µM ascorbic acid (AA, Sigma). On day eight, EBs with neuroepithelial outgrowth were triturated into smaller pieces and diluted in a 1:10 ratio. For following passages, 1x TrypLE Select Enzyme (Gibco)/0.5mM EDTA (Invitrogen) in 1x PBS was used and 10,000 to 20,000 cells per 96-well ultra-low attachment plate (round bottom, Corning) were seeded. The cells were always kept under 3D culture conditions and from passage 1 on cultured in N2B27 medium freshly supplemented with 2.5 µM SB, 100 nM LDN, 3 µM CHIR, 200 µM AA, and 0.5 µM SAG. After every cell split the ultra-low attachment plate was centrifuged for 3 min at 200 xg to assure the aggregation of single cells at the bottom of the well. Additionally, 5 µM ROCK inhibitor was added. The cells were split every 7 to 14 days and the medium was changed every third day. After four to five passages, mfNPCs were used as a starting population for hMOs.

Generation of midbrain-specific organoids

To start the generation of hMOs, 3,000 cells per well were seeded to an ultra-low attachment 96-well round bottom plate, centrifuged for 3 min at 200 xg and kept under maintenance conditions for seven days. LDN and SB were withdrawn of mfNPC expansion medium and after three additional days, the concentration of CHIR was reduced to 0.7 µM. On day nine of differentiation, medium was changed to neuronal maturation N2B27 medium including 10 ng/ml BDNF (Peprotech), 10 ng/ml GDNF (Peprotech), 200 µM AA (Sigma), 500 µM dbcAMP (Sigma), 1 ng/ml TGF-β3 (Peprotech), 2.5 ng/ml ActivinA (Life Technologies) and 10 µM DAPT (Cayman). The organoids were kept under static culture conditions with media changes every third day for 35 or 70 days. Detailed information about the generation of hMOs has been published recently (Smits et al., 2019).

Immunofluorescence

hMOs were fixed with 4 % PFA overnight at 4 °C and washed 3x with PBS for 15 min. After treatment, they were embedded in 3-4 % low-melting point agarose in PBS. The solid agarose block was sectioned with a vibratome (Leica VT1000s) into 50 µm sections. The sections were blocked on a shaker with 0.5 % Triton X-100, 0.1 % sodium azide, 0.1 % sodium citrate, 2 % BSA and 5 % normal goat or donkey serum in PBS for 90 min at RT. Primary antibodies were diluted in the same solution but with only 0.1 % Triton X-100 and were applied for 48 h at 4 °C.
After incubation with the primary antibodies (Table 2), sections were washed 3x with PBS and subsequently blocked for 30 min at RT on a shaker. Then sections were incubated with the secondary antibodies in 0.05 % Tween-20 in PBS for

two hours at RT and washed with 0.05 % Tween-20 in PBS and Milli-Q water before they were mounted in Fluoromount-G mounting medium (Southern Biotech).
STAINperfect Immunostaining Kit (ImmuSmol) was used according to manufacturer's protocol to detect dopamine, serotonin, GABA and L-glutamine. Nuclei were counterstained with Hoechst 33342 (Invitrogen).
For qualitative analysis, three randomly selected fields per organoid section were acquired with a confocal laser scanning microscope (Zeiss LSM 710) and images were further processed with OMERO Software. Three-dimensional surface reconstructions of confocal z-stacks were created using Imaris software (Bitplane).

Quantitative Image analysis
Immunofluorescence 3D images of hMOs were analysed in Matlab (Version 2017b, Mathworks). The in-house developed image analysis algorithms automate the segmentation of nuclei, astrocytes and neurons with structure-specific feature extraction. The image preprocessing for the segmentation of nuclei was computed by convolving the raw Hoechst channel with a gaussian filter. By selecting a pixel threshold to identify apoptotic cells, a pyknotic nuclei mask was identified and subtracted from the nuclei mask.
For the segmentation of neurons, a median filter was applied to the raw TUJ1 channels. The expression levels were expressed in two ways: i) positive pixel of the marker, normalised by the pixel count of Hoechst; ii) cells positive for a marker expressed as a percentage of the total number of cells. In this latter case, the nuclei were segmented and a watershed function was applied. Considering the high cell density of the specimens, steps to ensure high quality in the segmentation process were implemented and structure with a size higher than 10,000 pixels were removed (this indicated incorrected segmentation e.g. clumps). In the nuclei successfully segmented as a single element, a perinuclear zone was identified. In case the marker of interest was positive in at least 1 % of the perinuclear area, the corresponding cell was considered as positive.

Single-cell RNA-sequencing using Droplet-Sequencing (Drop-Seq)
scRNA-seq data were generated using the Droplet-Sequencing (Drop-Seq) technique (Macosko et al., 2015) as described previously (Walter, 2019). In this work, we performed scRNA-seq of hMOs derived from hiPSC line H4 (see Table 1). For each time point, 35 d and 70 d after dopaminergic differentiation, we pooled and analysed 30 hMOs each.

Pre-processing of the digital expression matrices from scRNA-seq
The result of the Drop-Seq scRNA-seq pipeline and subsequent bioinformatics processing is a digital expression matrix (DEM) representing the number of mRNA molecules captured per gene per droplet. Here, we obtained two DEMs, one corresponding to 35 d hMOs and the other to 70 d hMOs. After quality cut based on knee plots, we retained for each sample 500 cells with the highest number of total transcripts measured and performed normalisation of the DEM separately. Finally, the two DEMs were merged for the comparison analysis of the two time points based on 24,976 expressed genes in 1,000 cells. The data was analysed by our customized Python analysis pipeline (version 3.6.0, with anaconda version 4.3.1) including dimensionality reduction by t-distributed stochastic neighbourhood embedding (t-SNE) (van der Maarten and Hinton 2008) and differentially gene expression analysis.

Analysis of DEGs from scRNA-seq data
To determine, which and how many genes were differentially expressed between 35 d and 70 d hMOs, we applied one-way ANOVA test, a one-way ANOVA test on ranks (Kruskal-Wallis test), and a Mutual Information based test. The minimum p-value obtained for each gene across these

three tests was retained and statistical significance was set to $p < 0.01$ after Bonferroni correction for differentially expressed genes (DEG).

Cumulative gene expressions from scRNA-seq data

From literature, we extracted cell-type specific gene lists (Table 3) for stem cells, neurons, and neuronal subtypes (dopaminergic, glutamatergic, GABAergic and serotonergic neurons) (Reinhardt et al., 2013a; La Manno et al., 2016; Cho et al., 2017). Note, that not all genes listed therein have been measured in our dataset, these were highlighted in Table 3.

For each list we defined a score, which we refer to as cumulative gene expression, computed as the sum of the corresponding genes from normalized DEM for each cell. Since the expression levels were measured at single cell level, we can consider the cells distributions across the cumulative genes expression scores (Figure 1D and Figure 2A). These histograms exhibit the cumulative gene expression scores normalised to their maxima on the horizontal axis. Thus, on the horizontal axis, a value of 1 corresponds to the maximal cumulative gene expression for one list of genes, while 0 corresponds to no expression of any genes from that list. The vertical axis exhibits the number of cells falling into the corresponding bin of the histogram. In each subpanel the distributions for day 35 and for day 70 are shown. Population differences were assessed by Z-test of the means with Bonferroni correction.

Gene-gene correlations from scRNA-seq data

From the scRNA-seq data we also computed gene-gene Pearson correlation coefficients for stemness- and neuron-specific genes. Analysis was performed independently for the two samples (35d DA dif and 70d DA dif) resulting in two correlation matrices (Figure 1E).

In the lower triangular matrix all correlation values are shown, whereas the upper triangular matrix only statistical significant correlations (p-value < 0.05 after Bonferroni correction). For visual clarity, diagonal elements and not detected genes were excluded.

Fold changes of gene expression from scRNA-seq data

For individual genes, we considered the normalized gene expression across the cell populations. For each selected gene, we compared its expression within the 35 d cells with the one within the 70 d cells by computing the logarithmic fold change (log2FC). We performed this analysis for the neuron specific genes (Figure 1F) and neuronal subtypes including glutamatergic neurons, GABAergic neurons, and dopaminergic neurons (Figure 2B-D) where negative values indicate that a gene is less expressed at day 35 than at day 70 and positive numbers the opposite. p-value are based on Z-test with Bonferroni correction and significance levels correspond to * = p-value < 0.05, ** = p-value < 0.01, *** = p-value < 0.001, **** = p-value < 0.0001. Error bars represent SEM based on the individual sample average and error propagation.

TEM Morphology

63 day old hMO specimens were immersion-fixed in a solution of 2 % PFA and 2.5 % glutaraldehyde in 0.1 M sodium cacodylate buffer (pH 7.4, Electron Microscopy Sciences, Hatfield, PA) for 3 h, rinsed several times in cacodylate buffer and further post-fixed in 2 % glutaraldehyde in 0.1 M sodium cacodylate buffer for 2 h at room temperature on a gentle rotator; fixative was allowed to infiltrate an additional 48 h at 4 °C. Specimens were rinsed several times in cacodylate buffer, post-fixed in 1.0 % osmium tetroxide for 1 h at room temperature and rinsed several times in cacodylate buffer. Samples were then dehydrated through a graded series of ethanols to 100 % and dehydrated briefly in 100 % propylene oxide. Tissue was then allowed to pre-infiltrate 2 h in a 2:1 mix of

propylene oxide and Eponate resin (Ted Pella, Redding, CA), then transferred into a 1:1 mix of propylene oxide and Eponate resin and allowed to infiltrate overnight on a gentle rotator. The following day, specimens were transferred into a 2:1 mix of Eponate resin and propylene oxide for a minimum of 2 h, allowed to infiltrate in fresh 100 % Eponate resin for several hours, and embedded in fresh 100 % Eponate in flat molds; polymerization occurred within 24-48 h at 60 °C. Thin (70 nm) sections were cut using a Leica EM UC7 ultramicrotome, collected onto formvar-coated grids, stained with uranyl acetate and Reynold's lead citrate and examined in a JEOL JEM 1011 transmission electron microscope at 80 kV. Images were collected using an AMT digital imaging system with proprietary image capture software (Advanced Microscopy Techniques, Danvers, MA).

Microelectrode array

The Maestro microelectrode array (MEA, Axion BioSystems) platform was used to record spontaneous activity of the hMOs. A 48-well MEA plate containing a 16-electrode array per well was precoated with 0.1 mg/ml poly-D-lysine hydrobromide (Sigma-Aldrich). 60-70 days old organoids of two different passages were briefly treated for 5 min with 1X TrypLE Select Enzyme, resuspend in 10 µg/ml laminin (Sigma-Aldrich) and placed as a droplet onto the array. After 1 h incubation, neuronal maturation media was added and cells were cultured for 1-2 weeks. Spontaneous activity was recorded at a sampling rate of 12.5 kHz for 5 min at 37 °C over several days. Axion Integrated Studio (AxIS 2.1) was used to assay creation and analysis. A Butterworth band pass filter with 200-3000 Hz cutoff frequency and a threshold of 6x SD were set to minimise both false-positives and missed detections. The spike raster plots were analysed using the Neural Metric Tool (Axion BioSystems). Electrodes with an average of ≥5 spikes/min were defined as active, for the pharmacological treatment 24 electrodes were analysed. The organoids were consecutively treated with Gabazine, D-AP-5, NBQX (Cayman Chemical, end concentration: 50 mM each), and Quinpirole (Sigma Aldrich, end concentration: 5µM). To block all neuronal activity and thus verify spontaneous spiking activity of the cells, tetrodotoxin (TTX, Cayman Chemical, 1 µM) was applied at the end. The spike count files generated from the recordings were used to calculate the number of spikes/active electrode/minute. Further details regarding the MEA system were previously described (Bardy et al., 2015).

Statistical analyses

If not stated otherwise, experiments were performed with three independently generated organoid cultures from three different cell lines (n=9). Gaussian distribution was evaluated by performing D'Agostino & Pearson omnibus normality test. In case the data were normally distributed, Grubbs' test was performed to detect significant outliers. Unpaired t-test with Welch's correction or nonparametric Kolmogorov-Smirnov test were performed to evaluate statistical significance. Data are presented as mean ±SEM. The statistical analyses of scRNA-seq data are described in the corresponding sections.

Results

Characterisation of the neuronal differentiation dynamics in midbrain-specific organoids

Previously, we demonstrated that human iPSC-derived midbrain floor plate neural progenitor cells (mfNPCs) can give rise to 3D human organoids that contain high amounts of dopaminergic neurons (Smits et al., 2019). To have a better insight into the dynamics of the neuronal differentiation, we evaluated TUJ1 staining, as a marker for neuronal differentiation, at two time-points during the differentiation of hMOs (Figure 1A). An in-house developed image analysis algorithm was used to segment Hoechst positive nuclei and TUJ1 positive neurons to create specific

nuclear and neuronal masks. These masks contain all positive pixel counts for Hoechst and TUJ1, respectively.

The TUJ1 signal normalised to the Hoechst signal significantly increased after 70 days compared to 35 days, demonstrating a progressive differentiation into post-mitotic neurons. Whereas, the nuclear marker signal was significantly decreased at 70 days compared to 35 days, which might indicate selection in the cell population, as reported by Suzanne and Steller (2013) (Figure 1B). Along with these findings, we observed that the size of the organoids significantly increased during the course of the differentiation. This suggests that the increased TUJ1 volume and organoid size are due to the increased tissue complexity (e.g. neuronal arborisation) within the hMO (Figure 1B).

To further characterise the neuronal differentiation dynamics at the gene expression level, we performed scRNA-seq on samples from the two time-points mentioned above. The experiments were conducted using the Drop-Seq technique (Macosko et al., 2015), and the standard bioinformatics processing of the data resulted in two sample specific digital expression matrices (DEM), which were further normalised and merged (see Methods section).

To visualise the so-obtained high-dimensional single-cell data, we performed dimensionality reduction of the DEM by t-distributed stochastic neighbourhood embedding (t-SNE) (van der Maarten and Hinton 2008) where each dot corresponds to a cell (Figure 1C). This distribution shows that cells originating from organoids at 35 days and 70 days only partially cluster together (left panel in Figure 1C). This underlines that there are remarkable differences in the overall gene expression between the samples at days 35 and 70. The distribution of the cumulative gene expression (right panel in Figure 1C) shows that the neuronal gene expression is increased in a large fraction of the cells suggesting that this fraction of cells may not represent mature neurons.

To determine the differences in neuron-specific cumulative gene expression over time, we plotted the distributions of cells across the cumulative gene expression scores (Figure 1D). Here, we used the scores obtained from the lists of precursor cell-specific genes (indicated as "stemness genes") and those of neurons. While the distributions of cells across the cumulative gene expression for precursors is very similar between day 35 and 70 (upper panel), we observed a significant difference between the distributions of cells across the neuronal cumulative gene expression (lower panel). Cells at 35 days tend to express the neuron-specific genes significantly more than cells at 70 days.

To further investigate how the differentiation of precursor cells into neurons evolves over time, we computed the gene-gene correlation for the genes of the neuron-specific list and of the stemness-specific list, altogether. Comparing these two lists, we found that at 35 days there are low values of correlation between genes exclusively specific for neurons or stem cells and also between neuron- and stemness-specific genes (Figure 1E, left heatmap). Very few of the correlation values are significantly different from zero and were substituted by zeros in the upper triangular matrix (Figure 1E, left heatmap). While correlations between stemness genes and neuron-stemness correlations remain similar at day 70 to day 35, correlations between neuron-specific genes increased considerably at day 70. This significant increase of neuron-specific gene correlations indicates a higher commitment of the cells towards the neuronal fate at day 70 compared to day 35 and supports the finding of a progressive maturation of post-mitotic neurons (Figure 1E).

Next, we wanted to elucidate which individual genes contribute to the differences between the gene expression of cells at day 35 and cells at day 70. For this purpose, we performed an analysis of differentially expressed genes (DEGs) across the whole transcriptome. From the 24,976 distinct transcripts measured, 1,311 were significantly differentially expressed

between day 35 and 70 (approximately 5 % of all genes expressed, p-value < 0.01 after Bonferroni correction, see Supplementary Table 1). When intersecting the list of DEGs with the stemness-specific genes, we found that approximately 30 % of the stemness-specific genes are DEGs (see Table 4). Similarly, 42 % (corresponding to 11 genes) of the neuron-specific genes are differentially expressed (Table 3 and 4). Hence, the percentages of DEGs within the neuron-specific and stemness-specific lists are remarkably higher than the percentage of DEGs across the whole transcriptome. These notable changes further indicates the induction of the neuronal differentiation and progressive maturation.

Next, we focused on individual neuron-specific genes and compared their expression over time. For each gene we computed the log2 fold-change between the average expression at day 35 and day 70 (Figure 1F). Consistent with the findings shown in Figure 1D, the majority of genes were significantly higher expressed at day 35 than at day 70 based on Z-test analysis corrected for multiple hypotheses testing. Interestingly, among the genes expressed at day 35 we found genes that are involved in neurogenesis (EBF3 (Garcia-Dominguez et al., 2003)), neuronal migration and differentiation (L1CAM (Patzke et al., 2016)), whereas genes expressed at day 70 reflect more specific subpopulations of neurons, like GABAergic neurons (DLX1, CALB2 (Al-Jaberi et al., 2015)) in agreement with the separate DEG analysis across the whole transcriptome (see Table 4).

Midbrain-specific organoids consist of different neuronal subtypes

From previous studies we know that hMOs are rich in dopaminergic neurons (Jo et al., 2016; Qian et al., 2016; Monzel et al., 2017; Smits et al., 2019; Kim et al., 2019). We wanted to further explore which other neuronal subtypes develop besides midbrain dopaminergic neurons within the hMOs.

Therefore, we investigated the expression of genes typical for dopaminergic, glutamatergic, GABAergic, and serotonergic neurons by analysing the scRNA-seq data. We plotted the distributions of cells across the cumulative gene expression scores, which were obtained from the lists of genes specific of a neuronal subtype (Figure 2A). While the cell distribution over cumulative expression score for GABAergic neurons was very similar between the samples at 35 days and 70 days (Figure 2A, third panel), we detected statistically significant differences between the distributions of cells over scores for the other three types of neurons. The expression of the selected genes for the glutamatergic and dopaminergic neurons was increased at day 35 compared to day 70, which is consistent with the observations for the neuron specific score (Figure 1D). Interestingly, we discovered that the vast majority, approximately more than 700 of the 1000 cells, lacks completely expression of genes specific for serotonergic neurons (Figure 2C, fourth panel). Thus, we disregarded this neuronal subtype in the subsequent analyses and focused next on individual genes specific of dopaminergic, glutamatergic, and GABAergic neurons, by computing the log2 fold-change between the average gene expression at day 35 and at day 70 (Figure 2B-D). In each of the three lists, the majority of the genes for which a statistically significant difference is present are actually more expressed at 35 days than at 70 days, consistently with the findings of Figure 2A.

When intersecting the list of 1,311 DEGs across the whole transcriptome with the lists of dopaminergic, glutamatergic and GABAergic neurons, we found that 42 %, 34 %, and 17 % of the genes were DEGs within these lists, respectively (see Supplementary Table 1 and Table 4). Again, all of these percentages are considerably higher than the 5 % of DEGs across the whole transcriptome indicating that neuronal subtypes specific genes, in particular dopaminergic and glutamatergic, are highly represented within DEGs during hMO development.

Lastly, to verify the presence of the addressed neuronal subtypes we conducted an immunohistochemistry staining for the

respective neurotransmitters. This allowed us to robustly detect dopaminergic, glutamatergic and GABAergic neurons as well as even a few serotonergic neurons within hMOs (Figure 2E).

Midbrain-specific organoids express synaptic proteins

After identifying the presence of neurons and even specific neuronal subtypes on transcriptome expression levels by means of neurotransmitter staining and scRNA-seq, we investigated the actual interaction among the neuronal cells within the hMOs. We previously showed that hMOs synthesise and release the neurotransmitter dopamine (Smits et al., 2019). This already suggests the establishment of a functional neuronal network. The basic requirement for neuronal network formation is the development of synapses. Hence, we evaluated the presence of synaptic connections using the presynaptic marker SYNAPTOPHYSIN and the postsynaptic marker PSD95 in organoid sections after 70 days of culture (Figure 3A). Both proteins were detectable in a puncta-like organisation, which is expected for synapses. With a subsequent 3D surface reconstruction, we observed that the signals for SYNAPTOPHYSIN and PSD95 were localised in close proximity, forming pre- and postsynaptic puncta (Figure 3B). To further investigate whether actual functional synaptic connections were formed in the hMOs, we used a transmission electron microscopy (TEM) approach (Figure 3C). EM micrographs show excitatory synapses characterised by electron dense post-synaptic density proteins (full arrow) and pre-synaptic synapse (asterisks) loaded with synaptic vesicles.

Midbrain-specific organoids develop GABAergic, glutamatergic and dopaminergic electrophysiological activity

Non-invasive multielectrode array (MEA) measurements can give insights into physiological properties, like the generation of spontaneous neuronal activity of *in vitro* cultured and self-organised networks (Luhmann et al., 2016). As the assessment of neuronal activity is important to evaluate the functional maturation, we tested the spontaneous electrophysiological activity of hMOs by MEA measurements (Odawara et al., 2016). We measured extracellular field potentials, which are generated by action potentials. At days 50-60 of differentiation, hMOs were seeded in 48-well tissue culture MEA plates on a grid of 16 electrodes (Figure 4A and B). After 10-20 days of culturing, we recorded spontaneous activity, on several electrodes, over several days, in the form of mono- and biphasic spikes (Figure 4Aii). To investigate which neuronal subtypes were functionally active in the hMOs, we applied specific drugs following a previously reported experimental design (Illes et al., 2014). We recorded spiking patterns from 24 active electrodes: in Figure 4C and D representative recordings of one electrode are displayed. After treating the organoids with gabazine, a $GABA_A$ receptor antagonist, we detected an increase of spontaneous spiking (22.5 % increase, Figure 4Dii). Following the gabazine-induced disinhibition, we applied the AMPA/Kainate-receptor antagonist NBQX and the NMDA-receptor antagonist D-AP-5. The inhibition of the excitatory neurons resulted in a 28.1 % decrease of spontaneous activity (Figure 4Diii). After the inhibition of GABAergic and glutamatergic neurons in the hMOs, we added the D2/D3 receptor agonist quinpirole (Figure 4C and Div), which resulted in a 47.8 % decrease of neuronal activity. Confirming the findings displayed in Figure 2, we conclude from these experiments that hMOs contain functional GABAergic, glutamatergic and dopaminergic neurons.

Discussion

The *in vitro* human brain organoid technology has become a valuable tool allowing advances in the field of basic

research as well as in translational applications (Fatehullah et al., 2016). Organoids specifically modelling the human midbrain hold great promise for studying human development and for modelling Parkinson's disease (PD) (Jo et al., 2016; Monzel et al., 2017; Kim et al., 2019; Smits et al., 2019). In contrast to 2D monolayer cultures, hMOs can recapitulate complex interactions of midbrain dopaminergic neurons with other cell types of the central nervous system (CNS) in a 3D environment. However, human midbrain brain organoid research has so far focused mainly on dopaminergic neurons. In a detailed study of Borroto-Escuela et al. (2018) it has been described that released dopamine can diffuse into synaptic regions of glutamate and GABA synapses and directly affect other striatal cell types possessing dopamine receptors. Furthermore, *substantia nigra* dopaminergic neurons are directly controlled by GABAergic input (Tepper and Lee, 2007). Evidences from these studies suggest that the presence of other neuronal subtypes is important to model multifactorial disease like PD. In our study, we have demonstrated that the derivation of hMOs leads to functional neuronal networks, containing different neuronal subtypes of the human midbrain. Single-cell transcriptomic data from hMOs demonstrated that there is an increased expression of neuronal-specific genes in 35 days compared to 70 days old hMOs. On the other hand, the gene-gene correlations between only neuron-specific genes increased considerably at day 70, suggesting an increased commitment of cells towards the neuronal cell fate during the course of the organoid development. This further supports the finding of a progressive maturation of post-mitotic neurons (Figure 1D and E). The identification of these neuron-specific genes revealed that the genes upregulated at the earlier time point are relevant in the process of neurogenesis and neuronal migration and differentiation (EBF3 (Garcia-Dominguez et al., 2003), L1CAM (Patzke et al., 2016)). Whereas the upregulated genes at the later time point have been for instance implicated in subpopulations like GABAergic neurons (DLX1, CALB2 (Al-Jaberi et al., 2015)). (Figure 1F). This indicates a higher commitment of the cells toward their intended fate and a progressive maturation of the post-mitotic neurons within the hMOs. Furthermore, single-cell analysis of the hMOs also proved the presence of specific neuronal subtypes, like dopaminergic, glutamatergic and GABAergic neurons. While the scRNA-seq data were not fully conclusive concerning serotonergic neurons, a staining approach allowed to detect at least some of these neurons (Figure 2). Supporting the findings of currently published midbrain-specific organoid models (Jo et al., 2016; Qian et al., 2016; Monzel et al., 2017; Smits et al., 2019), we detected a significant upregulation of tyrosine hydroxylase (TH) within the cell population of 70 days old hMOs compared to 35 days old hMOs. The activity of neurons and their different receptors can be analysed by the specific response to chemical compounds. It has been shown that quinpirole, a specific D2/D3 receptor agonist, suppresses the firing in hMOs (Jo et al., 2016; Monzel et al., 2017). In addition to the previously reported analyses in hMOs, we blocked inhibitory and excitatory communication, to further isolate and attribute the recorded signals to neuronal subtypes. Gabazine induces a disinhibition of GABAergic neurons, whereas NMDA-receptor and AMPA/Kainate-receptor antagonists inhibit glutamatergic excitatory communication (Illes et al., 2014). Together with the characteristic hallmarks of synapse formation (Figure 3A-C) and the previous findings of dopamine release (Smits et al., 2019), these data confirm the presence of functional dopamine receptors in dopaminergic neurons as well as functional GABAergic and glutamatergic neurons within hMOs. As neurons do not exist in isolation in the CNS but form functional networks with other neurons and non-neuronal cells, it is important to expand our research of neurodegenerative diseases using 3D models that are able to recapitulate cell autonomous as well as non-cell autonomous aspects. Utilising 3D cell culture models that comprise a variety of neuronal subtypes

could lead to new insights into the selective vulnerabilities, which are observed in neurodegeneration. Indeed, evidence suggests that specific regulation of the excitability of dopaminergic neurons by other neuronal subtypes in the midbrain might explain their selective vulnerability in PD (Korotkova et al., 2004). This underlines the importance and the enormous potential for future disease modelling of the here described hMO model, as it contains functionally connected heterogeneous neuronal cell populations.

Acknowledgments

We would like to thank Dr. Sebastian Illes (University of Gothenburg, Sweden) for his help with the experimental MEA design and Diane Capen (Massachusetts General Hospital, Boston, USA) for her EM work. We thank Dr. Jared Sterneckert (Technical University of Dresden, Germany) and Dr. Bill Skarnes (The Wellcome Trust Sanger Institute, Cambridge, UK) for human iPSC lines. Furthermore, we would like to thank Yohan Jarosz from the LCSB Bioinformatics Core Group for his support in data management. This project was supported by the LCSB pluripotent stem cell core facility. The JCS lab is supported by the Fonds National de la Recherché (FNR) (CORE, C13/BM/5791363 and Proof-of-Concept program PoC15/11180855 & PoC16/11559169). This is an EU Joint Programme-Neurodegenerative Disease Research (JPND) project (INTER/JPND/14/02; INTER/JPND/15/11092422). Further support comes from the SysMedPD project which has received funding from the European Union's Horizon 2020 research and innovation programme under grant agreement No 668738. LMS is supported by fellowships from the FNR (AFR, Aides à la Formation-Recherche). Electron microscopy was performed in the Microscopy Core of the Center for Systems Biology/Program in Membrane Biology, which is partially supported by an Inflammatory Bowel Disease Grant DK043351 and a Boston Area Diabetes and Endocrinology Research Center (BADERC) Award DK057521. SM is supported by the University of Luxembourg and the National Research Fund through the CriTiCS DTU FNR PRIDE/10907093/CRITICS. KG and AS were supported by the Luxembourg National Research Fund (FNR) through the C14/BM/7975668/CaSCAD project and AS additionally by the National Biomedical Computation Resource (NBCR) through the NIH P41 GM103426 grant from the National Institutes of Health.

Author Contributions

LMS designed and performed cell culture and imaging experiments, prepared the figures and wrote the original draft. KG performed the scRNA-seq experiments and related bioinformatics approaches. SM performed the computational analysis of the single-cell RNA-Seq data, edited the manuscript and contributed to the figures. PMAA contributed to the development of 3D image analysis. RK supervised image analysis design. AS supervised the design and implementation of the single-cell experiments and associated computational data analysis. SB initiated the project, supervised it and edited the manuscript. JCS conceived and supervised the project, designed the experiments and edited the manuscript.

Competing financial interests

We declare no competing interests.

Data Availability

The data that support the findings of this study are public available at this doi: www.doi.org/10.17881/lcsb.20190326.01.

References

Abe-Fukasawa, N., Otsuka, K., Aihara, A., Itasaki, N., and Nishino, T. (2018). Novel 3D Liquid Cell Culture Method for Anchorage-independent Cell Growth, Cell Imaging and Automated Drug Screening. *Sci Rep* 8(1)**,** 3627. doi: 10.1038/s41598-018-21950-5.

Al-Jaberi, N., Lindsay, S., Sarma, S., Bayatti, N., and Clowry, G.J. (2015). The early fetal development of human neocortical GABAergic interneurons. *Cereb Cortex* 25(3)**,** 631-645. doi: 10.1093/cercor/bht254.

Bardy, C., van den Hurk, M., Eames, T., Marchand, C., Hernandez, R.V., Kellogg, M., et al. (2015). Neuronal medium that supports basic synaptic functions and activity of human neurons in vitro. *Proceedings of the National Academy of Sciences***,** 201504393. doi: 10.1073/pnas.1504393112.

Borroto-Escuela, D.O., Perez De La Mora, M., Manger, P., Narvaez, M., Beggiato, S., Crespo-Ramirez, M., et al. (2018). Brain Dopamine Transmission in Health and Parkinson's Disease: Modulation of Synaptic Transmission and Plasticity Through Volume Transmission and Dopamine Heteroreceptors. *Front Synaptic Neurosci* 10**,** 20. doi: 10.3389/fnsyn.2018.00020.

Cho, G.S., Lee, D.I., Tampakakis, E., Murphy, S., Andersen, P., Uosaki, H., et al. (2017). Neonatal Transplantation Confers Maturation of PSC-Derived Cardiomyocytes Conducive to Modeling Cardiomyopathy. *Cell Rep* 18(2)**,** 571-582. doi: 10.1016/j.celrep.2016.12.040.

Cooper, O., Seo, H., Andrabi, S., Guardia-Laguarta, C., Graziotto, J., Sundberg, M., et al. (2012). Pharmacological rescue of mitochondrial deficits in iPSC-derived neural cells from patients with familial Parkinson's disease. *Sci Transl Med* 4(141)**,** 141ra190. doi: 10.1126/scitranslmed.3003985.

Di Lullo, E., and Kriegstein, A.R. (2017). The use of brain organoids to investigate neural development and disease. *Nat Rev Neurosci* 18(10)**,** 573-584. doi: 10.1038/nrn.2017.107.

Fatehullah, A., Tan, S.H., and Barker, N. (2016). Organoids as an in vitro model of human development and disease. *Nature Publishing Group* 18**,** 246-254. doi: 10.1038/ncb3312.

Garcia-Dominguez, M., Poquet, C., Garel, S., and Charnay, P. (2003). Ebf gene function is required for coupling neuronal differentiation and cell cycle exit. *Development* 130(24)**,** 6013-6025. doi: 10.1242/dev.00840.

Illes, S., Jakab, M., Beyer, F., Gelfert, R., Couillard-Despres, S., Schnitzler, A., et al. (2014). Intrinsically active and pacemaker neurons in pluripotent stem cell-derived neuronal populations. *Stem Cell Reports* 2(3)**,** 323-336. doi: 10.1016/j.stemcr.2014.01.006.

Jo, J., Xiao, Y., Sun, A.X., Cukuroglu, E., Tran, H.D., Goke, J., et al. (2016). Midbrain-like Organoids from Human Pluripotent Stem Cells Contain Functional Dopaminergic and Neuromelanin-Producing Neurons. *Cell Stem Cell* 19(2)**,** 248-257. doi: 10.1016/j.stem.2016.07.005.

Kelava, I., and Lancaster, M.A. (2016). Dishing out mini-brains : Current progress and future prospects in brain organoid research. *Developmental Biology* 420**,** 199-209. doi: 10.1016/j.ydbio.2016.06.037.

Kim, H., Park, H.J., Choi, H., Chang, Y., Park, H., Shin, J., et al. (2019). Modeling G2019S-LRRK2 Sporadic Parkinson's Disease in 3D Midbrain Organoids. *Stem Cell Reports* 12(3)**,** 518-531. doi: 10.1016/j.stemcr.2019.01.020.

Korotkova, T.M., Ponomarenko, A.A., Brown, R.E., and Haas, H.L. (2004). Functional diversity of ventral midbrain dopamine and GABAergic neurons. *Mol Neurobiol* 29(3)**,** 243-259. doi: 10.1385/MN:29:3:243.

La Manno, G., Gyllborg, D., Codeluppi, S., Nishimura, K., Salto, C., Zeisel, A., et al. (2016). Molecular Diversity of Midbrain Development in Mouse, Human, and Stem Cells. *Cell* 167(2)**,** 566-580.e519. doi: 10.1016/j.cell.2016.09.027.

Lancaster, M.A., Renner, M., Martin, C.A., Wenzel, D., Bicknell, L.S., Hurles, M.E., et al. (2013). Cerebral organoids model human brain development and microcephaly. *Nature* 501(7467)**,** 373-379. doi: 10.1038/nature12517.

Luhmann, H.J., Sinning, A., Yang, J.W., Reyes-Puerta, V., Stuttgen, M.C., Kirischuk, S., et al. (2016). Spontaneous Neuronal Activity in Developing Neocortical Networks: From Single Cells to Large-Scale Interactions. *Front Neural Circuits* 10**,** 40. doi: 10.3389/fncir.2016.00040.

Macosko, E.Z., Basu, A., Satija, R., Nemesh, J., Shekhar, K., Goldman, M., et al. (2015). Highly Parallel Genome-wide Expression Profiling of Individual Cells Using Nanoliter Droplets. *Cell* 161(5)**,** 1202-1214. doi: 10.1016/j.cell.2015.05.002.

Matsui, T.K., Matsubayashi, M., Sakaguchi, Y.M., Hayashi, R.K., Zheng, C., Sugie, K., et al. (2018). Six-month cultured cerebral organoids from human ES cells contain matured neural cells. *Neurosci Lett* 670**,** 75-82. doi: 10.1016/j.neulet.2018.01.040.

Ming, G.L., Tang, H., and Song, H. (2016). Advances in Zika Virus Research: Stem Cell Models, Challenges, and Opportunities. *Cell Stem Cell* 19(6)**,** 690-702. doi: 10.1016/j.stem.2016.11.014.

Monzel, A.S., Smits, L.M., Hemmer, K., Hachi, S., Moreno, E.L., van Wuellen, T., et al. (2017). Derivation of Human Midbrain-Specific Organoids from Neuroepithelial Stem Cells. *Stem Cell Reports* 8(5)**,** 1144-1154. doi: 10.1016/j.stemcr.2017.03.010.

Muguruma, K., Nishiyama, A., Kawakami, H., Hashimoto, K., and Sasai, Y. (2015). Self-Organization of Polarized Cerebellar Tissue in 3D Culture of Human Pluripotent Stem Cells. *Cell Reports* 10**,** 537-550. doi: 10.1016/j.celrep.2014.12.051.

Nguyen, H.N., Byers, B., Cord, B., Shcheglovitov, A., Byrne, J., Gujar, P., et al. (2011). LRRK2 mutant iPSC-derived DA neurons demonstrate increased susceptibility to oxidative stress. *Cell stem cell* 8**,** 267-280. doi: 10.1016/j.stem.2011.01.013.

Odawara, A., Katoh, H., Matsuda, N., and Suzuki, I. (2016). Physiological maturation and drug responses of human induced pluripotent stem cell-derived cortical neuronal networks in long-term culture. *Sci Rep* 6**,** 26181. doi: 10.1038/srep26181.

Patzke, C., Acuna, C., Giam, L.R., Wernig, M., and Sudhof, T.C. (2016). Conditional deletion of L1CAM in human neurons impairs both axonal and dendritic arborization and action potential generation. *J Exp Med* 213(4)**,** 499-515. doi: 10.1084/jem.20150951.

Qian, X., Nguyen, H.N., Jacob, F., Song, H., and Ming, G.L. (2017). Using brain organoids to understand Zika virus-induced microcephaly. *Development* 144(6)**,** 952-957. doi: 10.1242/dev.140707.

Qian, X., Nguyen, H.N., Song, M.M., Hadiono, C., Ogden, S.C., Hammack, C., et al. (2016). Brain-Region-Specific Organoids Using Mini-bioreactors for Modeling ZIKV Exposure. *Cell* 165(5)**,** 1238-1254. doi: 10.1016/j.cell.2016.04.032.

Quadrato, G., Nguyen, T., Macosko, E.Z., Sherwood, J.L., Min Yang, S., Berger, D.R., et al. (2017). Cell diversity and network dynamics in photosensitive human brain organoids. *Nature* 545(7652)**,** 48-53. doi: 10.1038/nature22047.

Reinhardt, P., Glatza, M., Hemmer, K., Tsytsyura, Y., Thiel, C.S., Hoing, S., et al. (2013a). Derivation and expansion using only small molecules of human neural progenitors for neurodegenerative disease modeling. *PLoS One* 8(3)**,** e59252. doi: 10.1371/journal.pone.0059252.

Reinhardt, P., Schmid, B., Burbulla, L.F., Schondorf, D.C., Wagner, L., Glatza, M., et al. (2013b). Genetic correction of a LRRK2 mutation in human iPSCs links parkinsonian neurodegeneration to ERK-dependent changes in gene expression. *Cell Stem Cell* 12(3)**,** 354-367. doi: 10.1016/j.stem.2013.01.008.

Ryan, Scott D., Dolatabadi, N., Chan, Shing F., Zhang, X., Akhtar, Mohd W., Parker, J., et al. (2013). Isogenic Human iPSC Parkinson's Model Shows Nitrosative Stress-Induced Dysfunction in MEF2-PGC1α Transcription. *Cell* 155**,** 1351-1364. doi:

10.1016/j.cell.2013.11.009.

Sánchez-Danés, A., Richaud-Patin, Y., Carballo-Carbajal, I., Jiménez-Delgado, S., Caig, C., Mora, S., et al. (2012). Disease-specific phenotypes in dopamine neurons from human iPS-based models of genetic and sporadic Parkinson's disease. *EMBO molecular medicine* 4**,** 380-395. doi: 10.1002/emmm.201200215.

Smits, L.M., Reinhardt, L., Reinhardt, P., Glatza, M., Monzel, A.S., Stanslowsky, N., et al. (2019). Modeling Parkinson's disease in midbrain-like organoids. *npj Parkinson's Disease* in press. doi: 10.1038/s41531-019-0078-4

Spathis, A.D., Asvos, X., Ziavra, D., Karampelas, T., Topouzis, S., Cournia, Z., Qing, X., Smits, L.M., Dalla, C., Rideout, H.J. et al. (2017). Nurr1:RXRα heterodimer activation as monotherapy for Parkinson' s disease. *PNAS* 114.15, pp. 3999–4004.

Suzanne, M., and Steller, H. (2013). Shaping organisms with apoptosis. *Cell Death Differ* 20(5)**,** 669-675. doi: 10.1038/cdd.2013.11.

Takahashi, K., and Yamanaka, S. (2006). Induction of pluripotent stem cells from mouse embryonic and adult fibroblast cultures by defined factors. *Cell* 126(4)**,** 663-676. doi: 10.1016/j.cell.2006.07.024.

Tepper, J.M., and Lee, C.R. (2007). GABAergic control of substantia nigra dopaminergic neurons. *Prog Brain Res* 160**,** 189-208. doi: 10.1016/S0079-6123(06)60011-3.

Tieng, V., Stoppini, L., Villy, S., Fathi, M., Dubois-Dauphin, M., and Krause, K.H. (2014). Engineering of midbrain organoids containing long-lived dopaminergic neurons. *Stem Cells Dev* 23(13)**,** 1535-1547. doi: 10.1089/scd.2013.0442.

van der Maarten, L., and Hinton , G. (2008). "Visualizaing Data unsin t-SNE", in: *Journal of Machine Learning Research.*).

Walter, J. (2019). Neural stem cells of Parkinson's disease patients exhibit aberrant mitochondrial morphology and functionality. *Stem Cell Reports* in press.

Tables

Table 1

cell lines	Derivation conditions	Gender	Age at sampling	Geno-type	Source	hiPSC ID	Figure
H1	3D	Female	81	WT	Reinhardt *et al.,* 2013	2.0.0.10.1.0	1A, B C, 2A, B, C
H2	3D	Male	n.a	WT	Alstem (iPS15)	2.0.0.33.0.0	1A, B C, 2A, B, C
H3	3D	Female	n.a.	WT	Wellcome Trust Sanger Institute (Bill Skarnes)	2.0.0.19.0.0	1A, B C, 2A, B, C, 3A
H4	3D	Female	cord blood	WT	Gibco (A13777)	2.0.0.15.0.0	3A, B, C, D

Table 1: Cell lines used in this study to generate mfNPCs and midbrain-specific organoids. Human mfNPCs were derived under 2D conditions from human iPSCs of different origin. hMOs were generated as described in the experimental procedures section.

Table 2

Antibody	Species	Source	Ref.-No.	Dilution
Dopamine	rabbit	ImmuSmol	IS1005	1:500
GABA	chicken	ImmuSmol	IS1036	1:500
L-Glutamate	rabbit	ImmuSmol	IS018	1:500
MAP2	mouse	Millipore	MAB3418	1:1000
PSD-95	rabbit	Invitrogen	51-6900	1:300
SYP	mouse	Abcam	ab8049	1:50
TUJ1	mouse	BioLegend	801201	1:600
TUJ1	rabbit	Covance	PRB-435P-0100	1:600
TUJ1	chicken	Millipore	AB9354	1:600

Table 2: Antibodies used in this study.

Table 3

Stemness	Neuronal	Dopaminergic	Glutamatergic	GABAergic	Serotonergic
SOX2	BCL11A	NR4A2	SLC1A1	GAD1	SLC6A4
PAX6	CACNA2D2	PBX1	SLC1A2	GAD2	SLC18A2
HES5	CALB2	GRIA3	SLC1A3	GABARAP	*TPH1*
ASCL1	*CD274*	TH	SLC17A6	GABARAPL1	TPH2
SOX1	CELF4	EN1	SLC17A7	GABARAPL2	FEV
PAX3	CLSTN2	TMCC3	GLS	*GABARAPL3*	HTR1D
DACH1	DLX1	NTM	GLS2	ABAT	HTR1DP1
LMO3	DPYSL5	DDC	GRIN1		HTR1E
NR2F1	DYNC1I1	CAMK2N1	GRIN2A		HTR1F
PLAGL1	EBF3	*ALDH1A1*	GRIN2B		HTR2A
LIX1	FOSL2	APP	GRIN2C		HTR2A-AS1
HOXA2	ISLR2	PDZRN4	GRIN2D		HTR2B
FOXA2	L1CAM	PCDH10	*GRIN3A*		HTR2C
IRX3	*MEG3*	*MEG3*	GRIN3B		HTR3A
	NHLH2	ERBB4	GRINA		HTR3B
	NPAS4	SLC10A4	GRIA1		HTR3D
	NPY	BEX5	GRIA2		HTR4
	NXPH4	FOXA2	GRIA3		HTR5A
	RELN	*NPY1R*	GRIA4		HTR5A-AS1
	RGMB	GPC2			*HTR5BP*
	SLC17A6	KCNJ6			HTR7P1
	SLC32A1	LMX1B			HTRA1
	SST				HTRA2
	STMN2				HTRA3
	SYNGR3				HTRA4
	SYT4				
	TMEM130				
	VGF				
	VSTM2L				

Table 3: Gene lists used in this study. Genes that were not detected in the transcriptome are emphasised in italics.

Table 4

Stemness	Neuronal	Dopaminergic	Glutamatergic	GABAergic	Serotonergic
ASCL1	CALB2	APP	GRIA2	GAD2	HTRA1
FOXA2	CELF4	EN1	GRIN2A		SLC18A24
LMO3	CLSTN2	FOXA2	GRIN2B		
SOX2	DLX1	GPC2	SLC17A6		
	DPYSL5	NTM	SLC1A2		
	EBF3	PCDH10	SLC1A3		
	FOSL2	PDZRN4			
	SLC17A6	TH			
	SST				
	STMN2				
	VSTM2L				

Table 4: List of differentially expressed genes.

Figures

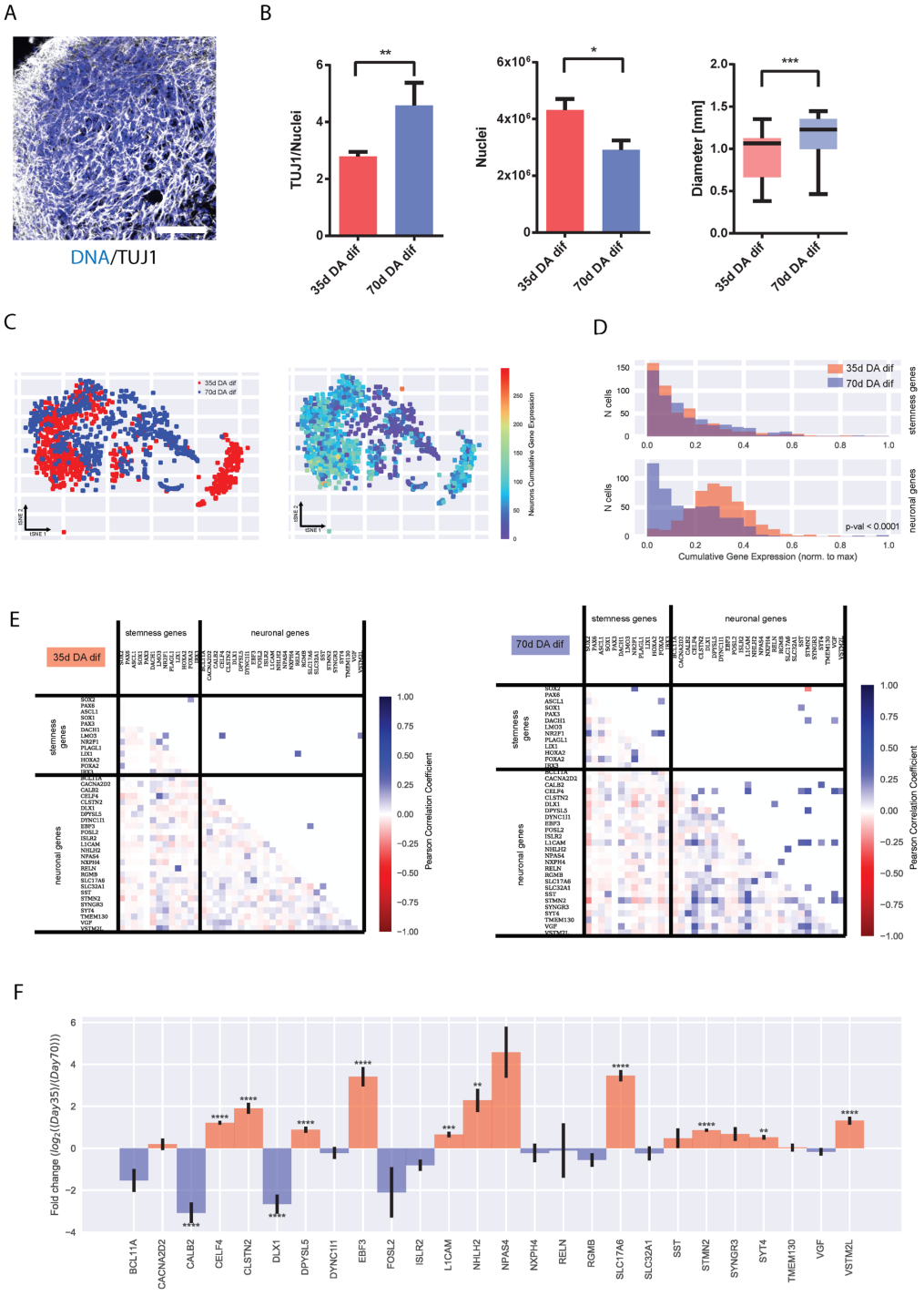

Figure 1: Identification of neuronal population in midbrain-specific organoids. (A) Immunohistological staining of TUJ1 expressing neurons in 35 d organoid sections (50 µm thickness, scale bar 100 µm). (B) The ratio of TUJ1 positive pixels normalised against Hoechst (35 d n=59, 70 d n=48). Quantification of Hoechst positive pixel (35 d n=22, 70 d n=29). Average size of four different organoid lines. Whiskers present minimum and maximum (35 d n=21, 70 d n=44). Data presented as mean ±SEM. (C) Dimensionality reduction of the scRNA-

seq data by tSNE underlies differences in gene expression between the samples at day 35 and day 70. Each dot corresponds to a cell. In the left panel, colours are used to indicate cells from the two time points. In the right panel, the colour scale indicates the score (cumulative gene expression) corresponding to neuron-specific genes for each cell. (D) Distributions (histograms) of cells across the cumulative gene expression scores, obtained from lists of genes specific for precursor cells (stemness genes) or neurons (stemness genes). (E) Gene-gene correlation matrices, for genes at day 35 on the left, and day 70 on the right. (F) Log2 fold-changes between day 35 and day 70 in gene expression for individual genes corresponding to the lists for neuron-specific genes.

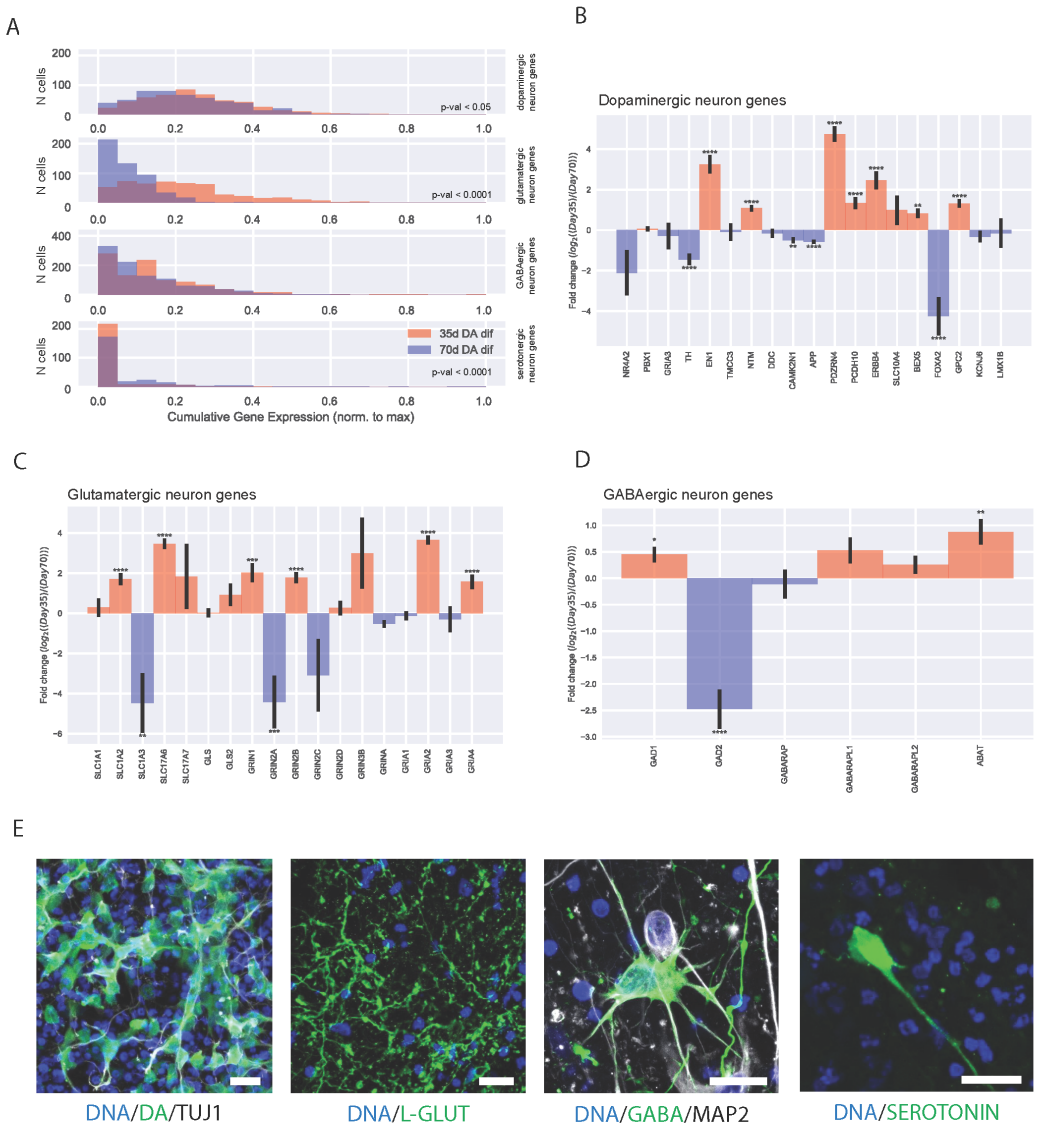

Figure 2: Neuronal subtypes in midbrain-specific organoids. (A) Distributions (histograms) of cells across the cumulative gene expression scores, obtained from the lists of genes specific

for the main neuronal subtypes present in the organoids, namely dopaminergic, glutamatergic, GABAergic, and serotonergic neurons. (B-D) Log2 fold-changes between day 35 and day 70 in gene expression for individual genes corresponding to the lists of genes typical of the neuronal subtypes: (B) dopaminergic neurons, (C) glutamatergic neurons, and (D) GABAergic neurons. (E) Immunohistological staining of 70 d organoid sections (50 µm thickness). Detection of the neurotransmitters dopamine, L-glutamine, GABA, and serotonin. Scale bar is 20 µm.

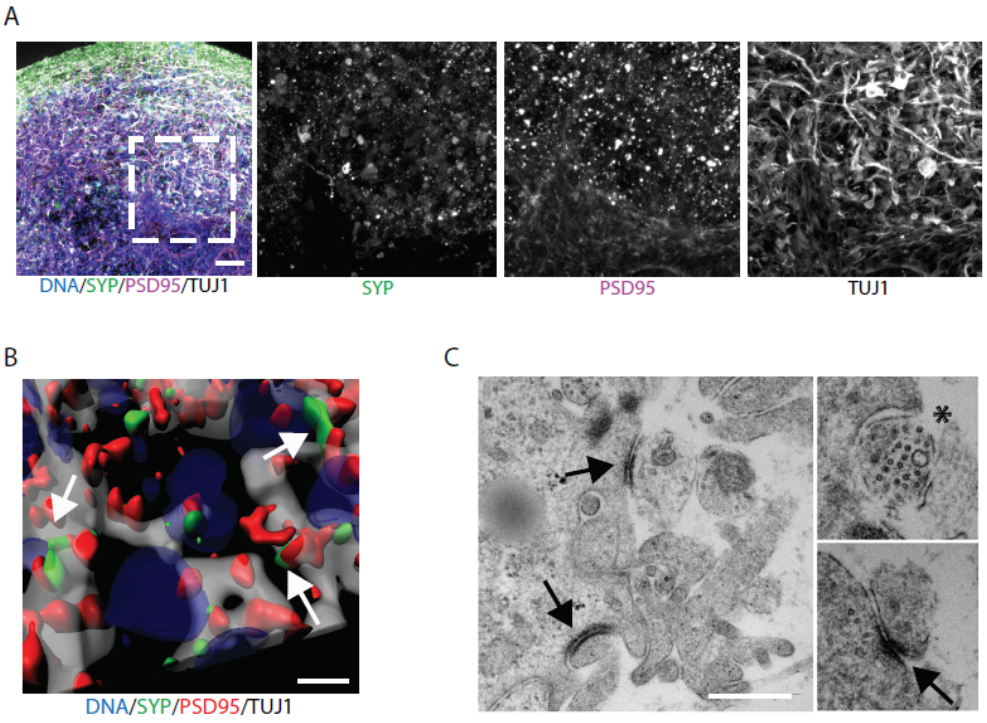

Figure 3: Midbrain-specific organoids express synaptic proteins. (A) Immunostaining of pre- and the postsynaptic markers at day 70. Dashed lines indicate the region of magnification. Scale bar is 50 µm. (B) 3D surface reconstructions of confocal z-stacks of an organoid at day 70 of differentiation. Scale bar is 10 µm. (C) Representative electron micrographs of synaptic terminals from 63 d organoids. Scale bar is 500 nm.

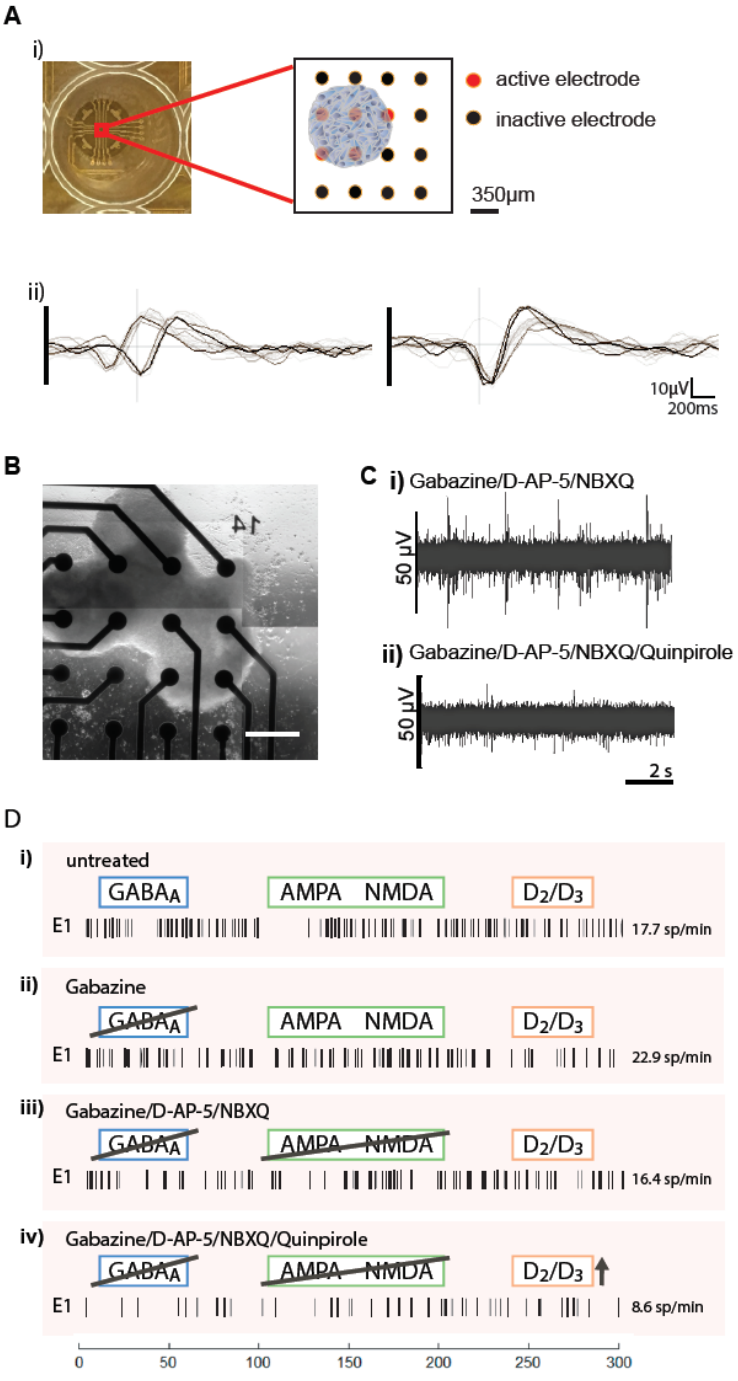

Figure 4: Electrophysiological activity in midbrain-specific organoids. (A) Representative scheme of positioned midbrain organoid on a 16-electrode array in a 48-well tissue culture plate (i). Examples of mono- and biphasic spikes detected by individual electrodes of a multielectrode array (MEA) system (ii). (B) Representative image of midbrain organoid positioned on a 16-electrode array in a 48-well tissue culture plate. Scale bar is 350 µm. (C-D) Evaluation of the spontaneous activity by addressing inhibitory (blue) and excitatory (green) neurotransmitter receptors using multielectrode array (MEA) system. (C) Representative raw data traces show the effect of Quinpirole in absence of inhibitory and excitatory synaptic communication. (D) Representative spike raster plots demonstrate effects of applied compounds.

CHAPTER 7

Original article: Modeling Parkinson's disease in midbrain–like organoids

This article has been published in the *npj Parkinson's Disease* journal.

7.1 Preface

The study of 3D cell culture models enables to bridge the gap between traditional 2D *in vitro* experiments and *in vivo* animal models (Xu, Jiao et al. 2018). Therefore, it offers an opportunity to better understand complex biology, for instance brain development, where conventional models have not proven successful. The so–called brain organoid technology provides a physiologically relevant context, like interactions between glia cells and neurons in a spatially organised microenvironment, which holds great potential for its application in modelling neurological diseases (Lee et al. 2017; Di Lullo et al. 2017). Here, we describe the derivation of hMOs that resemble key features of the human midbrain, like electrophysiologically functional mDANs producing and secreting DA. To investigate PD–relevant pathomechanisms, we derived hMOs from PD patients carrying the *LRRK2–G2019S* mutation and compared them to healthy control hMOs. Additionally to a reduced number and complexity of mDANs, we determined via automated high–content image analysis a significant increase of the stem cell marker FOXA2 in the patient–derived hMOs. This suggests a neurodevelopmental defect induced by a PD–specific mutation and emphasises the importance of advanced 3D stem cell–based *in vitro* models. The here described hMOs are suitable to reveal PD–relevant phenotypes, thus constitute as a powerful tool for human–specific *in vitro* disease modelling of neurological disorders.

This publication is the result of my PhD studies. I derived mfNPCs from hiPSCs under 3D conditions and generated all hMOs analysed in this manuscript. I designed and conducted the experiments that are shown in Figure 1 and 2 and Supplementary Figure 3) apart from the electrophysiological analyses that have been performed and evaluated by the above mentioned collaborators from Bolzano. Furthermore, A. Monzel supported the design of 3D experiments and performed Fontana Masson stainings. S. Bolognin and P. Antony elaborated the MATLAB scripts for the high–content image analysis. The initial conceptualisation and derivation of the mfNPC protocol as well as the detailed characterisation of these cells under 2D conditions was performed by the above mentioned collaborators from Dresden and Münster. They conducted microarray profiling of mfNPCs under maintenance conditions (Supplementary Figure 1), quantification of 2D mDAN differentiation efficiency by flow cytometry and analysis of electrophysiological functions via patch–clamp recordings (Supplementary Figure 2).

npj | Parkinson's Disease www.nature.com/npjparkd

BRIEF COMMUNICATION OPEN

Modeling Parkinson's disease in midbrain-like organoids

Lisa M. Smits[1], Lydia Reinhardt[2,3], Peter Reinhardt[2,3,6], Michael Glatza[2,3], Anna S. Monzel[1], Nancy Stanslowsky[4], Marcelo D. Rosato-Siri[5], Alessandra Zanon[5], Paul M. Antony[1], Jessica Bellmann[2], Sarah M. Nicklas[1], Kathrin Hemmer[1], Xiaobing Qing[1], Emanuel Berger[1], Norman Kalmbach[4], Marc Ehrlich[3], Silvia Bolognin[1], Andrew A. Hicks[5], Florian Wegner[4], Jared L. Sterneckert[2,3] and Jens C. Schwamborn[1]

Modeling Parkinson's disease (PD) using advanced experimental in vitro models is a powerful tool to study disease mechanisms and to elucidate unexplored aspects of this neurodegenerative disorder. Here, we demonstrate that three-dimensional (3D) differentiation of expandable midbrain floor plate neural progenitor cells (mfNPCs) leads to organoids that resemble key features of the human midbrain. These organoids are composed of midbrain dopaminergic neurons (mDANs), which produce and secrete dopamine. Midbrain-specific organoids derived from PD patients carrying the *LRRK2*-G2019S mutation recapitulate disease-relevant phenotypes. Automated high-content image analysis shows a decrease in the number and complexity of mDANs in *LRRK2*-G2019S compared to control organoids. The floor plate marker FOXA2, required for mDAN generation, increases in PD patient-derived midbrain organoids, suggesting a neurodevelopmental defect in mDANs expressing *LRRK2*-G2019S. Thus, we provide a robust method to reproducibly generate 3D human midbrain organoids containing mDANs to investigate PD-relevant patho-mechanisms.

npj Parkinson's Disease (2019)5:5 ; https://doi.org/10.1038/s41531-019-0078-4

INTRODUCTION

The current in vitro disease modeling approaches are typically conducted with cultures of neurons grown under two-dimensional (2D) conditions. However, 2D cultures neglect physiologically relevant characteristics like the interaction between glia cells and neurons in a spatially organized microenvironment. Recently, a new class of 3D in vitro models has been developed to compensate for this deficit, the so-called organoids. The complex 3D structure of organoids consists of multiple region-specific cell types, which allow studying functional interactions[1–8]. Therefore, organoids represent a promising tool to model cell autonomous and non-cell autonomous aspects of neurodegenerative diseases on an organ-like level in contrast to individual neuronal subtypes in 2D. In this study, we used a chemically defined derivation of midbrain floor plate neural progenitor cells (mfNPCs), which can be efficiently differentiated into 2D midbrain dopaminergic neurons (mDANs) and 3D human midbrain-specific organoids (hMOs). To investigate Parkinson's disease (PD)-relevant patho-mechanisms, we derived hMOs from PD patients carrying the *LRRK2*-G2019S mutation. We demonstrated that these organoids recapitulated key hallmarks of the pathology, such as reduced amounts of mDANs. Furthermore, we detected an increase of FOXA2 in patient-derived organoids compared to control organoids. This pinpoints at an impaired mDAN specification during hMO development. Thus, the generation of expandable mfNPCs provides an efficient and reproducible method to rapidly generate large quantities of functional mDANs suited for in vitro disease modeling.

RESULTS

Generation of midbrain-specific organoids

Our objective was to generate 3D organoids that resembled the complexity of the human midbrain. Based on previous findings[9], we first identified conditions that specifically promoted the formation of induced pluripotent stem cell (iPSC)-derived mfNPCs to generate a suitable starting population for the hMOs. The inhibition of bone morphogenetic protein (BMP) and tumor growth factor-β (TGFβ) signaling in combination with activation of SHH and WNT signaling enabled the generation of expandable neural stem cells (Supplementary Fig. 1a). Microarray profiling demonstrated that midbrain floor plate markers were highly expressed in these cells, in contrast to dorsal markers (IRX3, PAX3, PAX6), which were strongly downregulated (Supplementary Fig. 1b). Immunohistochemistry confirmed that these cells maintained the expression of midbrain floor plate markers EN1 and FOXA2 over several passages (Supplementary Fig. 1d). Differentiation efficiency of mfNPCs toward the dopaminergic lineage was determined by flow cytometry. After 14 days of mDAN differentiation, 59.94% (±10.6% SEM, mfNPC line P2-GC, $n = 3$) TH-positive cells were measured. Cells expressed multiple markers of mDAN fate and acquired essential functional electrophysiological properties during their differentiation (Supplementary Fig. 2). Therefore, mfNPCs represent an ideal starting population to generate hMOs.

After initiating the neuronal patterning of mfNPCs, 3D cultures were kept under differentiation conditions and were analyzed after 35 and 70 days (Fig. 1 and Supplementary Fig. 3).

[1]Luxembourg Centre for Systems Biomedicine (LCSB), Developmental and Cellular Biology, University of Luxembourg, Belvaux, Luxembourg; [2]DFG-Center for Regenerative Therapies, Technische Universität Dresden, Dresden, Germany; [3]Department of Cell and Developmental Biology, Max Planck Institute for Molecular Biomedicine, Münster, Germany; [4]Department of Neurology, Hannover Medical School, Hannover, Germany and [5]Institute for Biomedicine, Eurac Research, Affiliated Institute of the University of Lübeck, Bolzano, Italy
Correspondence: Jared L. Sterneckert (Jared.Sterneckert@tu-dresden.de) or Jens C. Schwamborn (jens.schwamborn@uni.lu)
[6]Present address: Neuroscience Discovery – Biology Department, AbbVie Deutschland GmbH & Co KG, Ludwigshafen, Germany
These authors contributed equally: Lisa M. Smits, Lydia Reinhardt

Received: 6 August 2018 Accepted: 7 March 2019
Published online: 05 April 2019

Published in partnership with the Parkinson's Foundation

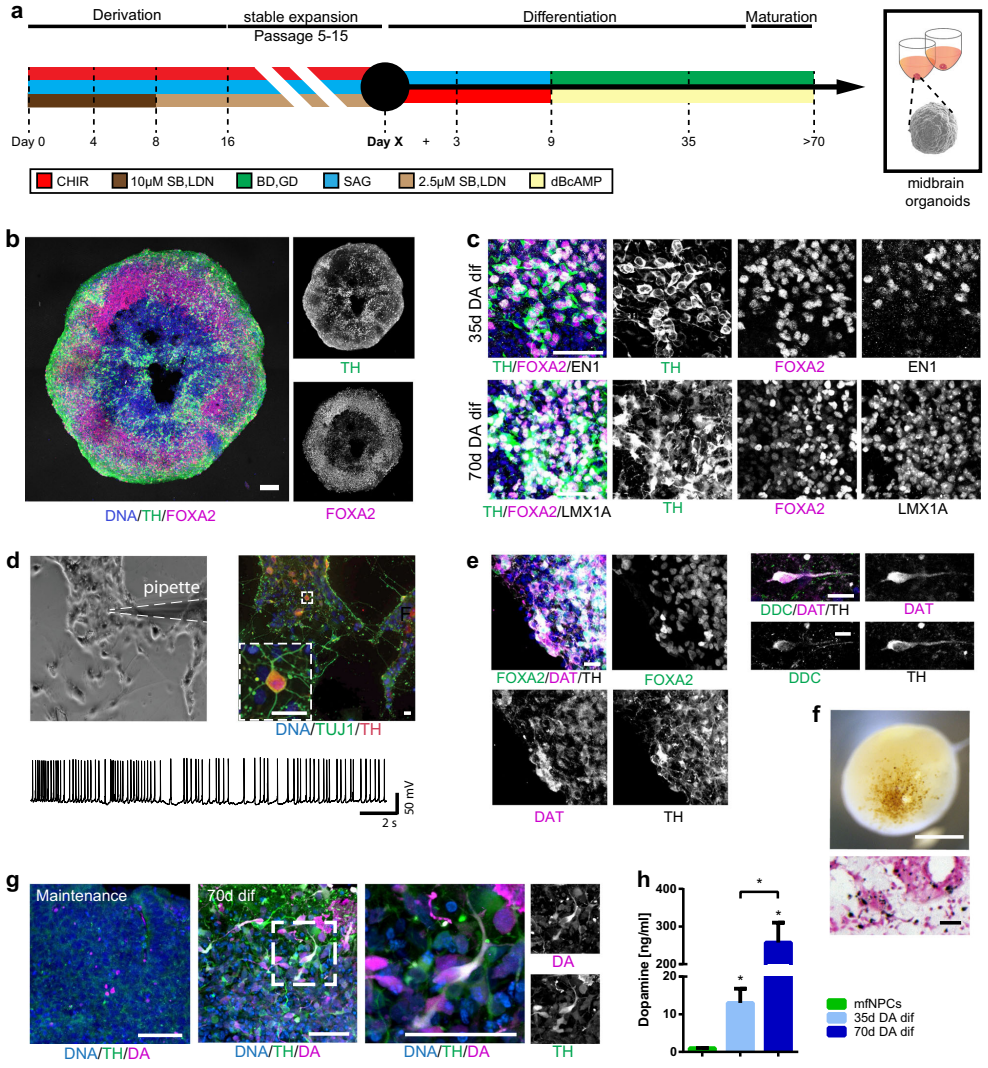

High-content image analysis revealed that hMOs showed high efficiency to form mDANs (62.38% ± 3.5% SEM TH-positive cells after 35 days and 54.12% ± 5.8% SEM after 70 days of differentiation, mfNPC line H3, $n = 7$, calculated as described in Supplementary Table 3). The markers TH, FOXA2, EN1, and LMX1A were abundantly expressed (Fig. 1b, c and Supplementary Fig. 3b) and we could also identify additional ventral and midbrain-specific markers (Supplementary Fig. 3d). Additionally, pace making and evoked firing activity was recorded in TH-positive cells by whole-cell patch-clamp measurements (this was detected in 12 out of 26 neurons, Fig. 1d and Supplementary Fig. 3c). A mean frequency of 9 ± 2 Hz was detected, 81% of the cells displayed sodium currents and 100% potassium currents. Immunofluorescence analysis demonstrated that the dopaminergic nature of the recorded cell (Supplementary Fig. 3d). Besides TH, bona fide mDANs are further characterized by the expression of dopamine decarboxylase (DDC) and the dopamine transporter (DAT). We identified neurons that co-expressed TH/FOXA2/DAT as well as TH/DDC/DAT (Fig. 1e). Occasionally, we detected the formation of neuromelanin inclusions in older hMOs (>100 days of differentiation) (Fig. 1f). The presence of dopamine in hMOs was subsequently confirmed by immunostainings and enzyme-linked immunosorbent assay (ELISA) (Fig. 1g, h). This indicates that mDANs in organoids are functional and can produce and secrete dopamine.

Fig. 1 Generation of midbrain-specific organoids. **a** Illustration of the conditions used to differentiate spherical midbrain floor plate neural progenitor cells (mfNPCs) into human midbrain-specific organoids (hMOs). mfNPCs are stably expandable up to passage 15; day X indicates the start of dopaminergic differentiation. SB = SB-431542, LDN = LDN-193189, SAG = sonic hedgehog agonist, BD = brain-derived neurotrophic factor, GD = glial cell-derived neurotrophic factor. **b** Maximum intensity projection of midbrain dopaminergic neuron (mDAN) markers TH and FOXA2 in 70-day-old hMO sections. Scale bar is 100 µm. hMOs derived from mfNPC lines H1–3 (image shows line H3). **c** Immunohistological stainings of mDAN markers TH, FOXA2, EN1, and LMX1A in the center of hMO sections. Scale bar is 50 µm. hMOs derived from mfNPC lines H1–3 (images shows line H2). **d** Bright-field image showing neurons obtained from three-dimensional (3D) culture of line H4 where a recorded cell is attached to the patch-clamp pipette tip (×10 magnification). Scale bar is 20 µm. Representative current-clamp trace of the pace-making firing activity obtained from the recorded mDAN is shown. Experiment conducted with mfNPC lines H4, P2-GC, and P3-GC, in total 26 cells have been recorded, 12 of these showed a similar pattern; representative images and traces of line H4. **e** Representative immunohistological stainings of mDAN markers FOXA2, TH, dopamine decarboxylase (DDC), and dopamine transporter (DAT) at the edge of an organoid. Scale bar is 20 µm. hMOs were derived from mfNPC lines H1–4 (images show lines H3 and H1). **f** Appearance of dark granules in hMOs at day 255, derived from mfNPC line H1. Scale bar is 500 µm. Fontana-Masson staining reveals neuromelanin-like granules at the edge of the organoid section after 100 days in culture, derived from mfNPCs line H4. Scale bar is 50 µm. **g** Representative immunohistological staining of spherical maintenance mfNPCs and 70-day hMO sections (50 µm thickness, taken at the edge of a section) for TH and neurotransmitter dopamine (DA). Scale bar is 50 µm. hMOs derived from mfNPC lines H1–3 (images show line H3). **h** Quantitative analysis of DA extracted from the supernatant of mfNPCs and hMOs, $*p < 0.05$. The two time points analyzed in all the experiments were 35 and 70 days of differentiation. Data are presented as mean ± SEM (mfNPC line H3, 4 different passages, $n = 4$)

Disease modeling of PD patient-specific midbrain-specific organoids

To assess the potential of mfNPC-derived hMOs for PD modeling, organoids were generated from healthy control (H-lines)- and from patient-specific iPSCs carrying the PD-associated *LRRK2*-G2019S mutation (P-lines). Their respective isogenic controls were also used in the study. The mutation was either introduced into the healthy control lines (H-G2019S lines) or corrected in the patient-specific lines (P-GC lines). mDANs were characterized after 10, 35, and 70 days of organoid differentiation with high-content image analysis (Fig. 2). At the beginning of the differentiation, hMOs from four different individuals (mfNPC line H3, H4, P2, and P3) as well as the corresponding isogenic controls (mfNPC line H3-G2019S, H4-G2019S, P2-GC, and P3-GC) developed similarly. Taking into consideration all analyzed features (see Supplementary Table 3), the heatmap shows that differences between the genotypes became evident when comparing hMOs at days 35 and 70 (Fig. 2b). For instance, healthy hMOs revealed a progressive increase in the TH percentage over time (d10 vs. d35, d10 vs. d70, H and H-G2019S), whereas patient-derived hMOs maintained lower levels throughout differentiation (d10 vs. d35, d10 vs. d70, P and P-GC). We detected a significant decrease of TH/FOXA2 double-positive signal in PD-derived compared to healthy control-derived hMOs after 35 days of differentiation (Fig. 2a). Introduction of the mutation into the healthy background or the correction of the mutation within the patient lines did not show the same effect (Fig. 2c). However, after evaluating the complexity of the dopaminergic neuronal network expressed as the number of nodes (dendrite bifurcation points) and links (number of branching)[10], we indeed identified a significant reduction of this complexity in the patient-derived TH-positive neurons compared to control mDANs (Fig. 2d). This phenotype was reproduced with the introduction of the LRRK2-*G2019S* mutation in the healthy background. Strikingly, we observed a significant increase of TH-negative but FOXA2-positive progenitor cells in the patient-specific hMOs (Fig. 2a, e). The same outcome became apparent when comparing 35-day-old hMOs generated from P and P-GC lines. This suggests that the disease-associated decrease in mDANs in patient-specific hMOs might be caused by a neurodevelopmental defect, leading to an altered specification of mDANs.

DISCUSSION

Disease modeling and drug discovery in the field of PD require enormous amounts of disease-relevant cells like mDANs that can be produced in a rapid and reproducible way. Numerous published protocols describe the generation of ventral mDANs from human PSCs by replicating mDAN specification in vivo[11–14]. Although current protocols are based on the generation of LMX1A/FOXA2-positive midbrain floor plate progenitors, differentiations starting from PSCs are time consuming and typically result in cultures containing various neuronal identities[12,13,15,16]. Here, we report an approach to efficiently differentiate mDANs and hMOs by generating expandable mfNPCs. As neurons form functional networks with other neurons and non-neuronal cells in the brain, it is essential to expand our research of neurodegenerative diseases using 3D models that are able to reproduce these interactions. So far, no phenotypes for PD have been shown in any of the published human brain organoid models. Here, we provide a proof-of-principle study that hMOs harboring the *LRRK2*-G2019S mutation show PD-relevant phenotypes, including reduced number and complexity of mDANs, which also occur in PD patients' brains[17,18]. Interestingly, we demonstrate a significant increase of FOXA2-positive progenitor cells in the patient-specific organoids. Since FOXA2 is required for the generation of mDANs, we hypothesize that this might be a compensatory response to an impaired specification of mDANs promoted by the mutated *LRRK2* gene. Similar compensatory mechanisms have been described in PD before[19] and might represent an attempt to counteract neurodevelopmental defects induced by PD-specific mutations. While introducing also isogenic control hMOs in this study, we could confirm that the introduction of the *LRRK2*-G2019S mutation caused deleterious effects on the complexity of mDANs within a healthy background. On the contrary, *LRRK2*-G2019S gene correction within a PD patient background is not sufficient to rescue this effect. This supports the hypothesis that the genetic background of PD patients can influence the degeneration of mDANs[10]. These findings show that mfNPCs and thereof derived mDANs as well as 3D hMOs represent powerful new tools for in vitro disease modeling. The patient-specific nature of these models also opens promising avenues for future personalized medicine approaches.

METHODS

Pluripotent stem cell culture and smNPC culture

The iPSCs used to derive neural progenitor cells were generated for and described in the study of Reinhardt et al.[9] and Qing et al.[20] and listed in the Supplementary Table 1. The cells were tested with the LookOut Mycoplasma PCR Detection Kit (Sigma-Aldrich) to exclude mycoplasma contamination. The cell line authentication via Sanger cell sequencing was performed by Microsynth Seqlab in Göttingen, Germany.

The generation of small molecule neural precursor cells (smNPCs) is described in detail in the study of Reinhardt et al.[9]

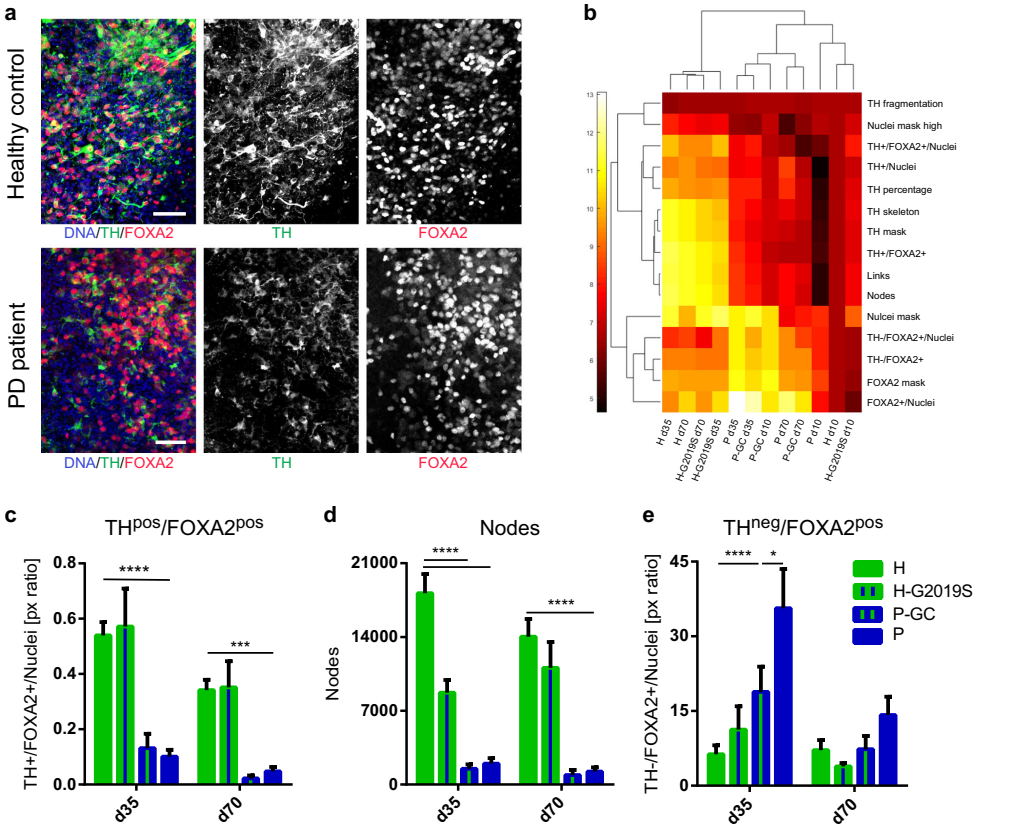

Fig. 2 Disease modeling of Parkinson's disease (PD) patient-derived midbrain-specific organoids. **a** Representative maximum intensity projection of TH-positive and FOXA2-positive cells in control and PD patient-specific human midbrain-specific organoids (hMOs) after 35 days of differentiation. Scale bar is 50 µm, magnification from the center of the organoid, images taken from line H3 and P3. **b** Heatmap comprising all features extracted by high-content automated image analysis. Dendrograms indicate clustering of genotypes and age (top) and features (left) and were obtained using the clustergram function in Matlab. **c**–**e** Quantification of **c** TH and FOXA2 double-positive signal, **d** number of nodes in the TH network, and **e** TH-negative, FOXA2-positive signal. Data are presented as mean ± SEM (and comprised of following numbers of hMO sections: healthy hMOs H (midbrain floor plate neural progenitor cell (mfNPC) line H3 and H4): $n = 26$ (d10), $n = 32$ (d35), $n = 38$ (d70); patient-derived hMOs P (mfNPC line P3 and P4): $n = 23$ (d10), $n = 36$ (d35), $n = 31$ (d70); isogenic control hMOs H-G2019S (mfNPC line H3-G2019S and H4-G2019S): $n = 18$ (d10), $n = 29$ (d35), $n = 28$ (d70); isogenic control hMOs P-GC (mfNPC line P3-GC and P4-GC): $n = 21$ (d10), $n = 38$ (d35), $n = 22$ (d70)). Relevant statistical significances determined by two-way analysis of variance (ANOVA), Tukey's multiple comparisons test are indicated with asterisks: *p <0.05, ***p <0.001, ****p <0.0001 (complete statistical evaluation shown in Supplementary Table 4)

Derivation of mfNPCs

For generation of mfNPCs from pluripotent stem cells, iPSCs were split as single cells and plated on feeder layers. Three to four days after splitting, colonies were detached using 2 mg/ml collagenase IV. Pieces of colonies were collected by sedimentation and resuspended in N2B27 medium supplemented with 10 µM SB-431542 (SB, Abcam), and 150 nM LDN-193189 (LDN, Millipore) for neural induction, as well as 5 µM ROCK inhibitor, 3 µM CHIR99021 (CHIR, Tocris), 200 µM ascorbic acid (AA, Sigma), and 0.5 µM SAG (Cayman). Cells were cultured in Petri dishes to prevent attachment. N2B27 medium consists of Dulbecco's modified Eagle's medium/Nutrient Mixture F12 (DMEM-F12) (Invitrogen)/Neurobasal (Invitrogen) 50:50 with 1:200 N2 supplement (Invitrogen), and 1:100 B27 supplement lacking vitamin A (Invitrogen) with 1% penicillin/streptomycin/glutamine (Biochrome). The medium was exchanged on days 2 and 4 with N2B27 medium supplemented with the same small molecule supplements, but without ROCK inhibitor. On day 6, embryoid bodies (EBs) showing neuroepithelial outgrowth without visible mesodermal/endodermal differentiation were collected and triturated with a 1000 µl pipette into smaller pieces. Then, they were plated on Matrigel-coated 12-well plates at a density of about 15–20 EBs per well in N2B27 medium supplemented with 10 µM SB, 150 nM LDN, 200 µM AA, 3 µM CHIR, and 0.5 µM SAG. Two days after plating the EBs, the medium was changed to mfNPC expansion medium (N2B27 medium with 2.5 µM SB, 100 nM LDN, 3 µM CHIR, 200 µM AA, and 0.5 µM SAG). The first split was performed 2–4 days after plating. During the early passages, it is important to keep the cells at high densities to increase survival. For the first split seed 500,000 cells per 12-well in mfNPC expansion medium containing an additional 5 µM ROCK inhibitor. In the next two passages, ~350,000 cells per 12 well are seeded to keep high densities and increase cell survival. All remaining splits are performed at a 1:5 to 1:10 ratio. After five passages, cultures are almost free of contaminating non-neuronal progenitor cells.

To derive mfNPCs under 3D conditions, iPSCs were detached using Accutase (Sigma) and collected in EB medium, consisting of knockout DMEM (Invitrogen) with 20% knockout serum replacement (Invitrogen), 100 µM β-mercaptoethanol (Gibco), 1% nonessential amino acids (Invitrogen), 1% penicillin/streptomycin/glutamine (Invitrogen), freshly supplemented with 10 µM SB-431542 (SB, Ascent Scientific), 250 nM LDN-193189 (LDN, Sigma), 3 µM CHIR99021 (CHIR, Axon Medchem), 0.5 µM SAG (Merck), and 5 µM ROCK inhibitor (Sigma). EBs were formed with 2,000 iPS cells each, using AggreWell 400 (Stemcell Technologies). EBs were harvested in EB medium without ROCK inhibitor after 24 h and transferred to a non-treated tissue culture plate (Corning). On day 2, the medium was replaced with N2B27 (as described above) supplemented with 10 µM SB, 250 nM LDN, 3 µM CHIR, and 0.5 µM SAG. The medium was exchanged with the same medium including 200 µM AA (Sigma) on days 4 and 6. On day 8, EBs with neuroepithelial outgrowth were collected, triturated with a 1000 µl pipette into smaller pieces, and transferred in a 1:10 ratio to an ultra-low attachment 24-well plate (Corning). For the following passages, cells were split with 1× TrypLE Select Enzyme (Gibco)/0.5 mM EDTA (Invitrogen) in 1× phosphate-buffered saline (PBS) and 10,000 to 20,000 cells per 96-well ultra-low attachment plate (round bottom, Corning) were seeded. The cells were always kept under 3D culture conditions and from passage 1 on cultured in N2B27 medium freshly supplemented with 2.5 µM SB, 100 nM LDN, 3 µM CHIR, 200 µM AA, and 0.5 µM SAG. After four to five passages, mfNPCs were used as a starting population for midbrain-specific organoids.

Expansion of mfNPCs

mfNPCs were cultured on Matrigel-coated 12-well cell-culture plates (Greiner). mfNPC expansion medium consisted of N2B27 freshly supplemented with SB, LDN, CHIR, SAG, and AA, with a medium change every 2 days. Typically, cells were split every 5 or 6 days at a ratio of 1:10 up to 1:15. For splitting, cells were digested into single cells for about 5 to 10 min at 37 °C with prewarmed Accutase (Sigma). Cells were diluted in DMEM (Biochrome) with 0.1% bovine serum albumin (BSA) fraction V (Invitrogen) for centrifugation at 200 × *g* for 5 min. The cell pellet was resuspended in fresh mfNPC expansion medium and plated on Matrigel-coated cell culture dishes. For coating, Matrigel was diluted to a final dilution of 1:100 in knockout DMEM (Invitrogen) prior to coating 500 µl per well of a 12-well plate overnight. Coated plates were wrapped with parafilm and kept in the fridge for up to one month.

To perform splitting of the 3D cultured mfNPCs, spherical colonies were collected and treated with 1× TrypLE Select Enzyme(Gibco)/0.5 mM EDTA (Invitrogen) in 1× PBS for about 5 to 10 min at 37 °C, followed by gentle pipetting to generate single cells. After re-seeding 10,000 to 20,000 cells per well of an ultra-low attachment, 96-well round bottom plate (Corning) was centrifuged for 3 min at 200 × *g* to assure the aggregation of single cells at the bottom of the well. Additionally, 5 µM ROCK inhibitor was added to the medium after passaging the cells. The cells were split every 7 to 14 days and the medium was changed every third day. mfNPCs were usually expanded from passages 5 to 15.

Differentiation of mfNPCs

For the differentiation into mDANs, 350,000 mfNPCs were seeded into a 12-well. Since SB and LDN are detrimental for differentiation, both small molecules were left out when seeding the cells. mfNPC expansion medium (without SB and LDN) was changed 2 days after seeding to N2B27 medium with 0.5 µM SAG, 0.7 µM CHIR, and 200 µM AA. After 4 days of patterning, maturation of the neurons was induced by changing the medium to N2B27 medium with 10 ng/ml brain-derived neurotrophic factor (BDNF, Peprotech), 10 ng/ml glial cell-derived neurotrophic factor (GDNF, Peprotech), 200 µM AA, 500 µM dibutyryl camp (Sigma), 1 ng/ml TGF-β3 (Peprotech), and 2.5 ng/ml ActivinA (Peprotech). When cultures became over-confluent during maturation, they were split into single cells using Accutase, or as small clumps using a cell scraper. To increase the maturation of differentiating cultures, the maturation medium was supplemented with 5–10 µM dual antiplatelet therapy (DAPT) (Cayman). Cultures were analyzed after 8–10 days under maturation conditions, unless otherwise indicated.

To generate midbrain-specific organoids, 3,000 cells were seeded per well to an ultra-low attachment 96-well round bottom plate and kept under maintenance conditions for 7 days. To start the pre-patterning, LDN and SB were withdrawn and after 3 additional days, the concentration of CHIR was reduced to 0.7 µM similar to 2D culturing. On day 9 of differentiation, the medium was changed to neuronal maturation medium including 10 µM DAPT, as described above. The organoids were kept under static culture conditions with media changes every third day for 10, 35, or 70 days.

Immunofluorescence staining

Cells were fixed for 20 min with 4% paraformaldehyde (PFA, Electron Microscopy Sciences) in PBS and washed twice with PBS (Lonza). Permeabilization and blocking were performed simultaneously using 0.1% Triton X-100 (Sigma), 1% BSA (Sigma), and 10% fetal calf serum in PBS for 45 min. The cells were washed with 0.1% BSA in PBS, and the primary antibodies were applied overnight at 4 °C in 0.1% BSA in PBS. The next day, the cells were washed with 0.1% BSA in PBS and incubated with secondary antibodies for 1 h at room temperature (RT). Finally, cells were washed three times with 0.1% BSA in PBS-T (0.005% Tween-20), including a Hoechst 33342 counterstaining for nuclei in the second washing step. Cells were mounted using Vectashield (Vector Labs) and imaged on a Zeiss PALM/Axiovert fluorescence microscope. When necessary, images were merged using ImageJ and Adobe Photoshop.

The primary antibodies used in this study are summarized in Supplementary Table 2. All secondary antibodies were obtained from Invitrogen and were conjugated to Alexa Fluor fluorochromes. Immunofluorescence staining for characterizing 2D-derived mfNPCs was performed with the cell lines mfNPC H1, P1-GC, and P2-GC (see Supplementary Table 1).

hMOs were fixed with 4% PFA overnight at 4 °C and washed three times with PBS for 15 min. After treatment, they were embedded in 3–4% low-melting point agarose in PBS. The solid agarose block was sectioned with a vibratome (Leica VT1000s) into 50 µm sections. The sections were blocked on a shaker with 0.5% Triton X-100, 0.1% sodium azide, 0.1% sodium citrate, 2% BSA, and 5% normal goat or donkey serum in PBS for 90 min at RT. Primary antibodies were diluted in the same solution but with only 0.1% Triton X-100 and were applied for 48 h at 4 °C.

After incubation with the primary antibodies (s. Supplementary Table 2), sections were washed three times with PBS and subsequently blocked for 30 min at RT on a shaker. Then, sections were incubated with the secondary antibodies in 0.05% Tween-20 in PBS for 2 h at RT and washed with 0.05% Tween-20 in PBS and Milli-Q water before they were mounted in Fluoromount-G mounting medium (Southern Biotech).

STAINperfect Immunostaining Kit (ImmuSmol) was used according to the manufacturer's protocol to detect dopamine. Sections were co-stained with chicken anti-TH primary antibody (Abcam), and nuclei were counterstained with Hoechst 33342 (Invitrogen).

For qualitative analyses, three randomly selected fields per organoid section were acquired with a confocal laser scanning microscope (Zeiss LSM 710) and images were further processed with the OMERO Software. For these immunofluorescence stainings of 3D derived mfNPCs and hMOs, the cell lines mfNPC H1, H2, H3, and H4 were used (see Supplementary Table 1).

Flow cytometry

Flow cytometry analysis was performed to quantify the differentiation efficiency of 2D mDAN cultures. To do so, we analyzed three independently differentiated wells of mfNPC P2-GC of three consecutive passages ($n = 3$) after 14 days of differentiation. In order to generate a single-cell suspension, differentiated cultures were washed once with PBS and subsequently dissociated at 37 °C using Accutase. Cells were further dissociated by pipetting gently up and down as well as by filtering them carefully through a 0.75 µm cell strainer. After centrifugation at 200 × *g* for 5 min, the cell pellet was resuspended in 2 ml PBS and the same volume of 8% PFA in PBS was added dropwise to fix the cells for 10 min at RT. Subsequently, the same volume of 0.1% BSA in PBS was added to the suspension. To remove the PFA, the cell suspension was centrifuged and washed once with 0.1% BSA in PBS. The pellet was resuspended in in 0.1% BSA in PBS and the suspension transferred into a 1.5 ml tube. After centrifugation, the cell pellet was resuspended in permeabilization/blocking solution (see section Immunofluorescence staining) and incubated for 20 min at RT. Permeabilization/blocking solution was withdrawn by centrifugation and the resulting cell pellet was resuspended in primary antibody solution. The incubation with the primary antibody rabbit anti-TH (1:300, Santa Cruz) was performed under shaking conditions overnight at 4 °C. On the following day, cultures were washed once with 0.1% BSA in PBS, and incubated with the secondary antibody for 1 h at RT. All

secondary antibodies were obtained from Invitrogen and were conjugated to Alexa Fluor fluorochromes. Finally, cells were washed twice with 0.1% BSA in PBS-T (0.005% Tween-20), including a Hoechst 33342 counter-staining for nuclei in the second washing step. After centrifugation, the pellet was resuspended in FACS buffer (0.1% BSA in PBS). To set the gates appropriately, we stained for each marker individually and included samples that have been stained with Hoechst individually. Flow cytometry was performed using BD LSRFortessa Cell Analyzer.

Image analysis

Immunofluorescence 3D images of hMOs were analyzed in Matlab (Version 2017b, Mathworks). The in-house developed image analysis algorithms automate the segmentation of nuclei and neurons, with structure-specific feature extraction (see Supplementary Table 3).

The image preprocessing for the segmentation of nuclei was computed by convolving the raw Hoechst channel with a Gaussian filter. By selecting a pixel threshold to identify apoptotic cells, a pyknotic nuclei mask was identified and subtracted from the nuclei mask.

For the segmentation of dopaminergic neurons, a median filter was applied to the raw TH channel to generate TH mask. A skeleton of the TH mask was generated with a thinning function and was used to identify nodes and links as total number of bifurcation points and total number of linking elements, respectively. For SOX2, CC3, and FOXA2 masks, a median filter was applied followed by a bwareaopen to remove all connected components smaller than 100. SOX2 and FOXA2 masks were identified within the nuclei masks of each image. The expression levels of the mentioned markers were expressed in two ways: (i) positive pixel of the marker, normalized by the pixel count of Hoechst; (ii) cells positive for a marker expressed as a percentage of the total number of cells. In this latter case, the nuclei were segmented and a watershed function was applied. Considering the high cell density of the specimens, steps to ensure high quality in the segmentation process were implemented and nuclei with a size higher than 10,000 pixels were removed. In the nuclei successfully segmented as a single element, a perinuclear zone was identified. In case the marker or interest was positive in at least 1% of the perinuclear area, that cell was considered positive.

For quantitative analyses of SOX2 and CC3 marker expression in hMOs, mfNPC lines H1, H2, and H3 were used. With a confocal laser scanning microscope (Zeiss LSM 710), three randomly selected fields per organoid section were acquired of three different organoid derivations. In total 27 images per time point were analyzed with above-described image analysis algorithms. To evaluate the TH signal, 21 field of hMOs derived of seven consecutive passages of mfNPC H3 were acquired.

For the comparison of PD patient-derived and healthy hMOs, as well as their isogenic controls, cell lines mfNPC H3, H3-G2019S, H4, H4-G2019S, P3, P3-GC, P4, and P4-GC were used (see Supplementary Table 1). hMOs were generated minimum five times per line from consecutive 3D mfNPC cultures. The entire organoid sections of 50 µm thickness were acquired with an Operetta High-Content Imaging System (Perkin -Elmer) and analyzed with above-described image analysis algorithms.

Dopamine ELISA

Dopamine Research ELISA (LDN) was performed for the quantitative determination of dopamine secreted by hMO cell line H3 (see Supplementary Table 1). Supernatant of 12 hMOs per condition was pooled, 200 µl was diluted 1:10 with a HCl buffer (0.01 N HCl, 4 mM $Na_2O_5S_2$, and 1 mM EDTA), and snap frozen in liquid nitrogen. Samples were selected from four independently generated hMO batches, and differentiated from consecutive 3D mfNPC cultures. The ELISA was performed according to the manufacturer's instructions with 10 µl sample volume.

Fontana–Masson staining

hMOs of line mfNPC H4 were fixed at day 100 in 4% PFA overnight at 4 °C on a shaker, washed three times in PBS, and dehydrated in 30% sucrose overnight until the organoid was entirely equilibrated with the sucrose solution. Next, cryosectioning was performed using a Cryostat (Leica) to a thickness of 10 µm. The sections were dried overnight and stained with a Fontana–Masson Staining Kit (Abcam) according to the manufacturer's protocol. The sections were mounted in Entellan® rapid mounting medium (Merck) and images were acquired using a stereomicroscope (Nikon SMZ25).

Quantitative RT-PCR

For total RNA extraction of 3D cultured cells, typically 8 spherical mfNPC colonies and 12 hMOs per line (mfNPC line H1–4, see Supplementary Table 1) were collected and snap frozen in liquid nitrogen. Afterwards, they were lysed with 1 ml QIAzol lysis reagent (Qiagen), homogenized first with a needle, and then with QIAshredder columns (Qiagen). According to the manufacturer's instructions, RNeasy Mini Kit (Qiagen) as well as DNase I Amplification Grade (Sigma-Aldrich) was used to isolate the RNA. After conducting reverse transcription by following the protocol of the High Capacity RNA to DNA Kit (Thermo Fisher Scientific), qRT-PCRs were performed using TaqMan Gene Expression Master Mix (Thermo Scientific), and the following Taqman® probes: RPL37A (Hs00902901_m1), FOXA2 (Hs00232764_m1), LMX1A (Hs00892663_m1), EN1 (Hs00154977_m1), and TH (Hs00165941_m1). Amplification of 5 ng of original RNA was performed in a LightCycler R480 (Roche) as follows: an initial denaturing step, 10 min at 95 °C, 40 cycles of denaturation for 15 s at 95 °C, annealing for 30 s at 60 °C, and elongation for 30 s at 72 °C. The expression levels were normalized relative to the expression of the housekeeping gene *RPL37A* using the comparative Ct method $2-\Delta\Delta Ct$. Expression patterns of hMOs were compared to the expression levels of mfNPCs cultured under 3D conditions, which were set to 1.

Whole-genome expression analysis

Microarray analysis was performed as described previously[21]. Briefly, 500 ng RNA of smNPCs and mfNPCs (cell lines P1-GC and P2-GC) were processed using a linear amplification kit (Ambion), quality controlled on a 2100 Bioanalyzer (Agilent), and hybridized on Illumina human-12 V3 expression BeadChips. Background subtraction, normalization, and differential expression analysis were performed using BeadStudio. Here smNPCs are used as a well-described[9] neural progenitor cell line to which the mfNPCs are compared.

Patch-clamp electrophysiology

mfNPC lines P1-GC and P2-GC were plated on Matrigel-coated 35-mm culture dishes (Greiner) and differentiated as 2D cultures described above for 2 or 4 weeks. Whole-cell patch-clamp recordings of neurons were performed at 20–22 °C under optical control (Zeiss inverted microscope) as reported previously[22]. The internal pipette solution consisted of 153 mM KCl, 1 mM $MgCl_2$, 10 mM HEPES, 5 mM EGTA, and 2 mM Mg-ATP, adjusted to pH 7.3 with KOH (305 mOsm). The external bath solution contained 142 mM NaCl, 8 mM KCl, 1 mM $CaCl_2$, 6 mM $MgCl_2$, 10 mM glucose, and 10 mM HEPES, adjusted to pH 7.4 with NaOH (325 mOsm). Neuronal recordings were low-pass filtered at 1–5 kHz, digitized at 10 kHz using an EPC-10 amplifier (HEKA), and analyzed with Patch Master (HEKA).

hMO lines H4, P2-GC, and P3-GC were dissociated after 60–65 days in culture using the NeuroCult™ Enzymatic Dissociation Kit for Adult CNS Tissue (Stemcell Technologies) according to the manufacturer's protocol and patch-clamp recordings ($n = 26$) were carried out 5–15 days after dissociation. Whole-cell recordings in voltage- and current-clamp modes were performed in a temperature-controlled recording chamber (35–37 °C) mounted on an inverted Eclipse-Ti microscope (Nikon, Tokyo, Japan) and using a MultiClamp 700B amplifier (Molecular devices, LLC). Voltage- and current-command protocols and data acquisition were performed using the pClamp 10.0 software and the Digidata 1550 interface (Molecular Devices, LLC). Data were low-pass filtered at 3 kHz and sampled at 10 kHz. Patch electrodes, fabricated from thick borosilicate glass capillaries, were made using a Sutter P-1000 puller (Sutter Instruments) to a final resistance of 4–6 MΩ when filled with the intracellular solution containing (in mM): 120 K-gluconate, 25 KCl, 10 EGTA, 10 HEPES, 1 $CaCl_2$, 4 Mg-ATP, 2 Na-GTP, and 4 Na2-phosphocreatine (pH 7.4, adjusted with KOH). Cells were perfused with a Krebs solution containing (in mM): 129 NaCl, 5 KCl, 2 $CaCl_2$, 1 $MgCl_2$, 30 D-glucose, 25 HEPES, pH 7.3, with NaOH. Voltage-clamp recordings ($Vh = -60$ mV) of evoked ionic currents were performed by applying a voltage step protocol (from −60 to +60 mV, 300 ms of duration). Spontaneous action potentials were recorded in a gap-free mode, while the evoked firing activity was evaluated by applying long steps at different current intensities (50 pA increments). Series resistance was monitored during the experiments and recordings with changes over 20% of its starting value were discarded.

Statistical analyses

2D experiments were performed with three different cell lines (mfNPC H1, P1-GC, and P2-GC), which have been published previously[9]. All hMO immunostainings and quantitative reverse transcription PCR experiments were performed with three independently generated organoid cultures from three to four different cell lines H1–4 ($n = 9$–12, see Supplementary Table 1). The dopamine ELISA was conducted with four different passages of mfNPC line H3 ($n = 4$). Gaussian distribution was evaluated by performing D'Agostino and Pearson omnibus normality test. According to this distribution, either a Grubbs' test to detect significant outliers and an unpaired *t* test with Welch's correction was carried out or a nonparametric Kolmogorov–Smirnov test was performed to evaluate statistical significance.

The image analysis for PD phenotyping was conducted with several passages of PD patient-derived and healthy hMOs, as well as their isogenic controls (mfNPC line H3, H3-G2019S, H4, H4-G2019S, P3, P3-GC, P4, and P4-GC, see Supplementary Table 1). A two-way analysis of variance and Tukey's multiple comparisons test was performed to evaluate statistical significance (see Supplementary Table 4). Data are presented as mean ± SEM.

All analyses were performed with multiple cell lines; in the figures always a representative image looking similar to the images obtained from all used lines is displayed.

Ethics statement

Informed consent was obtained from all individuals donating samples to this study prior to the donation using a written form and protocol previously approved by the institutional review board: Ethik-Kommission der Medizinischen Fakultät am Universitätsklinikum Tübingen. In vitro experiments were carried out with existing cell lines obtained from previous studies. Cell lines used in this study are summarized in Supplementary Table 1.

Reporting Summary

Further information on research design is available in the Nature Research Reporting Summary linked to this article.

DATA AVAILABILITY

The data that support the findings of this study are publically available at this https://doi.org/10.17881/lcsb.20192701.01. The microarray data that support the findings of this study have been deposited in Gene Expression Omnibus (GEO) under the accession code GSE127967.

CODE AVAILABILITY

The codes used for image analysis in this study are available via github: https://github.com/LCSB-DVB.

ACKNOWLEDGEMENTS

We are indebted to Martina Sinn, Inga Brüggemann, Thea van Wüllen, Antoine Treff, and Alexandros Lavdas for technical assistance. J.L.S. team was supported by funding from the Technische Universität Dresden, the Deutsche Forschungs Gemeinschaft (STE 1835/1-1), the DFG Research Center (DFG FZ 111, the Cluster of Excellence (DFG EXC 168), as well as the Bundesministerium für Bildung und Forschung (01EK1606A). M.G. and J.B. were supported by a fellowship from the Hans and Ilse Breuer Stiftung. The JCS lab is supported by the Fonds National de la Recherché (FNR) (Proof-of-Concept program PoC15/11180855 and PoC16/11559169). This is an EU Joint Programme-Neurodegenerative Disease Research (JPND) project (INTER/JPND/14/02; INTER/JPND/15/11092422) and M-ERA.NET project (INTER/M-ERA.NET/17/11760144). Further support comes from the SysMedPD project, which has received funding from the European Union's Horizon 2020 research and innovation programme under grant agreement no. 668738 and by a University Luxembourg Internal Research Project grant (MidNSCs). L.M.S., X.Q., and A.S.M. are supported by fellowships from the FNR (AFR, Aides à la Formation-Recherche). S.M.N. was supported by the FNR INTER Mobility program (INTER Mobility/16/11447821). This project was supported by the LCSB pluripotent stem cell core facility. N.K. and F.W. were supported by the Petermax-Müller-Stiftung in Hannover, Germany. In Bolzano, the work was supported by the Department of Educational Assistance, University and Research of the Autonomous Province of Bolzano.

AUTHOR CONTRIBUTIONS

L.M.S. and L.R. contributed equally and thus share first authorship. L.M.S., L.R., and P.R. designed experiments, prepared the figures, and wrote the original draft. M.G. performed microarray analysis. A.S.M. designed experiments. N.S. and F.W. performed patch-clamp analysis in 2D cultures. M.D.R.-S. and A.Z. performed patch-clamp analysis in 3D cultures. J.B. and E.B. designed and performed flow cytometry. S.M.N., K.H., P.M.A., and S.B. designed and performed image analysis and reconstruction. L.R., P.R., and X.Q. generated and provided iPSCs. N.K., M.E., S.B., and F.W. initiated the project, supervised it, and edited the manuscript. A.A.H., J.L.S., and J.C.S. conceived and supervised the project, designed the experiments, and edited the manuscript.

ADDITIONAL INFORMATION

Supplementary information accompanies the paper on the *npj Parkinson's Disease* website (https://doi.org/10.1038/s41531-019-0078-4).

Competing interests: The authors declare no competing interests.

Publisher's note: Springer Nature remains neutral with regard to jurisdictional claims in published maps and institutional affiliations.

REFERENCES

1. Lancaster, M. A. et al. Cerebral organoids model human brain development and microcephaly. *Nature* **501**, 373–379 (2013).
2. Muguruma, K., Nishiyama, A., Kawakami, H., Hashimoto, K. & Sasai, Y. Self-organization of polarized cerebellar tissue in 3D culture of human pluripotent stem cells. *Cell Rep.* **10**, 537–550 (2015).
3. Qian, X. et al. Brain-region-specific organoids using mini-bioreactors for modeling ZIKV exposure. *Cell* **165**, 1238–1254 (2016).
4. Di Lullo, E. & Kriegstein, A. R. The use of brain organoids to investigate neural development and disease. *Nat. Rev. Neurosci.* **18**, 573–584 (2017).
5. Lee, C. T., Bendriem, R. M., Wu, W. W. & Shen, R. F. 3D brain organoids derived from pluripotent stem cells: promising experimental models for brain development and neurodegenerative disorders. *J. Biomed. Sci.* **24**, 59 (2017).
6. Monzel, A. S. et al. Derivation of human midbrain-specific organoids from neuroepithelial stem cells. *Stem Cell Rep.* **8**, 1144–1154 (2017).
7. Jo, J. et al. Midbrain-like organoids from human pluripotent stem cells contain functional dopaminergic and neuromelanin-producing neurons. *Cell Stem Cell* **19**, 248–257 (2016).
8. Tieng, V. et al. Engineering of midbrain organoids containing long-lived dopaminergic neurons. *Stem Cells Dev.* **23**, 1535–1547 (2014).
9. Reinhardt, P. et al. Derivation and expansion using only small molecules of human neural progenitors for neurodegenerative disease modeling. *PLoS ONE* **8**, e59252 (2013).
10. Bolognin, S. et al. 3D cultures of Parkinson's disease-specific dopaminergic neurons for high content phenotyping and drug testing. *Adv. Sci. (Weinh.)* **6**, 1800927 (2019).
11. Nolbrant, S., Heuer, A., Parmar, M. & Kirkeby, A. Generation of high-purity human ventral midbrain dopaminergic progenitors for in vitro maturation and intracerebral transplantation. *Nat. Protoc.* **12**, 1962–1979 (2017).
12. Kirkeby, A. et al. Generation of regionally specified neural progenitors and functional neurons from human embryonic stem cells under defined conditions. *Cell Rep.* **1**, 703–714 (2012).
13. Kriks, S. et al. Dopamine neurons derived from human ES cells efficiently engraft in animal models of Parkinson's disease. *Nature* **480**, 547–551 (2011).
14. Doi, D. et al. Isolation of human induced pluripotent stem cell-derived dopaminergic progenitors by cell sorting for successful transplantation. *Stem Cell Rep.* **2**, 337–350 (2014).
15. Hargus, G. et al. Differentiated Parkinson patient-derived induced pluripotent stem cells grow in the adult rodent brain and reduce motor asymmetry in Parkinsonian rats. *Proc. Natl. Acad. Sci. USA* **107**, 15921–15926 (2010).
16. Grealish, S. et al. Human ESC-derived dopamine neurons show similar preclinical efficacy and potency to fetal neurons when grafted in a rat model of Parkinson's disease. *Cell Stem Cell* **15**, 653–665 (2014).
17. Bernheimer, H., Birkmayer, W., Hornykiewicz, O., Jellinger, K. & Seitelberger, F. Brain dopamine and the syndromes of Parkinson and Huntington. Clinical, morphological and neurochemical correlations. *J. Neurol. Sci.* **20**, 415–455 (1973).
18. Kordower, J. H. et al. Disease duration and the integrity of the nigrostriatal system in Parkinson's disease. *Brain* **136**, 2419–2431 (2013).
19. Blesa, J. et al. Compensatory mechanisms in Parkinson's disease: circuits adaptations and role in disease modification. *Exp. Neurol.* **298**, 148–161 (2017).

20. Qing, X. et al. CRISPR/Cas9 and piggyBac-mediated footprint-free LRRK2-G2019S knock-in reveals neuronal complexity phenotypes and α-Synuclein modulation in dopaminergic neurons. *Stem Cell Res.* **24**, 44–50 (2017).
21. Reinhardt, P. et al. Genetic correction of a LRRK2 mutation in human iPSCs links parkinsonian neurodegeneration to ERK-dependent changes in gene expression. *Cell Stem Cell* **12**, 354–367 (2013).
22. Stanslowsky, N. et al. Neuronal dysfunction in iPSC-derived medium spiny neurons from chorea-acanthocytosis patients is reversed by Src kinase inhibition and F-actin stabilization. *J. Neurosci.* **36**, 12027–12043 (2016).

Supplementary Material

Modeling Parkinson's disease in midbrain-like organoids

Lisa M. Smits[1,§], Lydia Reinhardt[2,3,§], Peter Reinhardt[2-4], Michael Glatza[2,3], Anna S. Monzel[1], Nancy Stanslowsky[5], Marcelo D. Rosato-Siri[6], Alessandra Zanon[6], Paul M Antony[1], Jessica Bellmann[2], Sarah M. Nicklas[1], Kathrin Hemmer[1], Xiaobing Qing[1], Emanuel Berger[1], Norman Kalmbach[5], Marc Ehrlich[3], Silvia Bolognin[1], Andrew A. Hicks[6], Florian Wegner[5], Jared L. Sterneckert[2,3*] and Jens C. Schwamborn[1*]

[1]Luxembourg Centre for Systems Biomedicine (LCSB), Developmental and Cellular Biology, University of Luxembourg, Belvaux Luxembourg

[2]DFG-Center for Regenerative Therapies, Technische Universität Dresden, Dresden, Germany

[3]Department of Cell and Developmental Biology, Max Planck Institute for Molecular Biomedicine, Münster, Germany

[4]Currently located at AbbVie Deutschland GmbH & Co KG, Neuroscience Discovery– Biology Department, Ludwigshafen, Germany

[5]Department of Neurology, Hannover Medical School, Hannover, Germany

[6]Institute for Biomedicine, Eurac Research, Affiliated Institute of the University of Lübeck, Bolzano, Italy

[§]These authors contributed equally and thus share first authorship.

[*]**Corresponding authors**

Prof. Dr. Jens C. Schwamborn
jens.schwamborn@uni.lu
Dr. Jared L. Sterneckert
Jared.Sterneckert@tu-dresden.de

Supplementary Figures and Tables

Supplementary Figure 1 Derivation of mfNPCs.

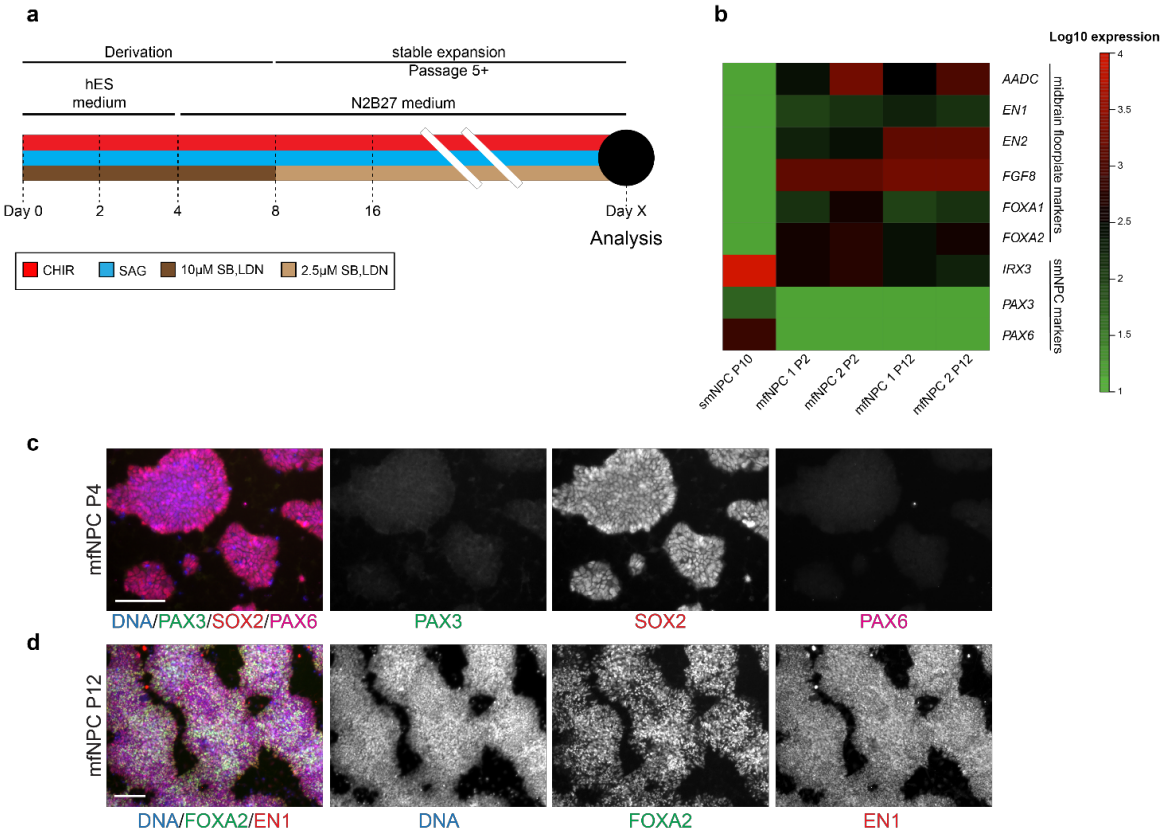

Supplementary Figure 1: Derivation of mfNPCs. (a) Schematic illustration of mfNPC derivation and expansion. SB = SB-431542, LDN = LDN-193189, SAG = sonic hedgehog agonist. (b) Microarray profiling displayed as a heatmap for selected markers of regional cell fate identity in small molecule neural precursor cells (smNPCs) and midbrain floor plate neural precursor cells (mfNPCs). (c) Immunostaining shows that mfNPCs lack PAX3 and PAX6, which are not expressed in the midbrain floor plate. Scale bar is 100 µm. (d) Immunofluorescence confirms that mfNPCs co-express FOXA2 and EN1, which are markers of the midbrain floor plate. Scale bar is 100 µm. Experiments were conducted with mfNPC lines H1, P1-GC, P2-GC, here representative images are shown for line P1-GC, which looked similar to the other cell lines.

Supplementary Figure 2 Differentiation potential of mfNPCs for mDANs.

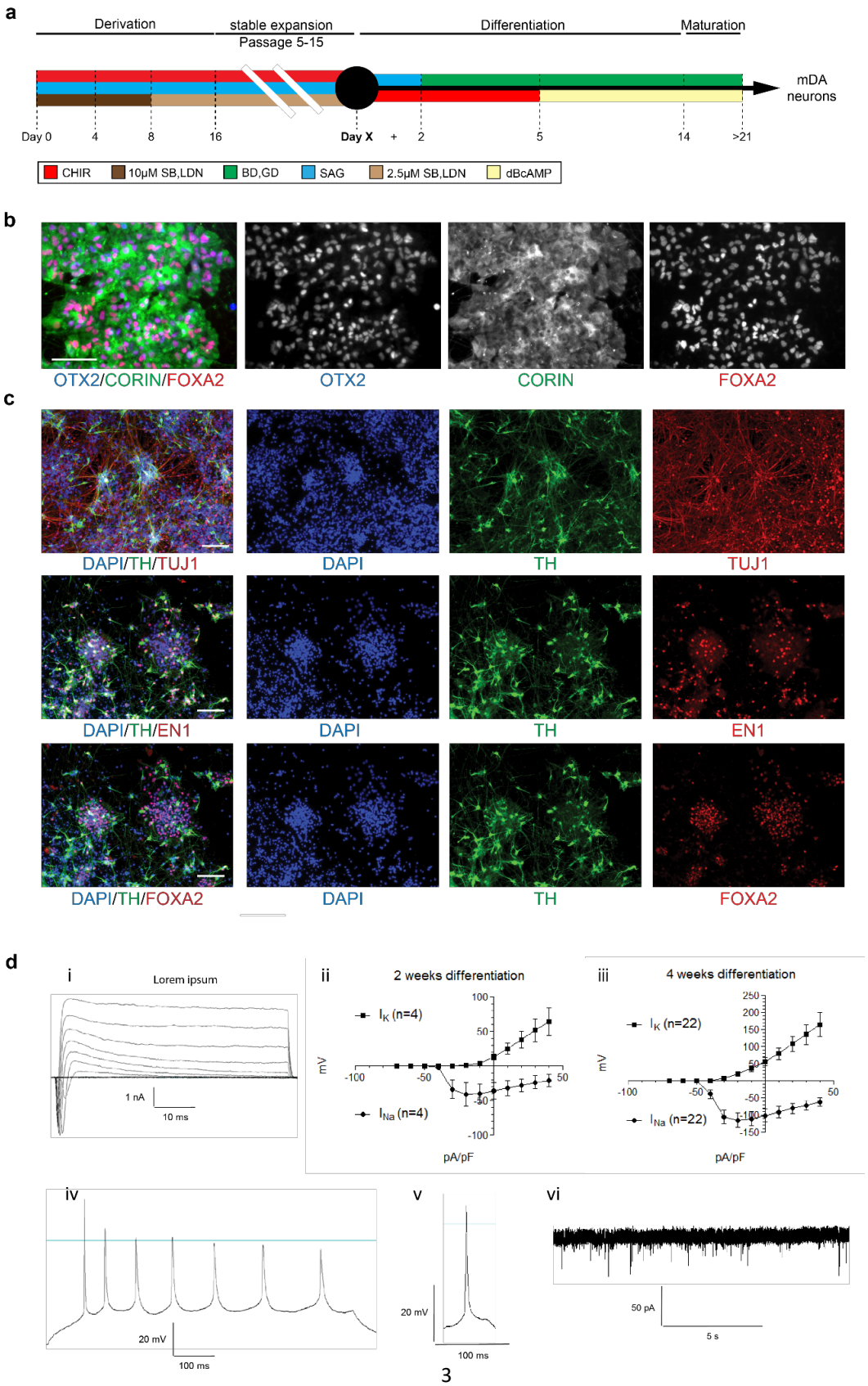

Supplementary Figure 2: Differentiation potential of mfNPCs for mDANs. Where indicated, analyses were performed with multiple cell lines (details see below) and a representative image looking similar to the images obtained from all used lines, is displayed. (a) Schematic illustration of the conditions used to differentiate mfNPCs into mDANs under 2D conditions. BD = BDNF, GD = GDNF. (b) mfNPCs were differentiated for four days and immunostained for CORIN and OTX2, which are markers of mDAN progenitors. (c) Immunostaining for the midbrain dopaminergic markers EN1, FOXA2, and TH after 14 days of differentiation. Scale bars are 100 µM. Stainings were performed with mfNPC lines H1, P1-GC, P2-GC, here representative images are shown for line P1-GC. (d) Patch-clamp recordings of voltage-gated ion currents, action potentials and synaptic activity of mfNPC-derived neurons after four weeks of differentiation indicate the development of essential functional properties during differentiation. (i) Representative voltage-gated sodium inward and potassium outward currents of a mfNPC-derived neuron recorded in whole-cell voltage-clamp mode by stepwise depolarizations in 10 mV increments from a holding potential of -70 to 40 mV. (ii-iii) Ion currents normalized for cell sizes based on the capacitance of the cell membrane (pA/pF) after differentiation for two weeks (ii) and four weeks (iii). Data are presented as means ± SEM. (iv) Example of neuron firing repetitive action potentials upon depolarization in the current-clamp mode. (v) Some neurons were also able to spike single action potentials spontaneously (same cell as in i after four weeks of differentiation). (vi) Spontaneous synaptic activity of neurons with miniature postsynaptic currents recorded in voltage-clamp mode. Recordings were performed with neurons derived from mfNPC lines P1-GC and P2-GC, four cells were recorded after two weeks of differentiation, 22 cells were recorded after four weeks of differentiation.

Supplementary Figure 3 Characterization of midbrain-specific organoids.

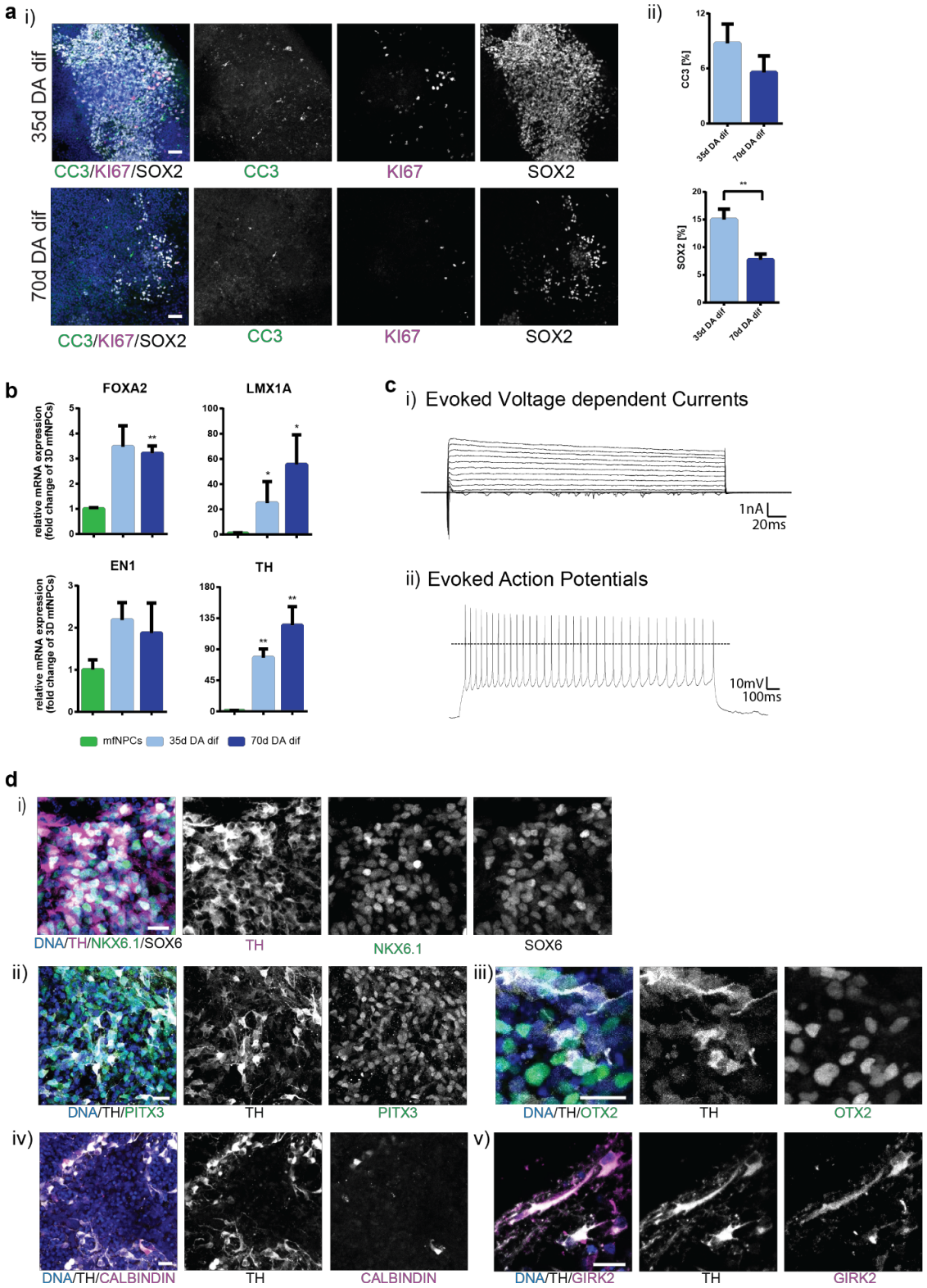

Supplementary Figure 3: Characterization of midbrain-specific organoids. Where indicated, analyses were performed with multiple cell lines (details see below) and a representative image looking similar to the images obtained from all used lines, is displayed. (a) (i) Immunohistological staining of apoptosis marker cleaved-caspase 3 (CC3), cell proliferation marker KI67, and stem cell marker SOX2 in an organoid quadrant. Scale bar is 50 µm. (ii) SOX2 and CC3 positive pixels expressed as a percentage of the total Hoechst signal (mfNPC lines H1-3, three passages each, n=9, here representative images are shown for line H1). (b) qRT-PCR analysis for mDAN markers FOXA2, LMX1A, EN1, and TH. Data presented as mean ±SEM, * p-value < 0.05, ** p-value < 0.01 (mfNPC lines H1-4, n=4). (c) Representative traces of voltage-gated sodium inward and potassium outward currents (i) evoked by stepwise depolarizations and sustained firing patterns of evoked action potentials (ii) upon a current-step application (i.e. 50 pA). These recordings were obtained from the same cell displayed in Figure 1 from a dissociated 3D culture of 75 days from line H4. Black plain line in (ii) indicates 0 mV. Experiment conducted with mfNPC line H4, P2-GC and P3-GC, in total 26 cells were recorded. (d) Immunostaining for indicated ventral midbrain markers of 35 old organoid middle (i)-(iv) and edge sections (v). Scale bars are 20 µm. hMOs derived from mfNPC lines H1-4, here representative images are shown for line H1 (i and iii) and line H2 (ii, iv, v).

Supplemetary Table 1

cell lines	Derivation conditions	Gender	Age at sampling	Genotype	Comment	hiPSC ID	Figure
H1	2D	Female	81	LRRK2 WT	Reinhardt *et al.*, 2013	2.0.0.10.1.0	S1C, D, S2B, C
	3D	Female	81	LRRK2 WT	Reinhardt *et al.*, 2013	2.0.0.10.1.0	1B, C, E, F, G, S3A, B, D
H2	3D	Male	n.a	LRRK2 WT	Alstem (iPS15)	2.0.0.33.0.0	1B, C, E, G, S3A, B, D
H3	3D	Female	n.a.	LRRK2 WT	Bill Skarnes, WTSI	2.0.0.19.0.0	1B, C, E, G, H, 2A, B, C, S3A, B, D
H3-G2019S (isogenic to H3)	3D	Female	n.a.	LRRK2 G2019S	Qing *et al.*, 2017	2.0.8.19.0.7	2B, C
H4	3D	Female	cord blood	LRRK2 WT	Gibco (A13777)	2.0.0.15.0.0	1D, F, 2A, B, C, S3B, C, D
H4-G2019S (isogenic to H4)	3D	Female	cord blood	LRRK2 G2019S	Qing *et al.*, 2017	2.0.8.15.0.7	2B, C
P1-GC	2D	Female	81	LRRK2 WT	Reinhardt *et al.*, 2013	2.1.2.11.2.0	S1B, C, D, S2B, C, D
P2	3D	Female	54	LRRK2 G2019S	Reinhardt *et al.*, 2013	2.1.1.46.0.0	2A, B, C
P2-GC (isogenic to P2)	2D	Female	54	LRRK2 WT	Reinhardt *et al.*, 2013	2.1.2.46.0.0	S1B, C, D, S2B, C, D
	3D	Female	54	LRRK2 WT	Reinhardt *et al.*, 2013	2.1.2.46.0.0	1D, S3C, 2B, C
P3	3D	Female	81	LRRK2 G2019S	Reinhardt *et al.*, 2013	2.1.1.11.3.0	2A, B, C
P3-GC (isogenic to P3)	3D	Female	81	LRRK2 WT	Reinhardt *et al.*, 2013	2.1.2.11.3.0	1D, S3C 2B, C

Supplementary Table 1 related to experimental procedures: Cell lines used in this study to generate 2D or 3D cultures. Human mfNPCs were derived from iPSCs that have been previously published [1,2]. Our data set includes iPSCs of healthy or diseased origin (H=healthy, P=PD patient with LRRK2-G2019S mutation). Additionally, cells were derived from isogenic controls, with either inserted LRRK2 mutation (H-G2019S) or gene corrected LRRK2 mutation (P-GC). The last column shows the contribution of each cell line to the data in the respective figure.

Supplementary Table 2

Antibody	Species	Source	Ref.-No.	Dilution
Calbindin	mouse	swant	300	1:500
CC3	rabbit	Cell Signaling Technology	9661	1:200
CORIN	rat	R&D systems	MAB2209	1:500
DAT	rat	Abcam	Ab5981	1:200
DDC	rabbit	Thermo Scientific	PA5-25450	1:25
Dopamine	rabbit	ImmuSmol	IS1005	1:500
EN1	goat	Santa Cruz	sc- 46101	1:300
FOXA2	mouse	Santa Cruz	sc-101060	1:250
GIRK2	goat	Abcam	Ab65096	1:200
KI67	mouse	BD Biosciences	550609	1:200
LMX1A	rabbit	Abcam	ab139726	1:200
LMX1A	rabbit	Sigma	HPA030088	1:1000
NKX6.1	mouse	DSHB	F55A10	1 mg/ml
OTX2	goat	R&D	AF1979	1:500
OTX2	goat	R&D	AF1979	1:500
PAX3	mouse	DSHB	Pax3	1 mg/ml
PAX6	rabbit	Covance	PRB-278P	1:300
PITX3	rabbit	Millipore	AB5722	1:200
SOX1	goat	R&D systems	AF3369	1:100
SOX2	goat	R&D systems	AF2018	1:200
SOX2	goat	Santa Cruz	Sc- 17320	1:400
SOX6	rabbit	Sigma	HPA001923	1:200
TH	chicken	Abcam	ab76442	1:1000
TH	rabbit	Abcam	ab112	1:1000
TH	rabbit	Santa Cruz	sc-14007	1:1000
TH	rabbit	Santa Cruz	14007	1:300
TH	mouse	Immunostar	22941	1:100
TH	rabbit	Millipore	657012	1:400
TUJ1	mouse	BioLegend	801201	1:600
TUJ1	rabbit	Covance	PRB-435P-0100	1:600
TUJ1	chicken	Millipore	AB9354	1:600
TUJ1	mouse	Covance	MMS-435P-100	1:1000

Supplementary Table 2 related to experimental procedures: Antibodies used in this study.

Supplementary Table 3

Feature	Description
Related to Figure 1:	**Generation of midbrain-specific organoids**
Nuclei mask	Count of nuclear positive pixels.
CC3 mask	Count of cleaved-caspase 3 positive pixels.
CC3 percentage	CC3 mask / Nuclei mask expressed as percentage.
SOX2 mask	Count of SOX2 positive pixels.
SOX2 percentage	SOX2 mask / Nuclei mask expressed as percentage.
Related to Figure 2:	**Disease modeling of PD patient-derived midbrain-specific organoids**
Nuclei mask	Count of nuclear positive pixels.
Nuclei mask high	Count of nuclear positive pixels higher than the threshold (4000) identifying pyknotic nuclei.
TH mask	Count of TH positive pixels.
TH skeleton	Count of TH skeleton pixel (red). Skeleton is calculated using a thinning function resulting in a simplified representation of the neuronal branching. The skeleton allows identifying nodes and links. 
Nodes	Total number of points located at a bifurcation of neuronal branching (red points), generated from the TH skeleton. 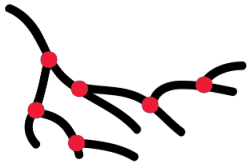
Links	Total number of connecting segments originated from the nodes (red lines), generated from the TH skeleton. 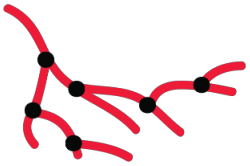
TH+/Nuclei	TH mask / Nuclei mask.
TH percentage	Percentage of number of neurons positive for TH. For this feature, nuclei

	were segmented with watershed function. Only nuclei segmented as single element were kept. The number of segmented nuclei positive for TH was calculated as a percentage of the total number of nuclei.
TH Fragmentation	Surface to volume ratio of TH mask.
FOXA2 mask	Count of FOXA2 positive pixels.
FOXA2+/Nuclei	FOXA2 mask / Nuclei mask.
TH+/FOXA2+	FOXA2 mask in TH positive neurons.
TH+/FOXA2+/Nuclei	FOXA2 mask identified in TH positive neurons/ Nuclei mask.
TH-/FOXA2	FOXA2 mask in TH negative perinuclear zone.
TH-/FOXA2+/ Nuclei	FOXA2 mask identified in TH negative neurons/ Nuclei mask.

Supplementary Table 3 related to Figure 1 and 2 and experimental procedures: Features from image analysis (adapted from Bolognin *et al.*, 2018[3]).

Supplementary Table 4

time point	comparison	THpos/FOXA2pos		Nodes		THneg/FOXA2pos	
d35	**H vs. H-G2019S**	ns	0.9851	****	< 0.0001	ns	0.8706
	H vs. P-GC	****	< 0.0001	****	< 0.0001	ns	0.1688
	H vs. P	****	< 0.0001	****	< 0.0001	****	< 0.0001
	H-G2019S vs. P-GC	****	< 0.0001	***	0.0007	ns	0.6202
	H-G2019S vs. P	****	< 0.0001	**	0.0022	***	0.0008
	P-GC vs. P	ns	0.9828	ns	0.9919	*	0.0239
d70	**H vs. H-G2019S**	ns	0.9995	ns	0.3920	ns	0.9544
	H vs. P-GC	**	0.0051	****	< 0.0001	ns	> 0.9999
	H vs. P	**	0.0041	****	< 0.0001	ns	0.6593
	H-G2019S vs. P-GC	**	0.0071	****	< 0.0001	ns	0.9627
	H-G2019S vs. P	**	0.0065	****	< 0.0001	ns	0.4017
	P-GC vs. P	ns	0.9940	ns	0.9986	ns	0.7679

Supplementary Table 4 related to Figure 2: Statistical evaluation of the image analysis for PD phenotyping. Several passages of PD patient-derived and healthy hMOs, as well as their isogenic controls (mfNPC H3, H3-G2019S, H4, H4-G2019S, P3, P3-GC, P4, and P4-GC, see Supplementary Table S1) were used. A 2way ANOVA, Tukey's multiple comparisons test was performed, asterisks and adjusted p values indicate significant differences between compared groups, * p-value < 0.05, ** p-value < 0.01, *** p-value < 0.001, **** p-value < 0.0001, ns= not significant.

Supplementary References

1 Qing, X., Walter, J., Jarazo, J., Arias-Fuenzalida, J., Hillje, A.-L. *et al.* CRISPR/Cas9 and piggyBac-mediated footprint-free LRRK2-G2019S knock-in reveals neuronal complexity phenotypes and α-Synuclein modulation in dopaminergic neurons. *Stem cell research* **24**, 44-50 (2017).

2 Reinhardt, P., Glatza, M., Hemmer, K., Tsytsyura, Y., Thiel, C. S. *et al.* Derivation and expansion using only small molecules of human neural progenitors for neurodegenerative disease modeling. *PloS one* **8**, e59252, doi:10.1371/journal.pone.0059252 (2013).

3 Bolognin, S., Fossepre, M., Qing, X., Jarazo, J., Scancar, J. *et al.* 3D Cultures of Parkinson's Disease-Specific Dopaminergic Neurons for High Content Phenotyping and Drug Testing. *Adv Sci (Weinh)* **6**, 1800927, doi:10.1002/advs.201800927 (2019).

CHAPTER 8

Discussion

The lack of advanced experimental *in vitro* models that truly recapitulate the complexity of the human brain is one of the main limitations in neuroscience and in the field of diesease modelling. Current *in vitro* approaches to model physiology and pathology of human neurons are mainly based on pure cultures of neurons grown under 2D conditions. Even though, the resulting cell culture monolayers have been proven as useful tools to study disease mechanisms and to identify potential neuroprotective compounds (Nguyen et al. 2011; Cooper et al. 2012; Sánchez-Danés et al. 2012; Reinhardt, Schmid et al. 2013; Ryan et al. 2013; Spathis et al. 2017), these culture conditions do not recapitulate several characteristics, which are relevant to the human brain. Features like cell–cell interactions and cyto–architecture might be crucial to predict the effectiveness of *in vitro* tested compounds in subsequent clinical trials (Abe-Fukasawa et al. 2018).

A valuable tool, offering an opportunity to understand complex biology in a physiologically relevant context and also allowing advances in translational applications, is the *in vitro* human brain organoid technology (Fatehullah et al. 2016). At the beginning, brain organoid approaches relied mainly on the endogenous capacity of PSCs to self–organise under 3D conditions and thereby to intrinsically recapitulate early steps of the brain development (Arlotta 2018). These approaches resulted in ectodermal derivatives with complex cyto–architechtures beyond what is possible

with 2D PSC derivatives (Kadoshima et al. 2013, Lancaster, Renner et al. 2013, Paşca et al. 2015). As neurons form functional networks with other neurons and non–neuronal cells in the brain, it is essential to expand our research of neurodegenerative diseases using 3D models that are able to reproduce these interactions. In general, 3D conditions are able to mimic more closely *in vivo* environments and therefore, enable an accelerated neuronal differentiation and neural network formation *in vitro* (Haycock 2011; D'Avanzo et al. 2015). Moreover, it has been shown that neurons developed in a 3D environment express neuronal genes more accurately than neurons derived in 2D conditions (Seidel et al. 2012). A monolayer of neurons cannot provide as many linkages between individual cells as a 3D neuronal culture. Along with this, the smaller synaptic distances in a 3D neuronal network promotes a functional signal transduction (Cullen et al. 2012; D'Avanzo et al. 2015). By creating a third dimension, neurons will develop in an environment that is more mature and relevant to human physiology and therefore gain morphological and physiological properties similar to those *in vivo*.

8.1 Derivation of midbrain–specific organoids

Organoids, specifically modelling the human midbrain, hold great promises for studying the human brain development and for modelling the neurodegenerative disorder PD. To achieve the *in vitro* derivation of a very distinct region, like the human midbrain, additional stimuli of specific pathways along with the 3D PSC culture are required. Up to this point, six 3D cell culture approaches have been published by different research groups for deriving tissue that resembles features of the human midbrain (Tieng et al. 2014; Qian et al. 2016; Jo et al. 2016; Monzel et al. 2017; Kim et al. 2019; Smits, Reinhardt et al. 2019). All of these approaches can be attributed to previous 2D cell culture experiments, which explored the fundamentals for the generation and characterisation of midbrain fate–specific cells, derived from PSC via exogenous patterning cues (Kriks et al. 2011; Kirkeby et al. 2012). The initial step for the derivation is the formation of EBs and induction of the neuroectoderm via dual–SMAD inhibition. In all of the here compared hMO protocols, SB was used to inhibit the Activin/TGF–β signalling pathway (see Table 8.1 on page 87). The further combination with BMP pathway inhibitors enabled a full neural conversion of the PSCs. The use of BMP antagonists Noggin, LDN, and DM

TABLE 8.1: **Comparison of hMO derivation protocols:** Overview of applied compounds to derive midbrain–specific neuralectoderm by neural induction. hMO protocols from TIENG (2014) and QIAN (2016) are based on 2D experiments by KRIKS et al. (2011); hMO protocols from JO (2016) and KIM (2019) are based on 2D experiments by CHAMBERS et al. (2009); hMO protocols from MONZEL (2017) and SMITS (2019) are based on 2D experiments by REINHARDT et al. (2013).

	TIENG (2014)	QIAN (2016)	JO (2016)	MONZEL (2017)	KIM (2019)	SMITS (2019)
Dual–SMAD inhibition						
SB	10 μM	10 μM	10 μM	10 μM	10 μM	10 μM
Noggin	—	—	200 ng/ml	—	200 ng/ml	—
LDN	100 nM	100 nM	—	—	—	150 nM
DM	—	—	—	1 μM	—	—
WNT activation						
CHIR	3 μM	3 μM	3 μM	3 μM	3 μM	3 μM
SHH activation						
SHH	100 ng/ml	100 ng/ml	100 ng/ml	—	100 ng/ml	—
PMA	2 μM	2 μM	—	0.5 μM	—	—
SAG	—	—	—	—	—	0.5 μM
FGF8 activation						
FGF8	100 ng/ml	100 ng/ml	100 ng/ml	—	100 ng/ml	—

has been shown in 2D (Chambers et al. 2009; Kriks et al. 2011; Reinhardt, Glatza et al. 2013) and applied in 3D stem cell cultures (see Table 8.1). To control the specification of the neural progenitor cells, CHIR, a potent, chemical inhibitor of GSK–3β, was used to dose–dependently activate the Wnt signalling (Kirkeby et al. 2012, see Table 8.1). The final patterning towards midbrain floor plate precursors requires a treatment with small molecule activators of the SHH signalling, like recombinant SHH, PMA or smoothened agonist (SAG) (Kriks et al. 2011; Smits, Reinhardt et al. 2019). This composition of exogenous patterning cues results in neural progenitors that can give rise to authentic, midbrain–specific DANs (Kriks et al. 2011, Kirkeby et al. 2012, Doi et al. 2014, Nolbrant et al. 2017). Moreover, the further development of these protocols allowed the derivation of 3D cultured hMO. In contrast to 2D monolayer cultures, hMOs can recapitulate complex interactions of mDANs with other cell types of the CNS in a 3D environment. An enormous amount of disease–relevant mDANs that can be produced in a rapid and reproducible way, is required for disease modelling and drug discovery in the field of PD. Numerous published protocols describe the generation of ventral mDANs from human PSCs in

2D, by replicating mDAN *in vivo*–specification *in vitro* (Kriks et al. 2011, Kirkeby et al. 2012, Doi et al. 2014, Nolbrant et al. 2017). Although current protocols are based on the generation of LMX1A/FOXA2 positive midbrain floorplate progenitors, differentiations starting from PSCs are time–consuming and typically result in cultures containing various neuronal identities (Hargus et al. 2010; Kriks et al. 2011; Kirkeby et al. 2012; Grealish et al. 2014). Typically, brain organoids are generated from PSCs by profiting from developmental processes (Lancaster, Renner et al. 2013; Clevers 2016) or by creating an environment favouring specific stem cell niches (Tieng et al. 2014; Qian et al. 2016; Jo et al. 2016; Kim et al. 2019). However, the utilisation of NSCs as a starting population for hMOs has the advantage that already patterned cells differentiate more efficiently into the desired structures. Other adult stem cell–derived organoid cultures have been established for instance, for the generation of intestinal or lung organoids. They contain cell types that are present in the organ from which they were derived and recapitulate some degree of its spatial organisation (Clevers 2013; Huch et al. 2015; Drost et al. 2017). Similarly and in contrast to other existing hMO derivation protocols, we were able to show the presence of midbrain–specific stem cell niches and clusters of mDANs in our NSC–derived hMO model (Monzel et al. 2017). Therefore, we report an approach to efficiently differentiate mDANs within hMOs by starting from expandable neural precursor cells (NPCs) (Monzel et al. 2017; Smits, Reinhardt et al. 2019; Smits, Magni et al. 2019, see Table 8.3 on page 93). Both hMO models have been already used in other studies (Jan et al. 2018; Berger et al. 2018).

Among the published hMO protocols, different approaches were presented to estimate the number of mDANs that arise during the organoid development (see Table 8.2 on page 89). Tieng and Qian dissociated their 3D structures and cultured the resulting single cells as a monolayer (Tieng et al. 2014; Qian et al. 2016). Their quantification resulted in more than 60 % TH–positive cells in 21 day–old cultures (Tieng et al. 2014) and around 55 % TH–positive cells after 65 days (Qian et al. 2016). A more straightforward method to quantify the mDAN population is flow cytometry via fluorescence–activated cell sorting (FACS), which also requires dissociated hMOs. By doing so, we showed that after 61 days of culture around 64 % cells were triple–positive for the mDAN markers TH, LMX1A, and FOXA2 (Monzel et al. 2017). Surprisingly, with the same method Jo and co–workers identified only around 22 % of MAP2–positive neurons co–expressing TH in their hMOs after 60 days of culture (Jo et al. 2016). A third approach to estimate the percentage of mDANs within hMOs has been described in our recent publication (Bolognin

TABLE 8.2: **Comparison of characteristics of different hMO derivation protocols:** Overview of hMO–specific features reported in Tieng et al. 2014, Qian et al. 2016, Jo et al. 2016, Monzel et al. 2017 (see Chapter 5), Kim et al. 2019, and Smits, Reinhardt et al. 2019 (see Chapter 7)/Smits, Magni et al. 2019 (see Chapter 6) (•different methods applied to determine and calculate TH content, °different methods applied to determine DA content, ⋆data not shown).

	TIENG (2014)	QIAN (2016)	JO (2016)	MONZEL (2017)	KIM (2019)	SMITS (2019)
mDANs						
TH•	>60 % (d21)	55 % (d65)	22 % (d60)	64 % (d61)	n/a	54 % (d70)
DAT	n/a	yes	yes	yes	yes	yes
DA°	yes	yes	yes	yes	yes	yes
NM	n/a	n/a	yes	yes	n/a	yes
glial cells						
oligodendrocytes	yes	n/a	yes	yes	n/a	yes⋆
myelination	yes	n/a	n/a	yes	n/a	yes⋆
astrocytes	yes	yes	yes	yes	n/a	yes⋆
neuronal subtypes						
GABAergic	no	n/a	yes	n/a	n/a	yes
glutamatergic	yes	n/a	n/a	n/a	n/a	yes
serotonergic	no	n/a	n/a	n/a	n/a	yes

et al. 2019; Smits, Reinhardt et al. 2019). With in–house developed image analysis algorithms, enabling the automated segmentation of nuclei and neurons, we quantified around 62 % TH–positive cells after 35 days and around 54 % TH–positive cells after 70 days of 3D culture. The application of high–content image–analysis allows us to examine entire organoid sections, rather than dissociated single cells, which preserves the original morphology and cell–cell interactions of the mDANs (Smits, Reinhardt et al. 2019).

TH is a marker commonly used for mDAN detection, as it is a rate–limiting enzyme for DA biosynthesis. However, it is also expressed in other catecholaminergic cell types and does not represent a unique marker specifically for mDANs, as it is the case for example for the DAT or the actual presence of the neurotransmitter DA (Abeliovich et al. 2007). DAT expression was reported in almost every hMO model (see Table 8.2 on page 89, Qian et al. 2016; Jo et al. 2016; Monzel et al. 2017; Kim et al. 2019; Smits, Reinhardt et al. 2019). TIENG and co–workers did not show the presence of DAT in their engineered nervous tissues (ENTs), but they were able

to prove the synthesis of DA via high–performance liquid chromatography (HPLC) after cell lysis (Tieng et al. 2014). Also Jo and Kim applied the same method to assess the DA content within the hMOs (Jo et al. 2016; Kim et al. 2019). To verify that the mDANs were not only able to produce DA, but actually to truly release the neurotransmitter, we did not lyse our organoids but analysed the supernatant of the 3D cultures with an enzyme–linked immunosorbent assay (ELISA). We determined a DA release that increased as the hMOs matured (Smits, Reinhardt et al. 2019).
An interesting observation was reported for the first time by Jo et al., they detected insoluble, dark–coloured deposits in their hMOs after approximately 60 days (Jo et al. 2016). With a Fontana–Masson staining they confirmed that these granules were NM, which is a byproduct of the DA biosynthesis and accumulates postnatally in the SNc of the human brain (Zecca et al. 2003; Pasca 2018; Kim et al. 2019). Also our hMO culture protocols stimulated the production of NM (Monzel et al. 2017; Smits, Reinhardt et al. 2019, see also Table 8.2 on page 89).

The presence of NM is a unique feature of the primate brain (Pasca 2018). It is neither apparent in mice brains nor murine midbrain–specific organoids (Dawson, Ko et al. 2010; Fedorow et al. 2005; Marton et al. 2016; Jo et al. 2016). Wild–type mDANs, derived and cultured in monolayer conditions, only produce NM after an artificial inductions of progerin expression, which is associated with premature ageing (Miller et al. 2013; Sterneckert et al. 2014). Membrane–bound, dense pigmented aggregates of NM was also detected in long–term cultures of homozygous DJ–1 mutant and idiopathic PD patient–derived mDANs (Burbulla et al. 2017). Currently, it is unknown whether NM has a protective or rather damaging effect on the cell survival, however it is proven that NM–containing mDANs of the SNc are especially vulnerable during the course of PD (Zecca et al. 2003; Marton et al. 2016; Jo et al. 2016). Therefore, the here presented hMOs have a great potential to be used for *in vitro* PD modelling, possibly revealing specific phenotypes that are not abundant in wild–type 2D cultures or murine models. Moreover, hMOs provide the basis for future studies about the role of NM in PD (Michel et al. 2016; Marton et al. 2016).
As mDANs are essential to model the human midbrain, hMO research has so far focused mainly on this specific type of neurons. Nevertheless, a detailed study of Borroto–Escuela, et al. (2018) described that the released DA can diffuse into synaptic regions of glutamate and γ–aminobutyric acid (GABA) synapses and directly affect other striatal cell types possessing DA receptors (Borroto-Escuela et al.

2018). Furthermore, *substantia nigra* (SN) dopaminergic neurons are directly controlled by GABAergic input (Tepper et al. 2007). Evidences from these studies suggest that the presence of other neuronal subtypes is important to be able to model multifactorial disease like PD.

A first transcriptional characterisation of hMO was performed by Jo and co–workers, showing that aspects of prenatal midbrain gene expression profiles were resembled in the organoids in contrast to the conventional 2D–derived mDANs (The GTEx Consortium 2015; Lin et al. 2016; Jo et al. 2016). For a further validation of the genetic expression profile during the course of hMO development they suggested conducting a single–cell transcriptome analysis, as it has been shown before for cerebral organoids (Camp et al. 2015; Kageyama et al. 2018).

In our recent study, we analysed single–cell transcriptomic data from hMOs (Smits, Magni et al. 2019). We demonstrated that there is an increased expression of neuronal– and stem cell–specific genes in 35 day– compared to 70 day–old hMOs, whereas exclusively the gene–gene correlations between only neuron–specific genes increased considerable at day 70. This signifies an increasing commitment of cells towards the neuronal cellular fate during the course of organoid development and further supports the finding of a progressive maturation of post–mitotic neurons. The identification of these neuron–specific genes revealed that the genes up–regulated at the earlier time point are rather relevant in the process of neurogenesis and neuronal migration and differentiation (for example early B–cell factor 3 (EBF3), Garcia-Dominguez 2003 and L1 cell adhesion molecule (L1CAM), Patzke et al. 2016), whereas the up–regulated genes at the later time point have been for instance implicated *in vivo* in a modulatory contribution to neurite extension (for example repulsive guidance molecule B (RGMB), Ma et al. 2011). This indicates a higher commitment of the cells toward their intended fate and thereof a progressive maturation of post–mitotic neurons within the hMOs.

As the presence of neuronal subtypes, like glutamatergic and GABAergic neurons has been reported in hMOs before (Tieng et al. 2014; Jo et al. 2016), we applied the high–resolution single-cell analysis to address residence of specific neuronal subtypes (Smits, Magni et al. 2019). We investigated the expression of genes typical for dopaminergic, glutamatergic, GABAergic, and serotonergic neurons and further confirmed their presence by immunohistochemistry staining for the respective neurotransmitters. This allowed us to robustly detect dopaminergic, glutamatergic and GABAergic neurons as well as a few serotonergic neurons within hMOs (see

Table 8.2 on page 89). However, not only the detailed characterisation of the neuronal population is crucial for an accurate modelling of the human midbrain. In addition, the presented models for hMOs have been characterised for astroglia and oligodendrocyte differentiation (see Table 8.2 on page 89). The presence of astrocytes is essential for the formation of synapses and regular neuronal activity (Chung et al. 2015). As astrocytes are specified later than neurons during development, astrocyte immunoreactivity is detectable in hMOs only after 35 days of cultivation (Molofsky et al. 2012; Chaboub et al. 2013; Monzel et al. 2017).

Interestingly, it has been shown that the application of a γ–secretase inhibitor, such as DAPT, during the the hMO maturation phase, also promotes the differentiation into glial fibrillary acidic protein (GFAP)–positive cells (Tieng et al. 2014). Along with this observation, we experienced an earlier development of glial cells in our hMO model treated with DAPT (GFAP–positive cells from day 35 on, data not shown, Smits, Reinhardt et al. 2019), compared to the model cultured without the addition of DAPT (GFAP–positive cells from day 61 on (see Table 8.3 on page 93, Monzel et al. 2017), indicating a stimulating effect on the differentiation of NSCs (Zhou et al. 2010). Fast information transmission between neurons depends on axonal myelination, which is achieved by oligodendrocytes. In most stem cell–based differentiation protocols, the differentiation into oligodendrocytes is extremely inefficient (Bunk et al. 2016, Jablonska et al. 2010). However, in our approach we achieved a differentiation into oligodendrocytes and detected myelination of non–dopaminergic neurons (Monzel et al. 2017). Some neurites in these hMOs are ensheathed by oligodendrocytes and even structures such as the nodes of Ranvier become apparent, which are of critical importance for saltatory transmission of signals in axons (Faivre-Sarrailh et al. 2013). The feature of unmyelinated or thinly myelinated neurons is particularly well described for SNc mDANs, and explains why we quantified only about 30 % of βIII Tubulin (TUJ1) and myelin basic protein (MBP) overlapping cells in our hMO system (Braak and Del Tredici 2004; Orimo et al. 2011; Sulzer and Surmeier 2013; Monzel et al. 2017). Interestingly, in our second and most recent hMO approach, we could already detect the expression of a myelin–associated enzyme (2', 3'–cyclic nucleotide 3'–phosphodiesterase (CNPase)) after 35 days of differentiation, however we were not able to detect an overlapping expression with neuronal markers (data not published, see Table 8.3 on page 93, Smits, Reinhardt et al. 2019).

To allow the future application and improve the impact of hMOs for pathophysiological and pharmacological studies, the electrical activity and functional maturity

TABLE 8.3: **Comparison of in–house hMO models:** Overview of selected features of hMOs approaches published in Monzel et al. 2017 (see Chapter 5) and Smits, Reinhardt et al. 2019 (see Chapter 7) (⋆different methods applied to determine TH content, °data not shown).

	MONZEL (2017)	SMITS (2019)
culture conditions		
used cell type	smNPCs	mfNPCs
number of cells	9,000	3,000
embedding	yes	no
agitation	yes	no
mDANs		
TH+ cells⋆	∼64 % (d61)	∼54 % (d70)
regionalisation	yes	no
A9/A10 specificity	yes	yes
DAT	yes (d61)	yes (d70)
D2/D3 receptor responsive	yes	yes
DA release	no	yes
NM	yes (>d149)	yes (>d100)
other cell types		
oligodendrocytes	yes (d61)	yes° (d35)
myelination	yes (d61)	no° (d70)
astrocytes	yes (d61)	yes° (d35)
neuronal subtypes	n/a	yes

of the midbrain–specific 3D cultures were assessed. Non–invasive recordings of extracellular field potentials can be achieved by a MEA system and allow insights into physiological properties of *in vitro* cultures (Luhmann et al. 2016). TIENG and co–workers detected spontaneous and evoked electrophysiological activities in their ENTs (Tieng et al. 2014). Furthermore, in the study of MONZEL et al., we detected spikes that occurred close in time on multiple electrodes, which indicates neuronal network synchronicity (Monzel et al. 2017).

To specifically determine the activity of different neuronal receptors within the organoid, the response to chemical compounds can be examined. The functionality of DA receptors has been tested with the application of quinpirole, a specific D2/D3 receptor agonist. It has been used already in several studies and it has been shown to affectively suppress the firing in hMOs (Jo et al. 2016; Monzel et al. 2017; Smits, Magni et al. 2019). Together with the reported DA production and release, this strongly suggests that TH-positive neurons, developed in hMOs, exhibit electrophysiological and biochemical qualities of mature mDANs and express

functional, quinpirole–responsive DA receptors. To further isolate and attribute the recorded signals to neuronal subtypes, we additionally blocked inhibitory and excitatory communication with specific drugs, following an established experimental design by Illes and co–workers. Gabazine induces a disinhibition of GABAergic neurons, whereas NMDA–receptor and AMPA/Kainate-receptor antagonists inhibit glutamatergic excitatory communication (Illes et al. 2014).
Together with the characteristic hallmarks of synapse formation, consisting of a direct contact between pre– and postsynapses and composing the prerequisite for electrophysiological and neuronal network functionality, these experiments confirmed additionally to the present functional DA receptors also functional GABAergic and glutamatergic neurons within the hMOs. As neurons do not exist in isolation in the CNS but rather form functional networks with other neurons and non–neuronal cells, it is important to expand our research of neurodegenerative diseases using 3D models that are able to recapitulate cell autonomous as well as non-cell autonomous aspects. Utilising 3D cell culture models that comprise a variety of neuronal subtypes could lead to new insights into the selective vulnerability, which are observed in neurodegeneration. Evidence suggests that specific regulation of the excitability of mDANs by other neuronal subtypes in the midbrain might explain their selective vulnerability in PD (Korotkova et al. 2004). This underlines the importance and the enormous potential for future disease modelling of the hMO model, as it contains functionally connected heterogeneous neuronal populations.

8.2 Disease modelling in midbrain–specific organoids

The second most common degenerative neurological disorder after AD is PD, defined by the selective loss of mDANs in the SNc of the human midbrain (see Section 1.1). The establishment of region–specific brain organoids offers new possibilities to study neuronal diseases that are linked to a specific part of the human brain, such as PD. With our recent publication, we provide a proof–of–principle study that either patient–derived or genetically modified hMOs harbouring the disease–associated G2019S mutation in the *LRRK2* gene show PD–relevant phenotypes including reduced number of mDANs (Smits, Reinhardt et al. 2019). By evaluating the number

of links (branching) and nodes (dendrite bifurcation points) of the mDANs developed within the different hMO groups, we identified a significant reduction of the dopaminergic network complexity in the patient–derived TH–positive neurons, which is also known to occur in PD patients' brain (Bernheimer et al. 1973; Kordower et al. 2013; Smits, Reinhardt et al. 2019). Based on another published hMO protocol, Kim and co–workers also derived organoids carrying the *LRRK2*–G2019S mutation (Jo et al. 2016; Kim et al. 2019). In line with our findings, Kim et al. discovered that the mDANs within the *LRRK2*–G2019S organoids reveal a decreased neurite length in comparison to the mDANs within the control organoids. They further assessed an overall decreased expression level of mDANs–specific markers, like TH, aromatic l–amino acid decarboxylase (AADC), and DAT in their engineered *LRRK2*–G2019S hMOs (Kim et al. 2019). They achieved a partial retrieval of the expression level of those genes after treating the *LRRK2*–G2019S mutant organoids with the *LRRK2* kinase inhibitor GSK2578215A. This *LRRK2* inhibitor suggests to have a positive impact on mDAN cell death and additionally proves that this 3D cell culture system is susceptible to investigating therapeutic strategies against PD (Kim et al. 2019). Kim and co–workers additionally determined, whether hMOs carrying the *LRRK2*–G2019S mutation exhibit an abnormal localisation of α–synuclein that is phosphorylated at serine 129 (pS129). They claim that pS129–α–synuclein is aberrantly expressed in mutated hMOs and they detected a *LRRK2*–G2019S mutation–dependent increase of thioflavin T–positive deposits in TH–positive neurons over time, even though the overall α–synuclein expression did not seem to increase (Kim et al. 2019). Here, methodological problems raise questions about these determined results, as these detected thioflavin T–positive deposits seem to be extracellular and are not clearly overlapping with the TH signal. Whether these finding would be reproducible with another analytical method, was not explored. Nevertheless, the assessment of PD–associated pathologies, like the synucleinopathies, in human–specific advanced cell culture models is crucial due to the inherent differences between human and mouse mDAN vulnerability and as existing murine transgenic models were not efficient to develop an accurate representation of the underlying disease mechanisms (Byers et al. 2012; Burbulla et al. 2017; Koh et al. 2018; Hemmer et al. 2018).

In the study of Smits et al., we demonstrated a significant increase of FOXA2–positive progenitor cells in the patient–specific organoids (Smits, Reinhardt et al. 2019). Since FOXA2 is required for the generation of mDANs, we hypothesise that

this might be a compensatory response to an impaired specification of mDANs promoted by the mutated *LRRK2* gene (Sasaki et al. 1997). Similar compensatory mechanisms have been described in PD before and might represent an attempt to counteract neurodevelopmental defects induced by PD–specific mutations (Blesa, Trigo-Damas et al. 2017). Neurodegenerative disorders, such as PD, are typically considered to be age–associated diseases (Sepe et al. 2016, Xu, Yang et al. 2016). However, there is accumulating evidence that PD has a strong neurodevelopmental component that probably defines the susceptibility to develop the disease (Garcia-Reitboeck et al. 2013; Le Grand et al. 2015; Schwamborn 2018). Our finding supports the importance of human brain development models to investigate the disease's underlying mechanisms.

While introducing also isogenic control hMOs in this study, we could confirm that the introduction of the *LRRK2*–G2019S mutation caused deleterious effects on the complexity of mDANs within a healthy background. On the contrary, *LRRK2*–G2019S gene correction within a PD patient background is not sufficient to rescue this effect. As *LRRK2*–G2019S is not fully penetrant and the probability of developing PD individually varies among the carriers, it is suggested that its pathological function comprises of additional pathways (Smith et al. 2006; Goldwurm et al. 2007). In this context, a permissive genetic background, due to cumulative genetic variants, might mediate and either enhance or diminish the *LRRK2*–induced neurodegeneration (Bolognin et al. 2019). Remarkably, in our analysis of all studied features, the PD patient–derived lines cluster together, independently of the presence or absence of the mutation (Smits, Reinhardt et al. 2019). This indicates that the genetic background of the PD patients, regardless of gene editing, accounts for most of the differences between the studied cell lines and seems to be a major discriminating factor. Thus, not the *LRRK2*–G2019S mutation but rather the genetic background of the patients constitutes the strongest contribution to the phenotypes and supports the hypothesis that the genetic background of PD patients can influence the degeneration of mDANs (Bolognin et al. 2019).

These findings show that 3D hMOs and the thereof derived mDANs represent powerful new tools for *in vitro* disease modelling. The patient–specific nature of these models also opens promising avenues for future personalised medicine approaches (Bu et al. 2016; Hillje et al. 2016; Smits, Reinhardt et al. 2019).

CHAPTER 9

Summary and Perspectives

The work presented in this thesis reveals novel findings in the field of advanced 3D *in vitro* cell culture systems. We aimed to generate and characterise two novel midbrain–specific organoid protocols and thereby provide sophisticated *in vitro* models to study both neurodevelopmental processes and neurodegenerative diseases of the human midbrain.

Contrary to previously published organoid models, we derived an organoid system from NSCs, committed to the ventral neural tube fate of the mesencephalon. A subsequent application of spatio–temporal specific signalling under 3D culture conditions, led to the establishment of two novel hMO methods. We evaluated the differentiation efficiency into true mDANs and assessed their cellular environment within the hMOs. A detailed *in vitro* characterisation of diverse developing cell populations and their functional properties, enabled us to evaluate the identity and composition of the hMOs.

Furthermore, we determined the potential of our midbrain–specific model for its application in modelling neurological diseases and we addressed, whether hMOs are suitable to reveal PD–relevant phenotypes. Focusing on the investigation of PD–specific pathomechanisms, we generated hMOs from PD patients carrying the *LRRK2*–G2019S mutation and compared them to healthy control hMOs. With that,

we were able to report for the first time PD–relevant phenotypes in PD patient–derived hMOs and proved that our newly derived method is a powerful tool for human–specific *in vitro* disease modelling of neurological disorders.

For such applications, an organoid model should be reproducible and stable for extended cultivation and manipulation. And even though the organoid technology is a powerful asset in the field of brain research, the hMO models show intrinsic disadvantages and limitations (Berger et al. 2018; Wang, Zhu et al. 2018).
The lack of a natural body axis or supportive tissue prevents an organoid organisation that is identical to the pattern of the *in vivo* human brain (Lancaster, Renner et al. 2013; Kelava et al. 2016a; Wang, Zhu et al. 2018). The identification of a specific brain region but also the reproducibility might be impaired, nevertheless it is unlikely to create the exact culture condition that can be found in the human brain *in utero* (Trujillo et al. 2018). A major limitation of the hMOs presented here, as well as other published brain organoid systems, is the absence of vasculature, which restricts the supply of oxygen and nutrition, especially in the inner part of the organoids (Kelava et al. 2016a; Wang, Zhu et al. 2018). It also might limit the growth of organoids beyond a certain size and the appearance of dead cells in the center of the organoids (Monzel et al. 2017; Berger et al. 2018; Giandomenico et al. 2017). Recently, brain organoids were successfully transplanted into a mouse brain and murine blood vessels could be detected in the grafts (Mansour et al. 2018). Even though the transplanted organoid mimicked more precisely the *in vivo* brain anatomy, this method bears the disadvantage of xenocontamination (Wang, Zhu et al. 2018; Trujillo et al. 2018).
The absence of microglia, the resident innate immune cells of the CNS, is another major disadvantage for disease modelling, as they are actively involved in the development and maturation of neurons. In the case of cerebral organoids, an adaptation for a microglia–containing organoid model has been recently published (Ormel et al. 2018). As our hMOs are derived from the neuroectoderm and microglia originate developmentally from the mesoderm, there is only the opportunity to integrate externally–derived microglia or their precursors to the developing hMO (Muffat et al. 2016; Haenseler et al. 2017; Abud et al. 2017; Trujillo et al. 2018; Wang, Zhu et al. 2018).

Future development of cell culture technologies will further improve brain–specific

organoid models and will support both the investigation of more complicated interactions in the human brain and the modelling of a larger range of neurological disorders (Di Lullo et al. 2017; Wang, Zhu et al. 2018).

Despite these limitations and taking aforesaid into consideration, we can come to the conclusion that the hMO system presented here along with other models may be a first step toward a more human patient–specific, probably even personalised, era of advanced disease modelling and therapy development.

CHAPTER 10

Appendices

APPENDIX A

Original article: Nurr1:RXRα heterodimer activation as monotherapy for Parkinson's disease

This article has been published in the *Proceedings of the National Academy of Sciences* journal.

Nurr1:RXRα heterodimer activation as monotherapy for Parkinson's disease

Athanasios D. Spathis[a,1], Xenophon Asvos[b], Despina Ziavra[a], Theodoros Karampelas[a], Stavros Topouzis[c], Zoe Cournia[a], Xiaobing Qing[d], Pavlos Alexakos[a], Lisa M. Smits[d], Christina Dalla[e], Hardy J. Rideout[a], Jens Christian Schwamborn[d], Constantin Tamvakopoulos[a], Demosthenes Fokas[b], and Demetrios K. Vassilatis[a,1]

[a]Center for Clinical Research, Experimental Surgery, and Translational Research, Biomedical Research Foundation of the Academy of Athens, Athens 11527, Greece; [b]Department of Materials Science and Engineering, University of Ioannina, Ioannina 45110, Greece; [c]Department of Pharmacy, University of Patras, Patras 26504, Greece; [d]Luxembourg Centre for Systems Biomedicine, University of Luxembourg, Esch-sur-Alzette L-4367, Luxembourg; and [e]Department of Pharmacology, Medical School, National and Kapodistrian University of Athens, Athens 11527, Greece

Edited by Michael K. Lee, University of Minnesota, Minneapolis, MN, and accepted by Editorial Board Member Gregory A. Petsko February 22, 2017 (received for review October 16, 2016)

Parkinson's disease (PD) is a progressive neurodegenerative disorder characterized by the loss of dopaminergic (DAergic) neurons in the substantia nigra and the gradual depletion of dopamine (DA). Current treatments replenish the DA deficit and improve symptoms but induce dyskinesias over time, and neuroprotective therapies are nonexistent. Here we report that Nuclear receptor-related 1 (Nurr1):Retinoid X receptor α (RXRα) activation has a double therapeutic potential for PD, offering both neuroprotective and symptomatic improvement. We designed BRF110, a unique in vivo active Nurr1:RXRα-selective lead molecule, which prevents DAergic neuron demise and striatal DAergic denervation in vivo against PD-causing toxins in a Nurr1-dependent manner. BRF110 also protects against PD-related genetic mutations in patient induced pluripotent stem cell (iPSC)-derived DAergic neurons and a genetic mouse PD model. Remarkably, besides neuroprotection, BRF110 up-regulates tyrosine hydroxylase (TH), aromatic l-amino acid decarboxylase (AADC), and GTP cyclohydrolase I (GCH1) transcription; increases striatal DA in vivo; and has symptomatic efficacy in two postneurodegeneration PD models, without inducing dyskinesias on chronic daily treatment. The combined neuroprotective and symptomatic effects of BRF110 identify Nurr1:RXRα activation as a potential monotherapeutic approach for PD.

Parkinson's disease | target validation | neuroprotection

Parkinson's disease (PD) is a common neurodegenerative disease characterized by the progressive loss of dopaminergic (DAergic) neurons in the substantia nigra (SN), leading to striatal dopamine (DA) deficiency (1). Current medications replenish DA and offer temporary symptomatic relief to patients; however, chronic treatments cause serious side effects in almost all patients, including abnormal involuntary movements (AIMs) and dyskinesias, limiting their efficacy (2). Moreover, DA replacement does not impede neurodegeneration, and PD pathology progresses (3). Despite considerable advances in our understanding of PD pathophysiology, pharmacologic strategies to prevent neurodegeneration remain elusive, and the disease remains incurable. Therefore, validation of novel targets that diminish DA replacement side effects and halt or slow disease progression is an urgent unmet clinical need (4).

Nurr1 (NR4A2), a nuclear receptor, is a promising candidate, implicated in both DA biosynthesis and DAergic neuron survival. Nurr1 is expressed in developing and mature DAergic neurons and is required for both survival and final complete DAergic differentiation (5, 6). Nurr1 enhances in vitro and in vivo transcription of tyrosine hydroxylase (TH), the rate-limiting enzyme of DA biosynthesis, and of GTP cyclohydrolase I (GCH1), the first enzyme in the biosynthesis of tetrahydrobiopterin (BH4), an essential cofactor for TH activity (7, 8). Decreased Nurr1 levels have been strongly associated with PD and reduced DAergic neuron survival. Nurr1 ablation in adult mice leads to dystrophic DAergic axons (9), loss of striatal DA (10), and behavioral features of parkinsonism during aging (11). Nurr1 mutations decreasing its mRNA have been found in patients with familial and sporadic PD (12, 13). Given the role of Nurr1 in PD, we theorized that pharmacologic activation of Nurr1 could serve as monotherapy for PD, offering both disease modification and symptomatic relief.

Nurr1 binds to DNA as a monomer, homodimer, or heterodimer with retinoid X receptor (RXR)α or RXRγ. Because Nurr1 heterodimerizes with RXRα in midbrain DAergic neurons (14), we postulated that synthetic ligands that bind to the RXRα-binding pocket would be the preferred approach. RXRα is a heterodimer partner of several nuclear receptors, and existing synthetic RXRα ligands activate several RXRα heterodimers (15). Two such ligands, XCT0135908 and bexarotene (14, 16), have been shown to activate Nurr1:RXRα as well as other RXRα heterodimers. Bexarotene, an approved antineoplastic agent activates RXRα heterodimers with liver X receptor (LXR), peroxisome proliferator-activated receptor gamma (PPARγ), and Nurr1, has shown promising results in animal models of Alzheimer's disease and PD (16, 17), but these results have not been replicated (18, 19). In vitro, XCT0135908 (14) activates Nurr1:RXRα heterodimers and RXRα:RXRα homodimers (17), but its bioavailability is unknown.

Here we show that XCT0135908 does not reach the brain and is essentially inactive in vivo. Rational compound design and synthetic chemistry enabled us to design BRF110, a selective Nurr1:RXRα agonist with combinatorial neuroprotective and symptomatic benefits in preclinical mouse models, validating Nurr1:RXRα heterodimer activation as a promising monotherapy for PD.

Significance

In Parkinson's disease (PD), dopamine (DA)-producing neurons gradually degenerate, leading to DA deficiency and to the main symptoms of PD. Current medications do not impede neurodegeneration, but relieve symptoms by replenishing DA; however, their chronic use causes serious side effects. We targeted a protein required for the development and function of DA neurons by designing a chemical compound that, by activating this protein, increases DA and improves symptoms without current treatment side effects while simultaneously preventing neuron loss in PD mice. Our findings point to a monotherapy that can both impede PD progression and concurrently improve symptoms of PD.

Author contributions: A.D.S., D.F., and D.K.V. designed research; A.D.S., X.A., D.Z., T.K., Z.C., X.Q., P.A., C.D., and H.J.R. performed research; L.M.S., J.C.S., C.T., and D.F. contributed new reagents/analytic tools; A.D.S., X.A., S.T., Z.C., X.Q., C.D., H.J.R., J.C.S., C.T., D.F., and D.K.V. analyzed data; and S.T. and D.K.V. wrote the paper.

The authors declare no conflict of interest.

This article is a PNAS Direct Submission. M.K.L. is a Guest Editor invited by the Editorial Board.

See Commentary on page 3795.

[1]To whom correspondence may be addressed. Email: dvassilatis@bioacademy.gr or thansp@hotmail.com.

This article contains supporting information online at www.pnas.org/lookup/suppl/doi:10.1073/pnas.1616874114/-/DCSupplemental.

Results

XCT0135908 in Vivo: Low Stability and Low Brain Penetration. XCT0135908 was administered to mice to test its bioactivity. Intraperitoneal or intracerebroventricular injections of XCT0135908 (1 and 10 mg/kg) did not result in any changes in expression of midbrain genes, such as c-jun or TH, at various time points after administration. LC-MS/MS (liquid chromatography-tandem mass spectrometry) analysis of blood plasma or brain homogenates and targeted search of the parent compound at 1 and 2 h after i.p. administration of XCT0135908 (1 μg/kg) indicated low compound stability and minimal brain penetration (brain/blood <0.03) (Fig. S1).

Discovery of the Nurr1:RXRα Activator BRF110. Because specific Nurr1:RXRα activators do not exist (20), we confronted the challenge to discover compounds that would be specific for Nurr1:RXRα heterodimers, stable in vivo, and brain-penetrant. Based on existing chemical structures and their function on RXRα in a variety of assays, we synthesized several series of compounds (termed BRFs). Human DAergic neuroblastoma SHSY-5Y cells cotransfected with a DR5-luciferase reporter construct, along with human Nurr1 and RXRα expression plasmids (Fig. 1 *A* and *B*), were treated with each of the experimental compounds at varying concentrations. Compounds active in vitro were routinely administered i.p. in mice (at 1 μg/kg), and brain penetration was evaluated by LC-MS/MS. This scheme and meticulous structure–activity relation analysis resulted in the identification of BRF110 (Fig. 1*C* and Figs. S2 and S3), which activates Nurr1:RXRα heterodimers (EC_{50} ~900 nM; Fig. S4).

In silico docking simulations show that BRF110 complements the hydrophobic L-shaped binding pocket of RXRα [Protein Data Bank (PDB) ID code 1MV9]. The carboxylic group of BRF110, with the participation of a water molecule, forms a hydrogen bond with the backbone amide of A327 and a salt bridge with the side chain of R316. The phenyl ring of BRF110 participates in π–π interactions with F346 and stabilizes the molecule in the RXRα-binding pocket, contributing to target affinity (calculated ΔG, −16.7 kcal/mol) (Fig. 1*D* and Fig. S5*A*). These simulations were validated by methyl or ethyl ester carboxylic group modifications, which abolished activation, increasing EC_{50} by 50- to 100-fold (Fig. S5*B*). In addition, halogenation of the BRF110 phenyl ring disturbs the π–π interactions with F346 and also increases the EC_{50} by approximately sevenfold (Fig. S5*C*).

Specificity of BRF110 for Nurr1:RXRα Heterodimers and Brain Penetration. BRF110 activated Nurr1:RXRα heterodimers (Fig. 1*E*), but did not activate Nurr1:RXRγ heterodimers (Fig. 1*F*), indicating that it is specific for RXRα and does not bind to Nurr1. In naïve SHSY-5Y cells, BRF110 activated endogenous Nurr1:RXRα heterodimers, as verified by loss of activity after knockdown of Nurr1 by ~60% using a retrovirus carrying shNurr1 sequences (Fig. 1*G*), indicating that Nurr1 is required for BRF110 activity (Fig. 1*H*).

To test off-target effects of BRF110 besides Nurr1:RXRα heterodimers, we fused the ligand-binding domains of Nurr1, RXRα, and a variety of related nuclear receptors to the GAL4 DNA-binding domain to create chimeric proteins, and also fused the ligand-binding domain of RXRα with VP16. These molecular chimeras were cotransfected in pairs with RXRα:VP16 along with a GAL4-responsive luciferase reporter in SHSY-5Y cells stimulated with BRF110. BRF110 strongly activated Nurr1GAL4:RXRαVP16 heterodimer chimeras, but failed to activate other RXRαVP16 heterodimer chimeras with vitamin D receptor VDRGAL4, RXRγGAL4, PPARγGAL4, or RXRαGAL4 homodimer chimeras (Fig. 1*I*). Nur77GAL4:RXRαVP16 heterodimers were partially activated, but Nur77, unlike Nurr1, is not associated with PD, and Nur77 knockdown enhances cell survival (21). The foregoing experiments indicate the high degree of selectivity of BRF110.

BRF110 (1 mg/kg) administered i.p. in mice reached the brain, with an approximate half-life of ~1.5 h in both blood and brain as assessed by LC-MS/MS (brain/blood concentration area under the curve ratio, 1.7; Fig. S6) and was bioactive, increasing midbrain c-jun expression. These experiments indicate that BRF110 has the necessary properties to test our monotherapeutic PD hypothesis of Nurr1:RXRα heterodimer activation.

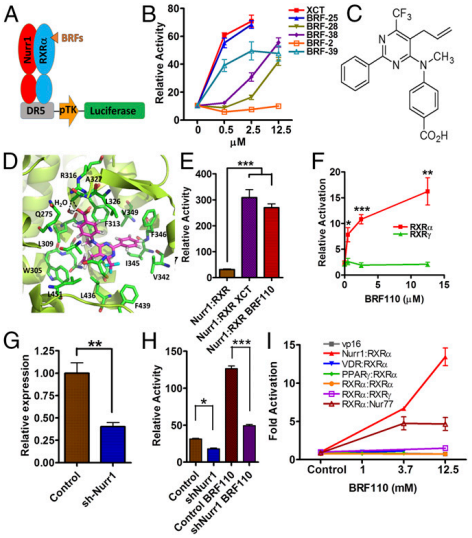

Fig. 1. Discovery of BRF110, specificity for Nurr1:RXRα heterodimers, and i.p. administration in mice. (*A*) Schematic representation of the screening transactivation assay. (*B*) Typical results. (*C*) Chemical structure of BRF110. (*D*) Schematic representation of BRF110 interactions within the RXRα (PDB ID code 1MV9)-binding pocket. BRF110 (magenta) docked onto RXRα (green; PDB ID code 1MV9). Hydrogen bonds and amino acids are indicated. (*E*) Comparison of DR5-Luc induction by BRF110 (1 μM) and XCT (1 μM) via activation of Nurr1:RXRα heterodimers. (*F*) Cellular assay indicating that BRF110 activates Nurr1:RXRα heterodimers but not Nurr1:RXRγ heterodimers. (*G*) Retroviral-mediated knockdown of endogenous Nurr1 in SHSY5Y cells as measured by qPCR. (*H*) Activation by BRF110 of DR5-luciferase reporter plasmid introduced into SHSY-5Y cells infected with either a control retrovirus or the retrovirus carrying shNurr1 sequences. (*I*) Gal4-DNA–binding domain and Nurr1, Nur77, VDR, RXRγ, PPARγ, and RXRα ligand-binding domain fusions cotransfected with RXRα:vp16 fusions activated by BRF110 at the indicated concentrations.

BRF110 Induces Transcription of DA Biosynthesis Genes and Protects DAergic Cell Lines and Human Induced Pluripotent Stem Cell-Derived DAergic Neurons Against PD-Associated Damage. Nurr1 regulates the transcription of DA biosynthesis genes (7, 8); however, whether this is mediated by Nurr1:RXRα heterodimers is unknown. In SHSY-5Y cells, BRF110 increased the expression of the three genes required for DA biosynthesis, TH by ~90% ($n = 6$; $P = 0.0374$, t test), aromatic L-amino acid decarboxylase (AADC) by ~70% ($n = 6$; $P < 0.0001$, t test), and GCH1 by ~42% ($n = 6$; $P < 0.0001$, t test) (Fig. 2*A*), indicating that this up-regulation depends on Nurr1:RXRα heterodimer activation.

We examined the neuroprotective capability of Nurr1:RXRα heterodimer activation in SHSY-5Y cells in which death was induced by either oxidative stress-related H_2O_2 or mitochondria complex I inhibitor 1-methyl-4-phenylpyridinium (MPP+) (Fig. 2*B*). BRF110 (12.5 μM) did not promote cell differentiation or cell proliferation, but significantly increased cell survival against varying concentrations of the toxic stimuli ($P < 0.0001$, two-way ANOVA) in a dose-dependent manner (Fig. 2*C*). The protection conferred by BRF110 was Nurr1-dependent, because it was abrogated by knockdown of

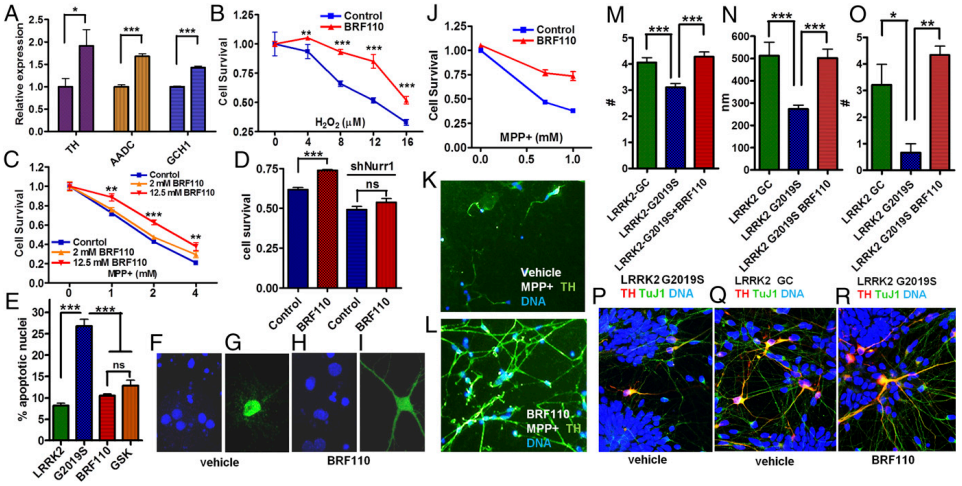

Fig. 2. Induction of DA biosynthesis gene expression and of neuroprotection in cell lines and in patient iPSC-derived DAergic neurons. (*A*) Expression levels of the three DA biosynthesis genes (TH, AADC, and GCH1) mediated by the activation of Nurr1:RXRα by BRF110 (12.5 μM), as assessed by qPCR. $n = 8$. (*B*) SHSY-5Y cell viability increases with BRF110 treatment, as measured by the 3-(4,5-dimethylthiazol-2-yl)-2,5-diphenyltetrazolium bromide (MTT) assay, after exposure to varying concentrations (0–16 μM) of H_2O_2. (*C*) BRF110 concentration-dependent SHSY-5Y cell viability, as measured by the MTT assay, after exposure to varying concentrations (0–4 mM) of MPP+. (*D*) BRF110-mediated SHSY-5Y cell viability against MPP+ (2 mM) is dependent on Nurr1 levels, as determined by retroviral knockdown of Nurr1. (*E*) BRF110 treatment of primary rat cortical neurons reduces apoptotic death induced by cotransfecting LRRK2-G2019S or control WT LRRK2 cDNAs with CMV GFP, as measured by DAPI staining. (*F–I*) Representative DAPI (*F* and *H*) and GFP (*G* and *I*) confocal images. (*J*) Survival of human iPSC-derived DAergic neurons exposed to MPP+ (0.5 and 1.0 mM for 24 h) and receiving vehicle or BRF110. (*K* and *L*) BRF110 treatment preserves DAergic neuron projections, as determined by TH immunofluorescence of surviving iPSC-derived DAergic neurons after exposure to MPP+. (*M–R*) PD patient iPSC-derived DAergic neurons with the LRRK2-G2019S mutation or corrected mutation (GC). BRF110 treatment rescues neurite number (*M*), neurite length (*N*), and neurite branching (*O*) phenotypes. (*P–R*) Representative images stained with TuJ, TH, and DAPI.

endogenous Nurr1 mRNA (Figs. 1*G* and 2*D*). The neuroprotective effects of BRF110 extend to damage induced by the PD-associated mutation G2019S in the leucine-rich repeat kinase 2 (LRRK2) gene, the most common genetic defect associated with clinical PD (22). Rat cortical neurons cotransfected with CMV-GFP (cytomegalovirus promoter-driven GFP) for identification and CMV-LRRK2-G2019S cDNAs show increased apoptosis, as assessed by DAPI staining and compared with control neurons cotransfected with a WT LRRK2 cDNA. We did not observe neuronal differentiation effects on BRF110 treatment, although it reduced apoptosis to control levels, comparable to those of the LRRK2 inhibitor GSK2578215A ($P < 0.0001$, one-way ANOVA) (Fig. 2 *E–I*).

The translational therapeutic potential of BRF110 was assessed in human midbrain-specific induced pluripotent stem cell (iPSC)-derived DAergic neurons, as indicated by positive staining and quantitative PCR (qPCR) for the neuronal markers MAP2, TH, FoxA2, Lmx1, and En1 (Fig. S7). BRF110 doubled the number of surviving MPP+-intoxicated neurons compared with vehicle ($P < 0.0008$, two-way ANOVA) (Fig. 2 *J–L*). The surviving control neurons had fewer and retreating projections, indicating compromised function (Fig. 2*K*), whereas the neurons that received BRF110 retained a complex network of projections and contacts (Fig. 2*L*).

In addition, we tested BRF110 in iPSC-derived DAergic neurons from a PD patient carrying the LRRK2-G2019S mutation. These neurons showed contracted neurites with reduced branching, phenomena that can be reversed on correction (LRRK2GC) of the LRRK2-G2019S mutation (22). Treatment of the LRRK2-G2019S DAergic neurons with BRF110 (12.5 μM) for 14 d (Fig. 2 *M–Q*) increased neurite length by 83% ($P < 0.0007$, one-way ANOVA; $P < 0.01$, Kruskal–Wallis test), neurite number by 38% ($P < 0.0001$, one-way ANOVA; $P < 0.001$, Kruskal–Wallis test), and neurite branching by 650% ($P < 0.01$, one-way ANOVA; $P < 0.05$, Kruskal–Wallis test) (Fig. 2 *M–O*). During the 14-d BRF110 treatment of these cells, we did not see any effect on TuJ1(+)/TH(−) neurons or on DAergic neurons with a WT genotype.

The foregoing experiments demonstrate the in vitro potential of Nurr1:RXRα activation to shield human DAergic neurons from diverse PD-related neuronal death stimuli, such as toxins and the LRRK2-G2019S mutation.

Neuroprotection of BRF110 in Vivo in Preclinical Mouse PD Models. We assessed the neuroprotective effects of Nurr1:RXRα heterodimer activation in vivo in two established preclinical C57BL/6 mouse PD models: acute 1-methyl-4-phenyl-1,2,3,6-tetrahydropyridine (MPTP) and unilateral 6-hydroxydopamine (6-OHDA) injection in the SN. Intraperitoneal injections of BRF110 (10 mg/kg) every 12 h, starting 12 h before toxin administration, were continued for 6 d in the MPTP model and for 14 d in the 6-OHDA model. To distinguish phenotypic effects, lasting 4–8 h (see below), from neuroprotection, BRF110 administration was discontinued 24–36 h before behavioral and histological examination of the mice. In the MPTP model, mice receiving BRF110 had considerably improved motor coordination (>100%) ($n = 5$; $P < 0.0001$, one-way ANOVA) compared with vehicle-injected mice, as assessed by the accelerating rotarod test (Fig. 3*A*). SN unbiased stereologic neuronal counting showed that TH(+) midbrain neuron survival per side was increased by 31% ($n = 5$; $P = 0.0003$, one-way ANOVA) in BRF110-treated mice, to a value not significantly different from that in control mice (Fig. 3 *B* and *C*). In addition, BRF110 protected SN axonal projections to the striatum, doubling the number of remaining terminals ($n = 5$; $P < 0.0001$, one-way ANOVA) (Fig. 3 *D* and *E*). This neuroprotective effect was BRF110-dependent,

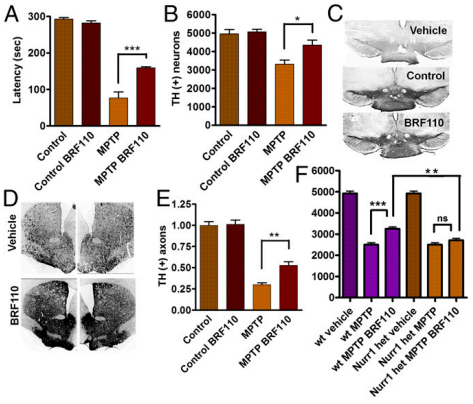

Fig. 3. BRF110 protects DAergic neurons against MPTP toxicity. (*A*) Improved rotarod test performance of C57BL/6 mice exposed to MPTP and receiving BRF110 treatment for 7 d. (*B*) Stereological counting of SN TH(+) neurons (average/side) in control C57BL/6 mice and mice exposed to MPTP and receiving either vehicle or BRF110 treatment. (*C*) Images of TH immunohistochemistry (IHC) in the SN of control C57BL/6 mice and mice exposed to MPTP and receiving either vehicle or BRF110 treatment. (*D*) Images of TH IHC of SN DAergic projections to the striatum in C57BL/6 mice exposed to MPTP and receiving either vehicle or BRF110 treatment. (*E*) Quantitation of TH IHC DAergic projections to the striatum of C57BL/6 mice exposed to MPTP and receiving either vehicle or BRF110 treatment. (*F*) Stereological counting of SN TH(+) neurons of control WT 129SV mice and mice exposed to MPTP and receiving either vehicle or BRF110 treatment (average/side) (first three bars) and of Nurr1$^{+/-}$ 129SV mice exposed to MPTP and receiving either vehicle or BRF110 treatment (last three bars).

because a once-daily injection regimen (20 mg/kg) was ineffective. BRF110 neuroprotection against MPTP toxicity was equally effective in 129sv WT mice (vehicle 2,500 ± 91 vs. BRF110 3,250 ± 92; $n = 4$; $P = 0.000571$, t test; $P < 0.001$, one-way ANOVA), but was abolished in Nurr1$^{+/-}$ 129sv mice. The number of TH(+) neurons was significantly lower in Nurr1$^{+/-}$ 129sv mice compared with 129sv WT mice (2,710 ± 91, $n = 4$ vs. 3,250 ± 92, $n = 4$; $P = 0.00298$, t test), confirming that the in vivo neuroprotective effects of BRF110 require Nurr1:RXRα heterodimers (Fig. 3*F*).

Nurr1:RXRα activation showed even more striking effects in the 6-OHDA model. Mice receiving BRF110 exhibited a dramatic reduction (by approximately eightfold) in apomorphine-induced contralateral turns ($n = 5$; $P = 0.0159$, Mann–Whitney U test) (Fig. 4*A*), whereas motor coordination was almost entirely restored to control levels, as evaluated by the rotarod test ($P < 0.0001$, one-way ANOVA; $P = 0.0079$, Mann–Whitney U test) (Fig. 4*B*). The number of surviving TH(+) neurons in the SN of BRF110-treated mice was increased by 47% ($P < 0.05$, one-way ANOVA; $P = 0.0317$, Mann–Whitney U test) to the level of complete restoration, as indicated by unbiased stereological neuronal counting (Fig. 4 *C* and *D*). Total midbrain neuronal determination by NueN staining showed similar results (Fig. S8*A*). Striatal innervation, which was practically obliterated in the vehicle-treated control mice, also showed a 10-fold higher preservation of TH(+) DAergic projections ($P < 0.0001$, one-way ANOVA; $P = 0.0159$, Mann–Whitney U test) (Fig. 4 *E* and *F*).

Because the predictive validity of toxin-based mouse PD models for neuroprotection in humans is questionable, we proceeded to test the effect of BRF110 in a mouse model, in which adeno-associated viruses (AAVs) overexpressing WT α-synuclein (ASYN) under the chicken β-actin promoter were injected unilaterally, along with contralateral injections of AAV-GFP. Treatment with BRF110 (10 mg/kg every 12 h for 2 wk) or vehicle was started the day after surgery. Unbiased stereology showed that the vehicle-treated AAV-ASYN–injected animals had a 44% decrease in TH(+) and NeuN(+) midbrain neurons compared with the AAV-GFP–injected side (Fig. 4 *G*–*I* and Fig. S8*B*). In contrast, in the BRF110-treated AAV-ASYN–injected animals, unbiased stereology showed that the number of TH(+) midbrain neurons was increased by ∼47% ($P < 0.05$, Wilcoxon test; $P = 0.00214$, Mann–Whitney U test) and NeuN(+) midbrain neurons ($P < 0.05$, Wilcoxon test; $P = 0.00214$, Mann–Whitney U test) compared with AAV-ASYN–injected animals treated with vehicle (Fig. 4*G*). Striatal innervation of unilaterally AAV-ASYN–injected brains resulted in a dramatic depletion of TH(+) axons by almost 85% in vehicle-treated mice, whereas in BRF110-treated mice, striatal TH(+) axons were increased by more than fivefold ($P < 0.001$, one-way ANOVA; $P < 0.0156$, Wilcoxon test) (Fig. 4 *J* *L*).

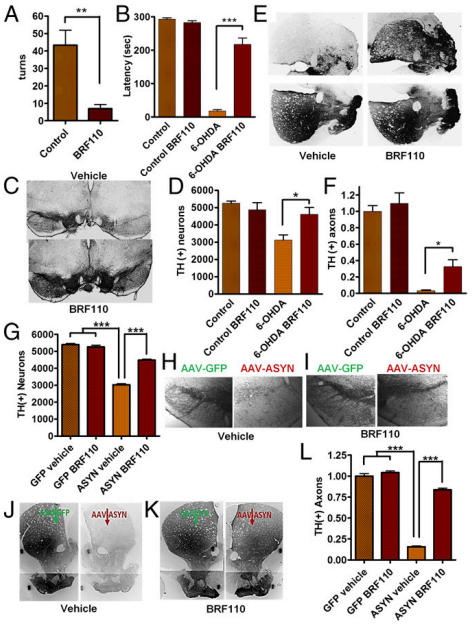

Fig. 4. BRF110 neuroprotection against 6-OHDA and AAV-ASYN toxicity in mice. (*A*) Decreased number of apomorphine-induced contralateral turns in C57BL/6 mice injected unilaterally with 6-OHDA and treated daily with either vehicle or BRF110 for 13 d, showing greater than eightfold improvement. $n = 5$. (*B*) Rotarod test of mice subjected to unilateral injection of 6-OHDA and receiving either vehicle or BRF110, showing 12-fold improvement with BRF110 treatment. $n = 5$. (*C*) SN TH IHC images of mice receiving unilateral injections of 6-OHDA and treated with either vehicle or BRF110. (*D*) Stereological counting of SN TH(+) neurons in mice receiving unilateral injections of 6-OHDA and treated daily with either vehicle or BRF110, which increased the number of TH(+) neurons by 47%. $n = 5$. (*E* and *F*) Striatum TH IHC of mice receiving 6-OHDA injections and treatment with either vehicle or BRF110, showing 10-fold increased innervation. $n = 5$. (*G*) Stereological counting of SN TH(+) neurons of mice receiving unilateral injections of AAV-ASYN and treated daily with either vehicle or BRF110, which increased the number of TH(+) neurons by 48%. $n = 7$. (*H* and *I*) SN TH IHC images of mice receiving unilateral injections of AAV-ASYN and contralateral injections of AAV-GFP and treated with either vehicle or BRF110. (*J* and *K*) Striatum TH IHC of mice receiving injections of AAV-ASYN or AAV-GFP and treated with either vehicle or BRF110, showing 10-fold increased innervation (*L*). $n = 7$.

The foregoing experiments demonstrate the DAergic neuroprotective effects of Nurr1:RXRα activation in both toxin-based and ASYN genetic preclinical animal models of PD.

A Single Dose of BRF110 Increases DA Biosynthesis in Vivo and Improves Symptoms in Two Postneurodegeneration PD Models. Based on the Nurr1:RXRα activation in the transcriptional regulation of DA biosynthesis genes, we tested whether BRF110 could increase DA levels in vivo. A single i.p. injection of BRF110 (10 mg/kg) in WT mice increased midbrain TH gene expression ($n = 4$; $P = 0.0396$, t test) within 4 h (Fig. 5*A*). Striatal DA and DA metabolite levels were increased as well, and their ratio remained constant, indicating physiological DA catabolism (Fig. 5*B*). Aiming to model PD based on human genetic data, we also tested whether BRF110 could increase DA levels in ASYN transgenic mice (23). A single i.p. injection of BRF110 (10 mg/kg) increased striatal DA levels ($n = 4$; $P = 0.01069$, t test) and DA metabolite levels in the ASYN transgenic mice compared with mice receiving vehicle (Fig. 5*C*). The effect of BRF110 was limited to DA biosynthesis, because noradrenaline levels remained unaffected (Fig. 5*D*).

We subsequently tested whether the DA increase could translate to symptomatic relief in postdegeneration PD mouse models based on MPTP or 6-OHDA (Fig. 5 *E* and *F*). A single dose of BRF110 (10 mg/kg i.p.) at 8 d after acute MPTP injection or 5–6 wk after unilateral 6-OHDA injection significantly improved temporarily motor coordination in both models ($P = 0.01$ and 0.0001, respectively, one-way ANOVA) at 4 h after dosing (Fig. 5 *G* and *H*) and induced contralateral turns in the 6-OHDA model ($P < 0.0001$, one-way ANOVA) (Fig. 5*I*), an effect similar to that of levodopa (L-DOPA). In these models, symptom improvement from BFF110 disappeared by 8 h after dosing. These experiments indicate that Nurr1:RXRα activation can indeed offer symptomatic relief in rodents, further supporting our monotherapy hypothesis.

BRF110 Chronic Dosing Does Not Induce Dyskinesias. We next compared BRF110 with L-DOPA in terms of causing AIMs. Mice treated daily with L-DOPA starting at 21 d after unilateral 6-OHDA injection exhibited severe hyperkinetic dyskinesias/AIMs within 7 d (Fig. 5 *J* and *K*). In contrast, similar daily BRF110 (10 mg/kg) administration for at least 2 wk resulted in consistently improved motor coordination (Fig. 5 *H* and *I*) without dyskinesias/AIMs ($P = 0.0061$, two-way ANOVA; $P = 0.0043$, Mann–Whitney U test) (Fig. 5*K*). These experiments exemplify the simultaneous symptomatic usefulness of Nurr1:RXRα activation devoid of undesirable complications.

Discussion

Drug discovery efforts for PD traditionally have been aimed either at symptomatic DA replacement treatments and alleviation of dyskinesias or at neuroprotection (24, 25). Neuroprotective approaches, although aimed at the core of PD pathology, so far have not delivered the expected results (26).

We selected Nurr1 as the target for disease-modifying and symptomatic relief for PD because it is strongly associated with PD. Nurr1 mutations have been identified in familial and sporadic cases of the disease (12, 13), and reduced levels of Nurr1 are associated with PD in both patients and animal models. In addition, Nurr1 is involved in DA biosynthesis (6, 7). We chose to target Nurr1 through its heterodimerization partner RXRα, limiting the activation of other Nurr1 molecules. Our data indicate that activation of Nurr1:RXRα by BRF110 can provide neuroprotection that can halt PD-associated neuronal loss in both toxin and genetic preclinical mouse models of PD. In addition, we have demonstrated that the

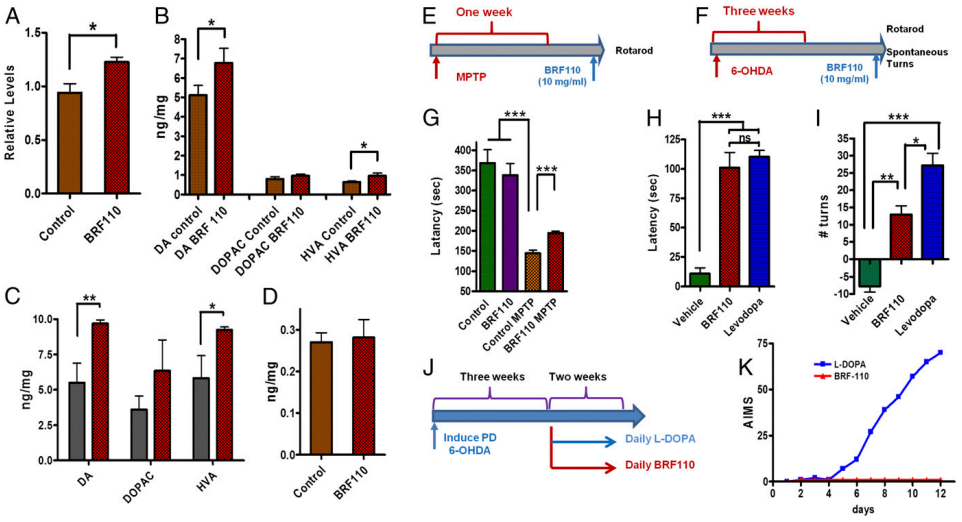

Fig. 5. BRF110 induces DA biosynthesis and symptomatic relief without dyskinesias in PD mouse models. (*A*) qPCR of TH expression levels in mouse midbrain at 4 h after i.p. administration of vehicle or BRF110 (10 mg/kg). (*B*) DA and DA metabolite levels at 4 h after i.p. administration of vehicle or BRF110 (10 mg/kg) in WT mice as assessed by HPLC. $n = 4$. (*C*) DA and DA metabolite levels at 4 h after i.p. administration of vehicle or BRF110 (10 mg/kg) in ASYN transgenic mice, as assessed by HPLC. $n = 4$. (*D*) Noradrenaline levels at 4 h after i.p. administration of vehicle or BRF110 (10 mg/kg), as assessed by HPLC. (*E* and *F*) Schematic representations of the treatment regimens. (*G*) Accelerating rotarod latency times of MPTP-treated mice at 4 h after i.p. administration of vehicle or BRF110 (10 mg/kg). (*H*) Accelerating rotarod latency times of 6-OHDA–treated mice at 4 h after i.p. administration of vehicle or BRF110 (10 mg/kg). (*I*) Spontaneous contralateral turns per minute of 6-OHDA–treated mice at 4 h after i.p. administration of vehicle, BRF110 (10 mg/kg), or L-DOPA. (*J* and *K*) Schematic of the treatment regimen (*J*) and AIMS (*K*) of mice at 5 wk after 6-OHDA treatment, after 2 wk of daily i.p. administration of BRF110 (10 mg/kg) or L-DOPA.

effects of BRF110 both in vitro and in vivo depend on Nurr1 expression, validating the therapeutic target. Because of the divergent toxin and genetic insults that we used in our PD models, our data indicate that various pathways leading to DAergic neuron demise can be overcome by BRF110 activation, implying coordinated control of a complex neuroprotective network by Nurr1:RXRα.

BRF110 also increases DA levels in vivo and offers symptomatic relief in two postdegeneration PD animal models at the neuroprotective dose. This dual activity indicates that unlike most efforts aimed at finding new therapeutic approaches for the treatment of PD, Nurr1:RXRα activation offers a unique combined efficacy distinct from that of other targets. Moreover, as opposed to the excessive DA stimulation induced by DA replacement therapies, BRF110 apparently finely regulates DA production in a more physiological manner via the transcriptional activation of the DA biosynthesis genes (TH, GCH1, and AADC), without affecting DA catabolism and without eliciting dyskinesias. This effect has been corroborated by the use of a lentiviral tricistronic vector expressing TH, GCH1, and AADC that alleviates PD symptoms in primates without dyskinesias (27). A current phase 1/2 clinical trial using a virtually identical lentiviral vector offers similar symptomatic relief in PD patients (28).

Our experiments show that a single molecule activating a single target achieves a double therapeutic advantage for PD in vivo. Because BRF110 neuroprotection extends to PD patient iPSC-derived DAergic neurons, Nurr1:RXRα activation has the potential to benefit PD patients. We believe that our findings strongly support the use of Nurr1:RXRα activation as a monotherapy for PD.

Materials and Methods

The materials and methods used in these experiments are described in detail in *SI Materials and Methods*.

In Vitro Studies in Neuroblastoma Cell Lines. Naive SH-SY5Y neuroblastoma cells were cultured in RPMI 1640 and 10% FBS and harvested at indicated time points. Transient transfections were performed using Lipofectamine 2000 (Invitrogen) for 4–6 h in Opti-MEM I (Invitrogen).

Mice. Mice were housed at the Animal Care Facilities of the Academy of Athens in a pathogen-free room under a controlled 12-h light/12-h dark cycle and with free access to food and water. Animal breeding and handling were performed in accordance with the European Communities Council Directive 86/609/EEC guidelines, and all animal procedures were approved by the Academy of Athens Institutional Animal Care and Use Committee (certified with ISO 9001:2008). PD mouse models for MPTP, 0.6-OHDA, and ASYN AAV were generated following established protocols. In brief, we used an acute MPTP regimen of four 20-mg/kg MPTP injections given 2 h apart. 6-OHDA-HCl in saline containing 0.02% ascorbic acid was injected intracerebrally and unilaterally at the level of the median forebrain bundle (MFB) in anesthetized mice. Recombinant AAVs (AAV-ASYN and AAV-GFP) were injected stereotactically into the right and left SN, respectively. Experimenters were blinded to the animal groups for all animal experiments and analyses.

Statistics. Statistical analyses were performed using GraphPad Prism 4. Significance was assessed with one-way ANOVA followed by Bonferroni's post hoc test and by the nonparametric Mann–Whitney *U* test or Kruskal–Wallis test unless indicated otherwise. A P value <0.05 was considered significant. In the figures, error bars represent ± SEM, and $*P < 0.05$, $**P < 0.01$, and $***P < 0.001$.

ACKNOWLEDGMENTS. We thank Drs. L. Stefanis, A. S. Charonis, K. Vougas, and A. Efstratiadis for encouragement; Drs. T. Perlmann and M. Spillantini for the Nurr1$^{+/-}$ and ASYN transgenic mice, respectively, and Dr. M. Makishima and RIKEN for constructs. This work was partially supported by the Michael J. Fox Foundation (D.K.V.), a Cooperation grant from the General Secretariat of Research and Technology (to D.K.V.), TransMed Grant EU FP7 REGPOT CT-2010-245928 (to D.K.V.), and SEE-DRUG Grant EU FP7 REGPOT CT-2011-285950 (to S.T.).

1. Meissner WG (2012) When does Parkinson's disease begin? From prodromal disease to motor signs. *Rev Neurol (Paris)* 168(11):809–814.
2. Athauda D, Foltynie T (2015) The ongoing pursuit of neuroprotective therapies in Parkinson disease. *Nat Rev Neurol* 11(1):25–40.
3. Fahn S (2006) A new look at levodopa based on the ELLDOPA study. *J Neural Transm Suppl* 70(Suppl):419–426.
4. Meissner WG, et al. (2011) Priorities in Parkinson's disease research. *Nat Rev Drug Discov* 10(5):377–393.
5. Zetterström RH, et al. (1997) Dopamine neuron agenesis in Nurr1-deficient mice. *Science* 276(5310):248–250.
6. Saucedo-Cardenas O, et al. (1998) Nurr1 is essential for the induction of the dopaminergic phenotype and the survival of ventral mesencephalic late dopaminergic precursor neurons. *Proc Natl Acad Sci USA* 95(7):4013–4018.
7. Kim KS, et al. (2003) Orphan nuclear receptor Nurr1 directly transactivates the promoter activity of the tyrosine hydroxylase gene in a cell-specific manner. *J Neurochem* 85(3):622–634.
8. Gil M, et al. (2007) Regulation of GTP cyclohydrolase I expression by orphan receptor Nurr1 in cell culture and in vivo. *J Neurochem* 101(1):142–150.
9. Kadkhodaei B, et al. (2009) Nurr1 is required for maintenance of maturing and adult midbrain dopamine neurons. *J Neurosci* 29(50):15923–15932.
10. Kadkhodaei B, et al. (2013) Transcription factor Nurr1 maintains fiber integrity and nuclear-encoded mitochondrial gene expression in dopamine neurons. *Proc Natl Acad Sci USA* 110(6):2360–2365.
11. Zhang L, Le W, Xie W, Dani JA (2012) Age-related changes in dopamine signaling in Nurr1-deficient mice as a model of Parkinson's disease. *Neurobiol Aging* 33(5):1001.e7–1001.e16.
12. Le WD, et al. (2003) Mutations in NR4A2 associated with familial Parkinson disease. *Nat Genet* 33(1):85–89.
13. Sleiman PM, et al. (2009) Characterisation of a novel NR4A2 mutation in Parkinson's disease brain. *Neurosci Lett* 457(2):75–79.
14. Wallen-Mackenzie A, et al. (2003) Nurr1-RXR heterodimers mediate RXR ligand-induced signaling in neuronal cells. *Genes Dev* 17(24):3036–3047.
15. Pérez E, Bourguet W, Gronemeyer H, de Lera AR (2012) Modulation of RXR function through ligand design. *Biochim Biophys Acta* 1821(1):57–69.
16. Cramer PE, et al. (2012) ApoE-directed therapeutics rapidly clear β-amyloid and reverse deficits in AD mouse models. *Science* 335(6075):1503–1506.
17. McFarland K, et al. (2013) Low-dose bexarotene treatment rescues dopamine neurons and restores behavioral function in models of Parkinson's disease. *ACS Chem Neurosci* 4(11):1430–1438.
18. Veeraraghavalu et al. (2013) Comment on "ApoE-directed therapeutics rapidly clear β-amyloid and reverse deficits in AD mouse models." *Science* 340(6135):924-f.
19. Volakakis N, et al. (2015) Nurr1 and retinoid X receptor ligands stimulate Ret signaling in dopamine neurons and can alleviate α-synuclein–disrupted gene expression. *J Neurosci* 35(42):14370–14385.
20. Vaz B, de Lera ÁR (2012) Advances in drug design with RXR modulators. *Expert Opin Drug Discov* 7(11):1003–1016.
21. Wei X, et al. (2016) Contra-directional coupling of Nur77 and Nurr1 in neurodegeneration: A novel mechanism for memantine-induced anti-inflammation and anti-mitochondrial impairment. *Mol Neurobiol* 53(9):5876–5892.
22. Reinhardt P, et al. (2013) Genetic correction of a LRRK2 mutation in human iPSCs links parkinsonian neurodegeneration to ERK-dependent changes in gene expression. *Cell Stem Cell* 12(3):354–367.
23. Tofaris GK, et al. (2006) Pathological changes in dopaminergic nerve cells of the substantia nigra and olfactory bulb in mice transgenic for truncated human alpha-synuclein(1-120): Implications for Lewy body disorders. *J Neurosci* 26(15):3942–3950.
24. Rascol O, Perez-Lloret S, Ferreira JJ (2015) New treatments for levodopa-induced motor complications. *Mov Disord* 30(11):1451–1460.
25. Schapira AH (2011) Monoamine oxidase B inhibitors for the treatment of Parkinson's disease: A review of symptomatic and potential disease-modifying effects. *CNS Drugs* 25(12):1061–1071.
26. Stocchi F (2014) Therapy for Parkinson's disease: What is in the pipeline? *Neurotherapeutics* 11(1):24–33.
27. Jarraya B, et al. (2009) Dopamine gene therapy for Parkinson's disease in a nonhuman primate without associated dyskinesia. *Sci Transl Med* 1(2):2ra4.
28. Palfi S, et al. (2014) Long-term safety and tolerability of ProSavin, a lentiviral vector-based gene therapy for Parkinson's disease: A dose-escalation, open-label, phase 1/2 trial. *Lancet* 383(9923):1138–1146.
29. Ho CC, Rideout HJ, Ribe E, Troy CM, Dauer WT (2009) The Parkinson disease protein leucine-rich repeat kinase 2 transduces death signals via Fas-associated protein with death domain and caspase-8 in a cellular model of neurodegeneration. *J Neurosci* 29(4):1011–1016.
30. Reinhardt P, et al. (2013) Derivation and expansion using only small molecules of human neural progenitors for neurodegenerative disease modeling. *PLoS One* 8(3):e59252.
31. Klein RL, King MA, Hamby ME, Meyer EM (2002) Dopaminergic cell loss induced by human A30P alpha-synuclein gene transfer to the rat substantia nigra. *Hum Gene Ther* 13(5):605–612.
32. Cao S, Theodore S, Standaert DG (2010) Fcγ receptors are required for NF-κB signaling, microglial activation, and dopaminergic neurodegeneration in an AAV-synuclein mouse model of Parkinson's disease. *Mol Neurodegener* 5:42.
33. Paxinos G, Franklin KBJ (2001) *The Mouse Brain in Stereotaxic Coordinates* (Academic, San Diego), 2nd Ed.
34. Vila M, et al. (2000) Alpha-synuclein up-regulation in substantia nigra dopaminergic neurons following administration of the parkinsonian toxin MPTP. *J Neurochem* 74(2):721–729.
35. Jackson-Lewis V, Przedborski S (2007) Protocol for the MPTP mouse model of Parkinson's disease. *Nat Protoc* 2(1):141–151.
36. Friesner RA, et al. (2006) Extra precision glide: docking and scoring incorporating a model of hydrophobic enclosure for protein-ligand complexes. *J Med Chem* 49(21):6177–6196.

APPENDIX B

Original article: Activity of translation regulator eukaryotic elongation factor–2 kinase is increased in Parkinson's disease brain and its inhibition reduces α–synuclein toxicity

This article has been published in the *Acta Neuropathologica Communications* journal.

Jan *et al. Acta Neuropathologica Communications* (2018) 6:54
https://doi.org/10.1186/s40478-018-0554-9

Acta Neuropathologica Communications

RESEARCH Open Access

Activity of translation regulator eukaryotic elongation factor-2 kinase is increased in Parkinson disease brain and its inhibition reduces alpha synuclein toxicity

Asad Jan[1*], Brandon Jansonius[3†], Alberto Delaidelli[2†], Forum Bhanshali[4], Yi Andy An[4], Nelson Ferreira[5], Lisa M. Smits[6], Gian Luca Negri[2], Jens C. Schwamborn[6], Poul H. Jensen[5], Ian R. Mackenzie[2], Stefan Taubert[4] and Poul H. Sorensen[2,3*]

Abstract

Parkinson disease (PD) is the second most common neurodegenerative disorder and the leading neurodegenerative cause of motor disability. Pathologic accumulation of aggregated alpha synuclein (AS) protein in brain, and imbalance in the nigrostriatal system due to the loss of dopaminergic neurons in the substantia nigra-pars compacta, are hallmark features in PD. AS aggregation and propagation are considered to trigger neurotoxic mechanisms in PD, including mitochondrial deficits and oxidative stress. The eukaryotic elongation factor-2 kinase (eEF2K) mediates critical regulation of dendritic mRNA translation and is a crucial molecule in diverse forms of synaptic plasticity. Here we show that eEF2K activity, assessed by immunohistochemical detection of eEF2 phosphorylation on serine residue 56, is increased in postmortem PD midbrain and hippocampus. Induction of aggressive, AS-related motor phenotypes in a transgenic PD M83 mouse model also increased brain eEF2K expression and activity. In cultures of dopaminergic N2A cells, overexpression of wild-type human AS or the A53T mutant increased eEF2K activity. eEF2K inhibition prevented the cytotoxicity associated with AS overexpression in N2A cells by improving mitochondrial function and reduced oxidative stress. Furthermore, genetic deletion of the eEF2K ortholog *efk-1* in *C. elegans* attenuated human A53T AS induced defects in behavioural assays reliant on dopaminergic neuron function. These data suggest a role for eEF2K activity in AS toxicity, and support eEF2K inhibition as a potential target in reducing AS-induced oxidative stress in PD.

Keywords: eEF2K, Parkinson disease, Alpha synuclein, Oxidative stress, Neurotoxicity

Introduction

Parkinson disease (PD) is the most common neurodegenerative cause of motor disability and is estimated to affect around 10 million people worldwide [33, 53]. Clinically, it presents as a movement disorder characterized by resting tremor, rigidity, and bradykinesia, and in a substantial number of patients the motor disability is compounded by non-motor symptoms such as cognitive impairment and autonomic dysfunction [33, 53]. Neuropathologically, loss of dopamine producing neurons in the midbrain *substantia nigra* (SN)-*pars compacta*, and intraneuronal inclusions of aggregated α-synuclein (AS) protein in multiple brain regions are hallmark features in PD [33, 53]. AS is a 14 kDa cytosolic protein (encoded by the *SNCA* gene) with putative roles in synaptic vesicle recycling, mitochondrial functions, and chaperone activity [39, 71]. Deposition of AS in the form of inclusions in neurons and/or nerve terminals, also known as Lewy body pathology, is also seen in other neurodegenerative diseases such as Alzheimer disease (AD), Lewy body dementia (LBD), and in

* Correspondence: ajan@aias.au.dk; psor@mail.ubc.ca
†Brandon Jansonius and Alberto Delaidelli contributed equally to this work.
[1]Aarhus Institute of Advanced Studies, Department of Biomedicine, Aarhus University, Høegh-Guldbergs Gade 6B, DK-8000 Aarhus, Denmark
[2]Department of Pathology and Laboratory Medicine, University of British Columbia, Vancouver, Canada
Full list of author information is available at the end of the article

oligodendrocytes in Multiple system atrophy (MSA) [67]. Idiopathic (non-inheritable) PD accounts for a vast majority of cases, while 5–10% of clinically diagnosed PD is attributable to genetic factors [53]. Missense mutations in *SNCA* resulting in N-terminal amino acid substitutions in the AS protein, or multiplications in *SNCA* gene locus leading to increased AS expression are the earliest known causes of autosomal-dominant inherited forms of PD [53, 54, 62]. There are additional genes associated with familial PD including autosomal-dominant and recessive inheritance (reviewed by [33, 53]), underlining the complex etiologic nature of PD.

Driven by the neuropathology and genetics, the neurotoxicity of AS has been a major area of research in PD towards the elucidation of disease-associated mechanisms and discovery of novel therapies. Based on studies in animal models and cell cultures, including neuronal cultures, substantial evidence implicates AS aggregation in triggering different alterations including synaptic dysfunction, calcium dyshomeostasis, mitochondrial impairment, endoplasmic reticulum (ER) stress, defective autophagy, neuroinflammation, and oxidative stress [27, 39, 59, 71]. In a broader perspective, a pathological role for dysregulation of some of these cellular mechanisms is also supported by the discovery of other genetic factors causing PD. For instance, autosomal-dominant mutations in leucine-rich repeat kinase 2 (*LRRK2*), which account for the most common cause of inherited PD [53], are associated with defective autophagy and mitochondrial dysfunction [68]. Similarly, mutations in *PARK2* (Parkin, an E3 ubiquitin ligase), *PINK1* (PTEN-induced putative kinase 1) and *PARK7* (DJ-1, a protein deglycase), which are associated with early onset (age less than 40 years) PD [33, 53], directly or indirectly affect mitochondrial function either by regulating mitophagy (Parkin and PINK1) or protecting mitochondria from oxidative stress (DJ-1) [5, 59]. Some studies have also reported that mitochondrial complex I protein expression and/or activity is reduced in PD substantia nigra [29, 60] and platelets [21]. Additionally, cultures of induced pluripotent stem cells (iPSCs) derived from PD patients show defects in oxygen consumption and mitochondrial function [3, 56]. Furthermore, exposure to several chemical toxins that inhibit complex I is well documented to induce dopaminergic neuron degeneration and a parkinsonian phenotype in humans (e.g., 1-methyl-4-phenyl-1,2,3,6-tetrahydropyridine, MPTP) and in animals (e.g., MPTP, rotenone, paraquat etc.) [33, 59].

The eukaryotic elongation factor-2 kinase (eEF2K), also known as calcium/calmodulin dependent kinase III, is an important regulatory molecule in cellular protein synthesis and also in diverse forms of synaptic plasticity [23]. Upon activation, eEF2K phosphorylates its major known substrate, the eukaryotic elongation factor-2 (eEF2), on threonine-56 (Thr56), thus leading to the dissociation of eEF2 from ribosomes and stalling of mRNA translation during the elongation phase [34, 57]. eEF2K activity is increased under condition of nutrient stress via the energy sensor AMP-activated kinase (AMPK), which positively regulates eEF2K activity by phosphorylation on serine residue 398 [34, 42]. We and others have observed increased eEF2K expression and/or activity in AD post-mortem brains [28, 43, 46], and in the brains of transgenic AD mice [28, 46]. We have also shown that eEF2K inhibition prevents the toxicity of amyloid-β (Aβ) oligomers in neuronal cultures by activating the NRF2 antioxidant response, and attenuates human Aβ-induced deficits in neuronal function in *C. elegans* [28].

Mitochondrial defects (directly or indirectly associated with the aggregation of AS protein) and oxidative stress are implicated in PD pathogenesis [5, 59], and eEF2K inhibition reduces reactive oxygen species (ROS) levels in cells [10, 28]. Therefore, we hypothesized that eEF2K inhibition may mitigate AS induced neurotoxicity by reducing oxidative stress. To test this hypothesis, we first examined markers of eEF2K activity,[1] i.e., phosphoryalation of eEF2 on serine residue 56, in postmortem PD brains in order to establish its relevance to human pathology, and subsequent to the induction of AS pathology in transgenic mouse M83 line expressing PD-associated mutant *Ala53Thr* (A53T) AS [20, 58]. Then, we probed the effects of eEF2K inhibition on cytotoxicity, mitochondrial function and oxidative stress in AS overexpressing dopaminergic N2A cells, and on dopaminergic neuronal function in *C. elegans* expressing mutant A53T AS. By using multiple experimental approaches, we elucidate the relevance of eEF2K in AS toxicity, and discuss the potential utility of eEF2K inhibition in PD and related synucleinopathies.

Materials and methods

Reagents and biochemical assays

Plasmids for overexpression of AS in mammalian cells were obtained under MTA from Addgene, and included human wild type AS (pHM6-alphasynuclein-WT, Addgene #40824) and human mutant A53T AS (pHM6-alphasynuclein-A53T, Addgene #40825). Additional reagents and biochemical assays employed during these studies include: pool of small interference RNAs (SiRNAs) targeting mouse eEF2K (Santa Cruz, #sc-39,012), Cell Titer Glo ATP measurement kit (Promega, #G7570), Lactate dehydrogenase (LDH) fluorometric assay (Novus Biologicals, #NBP2–54851), Seahorse Mito stress test kit (Agilent, #103015–100), 2′,7′-dichlorodihydrofluorescein diacetate (DCFDA) fluorescent ROS reagent (ThermoFisher, #D399), and MitoTracker Green fluorescent reagent for mitochondrial mass (ThermoFisher, #M7514). Biochemical

assays (LDH and ATP), Seahorse assays and flow cytometry assays were performed according to manufacturer's recommendations and are also outlined in details below.

Immunohistochemistry (IHC) and immunofluorescence studies on postmortem human brain sections

Five-micrometer formalin-fixed paraffin embedded separate post-mortem sections from midbrain and hippocampus of control or PD patients were provided by the laboratory of IM (co-author), as approved by the University of British Columbia Ethics Committee. Anonymized brain sections from 3 control individuals and 6 clinically and pathologically confirmed PD patients were obtained at autopsy and used in these experiments (Additional file 1: Table S1).

IHC on brain sections from human tissue was performed after deparaffinization and antigen retrieval. The following antibodies were employed to stain serial tissue sections, as indicated: antibody against phospho-eEF2 (Thr56) (Novus Biologicals, #NB100–92518) [28, 42], and antibody against phospho-alpha synuclein (pSer129; EMD Millipore, #MABN826), using the alkaline phosphatise conjugated streptavidin-biotin ABC kit (Vector Labs, # AK-5000). For destaining/bleaching neuromelanin in substantia nigra in the midbrain sections, the IHC protocol was modified slightly, as described [52] . Briefly, sections mounted on slides were incubated in a 60 °C degrees oven for 30 min and then were transferred into ambient distilled water. Then, the slides were placed in 0.25% potassium permanganate solution for 5 min. Subsequently, the slides were rinsed with distilled water. This was followed by incubation in 5% oxalic acid until section became clear. A final rinse in distilled water was performed before proceeding with the normal IHC staining as described above. Sections were counterstained with hematoxylin (Vector Labs, #H-3401). High resolution panoramic images of tissue sections for p-eEF2 and p-ASyn IHC analysis were acquired using a Leica Aperio digital slide scanner. IHC staining for p-eEF2 was quantified by manual counting of the DAB (3,3′-diaminobenzidine; Vector Labs, #SK-4100) positive cells.

For the detection of p-eEF2 (T56) and p-ASyn (S129) in the same tissue section, i.e., colocalization studies, immunofluorescence labelling was performed. For this purpose, after incubation of the tissue sections with primary antibodies as in the staining protocol described above, Alexa Fluor conjugated secondary fluorescent antibodies (Alexa Fluor 488 Goat anti-Mouse IgG, Thermo Fisher # A32723 and Alexa Fluor 594 Goat anti-Rabbit IgG, Thermo Fisher # R37119) were used for the detection. Image acquisition was performed using a Nikon Eclipse TE2000 confocal microscope.

Animal studies

Husbandry

Transgenic M83$^{+/+}$ PD mice [B6; C3-Tg (Prnp-SNCA*A53T) 83Vle/J] were kindly provided by the laboratory of Benoit Gaisson at the Centre for Translation Research in Neurodegenerative Diseases, University of Florida, USA to the laboratory of PHJ (co-author). These mice express the mutant human A53T AS under the direction of the mouse prion protein promoter [20]. The mice were housed at the Aarhus University Bartholin animal facility under conditions of 12 h light/dark cycles and received ad libitum standard laboratory chow diet. All procedures were performed in accordance with National rules and the European Communities Council Directive for the care and handling of laboratory animals. Both male and female mice were used for biochemical analyses. All genotypes were determined by PCR.

Intramuscular injections of alpha synuclein fibrils

Fibrillar mouse AS was prepared essentially according to an established protocol [58]. Tg M83$^{+/+}$ were bilaterally injected with recombinant mouse AS preformed fibrils (PFF) as described [58]. Briefly, 2–3 month-old mice were anesthetized with isoflurane (1–5%) inhalation and injected intramuscularly into the hindlimb biceps femoris bilaterally. The inoculum (5 μL of 2 mg/mL PFF or PBS) was injected using a 10-μL Hamilton syringe with a 25-gauge needle. Separate syringes were used for each type of inoculums (PBS or PFF) to avoid any cross-contamination. After the injection, mice were allowed to recover under close observation before being returned to their original cage.

Hindlimb clasping

Assessment of hindlimb clasping behaviour was performed with a modified tail suspension test [22]. Freely moving, non-anesthesized, Tg M83$^{+/+}$ were held by the tail and lifted in air for 10 s. Severity of clasping was assessed as follows: 1) No clasping (score 0), hindlimbs were consistently spread outward and away from the abdomen; 2) Mild clasping (score 1), one hindlimb was retracted toward the abdomen for more than 50% of the time; 3) Moderate clasping (score 2), both hindlimbs were partially retracted toward the abdomen for more than 50% of the time suspended; and 4) Severe clasping (score 3), hindlimbs were entirely retracted and touching the abdomen for more than 50% of the time suspended.

Quantitative RT-PCR

Total RNA from the whole brain homogenates was extracted using a commercial kit (Qiagen, #74134), and cDNA was synthesized using high capacity reverse transcriptase kit (Applied Biosystems, #4368814). The following gene specific primer pairs were used in qRT-PCR: Mouse *eef2k* (forward, 5'-CGCTTTGTACCGGGGATTCT-3′; reverse, 5′- AAGG

ATGGTCCTCCCACAGT-3′) and Mouse *Gapdh* (forward, 5′- CCCTTAAGAGGGATGCTGCC-3′; reverse, 5′-TACG GCCAAATCCGTTCACA-3′). The data were analyzed by relative ΔΔCT quantification method using *Gapdh* CT values as internal reference in each sample.

Cell culture

Midbrain organoid cultures

Midbrain organoids were generated with a modified protocol as reported previously [49], from human iPSCs essentially as described [3]. After 35 days of differentiation, RNA from snap frozen wild type or A53T mutation carrying organoids was isolated using a commercial kit (Qiagen, # 74104), and cDNA was synthesized using Applied Biosystems high capacity reverse transcriptase kit (Thermo Fisher, # 4368814). Following gene specific primer pairs were used in qRT-PCR: Human *EEF2K*, forward 5′- CCCAAGCAGGTGGACATCAT-3′ and reverse 5′-TTGCCCTCGATGTAGTGCTC-3′ and human glyceraldehyde 3-phosphate dehydrogenase (*GAPDH*), forward 5′- GACAGTCAGCCGCATCTTCT -3′ and reverse 5′- ACCAAATCCGTTGACTCCGA -3′.

N2A cultures

N2A neuroblastoma cells were obtained from ATCC (#CCL-131), and maintained in DMEM (4.5 g/L glucose; Gibco, #11965–084) supplemented with 1% antibiotic-antimycotic solution (Gibco, #15240062) and 10% Fetal Bovine Serum (FBS), Cells were cultured in 6-well (500, 000 cells/well) 12-well (250,000 cells/well) or 96-well (50,000 cells/well) plates. DNA plasmid transfections were performed using Lipofectamine 2000 (Invitrogen, #11668019), and Lipofectamine RNAiMAX (Invitroge, #13778150) for siRNAs, according to the recommended procedures. After 24 h, cells were briefly washed with phosphate-buffer saline (PBS) and allowed to differentiate into neurons in a modified culture medium [59] containing DMEM (Gibco, #21969035) supplemented with 500 μM L-glutamine, 1% antibiotic-antimycotic, 2% FBS and 500 μM Dibutyryladenosine 3′,5′-cyclic monophosphate (db cAMP; Sigma, #D0627) [28, 63]. Unless indicated otherwise, differentiated N2A cells which were mock transfected, or transfected with AS plasmids (ASyn-WT or ASyn-A53T; Addgene plasmid #40824 and #40825 respectively) +/− eEF2K kd, were used in the various assays described below after 72–76 h post-transfection.

Cytotoxicity assays

For the lactate dehydrogenase (LDH) release, 50 μl of culture medium was collected from each well into sterile tubes and cell debris was removed by centrifugation (1100 rpm, 10 min; 4 °C) in a tabletop centrifuge. Then, 5 μl of the supernatant were carefully transferred into a 96-well black microplate cooled and kept on ice. Then, the assay reagents, as recommended by the manufacturer were added to the wells. Fluorescence (Ex/Em = λ535/λ587 nm) was measured in a Tecan microplate reader equipped with necessary filters at room temperature. Measurements were acquired in a kinetics mode every minute, after 5 s of gentle shaking, over 20 min. Stabilized fluorescence signal from each sample was collected and analyzed. For the propidium iodide (PI) cell death detection assay, the cells were gently trypsinized (0.05% Trypsin-EDTA; Gibco, #25300054), centrifuged (1100 rpm, 5 min, 4 °C) and resuspended in 500 μl of sterile ice-cold PBS containing 20% FBS and 0.001% PI (ThermoFisher, #P3566). After transferring into FACS tubes, on ice, the cells were analyzed on a FACSCalibur-Tangerine flow cytometry instrument, as described [28]. Cellular ATP levels were measured using a bioluminescence firefly luciferase assay (Cell Titer Glo, Promega) with minor modifications to the manufacturer's instructions. Briefly, the cells were resuspended in the assay mix by thorough pipetting and transferred into a 96-well white assay plate, previously cooled on ice. Then luminescence signal was measured in a Tecan microplate reader at room temperature. Measurements were acquired in a kinetics mode every 3 min, after 5 s of gentle shaking, over 30 min. Stabilized luminescence signal from each sample was collected and analyzed.

Mitochondrial respiration and cellular mitochondrial content

Cellular oxygen consumption rate (OCR) was measured using the Seahorse Mito stress kit according to the supplier's instructions. Apart from the basal OCR, a combination of pharamcological agents (components of the Seahorse Mito Stress test) enables the assessment of different aspects of cellular respiration. These include non-mitochondrial (NM) respiration, maximal respiration (MR) and spare respiratory capacity (SRC). Optimal cell density and concentrations of drugs for the assay were established according to the kit instructions/parameters. Then, 30,000 cells/well were seeded in a 96-well microplate (included in the kit) and transfections were carried out (Mock, ASyn-WT or ASyn-A53, all ± eEF2K siRNA). OCR measurements were performed in a Seahorse XF analyzer according to the assay guidelines. Basal OCR was measured over 20 min (4 cycles, 5 min/cycle), followed by exposure to oligomycin, ATP synthase inhibitor (2 μM), carbonilcyanide p-triflouromethoxyphenylhydrazone-FCCP, oxidative phosphorylation uncoupler (0.5 μM) and rotenone/antimycin, complex I and III inhibitor respectively (0.5 μM). After injection with each drug, OCR was measured over 15 min (4 cycles, 5 min/cycle). After the assay completion, the cells were gently rinsed with PBS and homogenized by pipetting in ice cold 50 μl RIPA lysis buffer

(25 mM Tris-HCl pH 7.6, 150 mM NaCl, 1% NP-40, 1% sodium deoxycholate, 0.1% SDS, protease inhibitors and phosphatase inhibitors cocktail). Then, the cell lysate was transferred into microtubes, centrifuged (10,000 rpm, 10 min, 4 °C) and 25 μl of supernatant was transferred into a 96-well assay plate. Total protein in samples was determined by BCA protein assay (Pierce, #23225). OCR data was normalized to the protein content/well.

Mitochondrial content (mass) in differentiated N2A cells ± eEF2K kd was determined by labelling with Mitotracker fluorescent dye, and by quantification of mitochondrial DNA copy number. For the Mitotracker assay, cells were incubated with 50 nM Mitotracker Green FM reagent for 30 min in fresh medium. The cells were trypsinized, and centrifuged as described under the PI assay, and resuspended in 500 μl of sterile ice-cold PBS containing 20% FBS. Control cells without Mitotracker dye treatment were used as the background fluorescence signal. Separately, mitochondrial DNA (mtDNA) quantification was carried out by RT-PCR as described [47]. Briefly, nuclear DNA and mtDNA were isolated from differentiated N2A cells ± eEF2K using a Qiagen All Prep kit (#80204). Isolated samples were sonicated, then diluted to contain either 10 ng or 1 ng of DNA. This was used as an internal control to ensure that the ratio of mtDNA to nuclear DNA remained constant at different concentrations. qPCR was run on a Quant Studio 6 instrument using Fast SYBR Green Master Mix (ThermoFisher, #4309155). The primer sequences used for qPCR are as follows: mouse mitochondrial marker-*mMito* (forward, 5′-CTAGAAACCCCGAAACCAAA-3′; reverse, 5′-CCAGCTATCACCAAGCTCGT-3′) and mouse beta-2-microglobulin- *mB2M* (forward, 5′-ATGGGAAGC CGAACATACTG-3′; reverse: 5′-CAGTCTCAGTGGGG GTGAAT-3′). In each sample, mtDNA was quantified as a ratio of mtDNA to nuclear DNA (mtDNA/N) and were expressed as mtDNA copy numbers.

ROS measurements

For ROS detection, cells were incubated with 5 μg/mL 2, 7-dichlorofluorescein diacetate- DCFDA for 30 min in fresh medium. The cells were gently trypsinized (0.05% Trypsin-EDTA), centrifuged (1100 rpm, 5 min, 4 °C) and resuspended in 500 μl of sterile ice-cold PBS containing 20% FBS and 0.001% PI. After transferring into FACS tubes, on ice, the cells were analyzed on a FACSCalibur-Tangerine flow cytometry instrument as described previously [28]. During the analysis, dead cells were excluded from analysis based on PI staining. Control cells without DCDFA treatment were used as the background fluorescence signal.

Western blotting

Whole brain tissue homogenates from euthanized $M83^{+/+}$ mice were prepared in RIPA buffer (25 mM Tris-HCl pH 7.6, 150 mM NaCl, 1% NP-40, 1% sodium deoxycholate, 0.1% SDS, protease inhibitors and phosphatase inhibitors cocktail). For cellular assays, the cells were washed (ice cold PBS, 2–3 times) and lysed in RIPA buffer. Then, the mouse brain homogenates or cell lysates were briefly sonicated on ice and centrifuged (12,000 rpm, 15 min, 4 °C). Supernatant was collected and protein quantitation was done using BCA protein assay (Pierce, #23225). Then 25–40 μg of total proteins per sample were electrophoresed on 8% or 10% Bis-Tris acrylamide gels. Proteins were transferred onto a nitrocellulose membrane, incubated in blocking buffer (Li-Cor, #927–50,100]), and probed with following primary antibodies: eEF2K (Abcam, #46787), p-eEF2 Thr56 (Cell Signalling, #2331), eEF2 (Cell Signalling, #2332), ASyn (Santa Cruz #sc-12,767), p-ASyn Ser129 (Abcam, #168381, MJF-R13), and GAPDH (Cell Signaling 2118). Detection was performed using goat anti-mouse (Li-Cor, #925–32,210) or goat anti-rabbit (Li-Cor, #925–68,071) secondary antibodies conjugated with fluorescent infrared dyes using an Odyssey scanner (Li-Cor). Densitometry analysis was performed using ImageJ (NIH) [28].

C. elegans studies

Nematode strains and culture methods

C. elegans strains N2 wild-type (referred to as WT-N2), RB2588 *efk-1(ok3609)*, [28] (referred to as efk-1_{del}), JVR107 *Pdat-1::a-synuclein[A53T]*, [12] ((referred to as ASyn (A53T)), and STE120 *efk-1(ok3609); Pdat-1::a-synuclein[A53T]* ((generated herein, referred to as ASyn (A53T)/efk-1_{del})) were grown on Nematode Growth Medium (NGM) lite plates at 20 °C and with *E. coli* OP50 as food source, as described [28]. We used standard sodium hypochlorite bleaching and L1 stage starvation to generate synchronized populations, which were then allowed to grow for 72 h, i.e. until day two of adulthood; all assays were performed at that stage.

Dopamine-dependent behaviour assays

Ethanol avoidance assay

Ethanol avoidance assays were done as described [12], on an unseeded 15 mm × 60 mm plate divided into four quadrants with a circle of 1 cm in diameter in between. Then, $1cm^3$ agarose chunks were soaked in ice-cold ethanol overnight, and placed 0.5 cm from the edge of the plate in the centre of two opposing quadrants, while the other two quadrants remained untreated. Ethanol was allowed to diffuse in media for 2 h. Actively growing day 2 old adult worms were washed five times with M9 buffer, and 150–200 worms were placed in the centre of the plate, and allowed to move for 1 h at 20 °C. Then, worms were counted manually and ethanol avoidance was calculated as [(number of worms in control quadrants) – (number of worms in ethanol quadrants))/(total number of worms)]. Three assay plates were

used for each strain, and a minimum of three biological replicates was performed.

Pharyngeal pumping assay

The pharyngeal pumping rate was measured by manually counting the number of pumps made by each worm on seeded plate for 30 s using a Leica M205FA microscope. A total of 10–15 worms were used for each replicate. The assay was repeated at least three times on separate worms.

Area-restricted searching assay

Area-restricted searching assays were done as described [13]. Worms were washed very quickly to remove bacteria, and 10–15 worms were placed on an unseeded plate. To record the turning frequency, worms were videotaped at intervals of 5 and 30 min for one minute using a MoticamX camera mounted on a Leica M205FA microscope. Videotapes were analyzed manually to count the number of high-angled turns, i.e. those that exceeded 90°, including reversals and omega turns. The area-restricted searching ratio was calculated as [(number of turns/worm at 5 min)/(number of turns per worm at 30 min)]. A minimum of three replicates was performed for this assay.

Statistics

The data were analyzed in Graphpad Prism software (version 5) or Microsoft Excel 2010, and graphs were made in Microsoft Excel 2010. Statistical differences between two sets of data were calculated by Mann-Whitney nonparametric test or unpaired T-test, as indicated in the figure legends. Multiple column datasets were analyzed by One-way ANOVA followed by Bonferonni *posthoc* analysis. Longitudinal analysis was performed by Two-way ANOVA.

Results

eEF2K expression and activity are increased in PD brain

Using postmortem brain sections from midbrain and hippocampus of controls and PD patients (Additional file 1: Table S1), we performed immunohistochemistry (IHC) analysis of eEF2 phosphorylation on threonine residue 56 (p-eEF2, T56), which reflects eEF2K activity [42, 57]. In parallel, using serial sections, we also assessed the phosphorylation of AS on serine residue 129 (p-ASyn, S129) by IHC, as it is a robust marker for AS Lewy pathology (~ 90% S129 phosphorylated AS is found in inclusions) [2, 65]. To avoid ambiguity with neuromelanin pigment found in dopaminergic neurons in substantia nigra (SN) with DAB IHC staining, we employed a modified IHC protocol [52] in order to effectively destain/bleache neuromelanin in midbrain sections without adversely affecting p-eEF2 (T56) IHC staining (Additional file 1: Figure S1a-b). Our data show that p-eEF2 (T56) immunostaining is increased in SN and periaqueductal gray (PAG) matter (gray matter surrounding cerebral aqueduct) in PD midbrain sections compared to controls (Fig. 1a-b; additional controls shown in Additional file 1: Figure S2a; additional PD cases are shown in Additional file 1: Figure S3a; quantitation of p-eEF2 IHC staining is presented in Fig. 3a). We observed that p-eEF2 IHC staining was predominantly in neurons in SN and PAG in PD cases, and in some glial cells in SN (for instance in PD-2, Fig. 1b; PD-3 and PD-4, Additional file 1: Figure S3a). As expected, we observed Lewy body pathology (p-ASyn, S129) characteristic of PD in both of these midbrain regions in PD cases but not in controls (Fig. 1a-b; Additional file 1: Figure S2a, S3a). Accordingly, Lewy body inclusion pathology was seen in most PD cases both in SN and PAG, with some lewy neurites in SN (PD-2, Fig. 1b; PD-6, Additional file 1: Figure S3a) and PAG area (PD-2, Fig. 1b; PD-3 and PD-5, Additional file 1: Figure S3a). Then, by using immunofluorescence, we assessed whether p-eEF2 (T56) immunopositivity potentially colocalizes with p-ASyn (S129), or p-eEF2 (T56) is a possible component of lewy body pathology. While we observed some neurons in PD SN which were clearly positive for both p-eEF2 (T56) and p-ASyn (S129), we also found substantial p-eEF2 (T56) immunopositivity in cells without p-ASyn (S129) and vice versa (Additional file 1: Figure S4b).

Previous reports, including our own published data, show that phosphorylation of eEF2 (p-eEF2, T56) is strongly increased in postmortem hippocampus and mesial temporal cortex in AD, the major neurodegenerative disease with dementia [28, 43, 46]. Among the PD cases examined here, PD-1 and PD-5 were also clinically diagnosed with PD with dementia (PDD), which is usually seen in longstanding PD [1, 2]. Therefore, we assessed p-eEF2 (T56) in postmortem hippocampus sections from control and PD cases. We found increased p-eEF2 IHC staining in hippocampal CA1 and CA2 (CA, *cornu ammonis*) fields in PD cases compared to controls, predominantly in neurons (Fig. 2a-b; additional controls shown in Additional file 1: Figure S5a-b; additional PD cases shown in Additional file 1: Figure S6a, panoramic views; Additional file 1: Figure S7a-b, magnified field views; quantitation of p-eEF2 IHC staining in areas CA1-CA2 is presented in Fig. 3a). There was little or none p-eEF2 immunopositivity in CA3 and dentate gyrus (DG) in all PD cases, except PD-1 and PD-3 (CA3, Additional file 1: Figure S7a-b). We also assessed Lewy body pathology in hippocampal sections from these control and PD cases, since Lewy pathology in hippocampus is found at advanced neuropathological stages of PD (Braak PD staging, stages 4–6) [1, 36]. Our IHC analysis for p-ASyn (S129) showed varying degrees of Lewy body inclusions (PD-1 and PD-2, Fig. 2b; PD-3 and PD-6, Additional file 1: Figure S7b) and Lewy neurites pathology (PD-1 and PD-2, Fig. 2b; PD-6, Additional file 1: Figure S7b), with pronounced involvement of hippocampal

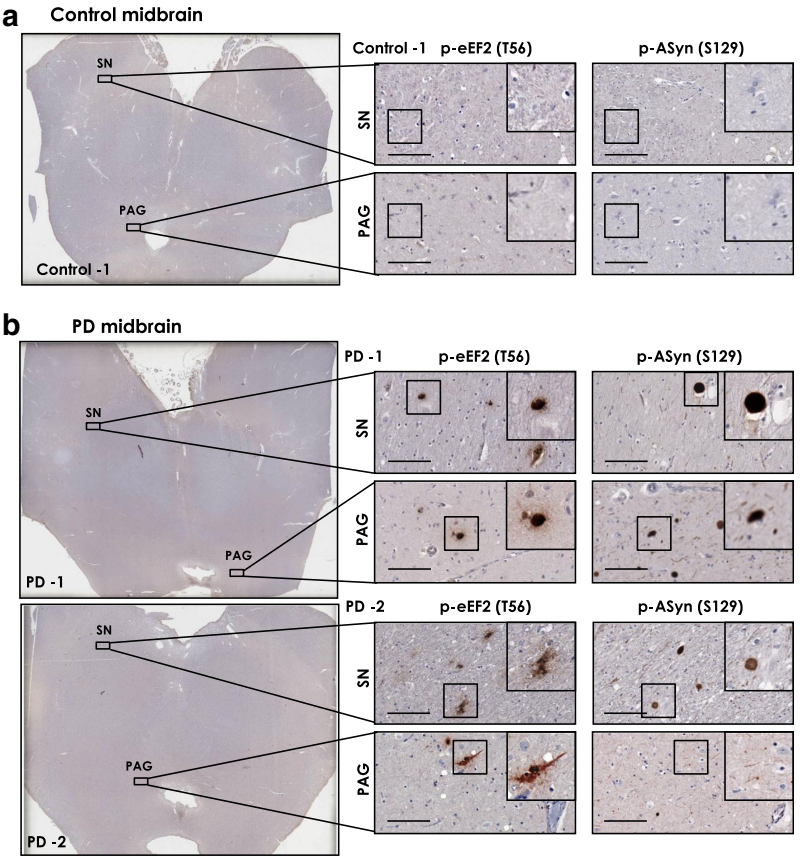

Fig. 1 Immunostaining for phospho-eEF2 (p-eEF2, Thr56) and phospho-AS (p-ASyn, Ser129) in postmortem control and PD midbrain serial sections. **a**-**b** p-eEF2 (T56) and p-ASyn (S129) IHC in postmortem midbrain serial sections from one control (**a**) and two PD cases (**b**). IHC staining for p-eEF2 is predominantly seen in neurons in both cases, and possibly glial cells in substantia nigra in PD-2. Substantia nigra in both cases shows involvement by lewy body-LB pathology (p-ASyn, S129); while in periaqueductal gray matter, LB inclusions are seen in PD-1 and some lewy neurites are seen in PD-2. Additional control and PD midbrain IHC data are presented in Additional file 1: Figure S2-S3, and case details are included in Additional file 1: Table S1. (SN- substantia nigra; PAG- periaqueductal gray matter; scale bar, 100 μm; insets show 40× magnified view in each image)

CA2 field in most PD cases (Fig. 2a-b and Additional file 1: Figure S7a-b).

We also queried multiple transcriptome datasets publicly available in the National Center for Biotechnology Information (NCBI) Gene Expression Omnibus (GEO) platform for eEF2K mRNA expression in PD brain. Significantly increased eEF2K mRNA expression was found in Striatum (Fig. 3b, GEO accession # GSE28894), medial substantia nigra (Fig. 3c, GEO accession # GSE8397), and dorsal nucleus of vagus (dmX) (Fig. 3d, GEO accession # GSE43490). Collectively, these data provide strong evidence for aberrant eEF2K expression and activity in PD brain. Finally, we also performed quantitative PCR in cultured midbrain organoids derived from human iPSCs [3, 49], and found significantly increased eEF2K mRNA expression in A53T mutant AS carrying organoids compared to wild type controls (Fig. 3e).

eEF2K expression and activity are increased in M83$^{+/+}$ transgenic PD mouse brains subsequent to induction of AS neuropathology

To further establish the relevance of eEF2K to AS-related pathology in PD, we analyzed brain eEF2K expression in transgenic PD M83$^{+/+}$ mice, subsequent to induction of AS pathology by intramuscular injection of pre-formed fibrillar PFF AS [20, 58]. Within 8–10 weeks post-injection, the PFF AS injected M83$^{+/+}$ mice show profound motor neuron loss, AS inclusions, progressive motor deficits and reduced survival at much earlier ages than native M83$^{+/+}$ mice [58]. For these analyses, PFF AS injected M83$^{+/+}$ mice (injected at 2–3 months of age) were used after 8–10 weeks

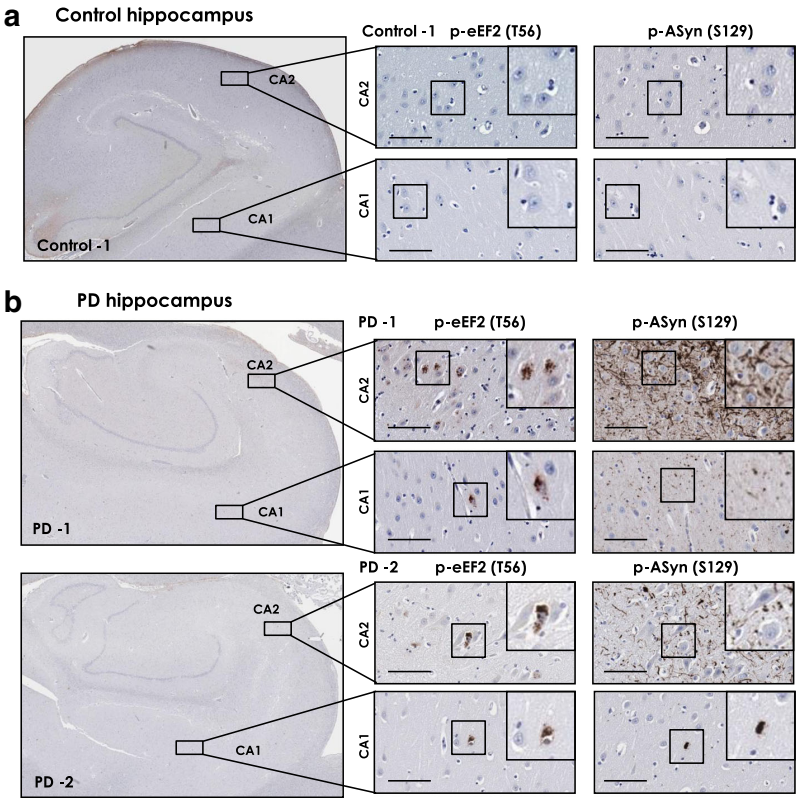

Fig. 2 Immunostaining for phospho-eEF2 (p-eEF2, Thr56) and phospho-AS (p-ASyn, Ser129) in postmortem control and PD hippocampus serial sections. **a**-**b** p-eEF2 (T56) and p-ASyn (S129) IHC in postmortem hippocampus serial sections from one control (**a**) and two PD cases (**b**). IHC staining for p-eEF2 in PD cases is seen predominantly in CA1 and CA2 neurons. Lewy body inclusions and neurites (p-ASyn, S129) are seen in both PD cases, with pronounced involvement of CA2. IHC data concerning CA3 and dentate gyrus from PD-1 and PD-2 are included in Additional file 1: Figure S7a. Additional control and PD hippocampus IHC data are presented in Additional file 1: Figure S5-S7, and case details are included in Additional file 1: Table S1 (CA1 and CA2- hippocampal cornu ammonis fields 1 and 2 respectively; scale bar, 100 μm; insets show 40× magnified view in each image)

post-injection when typical motor abnormalities such as hindlimb paralysis (Additional file 1: Figure S8a) and severe hindlimb clasping behaviour (Additional file 1: Figure S8b-c) were evident. Our data show that compared to PBS injected M83$^{+/+}$ mice, brain eEF2K mRNA expression is remarkably increased (~ 5–6 fold) in PFF AS injected M83$^{+/+}$ moribund (clasping score 3, see Materials and Methods) mice (Fig. 4a). Accordingly, we also found increased eEF2K activity (p-eEF2, T56) and induction of pathological AS phosphorylation (p-ASyn, S129) by western blotting in PFF AS injected M83$^{+/+}$ (Fig. 4b-c). These data further support our hypothesis regarding a role of eEF2K in AS neurotoxicity.

AS overexpression increases eEF2K activity, while eEF2K inhibition reduces AS cytotoxicity in dopaminergic N2A cells

As mentioned above, AS-induced neurotoxicity is considered to play an important role in neurodegeneration in PD [39, 71]. Indeed, overexpression of AS in cultured cells promotes AS aggregation, increases oxidative stress, and reduces cell survival [4, 8]. This has been observed for the wild-type and mutant forms of AS, including the A53T mutant AS, which accelerates AS aggregation and pathology [39, 41]. To study the effects of eEF2K inhibition on AS toxicity, we employed differentiated mouse neuroblastoma N2A cells overexpressing either wild-type AS (ASyn-WT) or the A53T mutant (ASyn-A53T) +/− siRNA mediated eEF2K knockdown (kd), and measured cytotoxicity in these cells. Differentiated N2A cells exhibit many features of mature dopaminergic neurons including functional neurotransmitter receptors [63], and are widely used to study the toxicity of amyloid proteins [14, 28].

Overexpression of ASyn-WT or ASyn-A53T increased p-eEF2 (T56) levels in N2A cells, which was reduced by eEF2K kd (Fig. 5a-b). We then assessed AS cytotoxicity by measuring the activity of lactate dehyrogenase (LDH) in

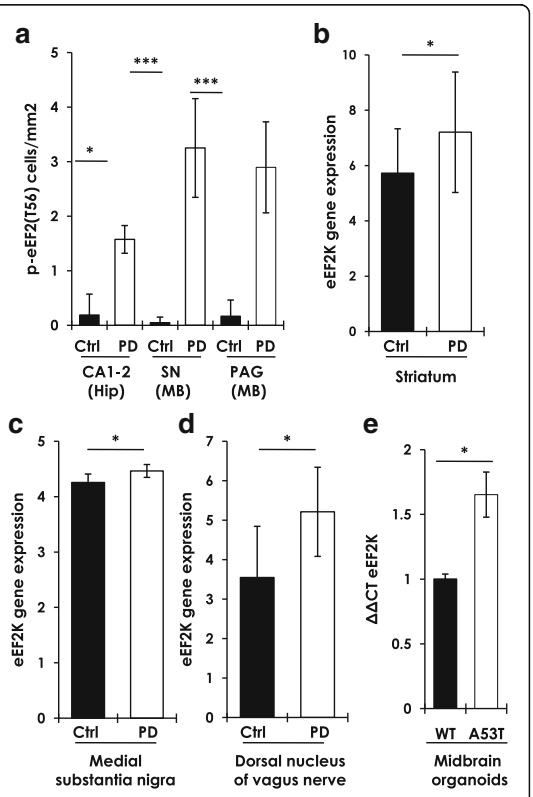

Fig. 3 eEF2K expression and activity in PD brain. **a** Quantitation of p-eEF2 (T56) IHC (3,3′-Diaminobenzidine-DAB staining) in postmortem hippocampus- Hip (CA1 and CA2 fields) and midbrain- MB (SN-substantia nigra, and PAG-peri-aqueductal gray matter) sections from 3 control and 6 PD cases (Additional file 1: Table S1; counts from at least 6 high power fields from each control or PD section; Mann–Whitney test, $*p < 0.05$, $***p < 0.005$; error bars indicate Mean ± S.D.). **b**-**d** eEF2K mRNA expression in control and PD striatum (**b**), medial substantia nigra (**b**) and dorsal nucleus of vagus nerve (**d**). The following publicly available transcriptomic profile datasets were analyzed on the National Center for Biotechnology Information (NCBI) Gene Expression Omnibus (GEO) platform: Striatum (**b**)- dataset GEO accession # GSE28894, Illumina human Ref-8 v2.0 expression beadchip platform, probe ID ILMN_1789171, controls $n = 15$ and PD $n = 15$; Medial substantia nigra (**c**)- dataset GEO accession # GSE8397, Affymetrix Human Genome U133B Array, probe ID 225546_at, controls $n = 8$ and PD $n = 15$; Dorsal nucleus of vagus (**d**)- dataset GEO accession # GSE43490, Agilent-014850 Whole Human Genome Microarray, probe ID A_24_P716162, controls $n = 6$ and PD $n = 7$. (Mann–Whitney test, $*p < 0.05$; error bars in 3b-d indicate Mean ± S.D.). **e** Relative eEF2K mRNA expression in human iPSCs derived cultured midbrain control (WT, $n = 3$) or A53T ($n = 2$) mutation carrying organoids (T-test, $*p < 0.05$; error bars indicate Mean ± S.D.)

the culture medium. LDH is a cytoplasmic enzyme released under conditions of cell membrane damage and during toxic stress in neuronal cultures [37]. As expected, overexpression of ASyn-WT or ASyn-A53T led to increased LDH release (72 h post-transfection), which was reduced significantly by eEF2K kd in both ASyn-WT or ASyn-A53T expressing cells (Fig. 5c). Next, we measured cytotoxicity in these cultures by labelling with propidium iodide (PI), another cell permeable marker of cell death. Overexpression of ASyn-WT or ASyn-A53T resulted in increased cell death (72 h post-transfection), as measured by flow cytometry analysis of PI staining, and eEF2K kd significantly improved viability in these cultures (Fig. 5d).

eEF2K inhibition mitigates AS induced mitochondrial dysfunction and oxidative stress in N2A cells

Next, we assessed whether the cytoprotective effects of eEF2K inhibition against AS toxicity are mediated by changes in mitochondrial function, since AS inhibits mitochondrial respiration and complex I activity [8, 55]. First, we characterized cellular respiration (oxygen consumption rate, OCR) in differentiated N2A cells following eEF2K kd without ASyn overexpression. This is important since eEF2K regulates highly energy consuming process of elongation during mRNA translation, and we wanted to assess if possible metabolic reprogramming in cells due to eEF2K inhibition does not impair mitochondrial function [15, 34]. Intriguingly, N2A cells with eEF2K kd exhibited significantly higher OCR under basal conditions, and maximal respiration subsequent to the treatment with FCCP (uncoupler of oxidative phosphorylation) than control cells (Additional file 1: Figure S9a). To investigate if the increased respiration in eEF2K kd cells under basal conditions is linked to an increase in the mitochondrial mass, we quantified mitochondrial content in control and eEF2K kd cells. However, there were no significant differences in mitochondrial mass by flow cytometry analysis using the fluorescent Mitotracker reagent (Additional file 1: Figure S9b), or by mitochondrial mtDNA quantification (Additional file 1: Figure S9c). These data demonstrate healthy mitochondrial function in eEF2K kd cells, and suggest that, compared to control cells, cellular respiration in eEF2K kd cells is increased predominantly due to enhanced mitochondrial respiration (Additional file 1: Figure S9a; compare changes in basal respiration and maximal respiration in control vs. eEF2K kd cells) without significant changes in mitochondrial content (Additional file 1: Figure S9b-c).

Having established that eEF2K kd per se does not negatively affect mitochondrial function in N2A cells, we proceeded to assess the effects of eEF2K kd on AS induced mitochondrial dysfunction [8, 27]. We investigated this activity in differentiated N2A cells with overexpression of ASyn-WT or ASyn-A53T +/− eEF2K kd (72 h post-transfection). There was a noticeable reduction in basal OCR in cells overexpressing ASyn-WT, or ASyn-A53T compared to mock transfected cells

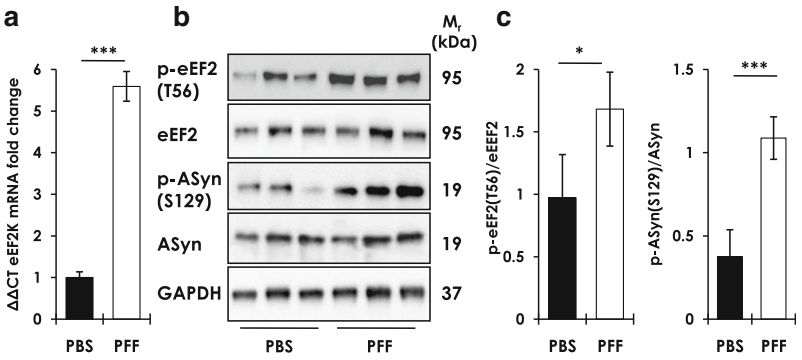

Fig. 4 Brain eEF2K expression and activity in transgenic M83$^{+/+}$ PD mice. **a** eEF2K mRNA levels in whole brain homogenates from transgenic M83$^{+/+}$ PD mice intramuscularly (IM) injected bilaterally with phosphate buffered saline (PBS, $n = 10$) or pre-formed fibrillar (PFF, $n = 13$) mouse wild type AS. (Mann–Whitney test, ***$p < 0.005$; error bars indicate Mean ± S.D.). **b**-**c** Western blot analysis of p-eEF2 (T56) and p-ASyn (S129) in whole brain homogenates from transgenic M83$^{+/+}$ PD mice intramuscularly (IM) injected bilaterally with phosphate buffered saline (PBS) or pre-formed fibrillar (PFF) mouse wild type AS (**b**), and corresponding densitometry analysis (**c**) ($n = 7$/group; Mann–Whitney test, *$p < 0.05$, ***$p < 0.005$; error bars indicate Mean ± S.D.)

(Fig. 6a). eEF2K kd led to significant improvement of the OCR under all conditions (compare Mock control vs. Mock+sieEF2K, ASyn-WT vs. ASyn-WT + sieEF2K and ASyn-A53T vs. ASyn-A53T + sieEF2K; Fig. 6a). Then, we measured cellular ATP levels under identical conditions, and found that overexpression of ASyn-WT or ASyn-A53T significantly reduced cellular ATP content reflecting AS toxicity (Fig. 6b). While eEF2K kd had negligible effect on ATP content in mock transfected cells, it attenuated the loss of ATP in ASyn overexpressing cells (compare ASyn-WT vs. ASyn-WT + sieEF2K and ASyn-A53T vs. ASyn-A53T + sieEF2K; Fig. 6b). Together, these data suggest that transient AS (WT or A53T) overexpression is associated with mitochondrial dysfunction in these dopaminergic cultures, which is rescued by eEF2K kd.

Mitochondrial dysfunction, including complex I inhibition, is associated with increased production of reactive oxygen species (ROS) and oxidative stress in cells [44]. As mentioned earlier, these processes, i.e., impaired mitochondrial function and increased ROS, are also implicated in AS toxicity [4]. Indeed, previous studies have shown that ROS levels are increased in AS overxpressing cells [27, 32]. Accordingly, we found that overexpression of ASyn-WT or ASyn-A53T increased ROS levels compared with mock transfected cells, as measured by flow cytometry analysis of the ROS detection reagent, DCFDA (Fig. 6c). Moreover, we found that eEF2K kd significantly reduced ROS in these cultures, in line with previously reported effects of eEF2K inhibition on cellular ROS levels [10, 28]. Collectively, these data suggest a role of eEF2K in AS toxicity (Fig. 5a-b), and demonstrate that eEF2K inhibition reduces AS toxicity by improving mitochondrial function and reducing ROS (Fig. 6a-c).

Deletion of efk-1 *improves dopaminergic neuronal function in a C. elegans model of AS neurotoxicity*

To assess the in vivo impact of eEF2K inhibition as a means of improving AS-mediated neurotoxicity, we used a *C. elegans* model of PD. *C. elegans* possess four bilaterally symmetric pairs of dopaminergic neurons that are critical for adaptations to mechanosensory stimuli, and for the regulation of complex behaviours such as foraging, movement, and egg-laying [50, 69]. Accordingly, this worm model is widely used in PD research to investigate the significance of specific mutations and variations, and to screen for candidate disease-modifying small molecules [70]. We studied a previously generated *C. elegans* strain that transgenically expresses human AS A53T mutant, which results in age-related degeneration of dopaminergic neurons and in defects in dopaminergic function in these worms [12]. Using this strain, we assessed dopaminergic neuron function with or without concomitant deletion of *efk-1*, the eEF2K ortholog in worms [(ASyn (A53T) and ASyn (A53T)/efk-1$_{del}$ strains; see Materials and Methods)]. We assessed the effects of *efk-1* deletion in A53T AS expressing worms in three behavioural responses that are considered to be mediated predominantly by dopaminergic neurons in worms: ethanol avoidance, pharyngeal pumping, and area restricted searching (see Materials and Methods). We hypothesized that, in view of the cytoprotective effects of eEF2K inhibition against AS toxicity in cultured dopaminergic N2A cells (Figs. 5-6), *efk-1* deletion would improve AS-A53T-induced dopaminergic neuron dysfunction in worms.

In ethanol avoidance assays, worms exhibit an aversive response to acute ethanol exposure and this response is dependent on adequate sensory motor co-ordination [40]. Notably, *efk-1* deletion alone had no significant effects on this response (Fig. 7a; compare WT (N2) worms with efk-1$_{del}$), while, as previously reported,

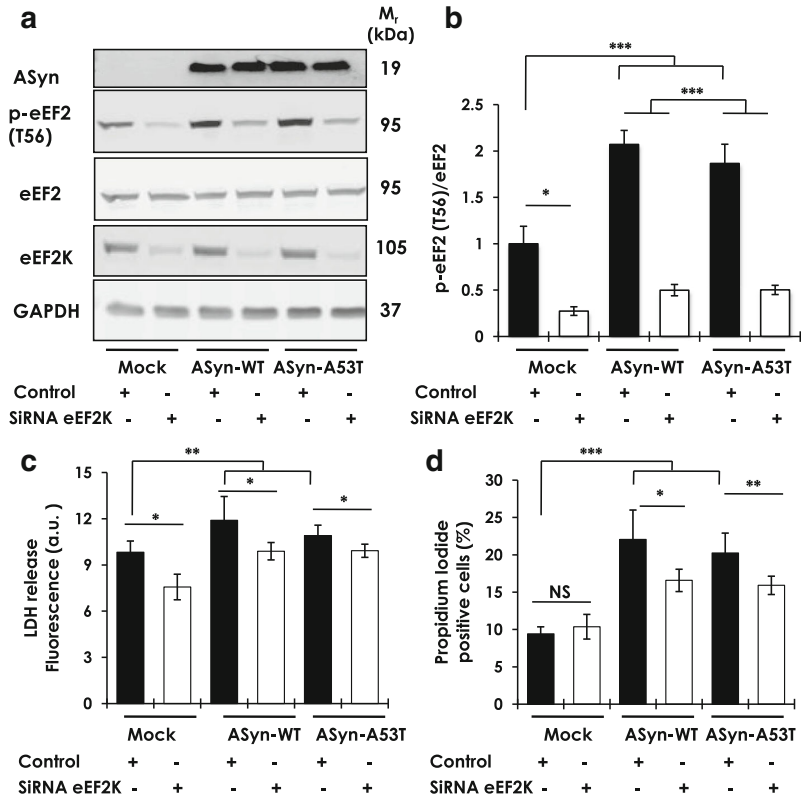

Fig. 5 Effects of eEF2K inhibition on human AS cytotoxicity in differentiated N2A cells. **a**-**b** Western blot analysis of p-eEF2 (T56) levels in N2A cells subsequent to transient overexpression of human wild type or mutant A53T AS, with or without siRNA mediated eEF2K knockdown (**a**), and corresponding densitometry analysis (**b**) ($n = 6$–9/group from three independent experiments; One-way ANOVA *post-hoc* Bonferroni test, $^{*}p < 0.05$, $^{***}p < 0.005$; error bars indicate Mean ± S.E.M). c Measurements of cytotoxicity by lactate dehydrogenase-LDH release in the culture medium (**c**) and FACS analysis of propidium iodide-PI staining (**d**) in N2A cells subsequent to transient overexpression of human wild type or mutant A53T AS, with or without siRNA mediated eEF2K knockdown ($n = 9$–12/group from three independent experiments; One-way ANOVA *post-hoc* Bonferroni test, $^{*}p < 0.05$, $^{**}p < 0.01$, $^{***}p < 0.005$, NS = not significant; error bars indicate Mean ± S.D.)

expression of ASyn-A53T led to a worsened response (Fig. 7a) [12]. Importantly, loss of *efk-1* completely rescued the reduced ethanol avoidance of ASyn-A53T expressing worms [(Fig. 7a; compare ASyn (A53T) with ASyn (A53T)/efk-1_{del})]. In pharyngeal pumping assays, rhythmic contractions (pumping) of the pharynx serve as marker of neuromuscular function and rely on a complex neural integration within the autonomic activity [64]. This response is essential for feeding and generation of consequent isthmus peristalsis. As expected, we observed no difference in the pharyngeal pumping activity between wild type worms and worms lacking *efk-1* [(Fig. 7b; compare WT (N2) with efk-1_{del})]. ASyn-A53T expressing worms showed a modest, but significant, reduction in pumping activity, which was restored significantly in ASyn-A53T worms with *efk-1* deletion [(Fig. 7b; compare ASyn (A53T) with ASyn (A53T)/efk-1_{del})]. Finally, the area-restricted search behaviour reflects foraging, such that the worms show an adaptive response by reducing turning frequency to the presence of food; this response is mediated by neural circuits involving dopaminergic and glutamatergic signalling [24]. As seen with the other two assays, *efk-1* deletion alone negligibly affected the performance of worms in the area restricted search assay [(Fig. 7c; compare WT (N2) worms with efk-1_{del})], whereas ASyn-A53T mutant expressing worms showed significant defects in this assay (Fig. 7c) as reported previously [12]. Critically, this defect was completely rescued in ASyn-A53T worms lacking *efk-1* [(Fig. 7c; compare ASyn (A53T) with ASyn (A53T)/efk-1_{del})]. Taken together, *efk-1* deletion improves three independent behaviours known to rely dominantly on normal dopaminergic neuron function. These data support our hypothesis and demonstrate that *efk-1* deletion mitigates the deleterious effects of ASyn (A53T) on the

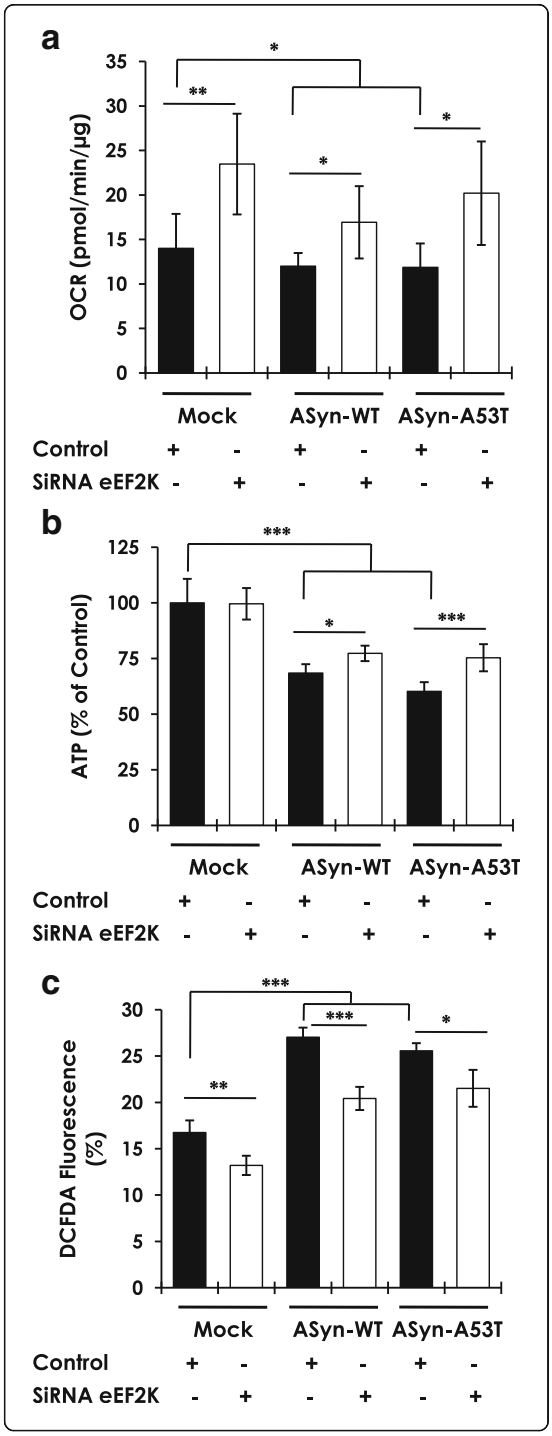

Fig. 6 Effects of eEF2K inhibition on mitochondrial dysfunction and oxidative stress induced by human AS in differentiated N2A cells. **a**-**b** Measurements of basal oxygen consumption rate-OCR (**b**) and ATP levels (**c**) in N2A cells subsequent to transient overexpression of human wild type or mutant A53T AS, with or without siRNA mediated eEF2K knockdown ($n = 9$–12/group from three independent experiments; Unpaired T-test, $^{*}p < 0.05$, $^{**}p < 0.01$, $^{***}p < 0.005$; error bars indicate Mean ± S.D.). **c** Flow cytometry analysis of reactive oxygen species (ROS), measured by DCFDA staining, in N2A cells subsequent to transient overexpression of human wild type or mutant A53T AS, with or without siRNA mediated eEF2K knockdown ($n = 9$/group from three independent experiments; Unpaired T-test, $^{*}p < 0.05$, $^{**}p < 0.01$, $^{***}p < 0.005$; error bars indicate Mean ± S.D.)

function of neural circuits involving dopaminergic neurons in *C. elegans*, and further point to an in vivo role for eEF2K signaling in AS-mediated neurotoxicity.

Discussion

Principally driven by the early genetic findings in inherited PD and PD neuropathology, a significant effort in the discovery of novel therapies in PD and other synucleinopathies has been to target AS production and/or aggregation [39, 71]. Although such studies have shown promising results in preclinical research, their translation into clinically implementable therapies has yet to be realized [71]. An additional area of research in potential therapies in PD has been to address AS neurotoxicity, and to target cellular mechanisms that potentially render neurons susceptible to AS neurotoxicity [38].

Our data suggest that eEF2K is one possible mechanism that is pathologically involved in AS-mediated toxicity, and that its inhibition represents a novel therapeutic strategy in PD. Our findings demonstrate that eEF2K activity is increased in postmortem PD midbrain (substantia nigra and periaqueductal gray matter) and in hippocampus (CA1 and CA2 regions), with the concomitant presence of Lewy pathology (phosphorylation of AS on Ser-129). Additionally, analysis of publicly available microarray datasets revealed increased eEF2K expression in striatum, medial substantia nigra and dorsal nucleus of vagus (dmX) in PD. Hence, dysregulated eEF2K expression and/or activity are observed in multiple brain regions that are affected in PD. We further show that induction of aggressive AS pathology in $M83^{+/+}$ transgenic PD mice, by intramuscular PFF AS injection, is associated with enhanced brain eEF2K expression and activity. In addition, transient overexpression of AS (WT or A53T mutant) is associated with cytotoxicity and oxidative stress in dopaminergic N2A cells, and leads to eEF2K activation in these cultures. Moreover, eEF2K inhibition mitigated the cytotoxic effects of AS overexpression in cells and prevented the deficits in dopaminergic function in *C. elegans* due to transgenic AS-A53T expression. These observations are supported by previous reports showing that eEF2K

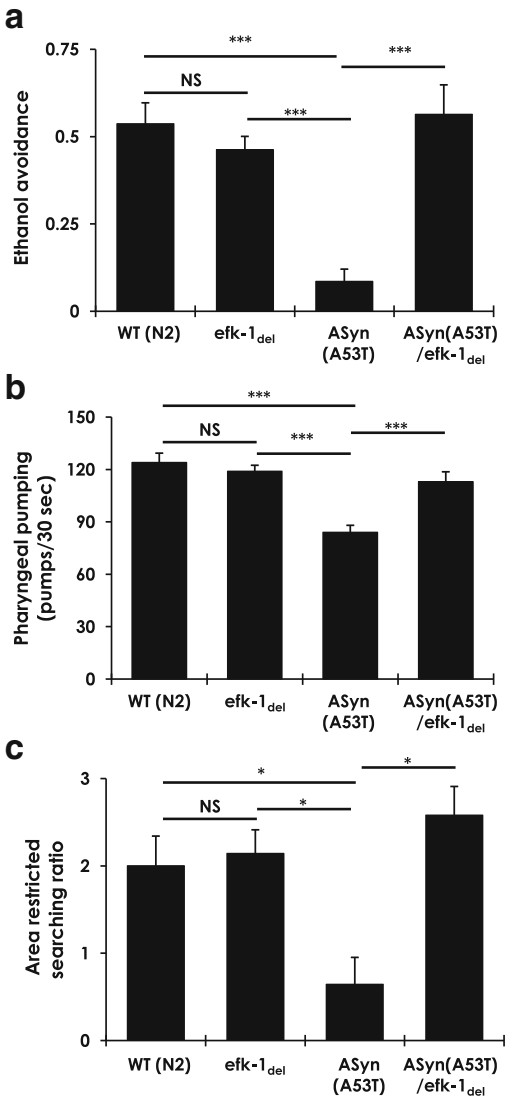

Fig. 7 Effects of efk-1 deletion on ethanol avoidance, pharyngeal pumping, and area restricted searching behavior in *C. elegans* expressing human AS-A53T. **a**-**c** Analysis of ethanol avoidance ($n = 100–150$ worms/measurement) (**a**), pharyngeal pumping ($n = 10–15$ worms/measurement) (**b**), and area restricted searching behavior ($n = 10–15$ worms/measurement) (**c**) in control (wild type N2) worms, in *efk-1(ok3609)* null mutant worms (efk-1_{del}), in worms expressing human mutant AS-A53T (*Pdat-1::α-synuclein[A53T]*), and in *efk-1(ok3609)* null mutant worms expressing AS-A53T (*efk-1(ok3609); Pdat-1::α-synuclein[A53T]*). Statistical analysis: one-way ANOVA with post-hoc Bonferroni test; $*p < 0.05$, $***p < 0.005$, NS = not significant; error bars indicate mean ± S.E.M. from at least three independent experiments

inhibition reduces oxidative and ER stress, processes associated with AS toxicity [6, 10, 28].

It is noteworthy that brain areas showing increased eEF2K activity in PD cases examined here are part of distinct neurotransmitter networks that are affected at different neuropathological stages in PD [7, 65]. Considering the neuronal populations found in these distinct anatomical brain areas and their connectivity, it has been postulated that the clinical spectrum of PD symptoms (i.e., motor, autonomic or cognitive) may arise depending on the extent of Lewy pathology and/or cell loss [7, 33]. From a neurological perspective, it is commonly thought that the lesions in the striatum or substantia nigra underlie the motor symptoms due to neurotransmitter imbalance in the nigrostriatal system causing defective motor control and muscle tone, and this assertion is supported by the studies in animal models [18]. Furthermore, the loss of cholinergic projections from dorsal nucleus of vagus (dmX) is implicated in the autonomic dysfunction in PD [65]. The periaqueductal gray (PAG) matter is also affected with AS inclusions in PD, Dementia with Lewy bodies (DLB), and Multiple system atrophy (MSA) [61]. This cell dense region harbours many distinct neuronal populations with projections linking forebrain and lower brain stem, and in mammals is involved in autonomic control, cardiovascular function, pain modulation, wakefulness, rapid eye movement (REM) sleep and vocalization [55]. Finally, Lewy body pathology is present in hippocampus at advanced neuropathological stages in PD, and thought to underlie cognitive symptoms [7, 33, 65].

The significance of enhanced eEF2K expression and/or activity in the aforementioned brain areas in PD remains unknown. Given the critical role of eEF2K in dendritic mRNA transaltion and synaptic integrity [34], it is plausible that aberrant eEF2K activity may underlie the dysfunction in these neuronal populations. Supporting this, some studies suggest a role for eEF2K in synaptic plasticity, in particular mGluR5-mediated long-term depression [66], a mechanism purported to underlie synaptic dysfunction in AD and other neuropsychiatric conditions [11]. Furthermore, eEF2K activity is also increased upon exposure to excitatory stimuli in neuronal cultures [23, 35, 66], and in response to nutrient deprivation (by energy sensor AMP-activated kinase). However, it remains to be established whether some of the aforementioned stimuli enhancing eEF2K activity also underlie increased eEF2K activity in PD. In this regard, activity of AMP-kinase, an important regulator of eEF2K in response to metabolic stimuli, is increased in cells and/or rodents after exposure to mitochondrial toxins (e.g., MPTP, rotenone) [9, 36]. In postmortem PD brain, activated AMPK has been detected near the rim of Lewy bodies in the cytoplasm as opposed to nuclear staining in controls [30]. However, the beneficial effects of AMPK inhibition in PD models have not been conclusively established [17], and in some studies

AMPK activation is protective [51]. A recent report showed aberrations in the expression of factors controlling protein synthesis (e.g., ribosomal proteins, translation initiation and elongation factors) in postrmortem PD brain, including reduced eEF2 levels in PD midbrain and cortex [19], supporting the notion of dysregulated mRNA translation in PD. Determining whether increased eEF2K activity plays a role in the synaptic defects of PD, or occurs due to aberrations within the translational machinery, represents a challenging task due to the complex nature of PD etiology and the possible involvement of multiple neurotransmitter systems as the disease progresses. For simplicity, it is plausible to suggest that increased eEF2K activity may be part of some stress-adaptive pathway, which plays a protective role in the short term under disturbed cellular homeostasis. However, chronic overactivation of this pathway in pathological states may be detrimental due to aberrations in mRNA translation and dendritic protein synthesis [28, 46].

From a therapeutic perspective, development of novel eEF2K inhibitors is actively being pursued towards novel experimental therapies in cancer due to its role in metabolic adaptations in cancer cells for survival under nutrient deprivation, including nervous system malignancies [16, 34, 42]. Here, we show that eEF2K inhibition augments mitochondrial respiration, reduces oxidative stress and prevents AS toxicity in dopaminergic N2A cells. The mechanism of increased mitochondrial function subsequent to eEF2K inhibition in dopaminergic N2A cells remains to be deciphered. We previously reported that eEF2K inhibition in dopaminergic N2A cells induces an NRF2 antioxidant response, and blocks the toxicity of Aβ oligomers in neuronal cultures [28]. NRF2 is a master regulator of cellular redox homeostasis under physiological and pathological conditions due to its ability in controlling the expression of antioxidant genes [31]. However, NRF2 is also known to regulate cellular metabolism (e.g., glutamine biogenesis), and affects mitochondrial structure and function such as ATP production, fatty acid oxidation and structural integrity [26, 48]. Accordingly, cells and mitochondria derived from NRF2 knockout mice show reduced respiration, lower ATP levels and impairments in mitochondrial fatty acid oxidation [25, 45]. Furthermore, several small molecules activators of NRF2 pathway have shown beneficial effects in restoring mitochondrial function under conditions of redox stress in cell cultures, and also in models of neurodegenerative diseases [26]. One such therapeutic molecule, dimethyl fumarate (DMF, Tecfidera), used to treat multiple sclerosis, exerts anti-inflammatory and antioxidant effects in cell culture and animal studies by activating NRF2 antioxidant response [1]. DMT administration prevents neurodegeneration in mice treated with MPTP [71], a mitochondrial toxin associated with chemically induced parkinsonism in humans and animals [1]. In this context, our findings raise the possibility that eEF2K can also be targeted in PD to mitigate AS-induced oxidative stress, and potentially neuronal dysfunction in this disease.

Conclusion

By employing multiple experimental models, our data support the relevance of eEF2K in PD, and of eEF2K inhibition in mitigating AS-induced oxidative stress and neuronal dysfunction. We anticipate that our findings will stimulate further mechanistic studies and a careful evaluation of eEF2K inhibition in PD, and potentially other neurodegenerative diseases.

Endnotes

[1]The term eEF2K activity in this manuscript denotes phosphorylation of eEF2, the major known substrate for eEF2K, on serine residue 56 assessed by immunohistochemistry, immunofluorescence or western blot.

Additional file

Additional file 1: Table S1. Control and PD cases; **Figure S1.** Melanin bleaching in postmortem midbrain sections and immunostaining for phospho-eEF2 (p-eEF2, Thr56); **Figure S2.** Immunostaining for phospho-eEF2 (p-eEF2, Thr56) and phospho-AS (p-ASyn, Ser129) in postmortem control midbrain sections; **Figure S3.** Immunostaining for phospho-eEF2 (p-eEF2, Thr56) and phospho-AS (p-ASyn, Ser129) in postmortem PD midbrain sections; **Figure S4.** Detection of phospho-eEF2 (p-eEF2, Thr56) and phospho-AS (p-ASyn, Ser129) in postmortem control and PD midbrain sections by immunofluorescence; **Figure S5.** Immunostaining for phospho-eEF2 (p-eEF2, Thr56) and phospho-AS (p-ASyn, Ser129) in postmortem control hippocampus sections; **Figure S6.** Immunostaining for phospho-eEF2 (p-eEF2, Thr56) in postmortem PD hippocampus sections-Panoramic views; **Figure S7.** Immunostaining for phospho-eEF2 (p-eEF2, Thr56) and phospho-AS (p-ASyn, Ser129) in postmortem PD hippocampus sections; **Figure S8.** Effects of intramuscularly injected pre-formed fibrillar (PFF) AS on motor phenotype and survival of transgenic M83+/+ PD mice and **Figure S9.** Mitochondrial respiration and mitochondrial mass in differentiated N2A cells subsequent to eEF2K knockdown. (PDF 2444 kb).

Abbreviations

AD: Alzheimer disease; AS: Alpha synuclein; eEF2: Eukaryotic elongation factor-2; eEF2K: Eukaryotic elongation factor-2 kinase; MPTP: 1-methyl-4-phenyl-1,2,3,6-tetrahydropyridine; PD: Parkinson disease; PFF: Pre-formed fibrils; ROS: Reactive oxygen species

Acknowledgements

The authors would like to thank following individuals their help and assistance during the study: (BCCRC) Amy Li, Jordan Cran, Bo Rafn, and Shawn Chafe, (PHJ lab) Rikke Hahn Kofoed.

Funding

This work was supported by funding to AJ in the form of AIAS-COFUND fellowship from European Union's Horizon 2020 Research and Innovation Programme under the Marie Skłodowska-Curie agreement (grant #754513) and the Lundbeckfonden, Denmark (grant #R250–2017-1131), Research grants to PHS from the Ride2Survive Brain Cancer Impact Grant of the Canadian Cancer Society and Brain Canada (grant #703205) and funds from the BC Cancer Foundation, Research support to ST by the Canadian Research Chair in Transcriptional Regulatory Networks and Canadian Institutes of Health Research Project Grant (grant #PJT-153199), NSERC USRA scholarship

to YAN, and support to PHJ by Lundbeckfonden Grant (grant # DANDRITE-R248–2016-2518 and R171–2014-591).

Availability of data and materials

The transcriptomic datasets analyzed during this study can be accessed on the National Center for Biotechnology Information (NCBI) Gene Expression Omnibus (GEO) platform (hyperlink: https://www.ncbi.nlm.nih.gov/geo/) with following accession IDs: GSE28894 (Platform, Illumina human Ref-8 v2.0 expression beadchip; eEF2K probe ID, ILMN_1789171), GSE8397 (Platform, Affymetrix Human Genome U133B Array; eEF2K probe ID, 225546_at), and GSE43490 (Agilent-014850 Whole Human Genome Microarray; eEF2K probe ID, A_24_P716162). Otherwise, all data generated and analyzed during this study are included in the main manuscript file or the supplementary files.

Authors' contributions

AJ, AD, BJ, ST and PHS designed the research, AJ, AD, BJ, FB, YAN, LMS and NF performed research, GLN helped with experimental design and dataset analysis, IM provided human postmortem research material, JCS provided research material from iPSCs derived midbrain organoids, and AJ, ST and PHS wrote the manuscript. AD and BJ contributed equally to this work. All authors read and approved the final manuscript.

Authors' information

AJ was formerly a Postdoctoral Fellow in the research laboratory of PHS at the University of British Columbia (Canada), and since October 2017 is affiliated with Aarhus University (Denmark) as AIAS-COFUND Junior Research Fellow.

Competing interests

The authors declare that they have no competing interests.

Publisher's Note

Author details

[1]Aarhus Institute of Advanced Studies, Department of Biomedicine, Aarhus University, Høegh-Guldbergs Gade 6B, DK-8000 Aarhus, Denmark. [2]Department of Pathology and Laboratory Medicine, University of British Columbia, Vancouver, Canada. [3]British Columbia Cancer Research Centre, 675 West 10th Avenue, Vancouver, BC V5Z 1L3, Canada. [4]Centre for Molecular Medicine and Therapeutics, BC Children's Hospital Research Institute, Department of Medical Genetics, University of British Columbia, Vancouver, BC V5Z 4H4, Canada. [5]Danish Research Institute of Translational Neuroscience, Department of Biomedicine, Aarhus University, Ole Worms Allé 3, DK-8000 Aarhus, Denmark. [6]Developmental and Cellular Biology, Luxembourg Centre for Systems Biomedicine (LCSB), University of Luxembourg, 7, avenue des Hauts-Fourneaux, 4362 Esch-sur-Alzette, Luxembourg.

Received: 6 May 2018 Accepted: 10 June 2018
Published online: 02 July 2018

References

1. Ahuja M, Ammal Kaidery N, Yang L, Calingasan N, Smirnova N, Gaisin A, Gaisina IN, Gazaryan I, Hushpulian DM, Kaddour-Djebbar I et al (2016) Distinct Nrf2 Signaling Mechanisms of Fumaric Acid Esters and Their Role in Neuroprotection against 1-Methyl-4-Phenyl-1,2,3,6-Tetrahydropyridine-Induced Experimental Parkinson's-Like Disease. J Neurosci 36:6332–6351. https://doi.org/10.1523/JNEUROSCI.0426-16.2016
2. Anderson JP, Walker DE, Goldstein JM, de Laat R, Banducci K, Caccavello RJ, Barbour R, Huang J, Kling K, Lee M et al (2006) Phosphorylation of Ser-129 is the dominant pathological modification of alpha-synuclein in familial and sporadic Lewy body disease. J Biol Chem 281:29739–29752. https://doi.org/10.1074/jbc.M600933200
3. Arias-Fuenzalida J, Jarazo J, Qing X, Walter J, Gomez-Giro G, Nickels SL, Zaehres H, Scholer HR, Schwamborn JC (2017) FACS-assisted CRISPR-Cas9 genome editing facilitates Parkinson's disease modeling. Stem Cell Rep 9:1423–1431. https://doi.org/10.1016/j.stemcr.2017.08.026
4. Behbehani MM (1995) Functional characteristics of the midbrain periaqueductal gray. Prog Neurobiol 46:575–605
5. Bose A, Beal MF (2016) Mitochondrial dysfunction in Parkinson's disease. J Neurochem 139(Suppl 1):216–231. https://doi.org/10.1111/jnc.13731
6. Boyce M, Py BF, Ryazanov AG, Minden JS, Long K, Ma D, Yuan J (2008) A pharmacoproteomic approach implicates eukaryotic elongation factor 2 kinase in ER stress-induced cell death. Cell Death Differ 15:589–599. https://doi.org/10.1038/sj.cdd.4402296
7. Braak H, Del Tredici K, Rub U, de Vos RA, Jansen Steur EN, Braak E (2003) Staging of brain pathology related to sporadic Parkinson's disease. Neurobiol Aging 24:197–211
8. Chinta SJ, Mallajosyula JK, Rane A, Andersen JK (2010) Mitochondrial alpha-synuclein accumulation impairs complex I function in dopaminergic neurons and results in increased mitophagy in vivo. Neurosci Lett 486:235–239. https://doi.org/10.1016/j.neulet.2010.09.061
9. Choi JS, Park C, Jeong JW (2010) AMP-activated protein kinase is activated in Parkinson's disease models mediated by 1-methyl-4-phenyl-1,2,3,6-tetrahydropyridine. Biochem Biophys Res Commun 391:147–151. https://doi.org/10.1016/j.bbrc.2009.11.022
10. Chu HP, Liao Y, Novak JS, Hu Z, Merkin JJ, Shymkiv Y, Braeckman BP, Dorovkov MV, Nguyen A, Clifford PM et al (2014) Germline quality control: eEF2K stands guard to eliminate defective oocytes. Dev Cell 28:561–572. https://doi.org/10.1016/j.devcel.2014.01.027
11. Collingridge GL, Peineau S, Howland JG, Wang YT (2010) Long-term depression in the CNS. Nat Rev Neurosci 11:459–473. https://doi.org/10.1038/nrn2867
12. Cooper JF, Dues DJ, Spielbauer KK, Machiela E, Senchuk MM, Van Raamsdonk JM (2015) Delaying aging is neuroprotective in Parkinson's disease: a genetic analysis in C. Elegans models. NPJ Parkinsons Dis 1:15022. https://doi.org/10.1038/npjparkd.2015.22
13. Cooper JF, Machiela E, Dues DJ, Spielbauer KK, Senchuk MM, Van Raamsdonk JM (2017) Activation of the mitochondrial unfolded protein response promotes longevity and dopamine neuron survival in Parkinson's disease models. Sci Rep 7:16441. https://doi.org/10.1038/s41598-017-16637-2
14. Dahlgren KN, Manelli AM, Stine WB Jr, Baker LK, Krafft GA, LaDu MJ (2002) Oligomeric and fibrillar species of amyloid-beta peptides differentially affect neuronal viability. JBiolChem 277:32046–32053
15. De Gassart A, Martinon F (2017) Translating the anticancer properties of eEF2K. Cell Cycle 16:299–300. https://doi.org/10.1080/15384101.2016.1254974
16. Delaidelli A, Negri GL, Jan A, Jansonius B, El-Naggar A, Lim JKM, Khan D, Zarni Oo H, Carnie CJ, Remke M et al (2017) MYCN amplified neuroblastoma requires the mRNA translation regulator eEF2 kinase to adapt to nutrient deprivation. Cell Death Differ 24:1564–1576. https://doi.org/10.1038/cdd.2017.79
17. Domise M, Vingtdeux V (2016) AMPK in neurodegenerative diseases. EXS 107:153–177. https://doi.org/10.1007/978-3-319-43589-3_7
18. Duty S, Jenner P (2011) Animal models of Parkinson's disease: a source of novel treatments and clues to the cause of the disease. Br J Pharmacol 164:1357–1391. https://doi.org/10.1111/j.1476-5381.2011.01426.x
19. Garcia-Esparcia P, Hernandez-Ortega K, Koneti A, Gil L, Delgado-Morales R, Castano E, Carmona M, Ferrer I (2015) Altered machinery of protein synthesis is region- and stage-dependent and is associated with alpha-synuclein oligomers in Parkinson's disease. Acta Neuropathol Commun 3:76. https://doi.org/10.1186/s40478-015-0257-4
20. Giasson BI, Duda JE, Quinn SM, Zhang B, Trojanowski JQ, Lee VM (2002) Neuronal alpha-synucleinopathy with severe movement disorder in mice expressing A53T human alpha-synuclein. Neuron 34:521–533
21. Haas RH, Nasirian F, Nakano K, Ward D, Pay M, Hill R, Shults CW (1995) Low platelet mitochondrial complex I and complex II/III activity in early untreated Parkinson's disease. Ann Neurol 37:714–722. https://doi.org/10.1002/ana.410370604
22. Hatzipetros T, Kidd JD, Moreno AJ, Thompson K, Gill A, Vieira FG (2015) A Quick Phenotypic Neurological Scoring System for Evaluating Disease Progression in the SOD1-G93A Mouse Model of ALS. J Vis Exp. https://doi.org/10.3791/53257
23. Heise C, Gardoni F, Culotta L, di Luca M, Verpelli C, Sala C (2014) Elongation factor-2 phosphorylation in dendrites and the regulation of dendritic mRNA translation in neurons. Front Cell Neurosci 8:35. https://doi.org/10.3389/fncel.2014.00035
24. Hills T, Brockie PJ, Maricq AV (2004) Dopamine and glutamate control area-restricted search behavior in Caenorhabditis elegans. J Neurosci 24:1217–1225. https://doi.org/10.1523/JNEUROSCI.1569-03.2004
25. Holmstrom KM, Baird L, Zhang Y, Hargreaves I, Chalasani A, Land JM, Stanyer L, Yamamoto M, Dinkova-Kostova AT, Abramov AY (2013) Nrf2 impacts cellular bioenergetics by controlling substrate availability for mitochondrial respiration. Biol Open 2:761–770. https://doi.org/10.1242/bio.20134853

26. Holmstrom KM, Kostov RV, Dinkova-Kostova AT (2016) The multifaceted role of Nrf2 in mitochondrial function. Curr Opin Toxicol 1:80–91. https://doi.org/10.1016/j.cotox.2016.10.002 S2468-2020(16)30025-0
27. Hsu LJ, Sagara Y, Arroyo A, Rockenstein E, Sisk A, Mallory M, Wong J, Takenouchi T, Hashimoto M, Masliah E (2000) Alpha-synuclein promotes mitochondrial deficit and oxidative stress. Am J Pathol 157:401–410
28. Jan A, Jansonius B, Delaidelli A, Somasekharan SP, Bhanshali F, Vandal M, Negri GL, Moerman D, MacKenzie I, Calon F et al (2017) eEF2K inhibition blocks Abeta42 neurotoxicity by promoting an NRF2 antioxidant response. Acta Neuropathol 133:101–119. https://doi.org/10.1007/s00401-016-1634-1
29. Janetzky B, Hauck S, Youdim MB, Riederer P, Jellinger K, Pantucek F, Zochling R, Boissl KW, Reichmann H (1994) Unaltered aconitase activity, but decreased complex I activity in substantia nigra pars compacta of patients with Parkinson's disease. Neurosci Lett 169:126–128
30. Jiang P, Gan M, Ebrahim AS, Castanedes-Casey M, Dickson DW, Yen SH (2013) Adenosine monophosphate-activated protein kinase overactivation leads to accumulation of alpha-synuclein oligomers and decrease of neurites. Neurobiol Aging 34:1504–1515. https://doi.org/10.1016/j.neurobiolaging.2012.11.001
31. Johnson DA, Johnson JA (2015) Nrf2–a therapeutic target for the treatment of neurodegenerative diseases. Free Radic Biol Med 88:253–267. https://doi.org/10.1016/j.freeradbiomed.2015.07.147
32. Junn E, Mouradian MM (2002) Human alpha-synuclein over-expression increases intracellular reactive oxygen species levels and susceptibility to dopamine. Neurosci Lett 320:146–150
33. Kalia LV, Lang AE (2015) Parkinson's disease. Lancet 386:896–912. https://doi.org/10.1016/S0140-6736(14)61393-3
34. Kenney JW, Moore CE, Wang X, Proud CG (2014) Eukaryotic elongation factor 2 kinase, an unusual enzyme with multiple roles. Adv Biol Regul 55:15–27. https://doi.org/10.1016/j.jbior.2014.04.003
35. Kenney JW, Sorokina O, Genheden M, Sorokin A, Armstrong JD, Proud CG (2015) Dynamics of elongation factor 2 kinase regulation in cortical neurons in response to synaptic activity. J Neurosci 35:3034–3047. https://doi.org/10.1523/JNEUROSCI.2866-14.2015
36. Kim TW, Cho HM, Choi SY, Suguira Y, Hayasaka T, Setou M, Koh HC, Hwang EM, Park JY, Kang SJ et al (2013) (ADP-ribose) polymerase 1 and AMP-activated protein kinase mediate progressive dopaminergic neuronal degeneration in a mouse model of Parkinson's disease. Cell Death Dis 4:e919. https://doi.org/10.1038/cddis.2013.447
37. Koh JY, Choi DW (1987) Quantitative determination of glutamate mediated cortical neuronal injury in cell culture by lactate dehydrogenase efflux assay. J Neurosci Methods 20:83–90
38. Kones R (2010) Mitochondrial therapy for Parkinson's disease: neuroprotective pharmaconutrition may be disease-modifying. Clin Pharmacol 2:185–198. https://doi.org/10.2147/CPAA.S12082 cpaa-2-185
39. Lashuel HA, Overk CR, Oueslati A, Masliah E (2013) The many faces of alpha-synuclein: from structure and toxicity to therapeutic target. Nat Rev Neurosci 14:38–48. https://doi.org/10.1038/nrn3406
40. Lee J, Jee C, McIntire SL (2009) Ethanol preference in C. Elegans. Genes Brain Behav 8:578–585. https://doi.org/10.1111/j.1601-183X.2009.00513.x
41. Lee MK, Stirling W, Xu Y, Xu X, Qui D, Mandir AS, Dawson TM, Copeland NG, Jenkins NA, Price DL (2002) Human alpha-synuclein-harboring familial Parkinson's disease-linked Ala-53 –> Thr mutation causes neurodegenerative disease with alpha-synuclein aggregation in transgenic mice. Proc Natl Acad Sci U S A 99:8968–8973. https://doi.org/10.1073/pnas.132197599
42. Leprivier G, Remke M, Rotblat B, Dubuc A, Mateo AR, Kool M, Agnihotri S, El-Naggar A, Yu B, Somasekharan SP et al (2013) The eEF2 kinase confers resistance to nutrient deprivation by blocking translation elongation. Cell 153:1064–1079. https://doi.org/10.1016/j.cell.2013.04.055
43. Li X, Alafuzoff I, Soininen H, Winblad B, Pei JJ (2005) Levels of mTOR and its downstream targets 4E-BP1, eEF2, and eEF2 kinase in relationships with tau in Alzheimer's disease brain. FEBS J 272:4211–4220. https://doi.org/10.1111/j.1742-4658.2005.04833.x
44. Lin MT, Beal MF (2006) Mitochondrial dysfunction and oxidative stress in neurodegenerative diseases. Nature 443:787–795. https://doi.org/10.1038/nature05292
45. Ludtmann MH, Angelova PR, Zhang Y, Abramov AY, Dinkova-Kostova AT (2014) Nrf2 affects the efficiency of mitochondrial fatty acid oxidation. Biochem J 457:415–424. https://doi.org/10.1042/BJ20130863
46. Ma T, Chen Y, Vingtdeux V, Zhao H, Viollet B, Marambaud P, Klann E (2014) Inhibition of AMP-activated protein kinase signaling alleviates impairments in hippocampal synaptic plasticity induced by amyloid beta. J Neurosci 34:12230–12238. https://doi.org/10.1523/JNEUROSCI.1694-14.2014
47. Malik AN, Czajka A, Cunningham P (2016) Accurate quantification of mouse mitochondrial DNA without co-amplification of nuclear mitochondrial insertion sequences. Mitochondrion 29:59–64. https://doi.org/10.1016/j.mito.2016.05.003
48. Mitsuishi Y, Taguchi K, Kawatani Y, Shibata T, Nukiwa T, Aburatani H, Yamamoto M, Motohashi H (2012) Nrf2 redirects glucose and glutamine into anabolic pathways in metabolic reprogramming. Cancer Cell 22:66–79. https://doi.org/10.1016/j.ccr.2012.05.016
49. Monzel AS, Smits LM, Hemmer K, Hachi S, Moreno EL, van Wuellen T, Jarazo J, Walter J, Bruggemann I, Boussaad I et al (2017) Derivation of Human Midbrain-Specific Organoids from Neuroepithelial Stem Cells. Stem Cell Reports 8:1144–1154. https://doi.org/10.1016/j.stemcr.2017.03.010
50. Nass R, Blakely RD (2003) The Caenorhabditis elegans dopaminergic system: opportunities for insights into dopamine transport and neurodegeneration. Annu Rev Pharmacol Toxicol 43:521–544. https://doi.org/10.1146/annurev.pharmtox.43.100901.135934
51. Ng CH, Guan MS, Koh C, Ouyang X, Yu F, Tan EK, O'Neill SP, Zhang X, Chung J, Lim KL (2012) AMP kinase activation mitigates dopaminergic dysfunction and mitochondrial abnormalities in Drosophila models of Parkinson's disease. J Neurosci 32:14311–14317. https://doi.org/10.1523/JNEUROSCI.0499-12.2012
52. Orchard GE, Calonje E (1998) The effect of melanin bleaching on immunohistochemical staining in heavily pigmented melanocytic neoplasms. Am J Dermatopathol 20:357–361
53. Poewe W, Seppi K, Tanner CM, Halliday GM, Brundin P, Volkmann J, Schrag AE, Lang AE (2017) Parkinson disease. Nat Rev Dis Primers 3:17013. https://doi.org/10.1038/nrdp.2017.13
54. Polymeropoulos MH, Lavedan C, Leroy E, Ide SE, Dehejia A, Dutra A, Pike B, Root H, Rubenstein J, Boyer R et al (1997) Mutation in the alpha-synuclein gene identified in families with Parkinson's disease. Science 276:2045–2047
55. Reeve AK, Ludtmann MH, Angelova PR, Simcox EM, Horrocks MH, Klenerman D, Gandhi S, Turnbull DM, Abramov AY (2015) Aggregated alpha-synuclein and complex I deficiency: exploration of their relationship in differentiated neurons. Cell Death Dis 6:e1820. https://doi.org/10.1038/cddis.2015.166
56. Ryan SD, Dolatabadi N, Chan SF, Zhang X, Akhtar MW, Parker J, Soldner F, Sunico CR, Nagar S, Talantova M et al (2013) Isogenic human iPSC Parkinson's model shows nitrosative stress-induced dysfunction in MEF2-PGC1alpha transcription. Cell 155:1351–1364. https://doi.org/10.1016/j.cell.2013.11.009
57. Ryazanov AG (2002) Elongation factor-2 kinase and its newly discovered relatives. FEBS Lett 514:26–29
58. Sacino AN, Brooks M, Thomas MA, McKinney AB, Lee S, Regenhardt RW, McGarvey NH, Ayers JI, Notterpek L, Borchelt DR et al (2014) Intramuscular injection of alpha-synuclein induces CNS alpha-synuclein pathology and a rapid-onset motor phenotype in transgenic mice. Proc Natl Acad Sci U S A 111:10732–10737. https://doi.org/10.1073/pnas.1321785111
59. Schapira AH (2008) Mitochondria in the aetiology and pathogenesis of Parkinson's disease. Lancet Neurol 7:97–109. https://doi.org/10.1016/S1474-4422(07)70327-7
60. Schapira AH, Cooper JM, Dexter D, Jenner P, Clark JB, Marsden CD (1989) Mitochondrial complex I deficiency in Parkinson's disease. Lancet 1:1269
61. Seidel K, Mahlke J, Siswanto S, Kruger R, Heinsen H, Auburger G, Bouzrou M, Grinberg LT, Wicht H, Korf HW et al (2015) The brainstem pathologies of Parkinson's disease and dementia with Lewy bodies. Brain Pathol 25:121–135. https://doi.org/10.1111/bpa.12168
62. Spillantini MG, Schmidt ML, Lee VM, Trojanowski JQ, Jakes R, Goedert M (1997) Alpha-synuclein in Lewy bodies. Nature 388:839–840. https://doi.org/10.1038/42166
63. Tremblay RG, Sikorska M, Sandhu JK, Lanthier P, Ribecco-Lutkiewicz M, Bani-Yaghoub M (2010) Differentiation of mouse Neuro 2A cells into dopamine neurons. J Neurosci Methods 186:60–67. https://doi.org/10.1016/j.jneumeth.2009.11.004
64. Trojanowski NF, Raizen DM, Fang-Yen C (2016) Pharyngeal pumping in Caenorhabditis elegans depends on tonic and phasic signaling from the nervous system. Sci Rep 6:22940. https://doi.org/10.1038/srep22940
65. Uchihara T, Giasson BI (2016) Propagation of alpha-synuclein pathology: hypotheses, discoveries, and yet unresolved questions from experimental and human brain studies. Acta Neuropathol 131:49–73. https://doi.org/10.1007/s00401-015-1485-1

66. Um JW, Kaufman AC, Kostylev M, Heiss JK, Stagi M, Takahashi H, Kerrisk ME, Vortmeyer A, Wisniewski T, Koleske AJ et al (2013) Metabotropic glutamate receptor 5 is a coreceptor for Alzheimer abeta oligomer bound to cellular prion protein. Neuron 79:887–902. https://doi.org/10.1016/j.neuron.2013.06.036
67. Vekrellis K, Xilouri M, Emmanouilidou E, Rideout HJ, Stefanis L (2011) Pathological roles of alpha-synuclein in neurological disorders. Lancet Neurol 10:1015–1025. https://doi.org/10.1016/S1474-4422(11)70213-7
68. Wang X, Yan MH, Fujioka H, Liu J, Wilson-Delfosse A, Chen SG, Perry G, Casadesus G, Zhu X (2012) LRRK2 regulates mitochondrial dynamics and function through direct interaction with DLP1. Hum Mol Genet 21:1931–1944. https://doi.org/10.1093/hmg/dds003
69. White JG, Southgate E, Thomson JN, Brenner S (1986) The structure of the nervous system of the nematode Caenorhabditis elegans. Philos Trans R Soc Lond Ser B Biol Sci 314:1–340
70. Wolozin B, Gabel C, Ferree A, Guillily M, Ebata A (2011) Watching worms whither: modeling neurodegeneration in *C. elegans*. Prog Mol Biol Transl Sci 100:499–514. https://doi.org/10.1016/B978-0-12-384878-9.00015-7
71. Wong YC, Krainc D (2017) Alpha-synuclein toxicity in neurodegeneration: mechanism and therapeutic strategies. Nat Med 23:1–13. https://doi.org/10.1038/nm.4269

APPENDIX C

Original article: *In vivo* Phenotyping of Human Parkinson's Disease–Specific Stem Cells Carrying the LRRK2–G2019S Mutation Reveals Increased α–Synuclein Levels but Absence of Spreading

This article has been published in the *Opera Medica et Physiologica* journal.

Kathrin Hemmer et al. In vivo Phenotyping of Human Parkinson's Disease-Specific Stem Cells Carrying the LRRK2-G2019S Mutation Reveals Increased A-Synuclein Levels but Absence of Spreading

OM&P

In vivo Phenotyping of Human Parkinson's Disease-Specific Stem Cells Carrying the LRRK2-G2019S Mutation Reveals Increased a-Synuclein Levels but Absence of Spreading

*Kathrin Hemmer, Lisa M. Smits, Silvia Bolognin, Jens C. Schwamborn**

Luxembourg Centre for Systems Biomedicine (LCSB), Developmental and Cellular Biology, University of Luxembourg, L-4367 Belvaux, Luxembourg.
* Corresponding e-mail: jens.schwamborn@uni.lu

Abstract. Parkinson's disease is a progressive age-associated neurological disorder. One of the major neuropathological hallmarks of Parkinson's disease is the appearance of protein aggregates, mainly consisting of the protein alpha-Synuclein. These aggregates have been described both in genetic as well as idiopathic forms of the disease. Currently, Parkinson's disease patient-specific induced pluripotent stem cells (iPSCs) are mainly used for in vitro disease modeling or for experimental cell replacement approaches. Here, we demonstrate that these cells can be used for in vivo disease modeling. We show that Parkinson's disease patient-specific, iPSC-derived neurons carrying the LRRK2-G2019S mutation show an upregulation of alpha-Synuclein after transplantation in the mouse brain. However, further investigations indicate that the increased human alpha-Synuclein levels fail to induce spreading or aggregation in the mouse brain. We therefore conclude that grafting of these cells into the mouse brain is suitable for cell autonomous in vivo disease modeling but has strong limitations beyond that. Furthermore, our results support the hypothesis that there might be a species barrier between human to mouse concerning alpha-Synuclein spreading.

Keywords: Parkinson's disease, LRRK2-G2019S, alpha-Synuclein, spreading, disease modeling

Introduction

Parkinson's disease is a progressive neurological disorder. It is the second most common neurodegenerative disease after Alzheimer's disease. Parkinson's disease is characterized by motor symptoms including tremor, rigidity, bradykinesia, and postural instability but also by non-motor symptoms as fatigue, depression, sleep disturbance, and dementia [1]. Although some symptomatic treatments exist, no preventive or disease-modifying therapies are currently available. The major hallmark of Parkinson's disease is the degeneration of dopaminergic neurons in the substantia nigra of the midbrain. It is estimated that about 30 % of the familial and 3-5 % of the sporadic cases are caused by monogenetic mutations [2]. The affected genes including SNCA, PINK1, Parkin, LRRK2, DJ1, ATP13A2 and VPS35 are involved in numerous, very different biochemical processes, emphasizing a complex etiopathogenesis. Among others, cellular processes like oxidative stress, dysfunctional protein degradation and clearance, calcium dysregulation, mitochondrial dysfunction as well as protein aggregation (prionopathy) have been implicated in the etiopathogenesis of Parkinson's disease. Although the majority of the Parkinson's disease cases is of idiopathic origin, the clinical symptoms and the histopathology do not differ from the genetic Parkinson's disease cases [2]. Therefore, to study genetic cases might serve as a tool to get more insights into the complex etiopathogenesis of the pathology. A major neuropathological hallmark of Parkinson's disease is protein aggregates that are detectable in many genetic as well as idiopathic cases. These aggregates are called Lewy bodies (LB) and Lewy neurites and consist mainly of the protein alpha-Synuclein (gene: SNCA). Several mutations in SNCA as well as increased SNCA gene doses have been previously described to cause Parkinson's disease (reviewed in [3]). Interestingly, neuropathological studies suggest that Lewy pathology ascends from peripheral autonomic ganglia to brainstem nuclei and subsequently toward the neocortex over time [4]. The associated prionopathy hypothesis posits that conformationally altered alpha-Synuclein is transmitted between neurons and initiates protein aggregation in susceptible neurons [4]. This hypothesis is supported by the observation that alpha-Synuclein fibrils induce LB pathology in primary neuronal cultures as well as in wild-type mice [5, 6]. However, whether increased levels of alpha-Synuclein in a subset of cells would be sufficient to induce such a prion-like spreading remains unclear so far.

The reprogramming of human somatic cells into induced pluripotent stem cells (iPSCs) was a breakthrough for in vitro disease modeling [7, 8]. iPSCs resemble embryonic stem cells in all their characteristics. Numerous studies used Parkinson's disease patient-specific iPSCs and thereof-derived neurons to gain insights into the mechanisms underlying the onset and progression of Parkinson's disease [9]. Among other findings, it was possible to demonstrate that even mutations in Parkinson's disease associated genes different from SNCA, can cause an upregulation of the alpha-Synuclein protein levels [10]. However, the usage of human iPSC-derived cellular models under physiological conditions, e.g. via grafting in mice, still remains unexplored.

In this study, we used an isogenic pair of Parkinson's disease patient-specific iPSCs with the G2019S mutation

in the gene LRRK2 and transplanted thereof-derived neuroepithelial stem cells (NESCs) into the striatum of mice. We demonstrated that in vivo differentiated neurons showed an upregulation of alpha-Synuclein under physiological conditions. However, we were unable to detect any spreading of alpha-Synuclein in the mouse brain. Our results suggest that human Parkinson's disease patient-derived iPSC models were able to recapitulate key characteristics of the disease in vivo. Furthermore, they support the hypothesis that murine alpha-Synuclein might actually inhibit seeding and propagation of human alpha-Synuclein.

Material and Methods

Stem cell culture

Human induced pluripotent stem cells (iPSCs) were derived from an 81 old, female Parkinson's disease patient carrying the LRRK2-G2019S mutation [11]. The iPSC line was gene corrected by using Zinc Finger Nucleases [11]. From these iPSCs, neuroepithelial stem cell (NESC) lines were generated and cultured as described elsewhere [12]. In brief, cells were cultured on Matrigel-coated plates in N2B27 medium (DMEM-F12 (Invitrogen)/ Neurobasal (Invitrogen) (50:50), 1:200 N2 supplement (Invitrogen,), 1:100 B27 supplement w/o Vitamin A (Invitrogen) 1:100 penicillin/streptomycin (Invitrogen), 1:100 L-Glutamine (Invitrogen) freshly supplemented with 0.5 µM Purmorphamine (Enzo Life Science), 3 µM CHIR (Axon Medchem), and 150 µM ascorbic acid (Sigma). Cells were split 1:10-1:15 once per week using Accutase. Differentiation was initiated by changing medium two days after splitting to N2B27 medium containing 1 µM PMA, 200 µM AA, 10 ng/mL BDNF (Peprotech), 10 ng/mL GDNF (Peprotech), 1 ng/mL TGF-b3 (Peprotech), and 500 µM dbcAMP (Sigma).

Transplantation

For surgeries 11-12 week old NOD.Cg-Prkdcscid Il2rgtm1Wjl/SzJ mice were deeply anesthetized by isoflurane (4 % v/v for induction and 2 % v/v for maintenance) and bupivacain (5 mg/kg s.c.) was given as supplementary local analgesia before surgery. Additionally, buprenorphine treatment (0.1 mg/kg; s.c.;) was used as analgesia before and one day after surgery. Two weeks before transplantation, 10 µg 6-OHDA (6-Hydroxydopamine hydrobromide, Sigma Aldrich) was stereotactically injected into the striatum using following coordinates in relation to bregma: anteroposterior: 0.5 mm, mediolateral: 2.0 mm, dorsoventral: 3.5 mm (below skull). Transplantation of NESCs was performed as described before [12, 13]. In brief, NESCs (Passage 10-13) were differentiated towards dopaminergic neurons for 6 days. For transplantation, cells were dissociated to single cells with Accutase and resuspended in N2B27 medium to a concentration of 5 x 104 cells per microliter. Three microliters of the cell suspension was injected into the 6-OHDA-lesioned striatum using a Hamilton 7005KH 5-µl syringe (LRRK2-G2019S n=6, LRRK2-WT n=3).From these iPSC

Perfusion, sectioning, and immunohistochemical analysis

Perfusion, sectioning, and immunohistochemical analysis were performed 11 weeks post-transplantation as described previously [12, 13]. The following primary antibodies were used: human Nuclei (mouse, 1:200, Millipore), human NCAM (mouse, 1:100, Santa Cruz), and alpha-Synuclein (rabbit, 1:600, Sigma). Alexa fluorophore-conjugated secondary antibodies (Invitrogen) and Hoechst 33342 (Invitrogen) were used to visualize primary antibodies and nuclei, respectively. Sections (40 µm) from the center of the graft were evaluated using a Zeiss LSM 710 confocal microscope. 3D surface structures of the z-stacks taken by the confocal microscope were created using IMARIS software (bitplane). For this, three different ROIs (graft, proximal to graft and distal to graft) were chosen and the values of the threshold (background substraction) were automatically set. The endogenous mouse stainings of the striatal myelinated fibers were not taken into consideration for the analysis.

Data and statistical analysis

The volume, the mean intensity, and maximum intensity of every created surface were defined by Imaris software. The average or the sum of the different parameters was calculated for each animal. Ratios of the different ROIs were created as indicated and t-tests were performed using SigmaPlot. n specifies the number of mice and statistical significance is considered to be $P < 0.05$. Prism 6.01 (GraphPad) was used for data illustration and data are presented as mean + SEM.

Results

Parkinson's disease-specific neurons, expressing LRRK2-G2019S, upregulated alpha-Synuclein in vivo

Previously, it has been shown in vitro that human neurons expressing the Parkinson's disease-associated G2019S mutation in the LRRK2 gene have elevated levels of alpha-Synuclein [10]. As a first step, we were aiming at determining whether this is also the case in vivo. Accordingly, we transplanted 1,5 x 105 human iPSC-derived NESCs that were pre-differentiated for the neuronal lineage (for details see Materials and Methods section), into the striatum of 11-12 week old NOD.SCID mice. In order to investigate the impact of the LRRK2-G2019S mutation, we used patient-derived cells expressing this mutation as well as a corresponding isogenic line where the mutation has been corrected. Human cells were distinguished from the surrounding mouse cells with human-specific antibodies against NCAM and human nuclei (Fig. 1A, B). 11 weeks after transplantation in the mouse striatum, we saw robust survival and neuronal differentiation for both lines as indicated with the anti-human-NCAM antibody (Fig. 1A). In order to detect the

 doi:10.20388/omp2018.001.0057

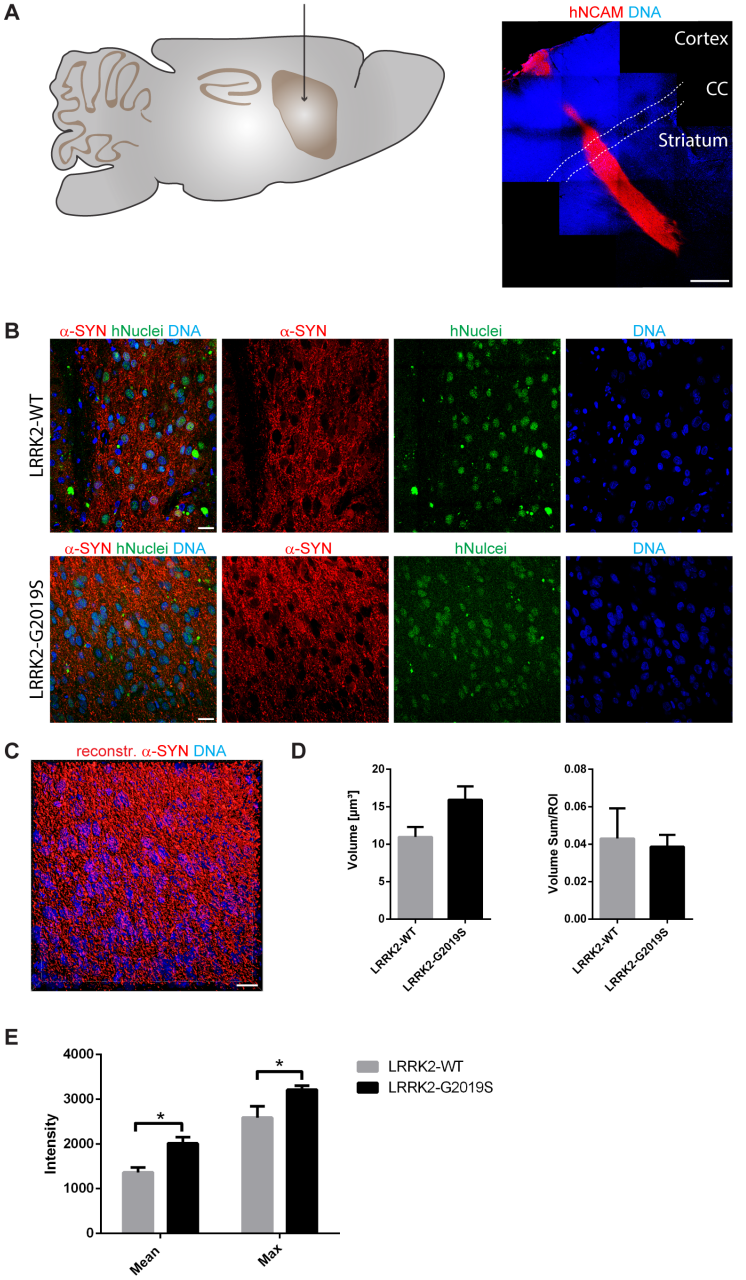

Figure 1. *LRRK2-G2019S mutation led to a higher expression of alpha-Synuclein in grafted neurons.* ***A*** *Schematic overview of the adult mouse brain (left) representing the stereotactic target side of the striatum for the transplantation. 11 weeks after transplantation, the species-specific antibody hNCAM revealed a sound survival and neuronal differentiation of the graft (right). Dashed lines indicate the corpus callosum.* ***B*** *Immunohistological stainings indicated the expression of alpha-Synuclein in both cell lines after transplantation.* ***C*** *Representative 3D surface reconstruction of alpha-Synuclein of the graft shown in the lower panel of B.* ***D*** *Quantification of the volume and volume sum/region of interest of the reconstructed alpha-Synuclein surfaces.* ***E*** *Quantification of the mean and maximum intensity of the reconstructed alpha-Synuclein surfaces. Scale bars: 500 µm (A) and 20 µm (B and C). Error bars represent mean + SEM (LRRK2-WT n=3, LRRK2-G2019S n=6); α-SYN: alpha-Synuclein, CC: corpus callosum, max: maximum, ROI: region of interest*

levels of alpha-Synuclein in the grafted cells, we stained with anti-alpha-Synuclein-specific antibodies (Fig. 1B). For quantification, we reconstructed the surfaces of the alpha-Synuclein signal in the grafts with IMARIS (Fig. 1C). The volume and the intensity of the alpha-Synuclein signal was quantified from the reconstruction (Fig. 1D, E). This quantification revealed that expression of LRRK-G2019S led to a negligible increase in the mean volume of the alpha-Synuclein signal (Fig. 1D). However, the mean and the maximum intensity of the alpha-Synuclein signal was significantly increased upon expression of the Parkinson's disease-associated LRRK2-G2019S mutation (Fig. 1E). These results indicate that human neurons carrying the LRRK2-G2019S mutation express higher levels of alpha-Synuclein under physiological conditions.

Grafted neurons did not induce alpha-Synuclein spreading in the mouse brain

Parkinson's disease is a progressive disorder characterized by the spreading of protein aggregates, mainly consisting of alpha-Synuclein. It has been hypothesized that this appearance of aggregates spreads in a prion-like fashion [4]. Aggregated alpha-Synuclein has the ability to induce further aggregation of soluble alpha-Synuclein. Hence, a seed of alpha-Synuclein aggregation would be sufficient to start the process.

In order to test whether our in vivo phenotyping approach would be able to recapitulate this spreading process, we analyzed the levels of endogenous mouse alpha-Synuclein in a region close (proximal) to the graft in comparison to a region far (distal) from the graft (Fig. 2A). Accordingly, a 3D surface reconstruction of the endogenous mouse alpha-Synuclein signal was performed with IMARIS (Fig. 2B and C). If alpha-Synuclein indeed would spread from the graft into the surrounding tissue, we expected to find significant differences in the volume (Fig. 2D) or intensity (Fig. 2E, F) of the alpha-Synuclein signal in a region proximal to the graft compared to a region distal to the graft when normalizing both regions to the graft. Particularly, we expected to see such differences in cases where cells with the LRRK2-G2019S mutation have been transplanted. Moreover, we compared the ratio of the two regions between the different genotypes. However, in none of the investigated parameters significant differences were detectable (Fig. 2D-F). We therefore conclude that in the here chosen paradigm Parkinson's disease-associated alpha-Synuclein spreading is not detectable.

Discussion

The spreading of alpha-Synuclein protein aggregates, in a prion-like fashion, is believed to be the underlying mechanism for the progression of Parkinson's disease pathology through the human brain [4]. Furthermore, somatic mutations occurring during embryogenesis can lead to genetic mosaicism in the brain. Typically, genotyping is conducted in mesoderm-derived lymphocytes. Therefore, mutations in ectoderm-derived neural cells will be missed [14]. Consequently, it is conceivable that Parkinson's disease patients that are classified as idiopathic, actually carry a Parkinson's disease-associated mutation in a subset of neurons. In fact, somatic mutations have been previously associated to neurodegenerative disorders. It was suggested that differences in Parkinson's disease phenotype in monozygotic twins with LRRK2 mutations are caused by additional somatic mutations [15, 16]. In the past, addressing the hypothesis of prion-like spreading of alpha-Synuclein and genetic mosaicism as potential source for aggregates of alpha-Synuclein was complicated because of the lack of appropriate models. In this study, we show that Parkinson's disease patient-specific iPSC-derived neurons upregulated alpha-Synuclein after transplantation which is believed to be a first important step to induce protein aggregation and spreading. Therefore, we conclude that this approach can be used for in vivo disease modeling. However, we further demonstrate that this alpha-Synuclein failed to spread in the mouse brain.

At first glance, it seems surprising not to see alpha-Synuclein spreading, because previous studies in vitro [5, 17] as well as in vivo [6, 18] have shown spreading. Furthermore, our finding that Parkinson's disease-specific cells with the LRRK2-G2019S mutation showed higher levels of alpha-Synuclein, supports their usability for modeling Parkinsons disease in vivo and indicates that they in principle might be able to induce alpha-Synuclein aggregation and spreading. However, it is noticeable that all these studies did not use a cross-species approach. Either human alpha-Synuclein spreading was investigated in human cells or in mice engineered to express human alpha-Synuclein. On the other hand, mouse alpha-Synuclein was tested in mouse cells or mice in vivo. Interestingly, a recent study using a cross-species approach reported that the mouse-alpha-Synuclein protein significantly attenuated the formation of aggregates of human-alpha-Synuclein [19]. In other words, the mouse-alpha-Synuclein inhibited the aggregation of the human form, which implies the existence of a species barrier. This finding is also supported by a report showing that mouse-alpha-Synuclein inhibited the fibrillization of human-alpha-Synuclein in vitro [20]. In this context, it is further interesting to note that the A53T mutation in human-alpha-Synuclein causes Parkinson's disease while the mouse version of alpha-Synuclein naturally expresses a Threonine at position 53. However, based on the here obtained results we cannot rule out that the failure to see alpha-Synuclein spreading in the mouse brain could be due to initially too low levels of human alpha-Synuclein in the transplanted cells. Additionally, we cannot exclude that an even longer duration of the experiment would have led to mouse alpha-Synuclein upregulation, aggregation, and spreading. Finally, the depletion of dopaminergic neurons in the striatum with 6-OHDA, preceding the transplantation, might have had a negative impact on the potential spreading.

Conclusion

Overall these results clearly indicate that it is of critical importance to choose the appropriate model and tools

 doi:10.20388/omp2018.001.0057

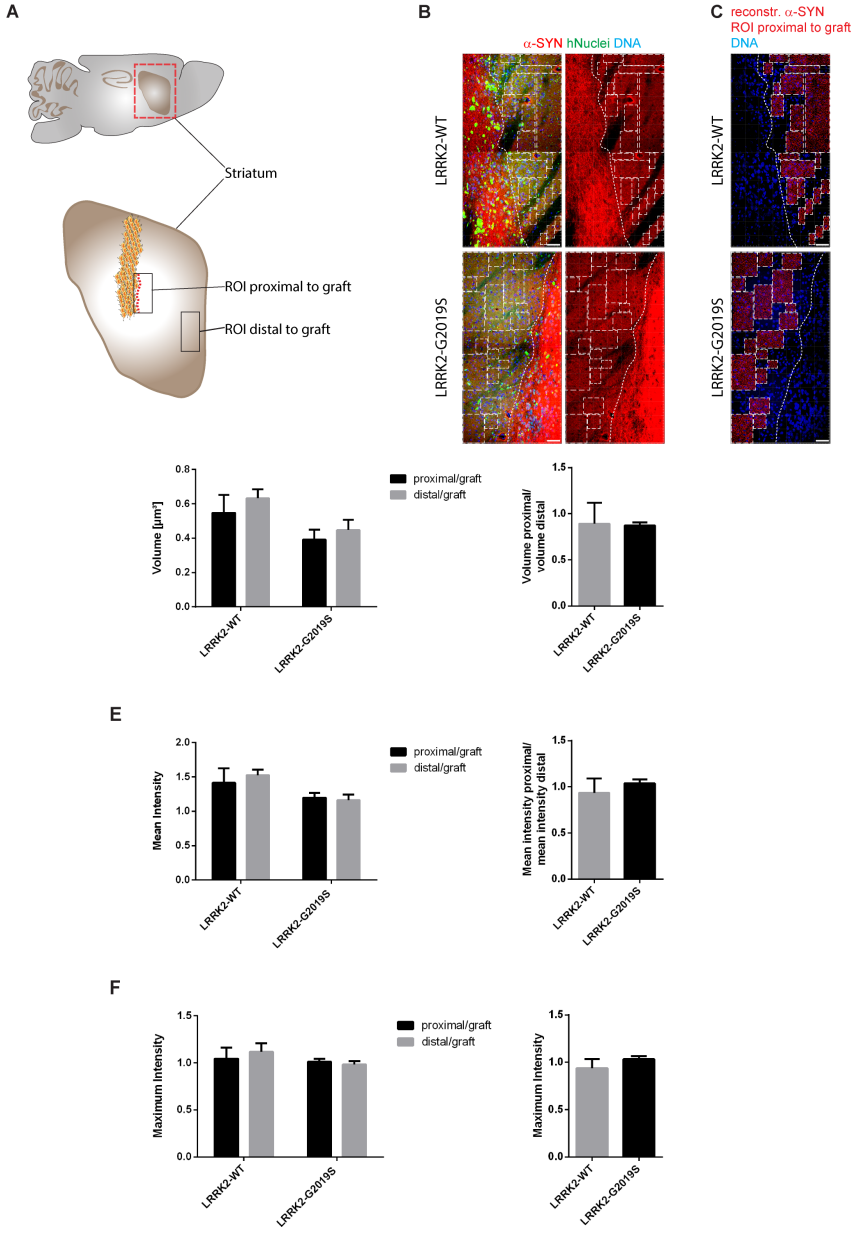

***Figure 2**. Alpha-Synuclein spreading from the graft was not detected in the surrounding tissue. **A** Schematic overview of the mouse adult brain indicating the ROIs that were chosen to analyse endogenous mouse alpha-Synuclein close (proximal) as well as far (distal) from the graft.**B** Representative images of the ROIs that were chosen proximal to the graft. Dashed lines define the edges of the graft. Squares mark the ROIs proximal to the graft that were used to create 3D surfaces shown in C. **C** 3D surface reconstruction of endogenous mouse alpha-Synuclein of the ROIs shown in B. **D-F** Quantification of the volume, the mean intensity and the maximum intensity of the reconstructed endogenous mouse alpha-Synuclein surfaces proximal to the graft and distal to the graft. Left: Proximal and distal ROIs of endogenous mouse alpha-Synuclein were normalized to the ROIs of the graft and eventually the different distances were compared to each other within the same cell line. Right: The ratio of the different regions of endogenous mouse alpha-Synuclein were compared between the different cell lines. Scale bars: 50 µm (B and C). Error bars represent mean + SEM (LRRK2-WT n=3, LRRK2-G2019S n=6); α-SYN: alpha-Synuclein, max: maximum, ROI: region of interest*

to study alpha-Synuclein aggregation and spreading. In particular, new human-specific organoid models recapitulating essential features of the human midbrain [21, 22] might represent interesting alternatives for the future. These models will allow combining the advantages of tissue-like specimens (complex system, in vivo, cellular heterogeneity) with high relevance for the human situation, particularly when they are derived from human Parkinson's disease patient-specific stem cells.

Abbreviations: α-SYN: alpha-Synuclein, CC: corpus callosum, iPSCs: induced pluripotent stem cells, LB: Lewy bodies, max: maximum, NESCs: neuroepithelial stem cells, ROI: region of interest

Ethical approval and consent to participate

All work with human iPSCs and thereof derived cells has been approved by the Ethics Review Panel (ERP) of the University Luxembourg as well as by the Luxembourgish Comité National d'Ethique de Recherche (CNER). The CNER reference number is 201305/04

All animal experimentation was approved by the appropriate Luxembourg governmental agencies (Ministry of Health and Ministry of Agriculture).

Consent for publication

Not applicable

Availability of data and materials

The datasets used and/or analysed during the current study available from the corresponding author on reasonable request.

Competing interests

The authors declare that they have no competing interests.

Funding

The JCS lab is supported by the Fonds National de la Recherche (FNR) (CORE, C13/BM/5791363). This is an EU Joint Programme. – Neurodegenerative Disease Research (JPND) project (INTER/JPND/14/02; INTER/JPND/15/11092422). Further support comes from the SysMedPD project which has received funding from the European Union's Horizon 2020 research and innovation program under grant agreement No 668738. KH received financial support from a private philanthropist as well as from the Fondation du Pélican de Mie et Pierre Hippert-Faber. LMS is supported by a fellowship from the FNR (AFR, Aides à la Formation-Recherche).

Authors' contributions

KH, SB, and JCS contributed to the conception and design of the study. KH and LMS performed experiments and analyzed data. JCS drafted the manuscript and KH prepared main figures. All authors read and approved the final manuscript.

Acknowledgments

The authors would like to thank Inga Brüggemann and Thea van Wüllen for excellent technical assistance. We further acknowledge support through the pluripotent stem cell facility at the LCSB.

References

Postuma RB, Lang AE, Gagnon JF, Pelletier A, Montplaisir JY: How does parkinsonism start? Prodromal parkinsonism motor changes in idiopathic REM sleep behaviour disorder. Brain 2012, 135(Pt 6):1860-1870.

Klein C, Westenberger A: Genetics of Parkinson's disease. Cold Spring Harb Perspect Med 2012, 2(1):a008888.

Kalinderi K, Bostantjopoulou S, Fidani L: The genetic background of Parkinson's disease: current progress and future prospects. Acta Neurol Scand 2016, 134(5):314-326.

Braak H, Del Tredici K: Neuroanatomy and pathology of sporadic Parkinson's disease. Adv Anat Embryol Cell Biol 2009, 201:1-119.

Volpicelli-Daley LA, Luk KC, Patel TP, Tanik SA, Riddle DM, Stieber A, Meaney DF, Trojanowski JQ, Lee VM: Exogenous alpha-synuclein fibrils induce Lewy body pathology leading to synaptic dysfunction and neuron death. Neuron 2011, 72(1):57-71.

Luk KC, Kehm V, Carroll J, Zhang B, O'Brien P, Trojanowski JQ, Lee VM: Pathological alpha-synuclein transmission initiates Parkinson-like neurodegeneration in nontransgenic mice. Science 2012, 338(6109):949-953.

Takahashi K, Yamanaka S: Induction of pluripotent stem cells from mouse embryonic and adult fibroblast cultures by defined factors. Cell 2006, 126(4):663-676.

Yu J, Vodyanik MA, Smuga-Otto K, Antosiewicz-Bourget J, Frane JL, Tian S, Nie J, Jonsdottir GA, Ruotti V, Stewart R et al: Induced pluripotent stem cell lines derived from human somatic cells. Science (New York, NY) 2007, 318(5858):1917-1920.

Hillje AL, Schwamborn JC: Utilization of stem cells to model Parkinson's disease – current state and future challenges. Future Neurology 2016, 11(2):171-186.

Sanchez-Danes A, Richaud-Patin Y, Carballo-Carbajal I, Jimenez-Delgado S, Caig C, Mora S, Di Guglielmo C, Ezquerra M, Patel B, Giralt A et al: Disease-specific phenotypes in dopamine neurons from human iPS-based models of genetic and sporadic Parkinson's disease. EMBO Mol Med 2012, 4(5):380-395.

Reinhardt P, Schmid B, Burbulla LF, Schondorf DC, Wagner L, Glatza M, Hoing S, Hargus G, Heck SA, Dhingra A et al: Genetic correction of a LRRK2 mutation in human iPSCs links parkinsonian neurodegeneration to ERK-dependent changes in gene expression. Cell stem cell 2013, 12(3):354-367.

Reinhardt P, Glatza M, Hemmer K, Tsytsyura Y, Thiel CS, Hoing S, Moritz S, Parga JA, Wagner L, Bruder

JM et al: Derivation and expansion using only small molecules of human neural progenitors for neurodegenerative disease modeling. PloS one 2013, 8:e59252.

Hemmer K, Zhang M, van Wullen T, Sakalem M, Tapia N, Baumuratov A, Kaltschmidt C, Kaltschmidt B, Scholer HR, Zhang W et al: Induced neural stem cells achieve long-term survival and functional integration in the adult mouse brain. Stem cell reports 2014, 3(3):423-431.

Proukakis C, Houlden H, Schapira AH: Somatic alpha-synuclein mutations in Parkinson's disease: Hypothesis and preliminary data. Movement Disorders 2013, 28:705-712.

Van Broeckhoven C: The future of genetic research on neurodegeneration. Nat Med 2010, 16(11):1215-1217.

Schneider SA, Johnson MR: Monozygotic twins with LRRK2 mutations: Genetically identical but phenotypically discordant. Movement Disorders 2012, 27:1203-1204.

Luk KC, Song C, Brien PO, Stieber A, Branch JR, Brunden KR, Trojanowski JQ, Lee VM: Exogenous alpha-synuclein fibrils seed the formation of Lewy body-like intracellular inclusions in cultured cells. PNAS 2009, 106.

Luk KC, Kehm VM, Zhang B, O'Brien P, Trojanowski JQ, Lee VM: Intracerebral inoculation of pathological alpha-synuclein initiates a rapidly progressive neurodegenerative alpha-synucleinopathy in mice. The Journal of experimental medicine 2012, 209(5):975-986.

Fares MB, Maco B, Oueslati A, Rockenstein E, Ninkina N, Buchman VL, Masliah E, Lashuel HA: Induction of de novo alpha-synuclein fibrillization in a neuronal model for Parkinson's disease. Proceedings of the National Academy of Sciences of the United States of America 2016, 113(7):E912-921.

Rochet JC, Conway KA, Lansbury PT, Jr.: Inhibition of fibrillization and accumulation of prefibrillar oligomers in mixtures of human and mouse alpha-synuclein. Biochemistry 2000, 39(35):10619-10626.

Jo J, Xiao Y, Sun AX, Cukuroglu E, Tran HD, Goke J, Tan ZY, Saw TY, Tan CP, Lokman H et al: Midbrain-like Organoids from Human Pluripotent Stem Cells Contain Functional Dopaminergic and Neuromelanin-Producing Neurons. Cell stem cell 2016, 19(2):248-257.

Monzel AS, Smits LM, Hemmer K, Hachi S, E. LM, van Wuellen T, Jarazo J, Walter J, Brüggemann I, Boussaad I et al: Derivation of human midbrain-specific organoids from neuroepithelial stem cells. Stem cell reports 2017, 8.

APPENDIX D

Curriculum Vitae: Lisa M. Smits

LISA M. SMITS

37 RUE GLESENER ◆ L-1631 LUXEMBOURG ◆ +352 661 898907 ◆LISA.SMITS@UNI.LU

PERSONAL INFORMATION

• NEUROSCIENTIST
  • enthusiastic • international experienced • multilingual
  • extensive science communication experiences

  • Date of Birth: 28th July 1989
  • Place of Birth: Goch, Germany
  • Nationality: German

EDUCATION

07/2015 – 06/2019	**PhD project at Luxembourg Centre for Systems Biomedicine (LCSB)** Developmental and Cellular Biology Group, University of Luxembourg, Funded by *Aides à la Formation-Recherche, Fonds National de la Recherche*
04/2013 – 05/2015	**Master of Science in Molecular Biomedicine** Westphalian Wilhelms University of Münster, Germany final mark: 1.2/1.0
10/2009 – 11/2012	**Bachelor of Science in Life Science** Gottfried Wilhelm Leibniz University of Hannover, Germany final mark: 1.2/1.0
08/2000 – 06/2009	**Abitur** Städtisches Gymnasium Goch, Germany Focus subjects: Biology, Mathematic final mark: 1.9/1.0

SCIENTIFIC EXPERIENCE

07/2015 – 06/2019	**Research project** (Funded by *Aides à la Formation-Recherche, FNR)* Luxembourg Centre for Systems Biomedicine, University of Luxembourg *Generation of midbrain organoids as a model to study Parkinson's disease.*
06/2015	**Summer School, Italy** Society for Neuroscience (SfN) and Federation of European Neuroscience Society (FENS), *Shared mechanisms and specificity in neurodegenerative diseases.*
05/2014 – 11/2014	**ERASMUS internship abroad, Luxembourg** Luxembourg Centre for Systems Biomedicine, University of Luxembourg *Characterisation of human induced pluripotent stem cells (hiPSCs).*

01/2013 – 03/2013	**Internship abroad, Austria** Department for Biomedical Technology, Danube University Krems, *Co-culturing of isolated hUVECs and hMSCs on Artificial Vascular Scaffolds.*
07/2010 – 12/2012	**Student assistant, Germany** Institute for Multiphase Processes, Gottfried Wilhelm Leibniz University of Hannover. Focus subject: *Biomedical Engineering*

- Conferences:

- JPND 3DPD Annual meeting Rotterdam, The Netherlands.
  Oral presentation, April 2018
- Development and 3-D Modeling of the Human Brain, New York, USA.
  Poster presentation, December 2017
- "Disease Modeling – Human-on-a-Chip. Steps to next generation" Lilienfeld, Austria.
  Poster presentation, July 2017
- EMBO|EMBL Symposium on Organoids: Modelling Organ Development and Disease in 3D Culture, Heidelberg, Germany.
  Poster presentation, October 2016
- 11th Annual Meeting of the GEoPD Consortium & 3rd International Parkinson´s Disease Symposium Belval, Luxembourg.
  Poster presentation, October 2016

- Publications:

Smits LM*, Reinhardt L*, Reinhardt P, Glatza M, Monzel AS, Stanslowsky N, Nicklas SM, Hemmer K, Anthony P, Qing X, Kalmbach N, Ehrlich M, Bolognin S, Kuhlmann T, Wegner F, Sterneckert JL*, Schwamborn JC*. Modelling Parkinson's disease in midbrain organoids. npj Parkinson's Disease, 2019 (in press)

Smits LM, Magni S, Grzyb K, Antony PMA, Krüger R, Skupin A, Bolognin S, Schwamborn JC. Single-cell transcriptomics reveal multiple neuronal cell types in midbrain-specific organoids. (submitted)

Smits LM, Magni S, Woods G, Grzyb K, Delcambre S, Luccarelli P, Jäger C, Antony PMA, Skupin A, Glaab E, Andersen J, Bolognin S*, Schwamborn JC*. LRRK2-G2019S mutation alters astrocytes development and induces senescence in midbrain organoids. (in preparation)

Jan A, Jansonius B, Delaidelli A, Bhanshali F, An YA, Ferreira N, **Smits LM**, Negri GL, Schwamborn JC, Jensen P, Mackenzie I, Taubert S, Sorensen P. Activity of translation regulator eukaryotic elongation factor-2 kinase is increased in Parkinson disease brain and its inhibition reduces alpha synuclein toxicity. Acta Neuropathologica Communications, 2018

Hemmer K, **Smits LM**, Bolognin S, Schwamborn JC. In Vivo Phenotyping Of Parkinson-Specific Stem Cells Carrying the LRRK2-G2019S Mutation Reveals Increased a-Synuclein Levels but Absence of Spreading. Opera Medica at Physiologica, 2018

Spathis AD, Asvos X, Ziavra D, Karampelas T, Topouzis S, Cournia Z, Qing X, Alexakos P, **Smits LM**, Dalla C, Rideout HJ, Schwamborn JC, Tamvakopoulos C, Fokas D, Vassilatis DK. Nurr1:RXRα heterodimer activation as monotherapy for Parkinson's disease. PNAS, 2017

Monzel AS*, **Smits LM***, Hemmer K*, Hachi S, Moreno EL, van Wuellen T, Jarazo J, Walter J, Brüggemann I, Boussaad I, Berger E, Fleming RMT, Bolognin S, Schwamborn JC. Derivation of Human Midbrain-Specific Organoids from Neuroepithelial Stem Cells. Stem Cell Reports, 2017

Smits, LM and Schwamborn JC. Hoffnungsträger Stammzelltherapie: Implantierte Nervenzellen werden Teil des Gehirn. Deutsche Zeitschrift für Klinische Forschung, 2015 Jan

- Prizes and Awards:

10/2016	**Poster prize**, 11th Annual Meeting of the GEoPD Consortium & 3rd International Parkinson´s Disease Symposium, Luxembourg
04/2016	**Biomedicine Award 2016**, Doctoral School University of Luxembourg
06/2015 – 06/2019	**AFR Individual - PhD grant**, *Aides à la Formation-Recherche, Fonds National de la Recherche* (#9137778)

Science Communication

- Publishing a scientific comic for the lay audience, Through the looking glass - *Using 'mini-brains' to investigate Parkinson's disease* (2019)
- Guiding laboratory tour for visitors of Open Day at University of Luxembourg (2019)
- Protagonist in RTL documentary *routwäissgro,* episode *'Brain is cool'* (2019)
- Welcoming and hosting visitors at LCSB for the Donor Event (2018)
- Participation in RTL TV reportage '*Mini-Gehirer an der Parkinson-Fuerschung*' (2017)
- Regularly supporting LCSB at public events, e.g. with participation at EPDA unity walk (2014), Public Pillow fight (2017) and giving laboratory tours for visitors (2015-2019)
- Member of organising committee for the Regional Student Group (RSG) conference in Luxembourg (2016)
- Guiding and teaching pupils within the framework of The Scienteens Lab – De Labo fir Jonker (2015)
- Publishing a scientific article for the lay audience, Deutsche Zeitschrift für Klinische Forschung, *Hoffnungsträger Stammzelltherapie: Implantierte Nervenzellen werden Teil des Gehirn.* (2015)
- Conceptualisation and organisation of a guided tour at Bayer AG within the framework of the Project Leader course of the University Münster (2014)
- Conceptualisation of a science booth and active contribution at IdeenExpo 2011 and 2013

Specific Skills

Computer	Mac OS X, MS Windows MS Office, Adobe Photoshop and Illustrator, LaTeX, MatLab
Certificates	Project Leader Certificate (by German law §15GenTS) FELASA B
Languages	German, native English, fluent Luxembourgish, good

Bibliography

Abe-Fukasawa, Natsuki, Otsuka, Keiichiro, Aihara, Ayako, Itasaki, Nobue and Nishino, Taito (2018). 'Novel 3D Liquid Cell Culture Method for Anchorage-independent Cell Growth, Cell Imaging and Automated Drug Screening'. In: *Scientific Reports* 8.1, pp. 1–12.

Abeliovich, Asa and Hammond, Rachel (2007). 'Midbrain dopamine neuron differentiation: Factors and fates'. In: *Developmental Biology* 304, pp. 447–454.

Abud, Edsel M, Ramirez, Ricardo N, Martinez, Eric S, Carson, Monica J, Poon, Wayne W, Blurton-jones, Mathew, Abud, Edsel M, Ramirez, Ricardo N, Martinez, Eric S, Healy, Luke M et al. (2017). 'iPSC-Derived Human Microglia-like Cells to Study Neurological Diseases'. In: *Neuron* 94.2, 278–293.e9.

Arlotta, Paola (2018). 'Organoids required! A new path to understanding human brain development and disease'. In: *Nature Methods* 15.1, pp. 27–29.

Austin, Kim Wieczorek, Ameringer, Suzanne Weil and Cloud, Leslie Jameleh (2016). 'An Integrated Review of Psychological Stress in Parkinson's Disease: Biological Mechanisms and Symptom and Health Outcomes'. In: *Parkinson's Disease* 2016, pp. 1–15.

Berger, Emanuel, Magliaro, Chiara, Paczia, Nicole, Monzel, Anna S., Antony, Paul, Linster, Carole L., Bolognin, Silvia, Ahluwalia, Arti and Schwamborn, Jens C. (Oct. 2018). 'Millifluidic culture improves human midbrain organoid vitality and differentiation'. In: *Lab on a Chip* 18.20, pp. 3172–3183.

Bernheimer, H., Birkmayer, W., Hornykiewicz, O., Jellinger, K. and Seitelberger, F. (Dec. 1973). 'Brain dopamine and the syndromes of Parkinson and Huntington

Clinical, morphological and neurochemical correlations'. In: *Journal of the Neurological Sciences* 20.4, pp. 415–455.

Berry, C, La Vecchia, C and Nicotera, P (2011). 'Paraquat and Parkinson's disease'. In: *Cell Death and Differentiation* 17, pp. 1115–1125.

Bian, Shan, Repic, Marko, Guo, Zhenming, Kavirayani, Anoop, Burkard, Thomas, Bagley, Joshua A., Krauditsch, Christian and Knoblich, Jürgen A. (2018). 'Genetically engineered cerebral organoids model brain tumor formation'. In: *Nature Methods* 15.8, pp. 631–639.

Blesa, Javier, Trigo-Damas, Inés, Dileone, Michele, Rey, Natalia Lopez Gonzalez del, Hernandez, Ledia F. and Obeso, José A. (2017). 'Compensatory mechanisms in Parkinson's disease: Circuits adaptations and role in disease modification'. In: *Experimental Neurology* 298.October, pp. 148–161.

Blesa, Javier, Trigo-Damas, Ines, Quiroga-Varela, Ana and Lopez-Gonzalez del Rey, Natalia (2016). 'Animal Models of Parkinson's Disease'. In: *Challenges in Parkinson's Disease*. IntechOpen. Chap. 10, pp. 195–216.

Bolognin, Silvia, Fossépré, Marie, Qing, Xiaobing, Jarazo, Javier, Ščančar, Janez, Moreno, Edinson Lucumi, Nickels, Sarah L, Wasner, Kobi, Ouzren, Nassima, Walter, Jonas et al. (Jan. 2019). '3D Cultures of Parkinson's Disease-Specific Dopaminergic Neurons for High Content Phenotyping and Drug Testing'. In: *Advanced Science* 6.1, p. 1800927.

Borroto-Escuela, Dasiel O., Perez De La Mora, Miguel, Manger, Paul, Narváez, Manuel, Beggiato, Sarah, Crespo-Ramírez, Minerva, Navarro, Gemma, Wydra, Karolina, Díaz-Cabiale, Zaida, Rivera, Alicia et al. (July 2018). 'Brain Dopamine Transmission in Health and Parkinson's Disease: Modulation of Synaptic Transmission and Plasticity Through Volume Transmission and Dopamine Heteroreceptors'. In: *Frontiers in Synaptic Neuroscience* 10.July.

Braak, Heiko and Del Tredici, Kelly (2004). *Poor and protracted myelination as a contributory factor to neurodegenerative disorders.*

Braak, Heiko, Del Tredici, Kelly, Rüb, Udo, De Vos, Rob a I, Jansen Steur, Ernst N H and Braak, Eva (2003). 'Staging of brain pathology related to sporadic Parkinson's disease'. In: *Neurobiology of Aging* 24, pp. 197–211.

Bu, Lu-Lu, Yang, Ke, Xiong, Wei-Xi, Liu, Feng-Tao, Anderson, Boyd, Wang, Ye and Wang, Jian (Jan. 2016). 'Toward precision medicine in Parkinson's disease.' In: *Annals of translational medicine* 4.2, p. 26.

Bunk, Eva C., Ertaylan, Gökhan, Ortega, Felipe, Pavlou, Maria A., Gonzalez Cano, Laura, Stergiopoulos, Athanasios, Safaiyan, Shima, Völs, Sandra, Cann, Marianne van, Politis, Panagiotis K. et al. (Aug. 2016). 'Prox1 Is Required for Oligodendrocyte Cell Identity in Adult Neural Stem Cells of the Subventricular Zone'. In: *STEM CELLS* 34.8, pp. 2115–2129.

Burbulla, Lena F, Song, Pingping, Mazzulli, Joseph R, Zampese, Enrico, Wong, Yvette C, Jeon, Sohee, Santos, David P, Blanz, Judith, Obermaier, Carolin D, Strojny, Chelsee et al. (2017). 'Dopamine oxidation mediates mitochondrial and lysosomal dysfunction in Parkinson's disease'. In: *Science* 357.6357, pp. 1255–1261.

Byers, Blake, Lee, Hsiao-lu and Reijo Pera, Renee (2012). 'Modeling Parkinson's Disease Using Induced Pluripotent Stem Cells'. In: *Current Neurology and Neuroscience Reports* 12, pp. 237–242.

Camp, J Gray, Badsha, Farhath, Florio, Marta, Kanton, Sabina, Gerber, Tobias, Wilsch-Bräuninger, Michaela, Lewitus, Eric, Sykes, Alex, Hevers, Wulf, Lancaster, Madeline et al. (2015). 'Human cerebral organoids recapitulate gene expression programs of fetal neocortex development.' In: *Proceedings of the National Academy of Sciences of the United States of America* 112.51, pp. 15672–7. arXiv: `arXiv:1408.1149`.

Chaboub, Lesley S. and Deneen, Benjamin (Dec. 2013). 'Astrocyte Form and Function in the Developing Central Nervous System'. In: *Seminars in Pediatric Neurology* 20.4, pp. 230–235.

Chambers, Stuart M, Fasano, Christopher A, Papapetrou, Eirini P, Tomishima, Mark, Sadelain, Michel and Studer, Lorenz (Mar. 2009). 'Highly efficient neural conversion of human ES and iPS cells by dual inhibition of SMAD signaling.' In: *Nature biotechnology* 27.3, pp. 275–80.

Chesselet, Marie Francoise, Fleming, Sheila, Mortazavi, Farzad and Meurers, Bernd (July 2008). 'Strengths and limitations of genetic mouse models of Parkinson's disease'. In: *Parkinsonism and Related Disorders* 14.SUPPL.2.

Choi, Se Hoon, Kim, Young Hye, Hebisch, Matthias, Sliwinski, Christopher, Lee, Seungkyu, D'Avanzo, Carla, Chen, Hechao, Hooli, Basavaraj, Asselin, Caroline, Muffat, Julien et al. (2014). 'A three-dimensional human neural cell culture model of Alzheimer's disease'. In: *Nature* 515.7526, pp. 274–278.

Choi, Se Hoon, Kim, Young Hye, Quinti, Luisa, Tanzi, Rudolph E. and Kim, Doo Yeon (2016). '3D culture models of Alzheimer's disease: a road map to a "cure-in-a-dish"'. In: *Molecular Neurodegeneration* 11.1, p. 75.

Chung, Won-Suk, Welsh, Christina A, Barres, Ben A and Stevens, Beth (Nov. 2015). 'Do glia drive synaptic and cognitive impairment in disease?' In: *Nature Neuroscience* 18.11, pp. 1539–1545.

Clevers, Hans (July 2013). 'The intestinal crypt, a prototype stem cell compartment'. In: *Cell* 154.2, p. 274.

— (2016). 'Modeling Development and Disease with Organoids'. In: *Cell* 165.7, pp. 1586–1597.

Cooper, Oliver, Seo, Hyemyung, Andrabi, Shaida, Guardia-Laguarta, Cristina, Graziotto, John, Sundberg, Maria, McLean, Jesse R, Carrillo-Reid, Luis, Xie, Zhong, Osborn, Teresia et al. (July 2012). 'Pharmacological rescue of mitochondrial deficits in iPSC-derived neural cells from patients with familial Parkinson's disease.' In: *Science translational medicine* 4.141, 141ra90.

Cugola, Fernanda R., Fernandes, Isabella R., Russo, Fabiele B., Freitas, Beatriz C., Dias, Joaõ L.M., Guimarães, Katia P., Benazzato, Cecília, Almeida, Nathalia, Pignatari, Graciela C., Romero, Sarah et al. (2016). 'The Brazilian Zika virus strain causes birth defects in experimental models'. In: *Nature* 534.7606, pp. 267–271.

Cullen, D. Kacy, Wolf, John A., Vernekar, Varadraj N., Vukasinovic, Jelena and LaPlaca, Michelle C. (June 2012). 'Neural Tissue Engineering and Biohybridized Microsystems for Neurobiological Investigation In Vitro (Part 1)'. In: *Critical Reviews in Biomedical Engineering* 39.3, pp. 201–240.

D'Avanzo, Carla, Aronson, Jenna, Kim, Young Hye, Choi, Se Hoon, Tanzi, Rudolph E. and Kim, Doo Yeon (Oct. 2015). 'Alzheimer's in 3D culture: Challenges and perspectives'. In: *BioEssays* 37.10, pp. 1139–1148.

Dang, Jason, Tiwari, Shashi Kant, Lichinchi, Gianluigi, Qin, Yue, Patil, Veena S and Eroshkin, Alexey M (2016). 'Zika Virus Depletes Neural Progenitors in Human Cerebral Organoids through Activation of the Innate Immune Receptor TLR3'. In: *Stem Cell* 19.2, pp. 258–265.

Dawson, Ted M., Ko, Han Seok and Dawson, Valina L. (June 2010). *Genetic Animal Models of Parkinson's Disease*.

Dawson, Ted M and Dawson, Valina L (2003). 'Molecular pathways of neurodegeneration in Parkinson's disease'. In: *Science* 302.5646, pp. 819–822.

Dettmer, Ulf, Selkoe, Dennis and Bartels, Tim (2016). 'New insights into cellular a-synuclein homeostasis in health and disease'. In: *Current Opinion in Neurobiology* 36, pp. 15–22.

Di Lullo, Elizabeth and Kriegstein, Arnold R (2017). 'The use of brain organoids to investigate neural development and disease'. In: *Nature Reviews Neuroscience* 18, pp. 573–584.

Doi, Daisuke, Samata, Bumpei, Katsukawa, Mitsuko, Kikuchi, Tetsuhiro, Morizane, Asuka, Ono, Yuichi, Sekiguchi, Kiyotoshi, Nakagawa, Masato, Parmar, Malin and Takahashi, Jun (Mar. 2014). 'Isolation of human induced pluripotent stem cell-derived dopaminergic progenitors by cell sorting for successful transplantation.' In: *Stem cell reports* 2.3, pp. 337–50.

Dorsey, E Ray and Bloem, Bastiaan R (2018). 'The Parkinson Pandemic — A Call to Action'. In: *JAMA Neurology* 75.1, pp. 9–10.

Drost, Jarno and Clevers, Hans (2017). 'Translational applications of adult stem cell-derived organoids'. In: *The Company of Biologists* 144, pp. 968–975.

Dutta, Devanjali, Heo, Inha and Clevers, Hans (2017). 'Disease Modeling in Stem Cell-Derived 3D Organoid Systems'. In: *Trends in Molecular Medicine* 23.5, pp. 393–410.

Eiraku, Mototsugu, Takata, Nozomu, Ishibashi, Hiroki, Kawada, Masako, Sakakura, Eriko, Okuda, Satoru, Sekiguchi, Kiyotoshi, Adachi, Taiji and Sasai, Yoshiki (Apr. 2011). 'Self-organizing optic-cup morphogenesis in three-dimensional culture'. In: *Nature* 472, p. 51.

Eiraku, Mototsugu, Watanabe, Kiichi, Matsuo-Takasaki, Mami, Kawada, Masako, Yonemura, Shigenobu, Matsumura, Michiru, Wataya, Takafumi, Nishiyama, Ayaka, Muguruma, Keiko and Sasai, Yoshiki (2008). 'Self-Organized Formation of Polarized Cortical Tissues from ESCs and Its Active Manipulation by Extrinsic Signals'. In: *Cell Stem Cell* 3.5, pp. 519–532.

Emborg, Marina E (2007). 'Nonhuman Primate Models of Parkinson's Disease'. In: *Institute for Laboratory Animal Research Journal* 48.4, pp. 339–355.

Engelhardt, Eliasz and Gomes, Marleide da Mota (July 2017). 'Lewy and his inclusion bodies: Discovery and rejection'. In: *Dementia & Neuropsychologia* 11.2, pp. 198–201.

Faivre-Sarrailh, Catherine and Devaux, Jérôme J (Oct. 2013). 'Neuro-glial interactions at the nodes of Ranvier: implication in health and diseases.' In: *Frontiers in cellular neuroscience* 7, p. 196.

Fatehullah, Aliya, Tan, Si Hui and Barker, Nick (2016). 'Organoids as an in vitro model of human development and disease'. In: *Nature Publishing Group* 18.3, pp. 246–254.

Fedorow, H., Tribl, F., Halliday, G., Gerlach, M., Riederer, P. and Double, K. L. (2005). 'Neuromelanin in human dopamine neurons: Comparison with peripheral melanins and relevance to Parkinson's disease'. In: *Progress in Neurobiology* 75.2, pp. 109–124.

Feigin, Valery L and Vos, Theo (2017). 'Articles Global , regional , and national burden of neurological disorders during 1990 – 2015 : a systematic analysis for the Global Burden of Disease Study 2015'. In: *Lancet Neurology* 16, pp. 877–897.

Fleming, Sheila M., Zhu, Chunni, Fernagut, Pierre Olivier, Mehta, Arpesh, DiCarlo, Cheryl D., Seaman, Ronald L. and Chesselet, Marie Françoise (2004). 'Behavioral and immunohistochemical effects of chronic intravenous and subcutaneous infusions of varying doses of rotenone'. In: *Experimental Neurology* 187.2, pp. 418–429.

Forno, Lysia S (1996). 'Neuropathology of Parkinson's Disease'. In: *Journal of Neuropathology and Experimental Neurology* 55.3, pp. 259–272.

Garcez, Patricia P., Loiola, Erick Correia, Da Costa, Rodrigo Madeiro, Higa, Luiza M., Trindade, Pablo, Delvecchio, Rodrigo, Nascimento, Juliana Minardi, Brindeiro, Rodrigo, Tanuri, Amilcar and Rehen, Stevens K. (2016). 'Zika virus impairs growth in human neurospheres and brain organoids'. In: *Science* 352.6287.

Garcia-Dominguez, M. (Dec. 2003). 'Ebf gene function is required for coupling neuronal differentiation and cell cycle exit'. In: *Development* 130.24, pp. 6013–6025.

Garcia-Reitboeck, Pablo, Anichtchik, Oleg, Dalley, Jeffrey W., Ninkina, Natalia, Tofaris, George K., Buchman, Vladimir L. and Spillantini, Maria Grazia (Oct. 2013). 'Endogenous alpha-synuclein influences the number of dopaminergic neurons in mouse substantia nigra'. In: *Experimental Neurology* 248, pp. 541–545.

Giandomenico, Stefano L. and Lancaster, Madeline A. (2017). 'Probing human brain evolution and development in organoids'. In: *Current Opinion in Cell Biology* 44, pp. 36–43.

Goldwurm, S, Zini, M, Mariani, L, Tesei, S, Miceli, R, Sironi, F, Clementi, M, Bonifati, V and Pezzoli, G (2007). 'Evaluation of LRRK2 G2019S penetrance: relevance for genetic counseling in Parkinson disease.' In: *Neurology* 68.14, pp. 1141–3.

Granado, Noelia, Ares-Santos, Sara and Moratalla, Rosario (Feb. 2013). 'Methamphetamine and Parkinson's Disease'. In: *Parkinson's Disease* 2013, pp. 1–10.

Grealish, Shane, Diguet, Elsa, Parmar, Malin, Bjo, Anders, Grealish, Shane, Diguet, Elsa, Kirkeby, Agnete, Mattsson, Bengt, Heuer, Andreas and Bramoulle, Yann (2014). 'Human ESC-Derived Dopamine Neurons Show Similar Preclinical Efficacy and Potency to Fetal Neurons when Grafted in a Rat Model of Parkinson ' s Clinical Progress Human ESC-Derived Dopamine Neurons Show Similar Preclinical Efficacy and Potency to Fetal Neur'. In: *Cell Stem Cell* 15, pp. 653–665.

Haenseler, Walther, Sansom, Stephen N., Buchrieser, Julian, Newey, Sarah E., Moore, Craig S., Nicholls, Francesca J., Chintawar, Satyan, Schnell, Christian, Antel, Jack P., Allen, Nicholas D. et al. (2017). 'A Highly Efficient Human Pluripotent Stem Cell Microglia Model Displays a Neuronal-Co-culture-Specific Expression Profile and Inflammatory Response'. In: *Stem Cell Reports* 8.6, pp. 1727–1742.

Hargus, Gunnar, Cooper, Oliver, Deleidi, Michela, Levy, Adam, Lee, Kristen, Marlow, Elizabeth, Yow, Alyssa, Soldner, Frank, Hockemeyer, Dirk, Hallett, Penelope J et al. (2010). 'Differentiated Parkinson patient-derived induced pluripotent stem cells grow in the adult rodent brain and reduce motor asymmetry in Parkinsonian rats.' In: *Proceedings of the National Academy of Sciences of the United States of America* 107.7, pp. 15921–15926.

Haycock, John W. (2011). '3D Cell Culture: A Review of Current Approaches and Techniques'. In: *Methods Molecular Biologyl Biol* 695, pp. 1–5.

Hegarty, Shane V., Sullivan, Aideen M. and O'Keeffe, Gerard W. (July 2013). 'Midbrain dopaminergic neurons: A review of the molecular circuitry that regulates their development'. In: *Developmental Biology* 379.2, pp. 123–138.

Hemmer, Kathrin, Smits, Lisa M, Bolognin, Silvia and Schwamborn, Jens C (May 2018). 'In vivo Phenotyping of Human Parkinson' s Disease-Specific Stem Cells Carrying the LRRK2 -G2019S Mutation Reveals Increased a-Synuclein Levels but Absence of Spreading'. In: *Opera Medica et Physiologica* 4.2.

Hillje, Anna-Lena and Schwamborn, Jens C (May 2016). 'Utilization of stem cells to model Parkinson's disease – current state and future challenges'. In: *Future Neurology* 11.2, pp. 171–186.

Hinkle, Kelly M., Yue, Mei, Behrouz, Bahareh, Dächsel, Justus C., Lincoln, Sarah J., Bowles, Erin E., Beevers, Joel E., Dugger, Brittany, Winner, Beate, Prots, Iryna et al. (2012). 'LRRK2 knockout mice have an intact dopaminergic system but display alterations in exploratory and motor co-ordination behaviors'. In: *Molecular Neurodegeneration* 7.1.

Howard, Christopher D., Keefe, Kristen A., Garris, Paul A. and Daberkow, David P. (Aug. 2011). 'Methamphetamine neurotoxicity decreases phasic, but not tonic, dopaminergic signaling in the rat striatum'. In: *Journal of Neurochemistry* 118.4, pp. 668–676.

Hubert, Christopher G., Rivera, Maricruz, Spangler, Lisa C., Wu, Qiulian, Mack, Stephen C., Prager, Briana C., Couce, Marta, McLendon, Roger E., Sloan, Andrew E. and Rich, Jeremy N. (2016). 'A Three-Dimensional Organoid Culture System Derived from Human Glioblastomas Recapitulates the Hypoxic Gradients and Cancer Stem Cell Heterogeneity of Tumors Found In Vivo'. In: *Cancer Research* 76.8, pp. 2465–2477.

Huch, Meritxell and Koo, Bon-kyoung (2015). 'Modeling mouse and human development using organoid cultures.' In: *Development (Cambridge, England)* 142.18, pp. 3113–25.

Illes, Sebastian, Jakab, Martin, Beyer, Felix, Gelfert, Renate, Couillard-Despres, Sébastien, Schnitzler, Alfons, Ritter, Markus and Aigner, Ludwig (2014). 'Intrinsically active and pacemaker neurons in pluripotent stem cell-derived neuronal populations'. In: *Stem Cell Reports* 2.3, pp. 323–336.

Jablonska, Beata, Aguirre, Adan, Raymond, Matthew, Szabo, Gabor, Kitabatake, Yasuji, Sailor, Kurt A, Ming, Guo-Li, Song, Hongjun and Gallo, Vittorio (May 2010). 'Chordin-induced lineage plasticity of adult SVZ neuroblasts after demyelination'. In: *Nature Neuroscience* 13.5, pp. 541–550.

Jackson-Lewis, Vernice and Przedborski, Serge (Feb. 2007). 'Protocol for the MPTP mouse model of Parkinson's disease'. In: *Nature Protocols* 2, p. 141.

Jagmag, Shail A., Tripathi, Naveen, Shukla, Sunil D., Maiti, Sankar and Khurana, Sukant (2016). 'Evaluation of models of Parkinson's disease'. In: *Frontiers in Neuroscience* 9.JAN.

Jan, Asad, Jansonius, Brandon, Delaidelli, Alberto, Bhanshali, Forum, An, Yi Andy, Ferreira, Nelson, Smits, Lisa M., Negri, Gian Luca, Schwamborn, Jens C., Jensen, Poul H. et al. (Dec. 2018). 'Activity of translation regulator eukaryotic elongation factor-2 kinase is increased in Parkinson disease brain and its inhibition reduces alpha synuclein toxicity'. In: *Acta Neuropathologica Communications* 6.1.

Jo, Junghyun, Xiao, Yixin, Xuyang Sun, Alfred, King Tan, Eng, Shawn Je, Hyunsoo, Ng, Huck-hui, Jo, Junghyun, Xiao, Yixin, Sun, Alfred Xuyang, Tan, Eng King et al. (2016). 'Midbrain-like Organoids from Human Pluripotent Stem Cells

Contain Functional Dopaminergic and Neuromelanin-Producing Neurons'. In: *Cell Stem Cell* 19.2, pp. 248–257.

Kadoshima, Taisuke, Sakaguchi, Hideya, Nakano, Tokushige, Soen, Mika, Ando, Satoshi and Eiraku, Mototsugu (2013). 'Self-organization of axial polarity, inside-out layer pattern , and species-specific progenitor dynamics in human ES cell-derived neocortex'. In: *Proceedings of the National Academy of Sciences* 110, pp. 20284–20289.

Kageyama, Jorge, Wollny, Damian, Treutlein, Barbara and Camp, J. Gray (2018). 'ShinyCortex: Exploring single-cell transcriptome data from the developing human cortex'. In: *Frontiers in Neuroscience* 12.MAY, pp. 10–13.

Kalia, Lorraine V and Lang, Anthony E (Mar. 2015). *Parkinson's Disease*.

Kamel, Freya, Goldman, Samuel M., Umbach, David M., Chen, Honglei, Richardson, Gina, Barber, Marie Richards, Meng, Cheryl, Marras, Connie, Korell, Monica, Kasten, Meike et al. (2014). 'Dietary fat intake, pesticide use, and Parkinson's disease'. In: *Parkinsonism and Related Disorders* 20.1, pp. 82–87.

Kelava, Iva and Lancaster, Madeline A (2016a). 'Dishing out mini-brains : Current progress and future prospects in brain organoid research'. In: *Developmental Biology* 420.2, pp. 199–209.

— (2016b). 'Stem Cell Models of Human Brain Development'. In: *Cell Stem Cell* 18.6, pp. 736–748.

Kim, Hongwon, Park, Hyeok Ju, Choi, Hwan, Chang, Yujung, Park, Hanseul, Shin, Jaein, Kim, Junyeop, Lengner, Christopher J., Lee, Yong Kyu and Kim, Jongpil (2019). 'Modeling G2019S-LRRK2 Sporadic Parkinson's Disease in 3D Midbrain Organoids'. In: *Stem Cell Reports* 12.3, pp. 518–531.

Kirkeby, Agnete, Grealish, Shane, Wolf, Daniel a, Nelander, Jenny, Wood, James, Lundblad, Martin, Lindvall, Olle and Parmar, Malin (June 2012). 'Generation of regionally specified neural progenitors and functional neurons from human embryonic stem cells under defined conditions.' In: *Cell reports* 1.6, pp. 703–14.

Klein, Christine and Westenberger, Ana (2012). 'Genetics of Parkinson's disease'. In: *Cold Spring Harbor Perspectives in Medicine* 2:a008888.

Koh, Yong Hui, Tan, Li Yi and Ng, Shi-yan (2018). 'Patient-Derived Induced Pluripotent Stem Cells and Organoids for Modeling Alpha Synuclein Propagation in Parkinson ' s Disease'. In: *Frontiers in Cellular Neuroscience* 12.November, pp. 1–12.

Kordower, Jeffrey H., Olanow, C. Warren, Dodiya, Hemraj B., Chu, Yaping, Beach, Thomas G., Adler, Charles H., Halliday, Glenda M. and Bartus, Raymond T. (Aug. 2013). 'Disease duration and the integrity of the nigrostriatal system in Parkinson's disease'. In: *Brain* 136.8, pp. 2419–2431.

Korotkova, Tatiana M., Ponomarenko, Alexei A., Brown, Ritchie E. and Haas, Helmut L. (2004). 'Functional diversity of ventral midbrain dopamine and GABAergic neurons'. In: *Molecular Neurobiology* 29.3, pp. 243–259.

Kriks, Sonja, Shim, Jae-Won, Piao, Jinghua, Ganat, Yosif M, Wakeman, Dustin R, Xie, Zhong, Carrillo-Reid, Luis, Auyeung, Gordon, Antonacci, Chris, Buch, Amanda et al. (Dec. 2011). 'Dopamine neurons derived from human ES cells efficiently engraft in animal models of Parkinson's disease.' In: *Nature* 480.7378, pp. 547–51.

Krüger, Rejko, Kuhn, Wilfried, Müller, Thomas, Woitalla, Dirk, Graeber, Manuel, Kösel, Sigfried, Przuntek, Horst, Epplen, Jörg T., Schöls, Ludger and Riess, Olaf (1998). 'Ala30Pro mutation in the gene encoding α-synuclein in Parkinson's disease'. In: *Nature Genetics* 18.2, pp. 106–108.

Lancaster, Madeline A. and Knoblich, Juergen A. (2014a). 'Generation of cardiomyocytes from human pluripotent stem cells'. In: *Nature protocols* 9.10, pp. 1–18.

— (2014b). 'Organogenesis in a dish: modeling development and disease using organoid technologies.' In: *Science (New York, N.Y.)* 345, p. 1247125.

Lancaster, Madeline A, Renner, Magdalena, Martin, Carol-Anne, Wenzel, Daniel, Bicknell, Louise S, Hurles, Matthew E, Homfray, Tessa, Penninger, Josef M, Jackson, Andrew P and Knoblich, Juergen A (Sept. 2013). 'Cerebral organoids model human brain development and microcephaly.' In: *Nature* 501.7467, pp. 373–9.

Langston, J. William (Mar. 2006). 'The parkinson's complex: Parkinsonism is just the tip of the iceberg'. In: *Annals of Neurology* 59.4, pp. 591–596.

Le Grand, Jaclyn Nicole, Gonzalez-Cano, Laura, Pavlou, Maria Angeliki and Schwamborn, Jens C. (Feb. 2015). 'Neural stem cells in Parkinson's disease: a role for neurogenesis defects in onset and progression'. In: *Cellular and Molecular Life Sciences* 72.4, pp. 773–797.

Lee, Chun-ting, Bendriem, Raphael M, Wu, Wells W and Shen, Rong-fong (2017). '3D brain Organoids derived from pluripotent stem cells : promising experimental models for brain development and neurodegenerative disorders'. In: *Journal of Cell Science* 24.59, pp. 1–12.

Lesage, Suzanne and Brice, Alexis (2009). *Parkinson's disease: From monogenic forms to genetic susceptibility factors*.

Li, Xianting, Tan, Yin Cai, Poulose, Shibu, Olanow, C. Warren, Huang, Xin Yun and Yue, Zhenyu (Oct. 2007). 'Leucine-rich repeat kinase 2 (LRRK2)/PARK8 possesses GTPase activity that is altered in familial Parkinson's disease R1441C/G mutants'. In: *Journal of Neurochemistry* 103.1, pp. 238–247.

Li, Yanping, Liu, Wencheng, Oo, Tinmarla F., Wang, Lei, Tang, Yi, Jackson-Lewis, Vernice, Zhou, Chun, Geghman, Kindiya, Bogdanov, Mikhail, Przedborski, Serge et al. (July 2009). 'Mutant LRRK2 R1441G BAC transgenic mice recapitulate cardinal features of Parkinson's disease'. In: *Nature Neuroscience* 12.7, pp. 826–828.

Lin, Lin, Göke, Jonathan, Cukuroglu, Engin, Dranias, Mark R., VanDongen, Antonius M.J. and Stanton, Lawrence W. (2016). 'Molecular Features Underlying Neurodegeneration Identified through In Vitro Modeling of Genetically Diverse Parkinson's Disease Patients'. In: *Cell Reports* 15.11, pp. 2411–2426.

Lindvall, Olle and Kokaia, Zaal (May 2009). 'Prospects of stem cell therapy for replacing dopamine neurons in Parkinson's disease.' In: *Trends in pharmacological sciences* 30.5, pp. 260–7.

Luhmann, Heiko J, Sinning, Anne, Yang, Jenq-wei and Reyes-puerta, Vicente (2016). 'Spontaneous Neuronal Activity in Developing Neocortical Networks : From Single Cells to Large-Scale Interactions'. In: *Frontiers in Neural Circuits* 10.May, pp. 1–14.

Ma, Chi H E, Brenner, Gary J, Omura, Takao, Samad, Omar A, Costigan, Michael, Inquimbert, Perrine, Niederkofler, Vera, Salie, Rishard, Sun, Chia Chi, Lin, Herbert Y et al. (2011). 'The BMP Coreceptor RGMb Promotes While the Endogenous BMP Antagonist Noggin Reduces Neurite Outgrowth and Peripheral Nerve Regeneration by Modulating BMP Signaling'. In: *Journal of Neuroscience* 31.50, pp. 18391–18400.

Mansour, Abed AlFatah, Gonçalves, J Tiago, Bloyd, Cooper W, Li, Hao, Fernandes, Sarah, Quang, Daphne, Johnston, Stephen, Parylak, Sarah L, Jin, Xin and Gage, Fred H (2018). 'An in vivo model of functional and vascularized human brain organoids'. In: *Nature Biotechnology* June 2017.

Mariani, Jessica, Coppola, Gianfilippo, Zhang, Ping, Pelphrey, Kevin A, Howe, R, Vaccarino, Flora M, Mariani, Jessica, Coppola, Gianfilippo, Zhang, Ping, Abyzov, Alexej et al. (2015). 'Glutamate Neuron Differentiation in Autism

FOXG1-Dependent Dysregulation of GABA / Glutamate'. In: *Cell* 162.2, pp. 375–390.

Maries, Eleonora, Dass, Biplob, Collier, Timothy J., Kordower, Jeffrey H. and Steece-Collier, Kathy (2003). 'The role of α-synuclein in Parkinson's disease: Insights from animal models'. In: *Nature Reviews Neuroscience* 4.9, pp. 727–738.

Marton, Rebecca M. and Paşca, Sergiu P. (2016). 'Neural Differentiation in the Third Dimension: Generating a Human Midbrain'. In: *Cell Stem Cell* 19.2, pp. 145–146.

McCormack, Alison L., Thiruchelvam, Mona, Manning-Bog, Amy B., Thiffault, Christine, Langston, J. William, Cory-Slechta, Deborah A. and Di Monte, Donato A. (2002). 'Environmental risk factors and Parkinson's disease: Selective degeneration of nigral dopaminergic neurons caused by the herbicide paraquat'. In: *Neurobiology of Disease* 10.2, pp. 119–127.

'Method of the Year 2017: Organoids' (Jan. 2018). In: *Nature Methods* 15, p. 1.

Michel, Patrick P, Hirsch, Etienne C and Hunot, Stéphane (May 2016). 'Understanding Dopaminergic Cell Death Pathways in Parkinson Disease.' In: *Neuron* 90.4, pp. 675–91.

Miller, Gary Wright (May 2007). 'Paraquat: The red herring of parkinson's disease research'. In: *Toxicological Sciences* 100.1, pp. 1–2.

Miller, Justine D., Ganat, Yosif M., Kishinevsky, Sarah, Bowman, Robert L., Liu, Becky, Tu, Edmund Y., Mandal, Pankaj K., Vera, Elsa, Shim, Jae Won, Kriks, Sonja et al. (2013). 'Human iPSC-based modeling of late-onset disease via progerin-induced aging'. In: *Cell Stem Cell* 13.6, pp. 691–705.

Miner, Jonathan J. and Diamond, Michael S. (2016). *Understanding how zika virus enters and infects neural target cells.*

Molofsky, Anna V, Krencik, Robert, Krenick, Robert, Ullian, Erik M, Ullian, Erik, Tsai, Hui-hsin, Deneen, Benjamin, Richardson, William D, Barres, Ben A and Rowitch, David H (May 2012). 'Astrocytes and disease: a neurodevelopmental perspective.' In: *Genes & development* 26.9, pp. 891–907.

Monzel, Anna S., Smits, Lisa M., Hemmer, Kathrin, Hachi, Siham, Moreno, Edinson Lucumi, Wuellen, Thea van, Jarazo, Javier, Walter, Jonas, Brüggemann, Inga, Boussaad, Ibrahim et al. (May 2017). 'Derivation of Human Midbrain-Specific Organoids from Neuroepithelial Stem Cells'. In: *Stem Cell Reports* 8.5, pp. 1–11.

Muffat, Julien, Li, Yun, Yuan, Bingbing, Mitalipova, Maisam, Omer, Attya, Corcoran, Sean, Bakiasi, Grisilda, Tsai, Li Huei, Aubourg, Patrick, Ransohoff, Richard M. et al. (Nov. 2016). 'Efficient derivation of microglia-like cells from human pluripotent stem cells'. In: *Nature Medicine* 22.11, pp. 1358–1367.

Muguruma, Keiko, Nishiyama, Ayaka, Kawakami, Hideshi, Hashimoto, Kouichi and Sasai, Yoshiki (2015). 'Self-Organization of Polarized Cerebellar Tissue in 3D Culture of Human Pluripotent Stem Cells'. In: *Cell Reports* 10, pp. 537–550.

Nass, Richard and Przedborski, Serge (2008). *Parkinson's Disease: Molecular and Therapeutic Insights From Model Systems*. Ed. by Richard Nass and Serge Przedbordki. 1st. Oxford: Elsevier Science, p. 686.

Nguyen, Ha Nam, Byers, Blake, Cord, Branden, Shcheglovitov, Aleksandr, Byrne, James, Gujar, Prachi, Kee, Kehkooi, Schüle, Birgitt, Dolmetsch, Ricardo E, Langston, William et al. (Mar. 2011). 'LRRK2 mutant iPSC-derived DA neurons demonstrate increased susceptibility to oxidative stress.' In: *Cell stem cell* 8.3, pp. 267–80.

Nolbrant, Sara, Heuer, Andreas, Parmar, Malin and Kirkeby, Agnete (2017). 'Generation of high-purity human ventral midbrain dopaminergic progenitors for in vitro maturation and intracerebral transplantation'. In: *Nature Protocols* 12.9, pp. 1962–1979.

Nowakowski, Tomasz J, Pollen, Alex A, Di Lullo, Elizabeth, Sandoval-Espinosa, Carmen, Bershteyn, Marina and Kriegstein, Arnold R (2016). 'Expression Analysis Highlights AXL as a Candidate Zika Virus Entry Receptor in Neural Stem Cells.' In: *Cell stem cell* 18.5, pp. 591–6.

Nuytemans, Karen, Theuns, Jessie, Cruts, Marc and Van Broeckhoven, Christine (2010). *Genetic etiology of Parkinson disease associated with mutations in the SNCA, PARK2, PINK1, PARK7, and LRRK2 genes: A mutation update.*

Obeso, José a, Rodríguez-Oroz, María C, Rodríguez, Manuel, Arbizu, Javier and Giménez-Amaya, José M (Apr. 2002). 'The basal ganglia and disorders of movement: pathophysiological mechanisms.' In: *News in physiological sciences : an international journal of physiology produced jointly by the International Union of Physiological Sciences and the American Physiological Society* 17, pp. 51–5.

Orimo, S., Uchihara, T., Kanazawa, T., Itoh, Y., Wakabayashi, K., Kakita, A. and Takahashi, H. (Dec. 2011). 'Unmyelinated axons are more vulnerable to degeneration than myelinated axons of the cardiac nerve in Parkinson's disease'. In: *Neuropathology and Applied Neurobiology* 37.7, pp. 791–802.

Ormel, Paul R., Vieira de Sa, Renata, Hol, Elly M., Pasterkamp, R. Jeroen, Vieira de Sá, Renata, Bodegraven, Emma J. van, Karst, Henk, Harschnitz, Oliver, Sneeboer, Marjolein A.M., Johansen, Lill Eva et al. (Dec. 2018). 'Microglia innately develop within cerebral organoids'. In: *Nature Communications* 9.1.

Parkinson, James (2002). 'An Essay on the Shaking Palsy'. In: *J Neuropsychiatry Clin Neurosci* 14.2, pp. 223–236.

Paşca, Anca M, Sloan, Steven a, Clarke, Laura E, Tian, Yuan, Makinson, Christopher D, Huber, Nina, Kim, Chul Hoon, Park, Jin-Young, O'Rourke, Nancy a, Nguyen, Khoa D et al. (2015). 'Functional cortical neurons and astrocytes from human pluripotent stem cells in 3D culture'. In: *Nature Methods* 12.7.

Pasca, Sergiu P. (2018). 'The rise of three-dimensional human brain cultures'. In: *Nature Review* 553.7689, pp. 437–445.

Patzke, Christopher, Acuna, Claudio, Giam, Louise R, Wernig, Marius and Südhof, Thomas C (2016). 'Conditional deletion of L1CAM in human neurons impairs both axonal and dendritic arborization and action potential generation'. In: *Journal of Experimental Medicine* 213.4, pp. 499–515.

Polymeropoulos, Mihael H., Lavedan, Christian, Leroy, Elisabeth, Ide, Susan E., Dehejia, Anindya, Dutra, Amalia, Pike, Brian, Root, Holly, Rubenstein, Jeffrey, Boyer, Rebecca et al. (June 1997). 'Mutation in the α-synuclein gene identified in families with Parkinson's disease'. In: *Science* 276.5321, pp. 2045–2047.

Potashkin, J. A., Blume, S. R. and Runkle, N. K. (2011). 'Limitations of animal models of Parkinson's disease'. In: *Parkinson's Disease* 2011.

Proukakis, Christos, Houlden, Henry and Schapira, Anthony H (2013). 'Somatic Alpha-Synuclein Mutations in Parkinson ' s Disease : Hypothesis and Preliminary Data'. In: *Movement Disorders* 28.6, pp. 705–712.

Qian, Xuyu, Nguyen, Ha Nam, Song, Mingxi M, Hadiono, Christopher, Ogden, Sarah C, Hammack, Christy, Yao, Bing, Hamersky, Gregory R, Jacob, Fadi, Zhong, Chun et al. (2016). 'Brain-Region-Specific Organoids Using Mini- bioreactors for Modeling ZIKV Exposure'. In: *Cell*, pp. 1–17.

Raja, Waseem K, Mungenast, Alison E, Lin, Yuan-ta, Ko, Tak, Abdurrob, Fatema, Seo, Jinsoo and Tsai, Li-huei (2016). 'Self-Organizing 3D Human Neural Tissue Derived from Induced Pluripotent Stem Cells Recapitulate Alzheimer ' s Disease Phenotypes'. In: *PLoS One*, pp. 1–18.

Ramonet, David, Daher, João Paulo L., Lin, Brian M., Stafa, Klodjan, Kim, Jaekwang, Banerjee, Rebecca, Westerlund, Marie, Pletnikova, Olga, Glauser, Liliane, Yang, Lichuan et al. (2011). 'Dopaminergic Neuronal loss, Reduced Neurite Complexity and Autophagic Abnormalities in Transgenic Mice Expressing G2019S Mutant LRRK2'. In: *PLoS ONE* 6.4.

Recasens, Ariadna and Dehay, Benjamin (2014). 'Alpha-synuclein spreading in Parkinson's disease'. In: *Frontiers in Neuroanatomy* 8.December, pp. 1–9.

Reinhardt, Peter, Glatza, Michael, Hemmer, Kathrin, Tsytsyura, Yaroslav, Thiel, Cora S, Hoing, Susanne, Moritz, Sören, Parga, Juan A, Wagner, Lydia, Bruder, Jan M et al. (Jan. 2013). 'Derivation and expansion using only small molecules of human neural progenitors for neurodegenerative disease modeling'. In: *PLoS One* 8.3, e59252.

Reinhardt, Peter, Schmid, Benjamin, Burbulla, Lena F., Schöndorf, David C., Wagner, Lydia, Glatza, Michael, Höing, Susanne, Hargus, Gunnar, Heck, Susanna A., Dhingra, Ashutosh et al. (2013). 'Genetic correction of a lrrk2 mutation in human iPSCs links parkinsonian neurodegeneration to ERK-dependent changes in gene expression'. In: *Cell Stem Cell* 12.3, pp. 354–367.

Renner, Magdalena, Lancaster, Madeline A, Bian, Shan, Choi, Heejin, Ku, Taeyun, Peer, Angela, Chung, Kwanghun and Knoblich, Juergen A (2017). 'Self-organized developmental patterning and differentiation in cerebral organoids'. In: *The EMBO Journal* 36, pp. 1316–1329.

Rodriguez, Manuel, Morales, Ingrid, Rodriguez-Sabate, Clara, Sanchez, Alberto, Castro, Rafael, Brito, Jose Miguel and Sabate, Magdalena (2014). 'The degeneration and replacement of dopamine cells in Parkinson's disease: the role of aging'. In: *Frontiers in Neuroanatomy* 8.August, pp. 1–7.

Roybon, Laurent, Christophersen, Nicolaj S, Brundin, Patrik and Li, Jia-Yi (2004). 'Stem cell therapy for Parkinson's disease: where do we stand?' In: *Cell and tissue research* 318, pp. 261–273.

Ruitenberg, Marit F.L., Duthoo, Wout, Santens, Patrick, Notebaert, Wim and Abrahamse, Elger L. (2015). 'Sequential movement skill in Parkinson's disease: A state-of-the-art'. In: *Cortex* 65, pp. 102–112.

Ryan, Scott D., Dolatabadi, Nima, Chan, Shing Fai, Zhang, Xiaofei, Akhtar, Mohd Waseem, Parker, James, Soldner, Frank, Sunico, Carmen R., Nagar, Saumya, Talantova, Maria et al. (2013). 'Isogenic Human iPSC Parkinson's Model Shows Nitrosative Stress-Induced Dysfunction in MEF2-PGC1α Transcription'. In: *Cell* 155.6, pp. 1351–1364.

Sachs, Charlotte and Jonsson, Gösta (Dec. 1975). 'Effects of 6-hydroxydopamine on central noradrenaline neurons during ontogeny'. In: *Brain Research* 99.2, pp. 277–291.

Sakaguchi, Hideya, Kadoshima, Taisuke, Soen, Mika, Narii, Nobuhiro, Ishida, Yoshihito, Ohgushi, Masatoshi, Takahashi, Jun, Eiraku, Mototsugu and Sasai, Yoshiki (Nov. 2015). 'Generation of functional hippocampal neurons from self-organizing human embryonic stem cell-derived dorsomedial telencephalic tissue'. In: *Nature Communications* 6, p. 8896.

Sánchez-Danés, Adriana, Richaud-Patin, Yvonne, Carballo-Carbajal, Iria, Jiménez-Delgado, Senda, Caig, Carles, Mora, Sergio, Di Guglielmo, Claudia, Ezquerra, Mario, Patel, Bindiben, Giralt, Albert et al. (May 2012). 'Disease-specific phenotypes in dopamine neurons from human iPS-based models of genetic and sporadic Parkinson's disease.' In: *EMBO molecular medicine* 4.5, pp. 380–95.

Sasaki, H, Hui, C, Nakafuku, M and Kondoh, H (1997). 'A binding site for Gli proteins is essential for HNF-3beta floor plate enhancer activity in transgenics and can respond to Shh in vitro.' In: *Development (Cambridge, England)* 124.7, pp. 1313–22.

Sato, Toshiro, Vries, Robert G, Snippert, Hugo J, Wetering, Marc van de, Barker, Nick, Stange, Daniel E, Es, Johan H van, Abo, Arie, Kujala, Pekka, Peters, Peter J et al. (Mar. 2009). 'Single Lgr5 stem cells build cryptvillus structures in vitro without a mesenchymal niche'. In: *Nature* 459, p. 262.

Schapira, Anthony H. V. and Gegg, Matthew (Apr. 2011). 'Mitochondrial Contribution to Parkinson's Disease Pathogenesis'. In: *Parkinson's Disease* 2011, pp. 1–7.

Schapira, Anthony H. and Jenner, Peter (May 2011). *Etiology and pathogenesis of Parkinson's disease*.

Schwamborn, Jens C. (Feb. 2018). 'Is Parkinson's Disease a Neurodevelopmental Disorder and Will Brain Organoids Help Us to Understand It?' In: *Stem Cells and Development* 27.14, pp. 968–975.

Seidel, Diana, Krinke, Dana, Jahnke, Heinz Georg, Hirche, Anika, Kloß, Daniel, Mack, Till G A, Striggow, Frank and Robitzki, Andrea (Nov. 2012). 'Induced Tauopathy in a Novel 3D-Culture Model Mediates Neurodegenerative Processes: A Real-Time Study on Biochips'. In: *PLoS ONE* 7.11.

Sepe, Sara, Milanese, Chiara, Gabriels, Sylvia, Derks, Kasper W J, Payan-Gomez, Cesar, IJcken, Wilfred F J van, Rijksen, Yvonne M A, Nigg, Alex L, Moreno,

Sandra, Cerri, Silvia et al. (2016). 'Inefficient DNA Repair Is an Aging-Related Modifier of Parkinson's Disease.' In: *Cell reports* 15.9, pp. 1866–75.

Setia, Harpreet and Muotri, Alysson R. (Mar. 2019). 'Brain organoids as a model system for human neurodevelopment and disease'. In: *Seminars in Cell & Developmental Biology* August 2018, pp. 0–1.

Shaikh, Komal T., Yang, Alvin, Youshin, Ekaterina and Schmid, Susanne (May 2015). 'Transgenic LRRK2 R1441G rats–a model for Parkinson disease?' In: *PeerJ* 3, e945.

Singleton, A. B., Farrer, M., Johnson, J., Singleton, A, Hague, S, Kachergus, J, Hulihan, M, Peuralinna, T, Dutra, A, Nussbaum, R et al. (2003). 'α-Synuclein Locus Triplication Causes Parkinson's Disease'. In: *Science* 302.5646, p. 841.

Smith, Wanli W., Pei, Zhong, Jiang, Haibing, Dawson, Valina L., Dawson, Ted M. and Ross, Christopher A. (Oct. 2006). 'Kinase activity of mutant LRRK2 mediates neuronal toxicity'. In: *Nature Neuroscience* 9.10, pp. 1231–1233.

Smits, Lisa M., Reinhardt, Lydia, Reinhardt, Peter, Glatza, Michael, Monzel, Anna S., Stanslowsky, Nancy, Rosato-Siri, Marcelo D., Zanon, Alessandra, Antony, Paul M., Bellmann, Jessica et al. (Dec. 2019). 'Modeling Parkinson's disease in midbrain-like organoids'. In: *npj Parkinson's Disease* 5.1, p. 5.

Smits, Lisa M, Magni, Stefano, Grzyb, Kamil, Antony, Paul MA, Krüger, Rejko, Skupin, Alexander, Bolognin, Silvia and Schwamborn, Jens C (2019). 'Single-cell transcriptomics reveals multiple neuronal cell types in human midbrain-specific organoids'. In: *bioRxiv*.

Spathis, Athanasios D, Asvos, Xenophon, Ziavra, Despina, Karampelas, Theodoros, Topouzis, Stavros, Cournia, Zoe, Qing, Xiaobing, Smits, Lisa M, Dalla, Christina, Rideout, Hardy J et al. (Apr. 2017). 'Nurr1:RXRα heterodimer activation as monotherapy for Parkinson' s disease'. In: *PNAS* 114.15, pp. 3999–4004.

Stefanis, Leonidas (2012). 'Alpha synuclein in Parkinson's disease'. In: *Cold Spring Harbor Perspectives in Medicine* 4:a009399.

Sterneckert, Jared L, Reinhardt, Peter and Schöler, Hans R (2014). 'Investigating human disease using stem cell models.' In: *Nature reviews. Genetics* 15.9, pp. 625–639.

Suga, Hidetaka, Kadoshima, Taisuke, Minaguchi, Maki, Ohgushi, Masatoshi, Soen, Mika, Nakano, Tokushige, Takata, Nozomu, Wataya, Takafumi, Muguruma, Keiko, Miyoshi, Hiroyuki et al. (Nov. 2011). 'Self-formation of functional adenohypophysis in three-dimensional culture'. In: *Nature* 480, p. 57.

Sulzer, David (Feb. 2011). 'How Addictive Drugs Disrupt Presynaptic Dopamine Neurotransmission'. In: *Neuron* 69.4, pp. 628–649.

Sulzer, David and Surmeier, D. James (Jan. 2013). *Neuronal vulnerability, pathogenesis, and Parkinson's disease.*

Takahashi, Kazutoshi, Tanabe, Koji, Ohnuki, Mari, Narita, Megumi, Ichisaka, Tomoko, Tomoda, Kiichiro and Yamanaka, Shinya (Nov. 2007). 'Induction of pluripotent stem cells from adult human fibroblasts by defined factors'. In: *Cell* 131.5, pp. 861–72.

Tanner, Caroline M., Kame, Freya, Ross, G. Webster, Hoppin, Jane A., Goldman, Samuel M., Korell, Monica, Marras, Connie, Bhudhikanok, Grace S., Kasten, Meike, Chade, Anabel R. et al. (June 2011). 'Rotenone, paraquat, and Parkinson's disease'. In: *Environmental Health Perspectives* 119.6, pp. 866–872.

Tepper, James M. and Lee, Christian R. (Jan. 2007). 'GABAergic control of substantia nigra dopaminergic neurons'. In: *Progress in Brain Research.* Vol. 160. Elsevier, pp. 189–208.

The GTEx Consortium (2015). 'The Genotype-Tissue Expression (GTEx) pilot analysis: Multitissue gene regulation in humans'. In: *Science* 348, pp. 648–660.

Tieng, Vannary, Stoppini, Luc, Villy, Sabrina, Fathi, Marc, Dubois-Dauphin, Michel and Krause, Karl-Heinz (2014). 'Engineering of midbrain organoids containing long-lived dopaminergic neurons.' In: *Stem cells and development* 23.13, pp. 1–32.

Tong, Y., Yamaguchi, H., Giaime, E., Boyle, S., Kopan, R., Kelleher, R. J. and Shen, J. (May 2010). 'Loss of leucine-rich repeat kinase 2 causes impairment of protein degradation pathways, accumulation of -synuclein, and apoptotic cell death in aged mice'. In: *Proceedings of the National Academy of Sciences* 107.21, pp. 9879–9884.

Trujillo, Cleber A. and Muotri, Alysson R. (2018). 'Brain Organoids and the Study of Neurodevelopment'. In: *Trends in Molecular Medicine* 24.12, pp. 982–990.

Tsika, Elpida, Kannan, Meghna, Foo, Caroline Shi Yan, Dikeman, Dustin, Glauser, Liliane, Gellhaar, Sandra, Galter, Dagmar, Knott, Graham W., Dawson, Ted M., Dawson, Valina L. et al. (2014). 'Conditional expression of Parkinson's disease-related R1441C LRRK2 in midbrain dopaminergic neurons of mice causes nuclear abnormalities without neurodegeneration'. In: *Neurobiology of Disease* 71.1, pp. 345–358.

Ungerstedt, Urban (1968). '6-hydroxy-dopamine induced degeneration of central monoamine neurons'. In: *European Journal of Pharmacology* 5.1, pp. 107–110.

Venda, Lara Lourenço, Cragg, Stephanie J, Buchman, Vladimir L and Wade-Martins, Richard (Dec. 2010). 'α-Synuclein and dopamine at the crossroads of Parkinson's disease.' In: *Trends in neurosciences* 33.12, pp. 559–68.

Wakabayashi, Koichi and Takahashi, Hitoshi (1997). 'Neuropathology of autonomic nervous system in Parkinson's disease'. In: *European Neurology* 38.

Wang, Xiao, Allen, William E, Wright, Matthew A, Sylwestrak, Emily L, Samusik, Nikolay, Vesuna, Sam, Evans, Kathryn, Liu, Cindy, Ramakrishnan, Charu, Liu, Jia et al. (2018). 'Three-dimensional intact-tissue sequencing of single-cell transcriptional states'. In: *Science* 361, pp. 1–9.

Wang, Yaqing, Zhu, Yujuan and Qin, Jianhua (2018). 'Human brain organoid-on-a-chip to model prenatal nicotine exposure'. In: *Lab on a Chip* 18.6, pp. 851–860.

Wells, Michael F., Salick, Max R., Wiskow, Ole, Ho, Daniel J., Worringer, Kathleen A., Ihry, Robert J., Kommineni, Sravya, Bilican, Bilada, Klim, Joseph R., Hill, Ellen J. et al. (2016). 'Genetic Ablation of AXL Does Not Protect Human Neural Progenitor Cells and Cerebral Organoids from Zika Virus Infection'. In: *Cell Stem Cell* 19.6, pp. 703–708.

Xi, Jiajie, Liu, Yan, Liu, Huisheng, Chen, Hong, Emborg, Marina E and Zhang, Su-Chun (Aug. 2012). 'Specification of midbrain dopamine neurons from primate pluripotent stem cells'. In: *Stem cells (Dayton, Ohio)* 30.8, pp. 1655–63.

Xu, Hanxiao, Jiao, Ying, Qin, Shuang, Zhao, Weiheng, Chu, Qian and Wu, Kongming (2018). 'Organoid technology in disease modelling, drug development, personalized treatment and regeneration medicine'. In: *Experimental Hematology & Oncology*, pp. 1–12.

Xu, Yaqian, Yang, Jing and Shang, Huifang (Dec. 2016). 'Meta-analysis of risk factors for Parkinson's disease dementia'. In: *Translational Neurodegeneration* 5.1, p. 11.

Zarranz, Juan J, Alegre, Javier, Gómez-Esteban, Juan C, Lezcano, Elena, Ros, Raquel, Ampuero, Israel, Vidal, Lídice, Hoenicka, Janet, Rodriguez, Olga, Atarés, Begoña et al. (2004). 'The New Mutation, E46K, of-Synuclein Causes Parkinson and Lewy Body Dementia'. In: *Ann Neurol* 55, pp. 164–173.

Zecca, Luigi, Zucca, Fabio A., Wilms, Henrik and Sulzer, David (2003). 'Neuromelanin of the substantia nigra: A neuronal black hole with protective and toxic characteristics'. In: *Trends in Neurosciences* 26.11, pp. 578–580.

Zhou, Zhi Dong, Kumari, Udhaya, Xiao, Zhi Cheng and Tan, Eng King (2010). 'Notch as a molecular switch in neural stem cells'. In: *IUBMB Life* 62.8, pp. 618–623.